Spin Asymmetry of Kaon Productions in polarized deep-inelastic Scattering on Deuterium Target by HERMES Experiment

by

Shigenobu Yoneyama

Thesis submitted to the Department of Physics
in partial fulfillment of the requirements for the degree of

Doctor of Science

at the

Tokyo Institute of Technology

February 2001

Abstract

The measurement of the spin asymmetry of kaon productions in deep-inelastic electron scattering on the polarized deuterium target at the HERMES experiment is reported in this thesis. The HERMES experiment is performed at DESY in Hamburg, Germany. It studies the spin structure of the nucleon. The HERMES experiment uses a longitudinally polarized target and the longitudinally polarized 27.5 GeV electron beam of the HERA storage ring. HERMES measures the electrons scattered off the target nucleon and identifies the hadrons in the final state in coincidence.

HERMES has installed a Ring Imaging Čerenkov (RICH) detector with a dual-radiator, aerogel and C_4F_{10} gas, just before the data taking period in 1998. Silica aerogel was used for the first time as a radiator of the RICH detector in the actual experiment. The RICH detector identifies kaons as well as pions and protons in a wide momentum range from 2 GeV to 15 GeV. The kaon is an important particle to study the contributions of the sea and strange quark spin to the nucleon spin as it has a strange quark as its constituent.

The spin asymmetry of kaon productions was measured in the kinematic range $0.023 < x < 0.6$ and $1\ \mathrm{GeV}^2 < Q^2 < 10\ \mathrm{GeV}^2$ using the polarized deuterium target data taken from 1998 to spring 1999. The result is shown as a function of x, the Bjorken's scaling variable. The spin asymmetry of kaon productions was measured for the first time in polarized deep-inelastic scattering. A clear difference between the asymmetries of K^+ ($u\bar{s}$) production and K^- ($\bar{u}s$) production was observed. K^- asymmetry provides the first direct experimental indication that the contribution of the sea quark spin to the nucleon spin is small. This result opened up a new technique of the polarized deep-inelastic scattering: π, K, p ($\bar{\mathrm{p}}$) identification and studies of quark flavor which contributes to the nucleon spin.

Contents

1 Introduction **19**

2 Deep-inelastic Scattering **21**

2.1 Kinematics of polarized deep-inelastic Scattering 21

2.1.1 Cross Section for deep-inelastic Scattering 23

2.1.2 Unpolarized Cross Section 24

2.2 Polarized Cross Section 26

2.2.1 Spin Asymmetries 29

2.2.2 Structure Functions in Quark Parton Model 32

2.2.3 Sum Rules 35

2.3 Semi-inclusive Measurement 38

2.3.1 Spin Asymmetry for semi-inclusive Measurement 38

2.3.2 Fragmentation Functions 39

3 The HERMES Experiment **41**

3.1 Overview of HERA 41

3.2 Polarized Beam of HERA 42

3.3 Polarized Deuterium Target 44

3.4 The HERMES Spectrometer 46

3.4.1 Tracking System 47

3.4.2 Particle Identification Detectors 51

3.4.3 Luminosity Monitor 52

3.4.4 Trigger System 53

3.4.5 Laser Alignment System 53

4 Dual-Radiator Ring Imaging Čerenkov Detector **57**

4.1 Introduction 57

4.1.1 Detector Design 58

4.2 Online Monitoring 65

4.2.1 Reconstruction and Particle Identification 67

4.2.2 Mirror Alignment 72
4.2.3 Detector Performance 72
4.2.4 Efficiencies and Contaminations 76

5 PID Performance of RICH Detector 79
5.1 Monte Carlo Programs 79
5.2 Optimization of RICH Detector in Software 80
5.2.1 Level of MC Program 80
5.2.2 Level of Reconstruction 81
5.3 Event Generation and Performance in Monte Carlo 82
5.3.1 Event Generation 82
5.3.2 Performance 82
5.4 Definitions of Identification Efficiencies and Probabilities 85
5.4.1 Definitions 86
5.4.2 Quality Parameters 88
5.5 Results of Identification Efficiencies, Purities and Contaminations . . 91
5.5.1 Conditions 91
5.5.2 Comparison of Charge Dependence 91
5.5.3 Results available for Analysis of Asymmetry 92

6 Extraction of Spin Asymmetries on Deuterium Target 103
6.1 Data Production 103
6.2 Data Quality Selection 104
6.2.1 Burst Level Criteria 104
6.3 Particle Identification and Event Selection 105
6.3.1 Particle Identification 105
6.3.2 Event Selection 109
6.4 Extraction of Spin Asymmetry 113
6.5 Corrections to Asymmetry 116
6.5.1 Background Corrections 116
6.5.2 Alignment Corrections 116
6.6 Results of Asymmetries 117
6.6.1 Result of inclusive Asymmetry 117
6.6.2 Kaon Asymmetry uncorrected for Contaminations 118
6.7 Summary of Kaon Asymmetry uncorrected for Contaminations 119

7 Corrections of Asymmetries for Hadron Contaminations 125
7.1 Method of Corrections 125
7.2 Corrected Kinematics 126

7.2.1 Momentum Distributions . . . 126
7.2.2 z Distributions . . . 128
7.2.3 x_F Distributions . . . 128
7.2.4 Relationship between kinematical Variables . . . 128
7.3 Conclusion for kinematical Cuts . . . 129
7.4 Test of central Limit Distribution Method . . . 135
7.5 Corrected Asymmetry . . . 138
7.6 Test of Asymmetry formed by inverse P Matrix . . . 146
7.7 Systematic Uncertainties on Asymmetry . . . 146
7.7.1 Uncertainties of Experiment . . . 147
7.7.2 Uncertainties of CLD Method . . . 150
7.7.3 Uncertainty of Flux . . . 150
7.8 Final Results of Asymmetries . . . 152

8 Conclusion 163

A Spin Asymmetry for combined Statistics of K^+ and K^- 181

B Tests for Stability of Asymmetry 185

C Particle Identification with direct Ray Tracing 189

D Tables of Results for P and Q Matrices 193
D.1 Elements of P and Q Matrices with the IRT Method . . . 194
D.2 Elements of P and Q Matrices with the DRT Method . . . 213

List of Figures

2.1 Schematic picture for a process of the deep-inelastic scattering 22
2.2 World data on the spin-independent structure function $F_2^{\mathrm{d}}(x, Q^2)$ of the deuteron 25
2.3 $R(x, Q^2)$ as a function of x in the different ranges of Q^2 27
2.4 Definition of scattering angles in polarized DIS 28
2.5 World data on the spin-dependent structure function $g_1^{\mathrm{p}}(x)$ of the proton 29
2.6 World data on the spin-dependent structure function $g_1^{\mathrm{d}}(x)$ of the deuteron and $g_1^{\mathrm{n}}(x)$ of the neutron 30
2.7 Schematic diagrams of the polarized deep-inelastic scattering in the level of QPM 34

3.1 Schematic picture of the HERA storage ring 42
3.2 Schematic diagrams of a spin rotator 43
3.3 Rise of the longitudinal polarization in the beam of HERA 44
3.4 Beam polarization versus run number for the data taking in the experiment 45
3.5 Schematic picture of the target system 46
3.6 Effective target polarization versus run number for the data taking in the experiment 47
3.7 Schematic side view of the HERMES spectrometer 48
3.8 Fresnel zone plate mounted on the BC1/2 55
3.9 Focusing image of the Fresnel zone plate and projected images 55

4.1 Čerenkov angle as a function of momentum 59
4.2 Ranges of momentum for the separation of pions, kaons and protons in aerogel and gas 60
4.3 Schematic view of the RICH detector for the upper half of the HERMES detector 61
4.4 Schematic view of the inner structure of the RICH detector in HERMES 62
4.5 Schematic view of the hexagonal close packed matrix 64

4.6 Two-dimensional tubemap for the lower half of the RICH detector . 66
4.7 Online display of a single electron event from the data 66
4.8 Average number of PMT hits for single electron events for the online data quality monitoring 67
4.9 Problem of the inverse ray tracing 68
4.10 Definition of the u and v axes and the angles in the Euclidean coordinate system 69
4.11 Spectra of the reconstructed Čerenkov angles 71
4.12 Number of fired PMTs for aerogel and gas as a function of momentum for the ideal tracks of pions 73
4.13 Reconstructed average angle for pions in the aerogel as a function of momentum 74
4.14 Reconstructed average angle for pions in the gas as a function of momentum 74
4.15 Reconstructed average angles in aerogel and gas as a function of momentum 75
4.16 Squared mass of hadrons calculated from the Čerenkov angles for aerogel and gas from the experimental data as a function of momentum 77

5.1 Schematic view of the geometry of the aerogel tiles in the RICH detector realized on the Monte Carlo program 81
5.2 Momentum distributions for pions, kaons and protons in the GEANT particle type as well as all hadrons 83
5.3 Histograms of the Čerenkov angle for aerogel and gas for the single tracks of electrons compared between the experimental and Monte Carlo data 84
5.4 Histograms of the number of fired PMTs for aerogel and gas for the single tracks of electrons compared between the experimental and Monte Carlo data 85
5.5 rQp distributions for particles identified as pions, kaons and protons as a function of momentum 90
5.6 Comparison of the identification efficiencies between positively and negatively charged particles in $N_{\mathrm{tracks}} = 1$ at $rQp > 0.0$ 93
5.7 Comparison of the identification efficiencies between positively and negatively charged particles in $N_{\mathrm{tracks}} = 2$ at $rQp > 0.0$ 94
5.8 Comparison of the identification efficiencies between positively and negatively charged particles in $N_{\mathrm{tracks}} > 2$ at $rQp > 0.0$ 95
5.9 Identification efficiencies for pions, kaons and protons in $N_{\mathrm{tracks}} = 1$ at $rQp > 0.0$ 96

5.10 Identification efficiencies for pions, kaons and protons in $N_{\text{tracks}} = 2$ at $rQp > 0.0$ 97
5.11 Identification efficiencies for pions, kaons and protons in $N_{\text{tracks}} > 2$ at $rQp > 0.0$ 98
5.12 Identification purities and contaminations for pions, kaons and protons in $N_{\text{tracks}} = 1$ at $rQp > 0.0$ 99
5.13 Identification purities and contaminations for pions, kaons and protons in $N_{\text{tracks}} = 2$ at $rQp > 0.0$ 100
5.14 Identification purities and contaminations for pions, kaons and protons in $N_{\text{tracks}} > 2$ at $rQp > 0.0$ 101

6.1 Responses of the particle identification detectors for the calorimeter, preshower counter and TRD in the experimental data 106
6.2 Distributions of PID likelihoods 108
6.3 Distributions of PID likelihoods for PID_2 and $\text{PID}_2 + \text{PID}_5$ shown in the two-dimensional plot 109
6.4 Distributions of z_{vertex}, r_{vertex}, θ_x, θ_y, horizontal and vertical positions at the calorimeter for electrons before and after the track selection criteria 112
6.5 Distributions of Q^2, W^2, y and calorimeter cluster energy E'_{Calo} for electrons before and after the DIS kinematical criteria 113
6.6 Result of the inclusive asymmetry on the deuterium target 120
6.7 Effect of the momentum threshold on the K^+ asymmetry 121
6.8 Effect of the momentum threshold on the K^- asymmetry 121
6.9 Comparison of statistics for pions, kaons and protons between the different quality parameters of $rQp > 0.0$, $rQp > 0.5$ and $rQp > 1.0$. 122
6.10 Distributions of the quality parameter for pions, kaons and protons . 123
6.11 Comparison of the K^+ asymmetry between the different quality parameters 124
6.12 Comparison of the K^- asymmetry between the different quality parameters 124

7.1 Procedures for the assignment of the true type of hadron to the identified type of hadron in the CLD method 127
7.2 Momentum distributions for pions, kaons and protons 130
7.3 Corrected distributions of z for all hadrons, pions, kaons and protons 131
7.4 Corrected distributions of x_{F} for all hadrons, pions, kaons and protons 132
7.5 Relationship between z and x_{F} for pions, kaons and protons 133
7.6 Relationship between momentum and z for pions, kaons and protons 134

7.7 Distributions of statistics $N^{\vec{\Rightarrow}}$ and $N^{\vec{\Leftarrow}}$ for pions and kaons resulting from the execution more than 600 times for the assignment of the true type of hadron to the identified type of hadron 137

7.8 Distributions for the mean value of the K^+ asymmetry in each bin of x resulting from the execution more than 600 times for the assignment of the true type of hadron to the identified type of hadron 141

7.9 Distributions for the statistical uncertainty of the K^+ asymmetry in each bin of x resulting from the execution more than 600 times for the assignment of the true type of hadron to the identified type of hadron 142

7.10 Distributions for the mean Bjorken x of the K^+ asymmetry in each bin of x resulting from the execution more than 600 times for the assignment of the true type of hadron to the identified type of hadron 143

7.11 Comparison of the K^+ asymmetry between uncorrected and corrected by the CLD method 144

7.12 Comparison of the K^- asymmetry between uncorrected and corrected by the CLD method 144

7.13 Distributions of the virtual photon depolarization factor and kinematical factor $1/(1+\eta\gamma)$ for the DIS events, positively and negatively charged kaons in coincidence with the DIS events in each bin of x . . 145

7.14 Comparison of the K^+ asymmetry formed by the numbers $\vec{\mathsf{N}}$ of the true type of hadron to the one obtained from the CLD method . . . 147

7.15 Spin-dependent structure function $x \cdot g_2^{\mathrm{d}}$ of the deuteron 149

7.16 Flux ratios of the experimental data to the Monte Carlo data for pions, kaons and protons 152

7.17 Result of the K^+ asymmetry on the deuterium target 154

7.18 Result of the K^- asymmetry on the deuterium target 155

7.19 Result of the π^+ asymmetry on the deuterium target 156

7.20 Result of the π^- asymmetry on the deuterium target 157

7.21 Result of the proton asymmetry on the deuterium target 158

7.22 Result of the anti-proton asymmetry on the deuterium target 159

7.23 Result of the h^+ asymmetry on the deuterium target 160

7.24 Result of the h^- asymmetry on the deuterium target 161

A.1 Result of the $K^+ + K^-$ asymmetry on the deuterium target 182

B.1 Comparison of the π^+ asymmetry between the mass of proton and the mass of pion 186

B.2 Comparison of the π^- asymmetry between the mass of proton and the mass of pion 186

B.3 Comparison of the K^+ asymmetry between no cut and with cut on z and x_F . . . 188
B.4 Comparison of the K^- asymmetry between no cut and with cut on z and x_F . . . 188

C.1 Definition of the vectors and the angles in the direct ray tracing . . . 190

List of Tables

3.1 Properties of the tracking chambers 50

4.1 Thresholds of the Čerenkov radiation for pions, kaons and protons . 58
4.2 Maximum separation momenta $p_{\max}$ for aerogel and gas in the RICH detector 60
4.3 Individual contributions to the single photon resolution in aerogel and gas 61
4.4 Additional contributions to the single photon resolution in aerogel and gas 76

5.1 Width of each bin in the different momentum regions 91

6.1 List of criteria for the burst level quality 105
6.2 List of criteria for the event selection 111
6.3 Definition of the binning in x 115

7.1 Comparison of statistics between before and after the corrections of the K^+ asymmetry 140
7.2 Comparison of statistics between before and after the corrections of the K^- asymmetry 140

8.1 Inclusive deuteron asymmetry A_1, x, y, Q^2, statistics in each spin state of beam and target, and their total 166
8.2 Semi-inclusive deuteron asymmetry $A_1^{h^+}$, x, y, Q^2, statistics in each spin state of beam and target, and their total 167
8.3 Semi-inclusive deuteron asymmetry $A_1^{h^-}$, x, y, Q^2, statistics in each spin state of beam and target, and their total 167
8.4 Semi-inclusive deuteron asymmetry $A_1^{\pi^+}$, x, y, Q^2, statistics in each spin state of beam and target, and their total 168
8.5 Semi-inclusive deuteron asymmetry $A_1^{\pi^-}$, x, y, Q^2, statistics in each spin state of beam and target, and their total 168
8.6 Semi-inclusive deuteron asymmetry $A_1^{K^+}$, x, y, Q^2, statistics in each spin state of beam and target, and their total 169

8.7 Semi-inclusive deuteron asymmetry $A_1^{K^-}$, x, y, Q^2, statistics in each spin state of beam and target, and their total . . . 169
8.8 Semi-inclusive deuteron asymmetry A_1^{p}, x, y, Q^2, statistics in each spin state of beam and target, and their total . . . 170
8.9 Semi-inclusive deuteron asymmetry $A_1^{\bar{p}}$, x, y, Q^2, statistics in each spin state of beam and target, and their total . . . 170
8.10 Systematic uncertainties of the experiment for the inclusive deuteron asymmetry A_1 . . . 171
8.11 Systematic uncertainties of the CLD method and systematic uncertainty of the flux for hadrons for the semi-inclusive deuteron asymmetry $A_1^{h^+}$ . . . 172
8.12 Systematic uncertainties of the experiment for the semi-inclusive deuteron asymmetry $A_1^{h^+}$ . . . 172
8.13 Systematic uncertainties of the CLD method and systematic uncertainty of the flux for hadrons for the semi-inclusive deuteron asymmetry $A_1^{h^-}$ . . . 173
8.14 Systematic uncertainties of the experiment for the semi-inclusive deuteron asymmetry $A_1^{h^-}$ . . . 173
8.15 Systematic uncertainties of the CLD method and systematic uncertainty of the flux for hadrons for the semi-inclusive deuteron asymmetry $A_1^{\pi^+}$ . . . 174
8.16 Systematic uncertainties of the experiment for the semi-inclusive deuteron asymmetry $A_1^{\pi^+}$ . . . 174
8.17 Systematic uncertainties of the CLD method and systematic uncertainty of the flux for hadrons for the semi-inclusive deuteron asymmetry $A_1^{\pi^-}$ . . . 175
8.18 Systematic uncertainties of the experiment for the semi-inclusive deuteron asymmetry $A_1^{\pi^-}$ . . . 175
8.19 Systematic uncertainties of the CLD method and systematic uncertainty of the flux for hadrons for the semi-inclusive deuteron asymmetry $A_1^{K^+}$ . . . 176
8.20 Systematic uncertainties of the experiment for the semi-inclusive deuteron asymmetry $A_1^{K^+}$ . . . 176
8.21 Systematic uncertainties of the CLD method and systematic uncertainty of the flux for hadrons for the semi-inclusive deuteron asymmetry $A_1^{K^-}$ . . . 177
8.22 Systematic uncertainties of the experiment for the semi-inclusive deuteron asymmetry $A_1^{K^-}$ . . . 177
8.23 Systematic uncertainties of the CLD method and systematic uncertainty of the flux for hadrons for the semi-inclusive deuteron asymmetry A_1^{p} . . . 178

8.24 Systematic uncertainties of the experiment for the semi-inclusive deuteron asymmetry A_1^{p} . . . 178

8.25 Systematic uncertainties of the CLD method and systematic uncertainty of the flux for hadrons for the semi-inclusive deuteron asymmetry $A_1^{\bar{\mathrm{p}}}$ . . . 179

8.26 Systematic uncertainties of the experiment for the semi-inclusive deuteron asymmetry $A_1^{\bar{\mathrm{p}}}$ . . . 179

A.1 Semi-inclusive deuteron asymmetry $A_1^{\mathrm{K}^+ + \mathrm{K}^-}$, x, y, Q^2, statistics in each spin state of beam and target, and their total . . . 183

A.2 Systematic uncertainties of the CLD method and systematic uncertainty of the flux for hadrons for the semi-inclusive deuteron asymmetry $A_1^{\mathrm{K}^+ + \mathrm{K}^-}$ . . . 184

A.3 Systematic uncertainties of the experiment for the semi-inclusive deuteron asymmetry $A_1^{\mathrm{K}^+ + \mathrm{K}^-}$ . . . 184

B.1 Comparison of statistics with application of the mass of proton and the mass of pion in the π^+ asymmetry . . . 187

B.2 Comparison of statistics with application of the mass of proton and the mass of pion in the π^- asymmetry . . . 187

D.1 Identification efficiencies for pions, kaons and protons in $N_{\mathrm{tracks}} = 1$ with the IRT method at $rQp > 0.0$ . . . 195

D.2 Identification efficiencies for pions, kaons and protons in $N_{\mathrm{tracks}} = 2$ with the IRT method at $rQp > 0.0$ . . . 196

D.3 Identification efficiencies for pions, kaons and protons in $N_{\mathrm{tracks}} > 2$ with the IRT method at $rQp > 0.0$ . . . 197

D.4 Identification purities and contaminations for pions, kaons and protons in $N_{\mathrm{tracks}} = 1$ with the IRT method at $rQp > 0.0$ . . . 198

D.5 Identification purities and contaminations for pions, kaons and protons in $N_{\mathrm{tracks}} = 2$ with the IRT method at $rQp > 0.0$ . . . 199

D.6 Identification purities and contaminations for pions, kaons and protons in $N_{\mathrm{tracks}} > 2$ with the IRT method at $rQp > 0.0$ . . . 200

D.7 Identification efficiencies for pions, kaons and protons in $N_{\mathrm{tracks}} = 1$ with the IRT method at $rQp > 0.5$ . . . 201

D.8 Identification efficiencies for pions, kaons and protons in $N_{\mathrm{tracks}} = 2$ with the IRT method at $rQp > 0.5$ . . . 202

D.9 Identification efficiencies for pions, kaons and protons in $N_{\mathrm{tracks}} > 2$ with the IRT method at $rQp > 0.5$ . . . 203

D.10 Identification purities and contaminations for pions, kaons and protons in $N_{\mathrm{tracks}} = 1$ with the IRT method at $rQp > 0.5$ . . . 204

D.11 Identification purities and contaminations for pions, kaons and protons in $N_{\text{tracks}} = 2$ with the IRT method at $rQp > 0.5$ 205
D.12 Identification purities and contaminations for pions, kaons and protons in $N_{\text{tracks}} > 2$ with the IRT method at $rQp > 0.5$ 206
D.13 Identification efficiencies for pions, kaons and protons in $N_{\text{tracks}} = 1$ with the IRT method at $rQp > 1.0$ 207
D.14 Identification efficiencies for pions, kaons and protons in $N_{\text{tracks}} = 2$ with the IRT method at $rQp > 1.0$ 208
D.15 Identification efficiencies for pions, kaons and protons in $N_{\text{tracks}} > 2$ with the IRT method at $rQp > 1.0$ 209
D.16 Identification purities and contaminations for pions, kaons and protons in $N_{\text{tracks}} = 1$ with the IRT method at $rQp > 1.0$ 210
D.17 Identification purities and contaminations for pions, kaons and protons in $N_{\text{tracks}} = 2$ with the IRT method at $rQp > 1.0$ 211
D.18 Identification purities and contaminations for pions, kaons and protons in $N_{\text{tracks}} > 2$ with the IRT method at $rQp > 1.0$ 212
D.19 Identification efficiencies for pions, kaons and protons in $N_{\text{tracks}} = 1$ with the DRT method at $rQp > 0.0$ 214
D.20 Identification efficiencies for pions, kaons and protons in $N_{\text{tracks}} = 2$ with the DRT method at $rQp > 0.0$ 215
D.21 Identification efficiencies for pions, kaons and protons in $N_{\text{tracks}} > 2$ with the DRT method at $rQp > 0.0$ 216
D.22 Identification purities and contaminations for pions, kaons and protons in $N_{\text{tracks}} = 1$ with the DRT method at $rQp > 0.0$ 217
D.23 Identification purities and contaminations for pions, kaons and protons in $N_{\text{tracks}} = 2$ with the DRT method at $rQp > 0.0$ 218
D.24 Identification purities and contaminations for pions, kaons and protons in $N_{\text{tracks}} > 2$ with the DRT method at $rQp > 0.0$ 219
D.25 Identification efficiencies for pions, kaons and protons in $N_{\text{tracks}} = 1$ with the DRT method at $rQp > 0.5$ 220
D.26 Identification efficiencies for pions, kaons and protons in $N_{\text{tracks}} = 2$ with the DRT method at $rQp > 0.5$ 221
D.27 Identification efficiencies for pions, kaons and protons in $N_{\text{tracks}} > 2$ with the DRT method at $rQp > 0.5$ 222
D.28 Identification purities and contaminations for pions, kaons and protons in $N_{\text{tracks}} = 1$ with the DRT method at $rQp > 0.5$ 223
D.29 Identification purities and contaminations for pions, kaons and protons in $N_{\text{tracks}} = 2$ with the DRT method at $rQp > 0.5$ 224
D.30 Identification purities and contaminations for pions, kaons and protons in $N_{\text{tracks}} > 2$ with the DRT method at $rQp > 0.5$ 225

D.31 Identification efficiencies for pions, kaons and protons in $N_{\text{tracks}} = 1$ with the DRT method at $rQp > 1.0$ 226
D.32 Identification efficiencies for pions, kaons and protons in $N_{\text{tracks}} = 2$ with the DRT method at $rQp > 1.0$ 227
D.33 Identification efficiencies for pions, kaons and protons in $N_{\text{tracks}} > 2$ with the DRT method at $rQp > 1.0$ 228
D.34 Identification purities and contaminations for pions, kaons and protons in $N_{\text{tracks}} = 1$ with the DRT method at $rQp > 1.0$ 229
D.35 Identification purities and contaminations for pions, kaons and protons in $N_{\text{tracks}} = 2$ with the DRT method at $rQp > 1.0$ 230
D.36 Identification purities and contaminations for pions, kaons and protons in $N_{\text{tracks}} > 2$ with the DRT method at $rQp > 1.0$ 231

Chapter 1

Introduction

The investigation of the spin structure of the nucleon is important for quantum chromodynamics (QCD). Polarized deep-inelastic scattering (DIS) provides the experimentally powerful tool to study the spin structure of the nucleon. In the naive quark parton model (QPM) it has been believed for a long time that the spin of the nucleon is composed of the vector sum of the spins of the three valence quarks. This means that the spin of the nucleon is carried by the spin of the quarks by nature. The nucleon and each valence quark have the spin of one half. However, it was experimentally found by the EMC experiment at CERN in 1987 [1] that the contribution of the quark spin to the nucleon spin is smaller than expected. New experiments at SLAC and SMC at CERN followed to measure the spin contents of the nucleon more precisely. Their results, both on proton and neutron targets, confirmed the EMC's finding. The most recent results of the spin contents of the nucleon were presented by the HERMES experiment [2] and implied that the contribution of the quark spin to the nucleon spin is about 30 %. Presently the contribution of the quark spin in the world data varies from 20 % to 30 %.

The spin of the nucleon is mathematically expressed in terms of each contribution of the quarks, gluons and orbital angular momenta as [3]:

$$s_z^{\mathrm{N}}/\hbar = \frac{1}{2} = \frac{1}{2}\Delta\Sigma + \Delta g + L_q + L_g, \tag{1.1}$$

where $\Delta\Sigma$ is decomposed into the terms of the spin contribution of each quark like $\Delta\Sigma = \Delta u + \Delta\bar{u} + \Delta d + \Delta\bar{d} + \Delta s + \Delta\bar{s}$, Δg is the contribution of the gluon spin, and L_q and L_g are the orbital angular momenta of the quarks and gluons respectively. HERMES [2] measured each term of $\Delta\Sigma$ and found from the analyses using the spin asymmetries on the polarized hydrogen and ^{3}He targets that the sea quark distribution Δs had a small contribution of $-0.01 \pm 0.03(\mathrm{stat.}) \pm 0.04(\mathrm{syst.})$. No direct measurement of the polarized distributions for the sea and strange quarks has ever been done up to now.

The HERMES experiment at DESY (Deutsches Elektronen-Synchrotron) investigates the spin structure of the nucleon in the deep-inelastic scattering using the polarized beam of HERA and a polarized gas target in a storage cell installed into

the HERA ring. HERMES measures electrons (positrons) of the HERA beam scattered off the nucleon and identifies the produced hadrons in coincidence with the scattered electrons (positrons). Additionally in 1998 the threshold type Čerenkov detector was converted to a Ring Imaging Čerenkov (RICH) detector, which has been operated presently. The RICH detector identifies pions, kaons and protons in a wide momentum range from 2 GeV to 15 GeV. Especially it is important to measure kaons in order to investigate the spin contribution of the sea and strange quarks as K^- ($\bar{u}s$) is composed of the sea objects alone.

In this thesis the asymmetry of kaon productions on the deuterium target in the polarized deep-inelastic scattering is reported using the RICH detector in the kinematic range of $0.023 < x < 0.6$ and $1\ \mathrm{GeV}^2 < Q^2 < 10\ \mathrm{GeV}^2$. The asymmetry of kaon productions allows to provide detailed information for the spin of the sea and strange quarks. Additionally the asymmetries of pion productions and proton productions as well as hadron productions are reported.

Chapter 2

Deep-inelastic Scattering

2.1 Kinematics of polarized deep-inelastic Scattering

In the process of deep-inelastic scattering (DIS) the virtual photon is exchanged between the incoming charged lepton and the target nucleon via electromagnetic interaction. As the photon is absorbed by the nucleon and interacts with a quark in the nucleon, it is a good probe to investigate the inner structure of the nucleon. Figure 2.1 shows a process of the DIS between the lepton beam l and the target nucleon N in the one photon exchange approximation. l' is the lepton scattered off the nucleon and X are in the hadronic final states produced from the nucleon. In the inclusive measurement only l' is detected and in the semi-inclusive measurement parts of X are detected as well as l'. Exclusive measurement detects l' and all other particles produced in the final state of the process. k is the four-momentum of the incoming lepton with energy E and three-momentum $\vec{q}$ and k' the scattered one with energy E' and three-momentum $\vec{q'}$. The nucleon N has a four-momentum P. The first element in P is energy M, the mass of the nucleon. The three-momentum is zero in the laboratory system. θ is the scattering angle between the incoming and outgoing lepton. The Planck constant $\hbar$ and the speed of light c are set to 1 in this thesis as long as it is not noted otherwise. The firstly two important variables of the DIS kinematics are Q^2 and ν defined as:

$$Q^2 = -q^2 = -(k - k')^2 > 0 \tag{2.1}$$

and

$$\nu = \frac{P \cdot q}{M}. \tag{2.2}$$

In the Breit frame, which is the frame where the virtual photon has no energy, the helicity of the quark in the nucleon changes its direction to the opposite one with no change of the absolute value of the momentum after the absorption of the photon. The dimensionless scaling variables x and y, which are well used in the DIS process,

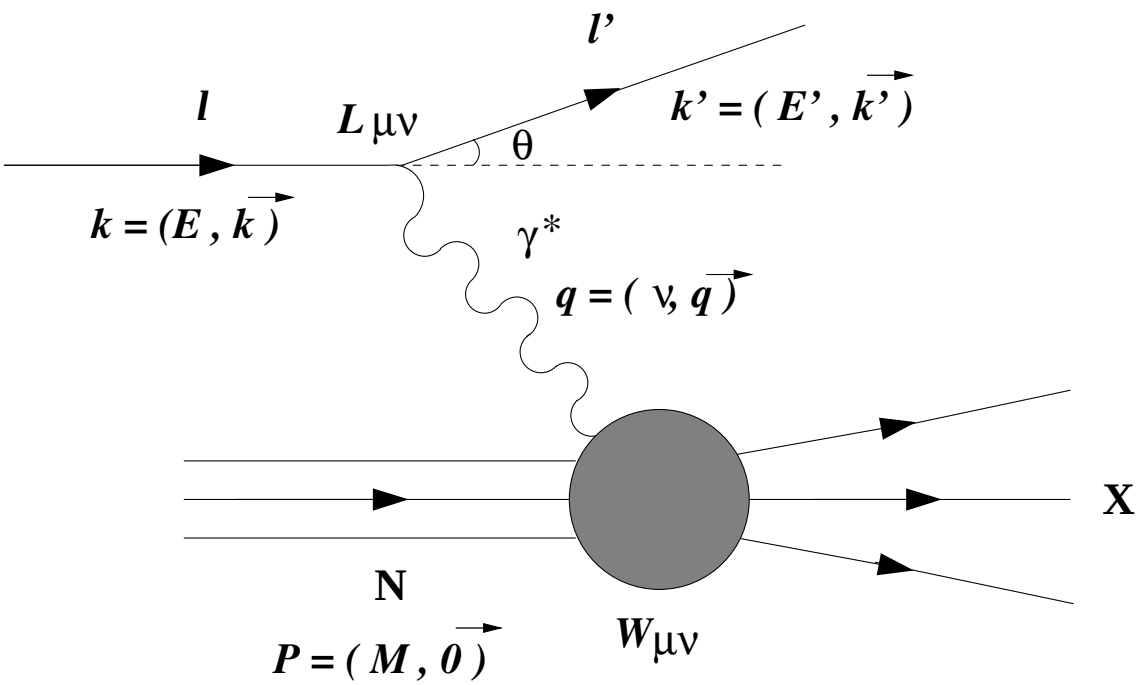

Figure 2.1: Schematic picture for a process of the deep-inelastic scattering in the one photon exchange approximation between the lepton and the nucleon.

are defined as:

$$x = \frac{Q^2}{2(P \cdot q)} \tag{2.3}$$

and

$$y = \frac{P \cdot q}{P \cdot k}. \tag{2.4}$$

For the laboratory system (lab) of a fixed target experiment, like HERMES, neglecting the mass m of the electron which is small compared to its momentum. One has:

$$x \overset{\text{lab}}{=} \frac{Q^2}{2M\nu} \tag{2.5}$$

and

$$y \overset{\text{lab}}{=} \frac{\nu}{E}. \tag{2.6}$$

x is called the Bjorken scaling variable, which is regarded as the fraction of the momentum of the nucleon carried by a quark. The variable y means the fractional energy transfer of the virtual photon. The kinematically allowed range of x and y are:

$$0 \leq x \leq 1, \tag{2.7}$$

$$0 \leq y < \frac{1}{1 + xM/2E} \leq 1. \tag{2.8}$$

The squared invariant mass of the hadronic final state is defined as:

$$W^2 = (P+q)^2 = M^2 + 2M\nu - Q^2. \tag{2.9}$$

As the mass of the electron can be neglected, the variables Q^2 and ν in the laboratory system are represented as:

$$Q^2 \overset{\text{lab}}{\simeq} 4EE' \sin^2 \frac{\theta}{2}, \tag{2.10}$$

$$\nu \overset{\text{lab}}{=} E - E'. \tag{2.11}$$

Q^2 means the squared invariant mass of the virtual photon and ν the energy transfer from the incoming lepton to the target nucleon.

In the semi-inclusive measurement a scaling variable z for the hadron of the final state with energy E_h and three-momentum $\vec{p_h}$, which correspond to four-momentum $p_h = (E_h, \vec{p_h})$, is introduced as:

$$z = \frac{P \cdot p_h}{P \cdot q} \overset{\text{lab}}{=} \frac{E_h}{\nu}, \tag{2.12}$$

$$0 \leq z \leq 1. \tag{2.13}$$

z is the fraction of the energy of the virtual photon transfered to the hadron. Another variable which characterizes the kinematics of the hadron is x_{F}, the x Feynman, as follows:

$$x_{\mathrm{F}} = \frac{2p_h^{\mathrm{L}}}{W}, \tag{2.14}$$

$$-1 \leq x_{\mathrm{F}} \leq 1. \tag{2.15}$$

p_h^{L} is the longitudinal three-momentum of the hadron along the three-momentum of the virtual photon in the virtual photon-nucleon center mass system. We call the hadron with $x_{\mathrm{F}} > 0$ the current fragment, which comes from the quark struck by the virtual photon. The hadron with $x_{\mathrm{F}} < 0$ is the target remnant, which does not directly come from the interacting quark.

2.1.1 Cross Section for deep-inelastic Scattering

In the lowest order quantum electrodynamics (QED) the inclusive DIS differential cross section of the one photon exchange in figure 2.1 is written in the contraction of the vertex factors of both a lepton tensor $L_{\mu\nu}$ and a hadron tensor $W_{\mu\nu}$ when the outgoing lepton is detected in a solid angle $d\Omega$ and in a range of the energy $[E', E' + dE']$ [4]:

$$\begin{aligned} \frac{d^2\sigma}{d\Omega\, dE'} &= \frac{\alpha^2}{Q^4}\frac{E'}{E} L_{\mu\nu} W^{\mu\nu} \\ &= \frac{\alpha^2}{Q^4}\frac{E'}{E}\left(L_{\mu\nu}^{(\mathrm{S})} W^{\mu\nu(\mathrm{S})} - L_{\mu\nu}^{(\mathrm{A})} W^{\mu\nu(\mathrm{A})}\right), \end{aligned} \tag{2.16}$$

where α is the electromagnetic coupling constant with 1/137.04. The lepton tensor $L^{\mu\nu}$ has a polarization-independent symmetric part $L^{(\mathrm{S})}_{\mu\nu}$ and a polarization-dependent anti-symmetric part $L^{(\mathrm{A})}_{\mu\nu}$:

$$L_{\mu\nu} = L^{(\mathrm{S})}_{\mu\nu} + iL^{(\mathrm{A})}_{\mu\nu}. \tag{2.17}$$

In the case of unpolarized lepton and target, both initial spin states of the incoming lepton are averaged and the polarization-independent symmetric part is written as:

$$L^{(\mathrm{S})}_{\mu\nu}(k;k') = 2[k'_\mu k_\nu + k_\mu k'_\nu - g_{\mu\nu}(k\cdot k' - m^2)], \tag{2.18}$$

where $g_{\mu\nu}$ is the metric tensor. The polarization-dependent anti-symmetric part is:

$$L^{(\mathrm{A})}_{\mu\nu}(k,s;k') = 2m\ \varepsilon_{\mu\nu\alpha\beta}\ s^\alpha (k-k')^\beta. \tag{2.19}$$

Here s_α is the spin four-vector of the incident lepton, $\varepsilon_{\mu\nu\alpha\beta}$ the totally anti-symmetric Levi-Civita tensor. The hadronic tensor $W_{\mu\nu}$ describes the interaction at the photon-nucleon vertex. Similarly the hadronic tensor is separated into two parts, the polarization-independent symmetry part $W^{(\mathrm{S})}_{\mu\nu}$ and the polarization-dependent anti-symmetry part $W^{(\mathrm{A})}_{\mu\nu}$ as:

$$W_{\mu\nu} = W^{(\mathrm{S})}_{\mu\nu} + iW^{(\mathrm{A})}_{\mu\nu}. \tag{2.20}$$

2.1.2 Unpolarized Cross Section

In the calculation of the unpolarized cross section the polarization-dependent anti-symmetric part of equation (2.16) is canceled out as both spin states of the incoming lepton are averaged. Though the structure of the hadron cannot be calculated by QCD, under the symmetric arguments and the conservation laws of QED the polarization-independent symmetric part $W^{(\mathrm{S})}_{\mu\nu}$ is parameterized by W_1 and W_2:

$$\begin{aligned} W^{(\mathrm{S})}_{\mu\nu}(q;P) &= W_1(\nu,Q^2)\left(-g_{\mu\nu} + \frac{q_\mu q_\nu}{q^2}\right) \\ &+ \frac{W_2(\nu,Q^2)}{M^2}\left(P_\mu - \frac{P\cdot q}{q^2}q_\mu\right)\left(P_\nu - \frac{P\cdot q}{q^2}q_\nu\right). \end{aligned} \tag{2.21}$$

W_1 and W_2 are called the structure functions and depend on the kinematical variables Q^2 and ν. The unpolarized cross section is given using W_1 and W_2:

$$\frac{d^2\sigma}{d\Omega\ dE'} = \frac{(2\alpha E')^2}{Q^4}\left(2W_1(\nu,Q^2)\sin^2\frac{\theta}{2} + W_2(\nu,Q^2)\cos^2\frac{\theta}{2}\right). \tag{2.22}$$

The dimensionless structure functions, so called spin-independent structure functions, F_1 and F_2, are introduced replacing the variable ν by the dimensionless variable x:

$$F_1(x,Q^2) = MW_1(\nu,Q^2), \tag{2.23}$$

$$F_2(x,Q^2) = \nu W_2(\nu,Q^2). \tag{2.24}$$

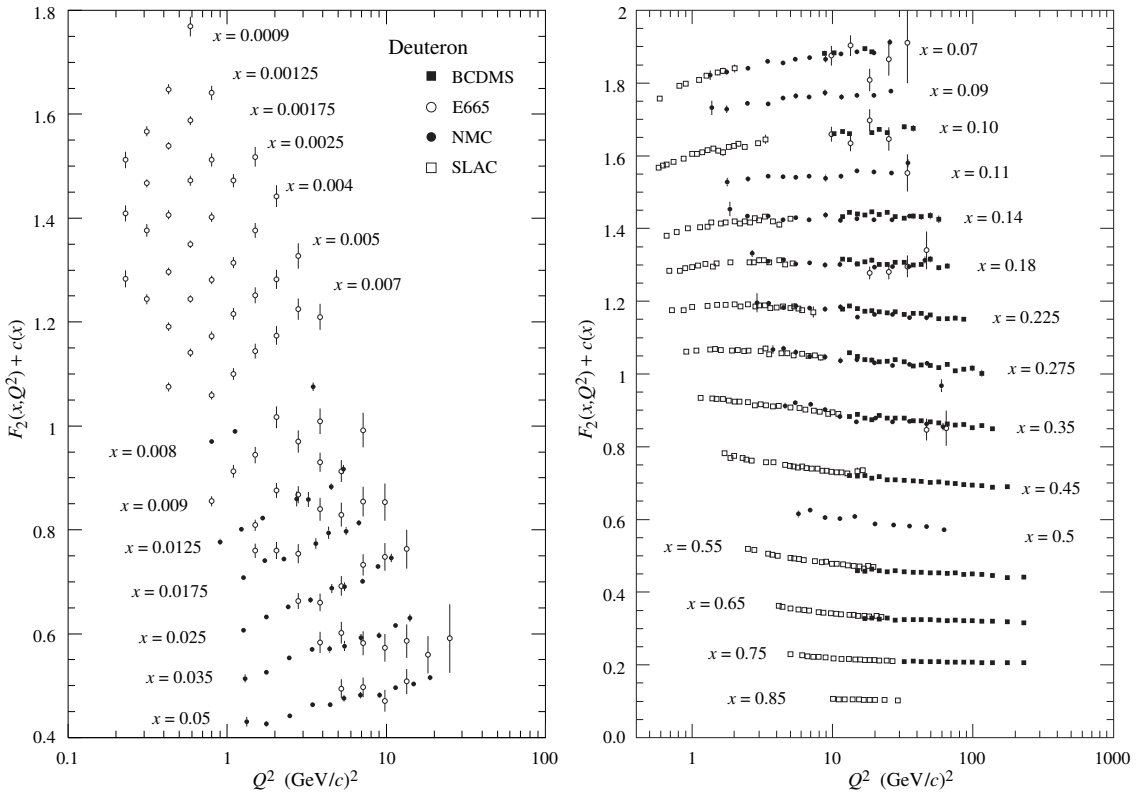

Figure 2.2: World data [5] on the spin-independent structure function $F_2^{\mathrm{d}}(x, Q^2)$ of the deuteron measured in deep-inelastic scattering of electrons (SLAC [6]) and muons (BCDMS [7], E665 [8], NMC [9]) as a function of Q^2 for bins at fixed x. Only statistical errors are shown. For the purpose of the plotting, a constant $c(x) = 0.1 i_x$ is added to $F_2^{\mathrm{d}}(x, Q^2)$ where i_x is the number of the x bin, ranging from 1 ($x = 0.05$) to 14 ($x = 0.0009$) on the left side figure, and from 1 ($x = 0.85$) to 15 ($x = 0.07$) on the right side figure.

The unpolarized cross section is expressed by F_1 and F_2 as:

$$\frac{d^2\sigma}{dx\ dQ^2} = \frac{4\pi\alpha^2}{Q^4}\left[F_1(x,Q^2)\cdot y^2 + \frac{F_2(x,Q^2)}{x}\cdot\left(1 - y - \frac{Mxy}{2E}\right)\right]. \tag{2.25}$$

Figure 2.2 shows the structure function $F_2^{\mathrm{d}}(x, Q^2)$ on the deuteron measured by BCDMS, E665, NMC and SLAC. The figure shows that the scaling of $F_2^{\mathrm{d}}(x, Q^2)$ is clearly violated; It depends on the variable Q^2. The scaling is valid only around $x \simeq 0.2$. In $x < 0.2$ and $x > 0.2$ $F_2^{\mathrm{d}}(x, Q^2)$ has some slopes.

The unpolarized cross section can be related to the photo-absorption cross section for the longitudinally (σ_{L}) polarized and transversely (σ_{T}) polarized photons:

$$\frac{d^2\sigma}{dx\ dQ^2} = \Gamma[\sigma_{\mathrm{T}}(x,Q^2) + \varepsilon\sigma_{\mathrm{L}}(x,Q^2)], \tag{2.26}$$

where Γ is the flux of the virtual photons and expressed as:

$$\Gamma = \frac{\alpha E'}{4\pi^2 ME}\left(\frac{1}{x}-1\right)\frac{1}{1-\varepsilon}. \tag{2.27}$$

ε represents the degree of the transverse polarization of the virtual photons:

$$\varepsilon = \frac{4(1-y)-\gamma^2 y^2}{4(1-y)+2y^2+\gamma^2 y^2}, \tag{2.28}$$

where

$$\gamma = \frac{2Mx}{\sqrt{Q^2}}. \tag{2.29}$$

We define the ratio $R(x,Q^2)$ as:

$$R(x,Q^2) = \frac{\sigma_{\mathrm{L}}(x,Q^2)}{\sigma_{\mathrm{T}}(x,Q^2)}. \tag{2.30}$$

$R(x,Q^2)$ is related to the structure functions $F_1(x,Q^2)$ and $F_2(x,Q^2)$:

$$\frac{1+R(x,Q^2)}{1+\gamma^2} = \frac{F_2(x,Q^2)}{2xF_1(x,Q^2)}. \tag{2.31}$$

$R(x,Q^2)$ on the proton and deuteron has been measured at SLAC [10, 11], NMC [12] and several other experiments and was found to be identical for the proton and deuteron within the experimental uncertainties. In figure 2.3 $R(x,Q^2)$ [10] was fitted and newly parameterized to the world data as $R1998$. In the scaling limit where Q^2 is large and where γ vanishes $R(x,Q^2)$ approaches zero as $\sigma_{\mathrm{L}}(x,Q^2)$ decreases to zero. Then F_1 and F_2 become independent of Q^2 [13, 14, 15]:

$$F_1(x,Q^2), F_2(x,Q^2) \overset{Q^2,\nu\to\infty}{\longrightarrow} F_1(x), F_2(x). \tag{2.32}$$

As a result, one obtains the so called Callan-Gross relation [16]:

$$\frac{2xF_2(x)}{F_1(x)} = 1. \tag{2.33}$$

The equation (2.32) and (2.33) follow from the fact that the scattering comes from the nucleon's constituents, point-like particles with the spin 1/2, which we call the partons.

2.2 Polarized Cross Section

The polarized differential cross section, in the case of the polarized lepton scattering off the polarized nucleon target, is represented in two scattering angles θ and ϕ:

$$\frac{d^3\sigma}{d\cos\theta\ d\phi\ dE'} = \frac{\alpha^2}{Q^4}\frac{E'}{E}L_{\mu\nu}W^{\mu\nu}. \tag{2.34}$$

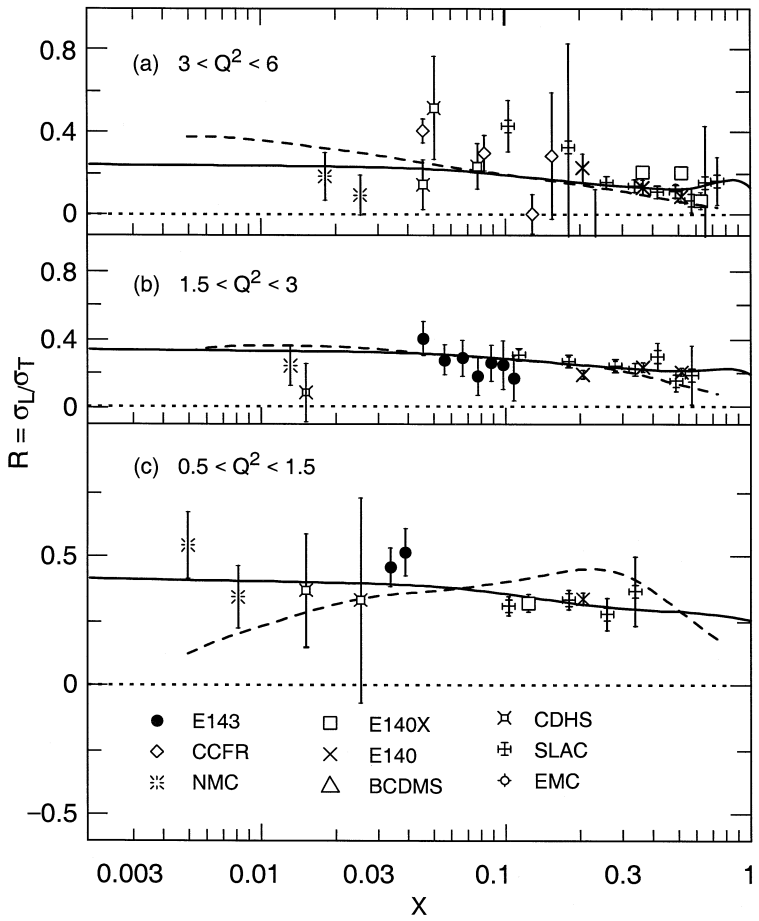

Figure 2.3: $R(x, Q^2)$ [10] as a function of x in the different ranges of Q^2: (a) 3 GeV^2 $\leq Q^2 \leq$ 6 GeV^2; (b) 1.5 GeV^2 $\leq Q^2 \leq$ 3 GeV^2; (c) 0.5 GeV^2 $\leq Q^2 \leq$ 1.5 GeV^2 measured by the different experiments. The solid curve is the fit of $R1998$ and the dashed curve the prediction of the next next leading order perturbative QCD.

The scattering angles are defined in figure 2.4. In the DIS cross section in equation (2.16) the polarization-independent symmetric part and polarization-dependent anti-symmetric part have contributions to the cross section. To cancel out the polarization-independent symmetric part in equation (2.16) we use the cross section difference between two spin states so that only the polarization-dependent anti-symmetric part remains. The polarization-dependent anti-symmetric part for the hadron tensor is given by:

$$\begin{aligned} W_{\mu\nu}^{(\mathrm{A})}(q; P, S) &= G_1(\nu, Q^2) M i\, \varepsilon_{\mu\nu\lambda\sigma}\, q^\lambda S^\sigma \\ &+ \frac{G_2(\nu, Q^2)}{M} i\, \varepsilon_{\mu\nu\lambda\sigma}\, q^\lambda \left[(P \cdot q) S^\sigma - (S \cdot q) P^\sigma\right]. \end{aligned} \tag{2.35}$$

Here S is the polarization vector of the longitudinally polarized nucleon target with spin 1/2, which satisfies $S \cdot S = -1$ and $P \cdot S = 0$ in the laboratory frame. In analogy to the unpolarized cross section the dimensionless spin-dependent structure

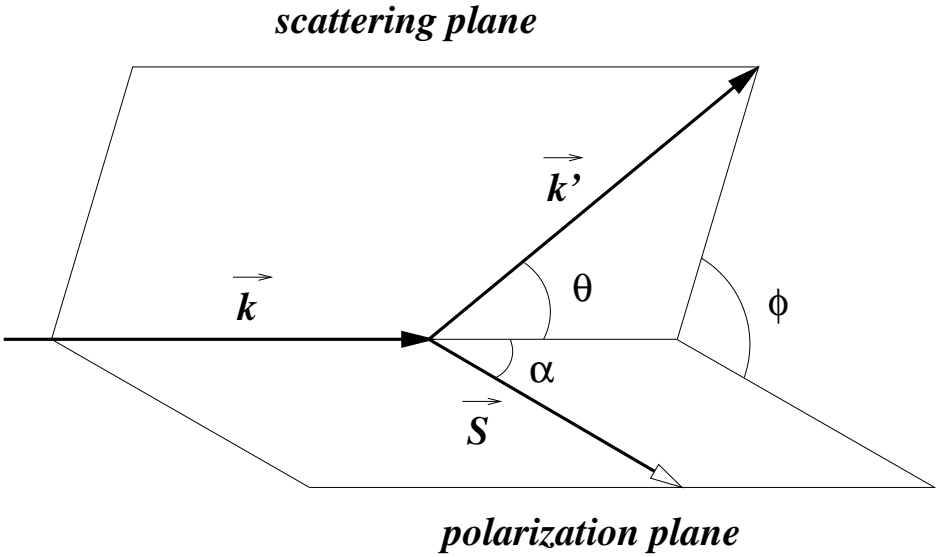

Figure 2.4: Definition of scattering angles in polarized DIS. The angles θ and ϕ are the polar and azimuthal angle between the incoming lepton $\vec{k}$ and the scattered lepton $\vec{k'}$. α is the angle between $\vec{k}$ and the direction of the target polarization $\vec{S}$.

functions are introduced as:

$$g_1(x,Q^2) = M^2\nu G_1(\nu,Q^2), \tag{2.36}$$
$$g_2(x,Q^2) = M\nu^2 G_2(\nu,Q^2). \tag{2.37}$$

For the longitudinally polarized incoming lepton the cross section difference for the direction of the target polarization $\vec{S}$ parallel or anti-parallel is given by:

$$\frac{d^3\sigma(\alpha)}{dx\ dQ^2\ d\phi} - \frac{d^3\sigma(\alpha+\pi)}{dx\ dQ^2\ d\phi} = -\frac{e^4}{4\pi^2 Q^2}\left[\cos\alpha\left(\left[1-\frac{y}{2}-\frac{y^2}{4}\gamma^2\right]g_1(x,Q^2)\right.\right.$$
$$\left.-\frac{y}{2}\gamma^2 g_2(x,Q^2)\right) - \sin\alpha\cos\phi\sqrt{\gamma^2\left[1-y-\frac{y^2}{4}\gamma^2\right]}\left(\frac{y}{2}g_1(x,Q^2)\right.$$
$$\left.\left.+g_2(x,Q^2)\right)\right]. \tag{2.38}$$

For the configurations of the target spin parallel ($\vec{\Rightarrow}$) or anti-parallel ($\vec{\Leftarrow}$) to the spin of the incoming lepton, which corresponds to $\alpha = 0$, above equation (2.38) becomes:

$$\frac{d^3\sigma^{\vec{\Rightarrow}}}{dx\ dQ^2\ d\phi} - \frac{d^3\sigma^{\vec{\Leftarrow}}}{dx\ dQ^2\ d\phi} = -\frac{e^4}{4\pi^2 Q^2}\left[\left(1-\frac{y}{2}-\frac{y^2}{4}\gamma^2\right)g_1(x,Q^2)\right.$$
$$\left.-\frac{y}{2}\gamma^2 g_2(x,Q^2)\right]. \tag{2.39}$$

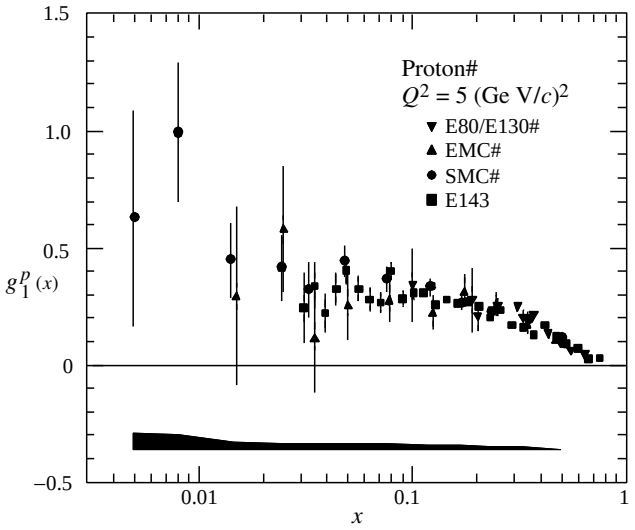

Figure 2.5: World data on the spin-dependent structure function $g_1^{\mathrm{p}}(x)$ of the proton measured in deep-inelastic scattering of polarized electrons (E80 [17], E130 [18], E143 [19]) and polarized muons (EMC [20], SMC [21]) as a function of x at $Q^2 = 5$ GeV^2. Only statistical errors are shown with the data points. As an example, the systematic errors of the SMC data are indicated by the shaded band.

For the configurations of the target spin perpendicular to the spin of the incoming lepton, which corresponds to $\alpha = \pi/2$, equation (2.38) becomes another formula:

$$\frac{d^3\sigma^{\rightarrow\Uparrow}}{dx\ dQ^2\ d\phi} - \frac{d^3\sigma^{\rightarrow\Downarrow}}{dx\ dQ^2\ d\phi} = \frac{e^4}{4\pi^2 Q^2}\cos\phi\left[\sqrt{\gamma^2\left[1-y-\frac{y^2}{4}\gamma^2\right]}\left(\frac{y}{2}g_1(x,Q^2) + g_2(x,Q^2)\right)\right]. \tag{2.40}$$

In figures 2.5 and 2.6 g_1 of the proton, deuteron and neutron on the world data are shown as a function of x respectively.

2.2.1 Spin Asymmetries

The spin-dependent structure functions g_1 and g_2 in the previous section are experimentally determined by the cross section difference between the longitudinally ($\alpha = 0, \pi$) and transversely ($\alpha = \pi/2,\ 3\pi/2$) polarized nucleon target and the longitudinally polarized incoming lepton. A single cross section difference of equation (2.39) or (2.40), however, can determine only a combination of g_1 and g_2. To derive g_1 and g_2 separately the asymmetries of the cross section difference between longitudinally and transversely polarized nucleon target and the longitudinally polarized incoming lepton, which are experimentally measured, are used:

$$A_{||} = \frac{\sigma^{\rightleftarrows} - \sigma^{\rightrightarrows}}{\sigma^{\rightleftarrows} + \sigma^{\rightrightarrows}}, \tag{2.41}$$

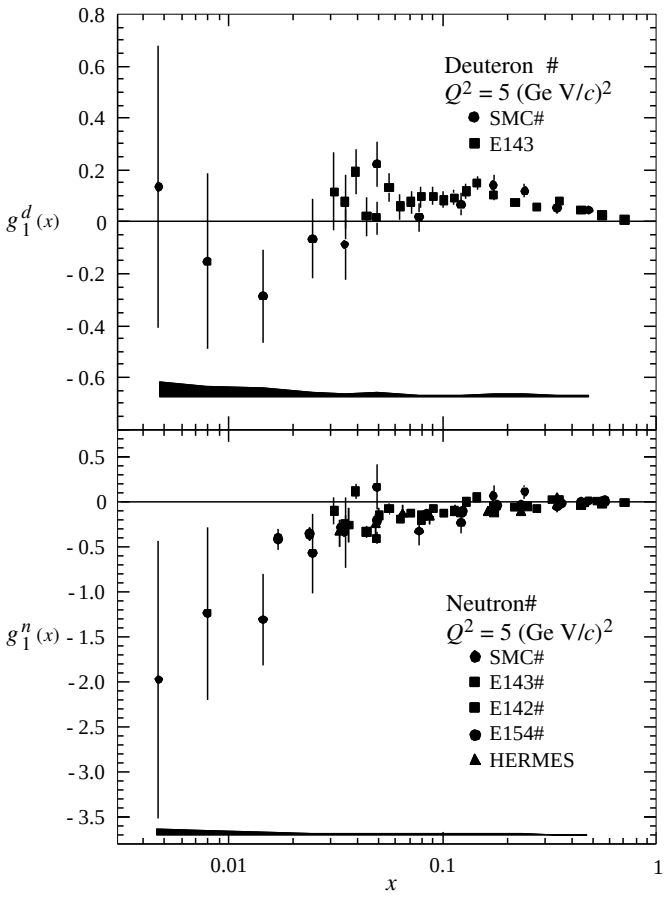

Figure 2.6: World data on the spin-dependent structure function $g_1^{\mathrm{d}}(x)$ of the deuteron (top) and $g_1^{\mathrm{n}}(x)$ of the neutron (bottom) measured in deep-inelastic scattering of polarized electrons (E142 [22], E143 [23], E154 [24], HERMES [25]) and muons (SMC [26]). The results of SMC and E143 for the neutron are evaluated from the difference of the deuteron and the proton data. The results of E142, E154 and HERMES were obtained with polarized ^{3}He targets. Only statistical errors are shown with the data points. As an example, the systematic error of the SMC data is indicated by the shaded band. All results except the HERMES data are shown at $Q^2 = 5$ GeV^2. The results of HERMES are shown at the average Q^2 of the respective data point which varies from $Q^2 = 1.22$ GeV^2 at $x = 0.033$ to $Q^2 = 5.25$ GeV^2 at $x = 0.464$.

$$A_{\perp} = \frac{\sigma^{\rightarrow\Downarrow} - \sigma^{\rightarrow\Uparrow}}{\sigma^{\rightarrow\Downarrow} + \sigma^{\rightarrow\Uparrow}}. \quad (2.42)$$

Here $\sigma^{\overrightarrow{\Rightarrow}\ (\overrightarrow{\Leftarrow})}$ and $\sigma^{\rightarrow\Uparrow\ (\rightarrow\Downarrow)}$ in above equations are short expressions for $d^2\sigma^{\overrightarrow{\Rightarrow}(\overrightarrow{\Leftarrow})}/dxdQ^2$ and $d^2\sigma^{\rightarrow\Uparrow(\rightarrow\Downarrow)}/dxdQ^2$. One photon exchange between the incoming lepton and target nucleon is the dominant process in deep-inelastic scattering. The virtual photon-nucleon asymmetries A_1 and A_2 are defined in the cross section difference and expressed in the spin-independent structure function F_1 and spin-dependent structure functions g_1 and g_2:

$$A_1 = \frac{\sigma^{\frac{1}{2}} - \sigma^{\frac{3}{2}}}{\sigma^{\frac{1}{2}} + \sigma^{\frac{3}{2}}} = \frac{g_1 - \gamma^2 g_2}{F_1}, \quad (2.43)$$

$$A_2 = \frac{2\sigma_{\mathrm{I}}}{\sigma^{\frac{1}{2}} + \sigma^{\frac{3}{2}}} = \gamma\frac{g_1 + g_2}{F_1}. \quad (2.44)$$

Here $\sigma^{\frac{1}{2}\ (\frac{3}{2})}$ is the virtual photon absorption cross section when the projection of the total photon and target nucleon spin is $\frac{1}{2}$ $(\frac{3}{2})$ along the direction of the photon momentum. σ_{I} is the interference cross section between the transverse and longitudinal polarization of the virtual photon. $\sigma^{\frac{1}{2}} + \sigma^{\frac{3}{2}}$ in the denominator of equations (2.44) is simply twice σ_{T} of the transverse photon absorption cross section like $\sigma_{\mathrm{T}} = (\sigma^{\frac{1}{2}} + \sigma^{\frac{3}{2}})/2$. The virtual photon-nucleon asymmetries A_1 and A_2 have a positivity limit:

$$|A_1| \leq 1, \quad (2.45)$$

$$|A_2| = \frac{\sigma_{\mathrm{I}}}{\sigma_{\mathrm{T}}} \leq \sqrt{\frac{\sigma_{\mathrm{L}}\sigma_{\mathrm{T}}}{(\sigma_{\mathrm{T}})^2}} = \sqrt{R(x,Q^2)}. \quad (2.46)$$

The virtual photon-nucleon asymmetries A_1 and A_2 are related to the experimentally measured asymmetries $A_{||}$ and $A_{\perp}$ with some kinematical variables:

$$A_{||} = D(A_1 + \eta A_2), \quad (2.47)$$

$$A_{\perp} = d(A_2 - \xi A_1). \quad (2.48)$$

Here the kinematical variables D, η, d and ξ are:

$$D = \frac{1 - (1-y)\varepsilon}{1 + \varepsilon R}, \quad (2.49)$$

$$\eta = \frac{\varepsilon\gamma y}{1 - \varepsilon(1-y)}, \quad (2.50)$$

$$d = D\sqrt{\frac{2\varepsilon}{1+\varepsilon}}, \quad (2.51)$$

$$\xi = \eta\frac{1+\varepsilon}{2\varepsilon}. \quad (2.52)$$

From the combination of equations (2.43), (2.44) and (2.47) the virtual photon-nucleon asymmetry can be obtained like:

$$A_1 = \frac{A_{||}}{D(1+\eta\gamma)} - \frac{\eta\gamma(1+\gamma^2)}{1+\eta\gamma}\frac{g_2}{F_1}. \quad (2.53)$$

g_2 can be regarded to be approximately zero and then:

$$A_1 \simeq \frac{A_{||}}{D(1+\eta\gamma)}. \tag{2.54}$$

The systematic uncertainty which arises from this approximation on the virtual photon-nucleon asymmetry A_1 is taken into account in the analysis at present.

2.2.2 Structure Functions in Quark Parton Model

In the quark parton model (QPM), which was developed by Feynman [27], Bjorken and Paschos [28], the nucleon consists of point-like scattering centres called partons. In the naive QPM the structure functions are expressed in the quark momentum distribution functions $q_f^+(x)$ and $q_f^-(x)$ of the flavor f. $q_f^{+(-)}(x)$ is the the probability of finding a quark with a momentum fraction x to the momentum of the nucleon when the direction of the quark spin is parallel (anti-parallel) to the direction of the nucleon spin. The spin-independent and spin-dependent structure functions are expressed in the quark momentum distribution functions $q_f^{+(-)}(x)$:

$$F_1(x) = \frac{1}{2}\sum_f e_f^2 \left(q_f^+(x) + q_f^-(x)\right), \tag{2.55}$$

$$F_2(x) = \sum_f e_f^2 x \left(q_f^+(x) + q_f^-(x)\right), \tag{2.56}$$

$$g_1(x) = \frac{1}{2}\sum_f e_f^2 \left(q_f^+(x) - q_f^-(x)\right), \tag{2.57}$$

$$g_2(x) = 0. \tag{2.58}$$

The summation over f is performed for all quarks and anti-quarks which contribute to the structure functions at x.

Unpolarized Quark Distribution Function

The spin-independent structure function $F_2(x)$ reflects the momentum distribution of the quarks. The unpolarized quark distribution function is defined as the addition of $q_f^+(x)$ and $q_f^-(x)$:

$$q_f(x) = q_f^+(x) + q_f^-(x). \tag{2.59}$$

In the QPM:

$$1 = \sum_f \int_0^1 dx\ x q_f(x). \tag{2.60}$$

This means that the sum of the momentum of the quarks in the nucleon is equal to the whole momentum of the nucleon. Again in the QPM we see the Callan-Gross relation from equation (2.55) and (2.56) directly.

$$F_1(x) = 2xF_2(x). \tag{2.61}$$

When the distribution function for valence and sea quarks is defined as:

$$q_{\mathrm{v}}(x) = q(x) - \bar{q}(x), \tag{2.62}$$

where q_{v} and $\bar{q}$ are the distribution functions of valence and sea quarks respectively. From equation (2.56) the spin-independent structure function of the proton is:

$$\begin{aligned} \frac{1}{x}F_2^{\mathrm{p}}(x) &= \frac{4}{9}[u(x)+\bar{u}(x)] + \frac{1}{9}[d(x)+\bar{d}(x)] + \frac{1}{9}[s(x)+\bar{s}(x)] \\ &= \frac{4}{9}u_{\mathrm{v}}(x) + \frac{1}{9}d_{\mathrm{v}}(x) + \frac{12}{9}q_{\mathrm{sea}}(x), \end{aligned} \tag{2.63}$$

where the sea quark distribution is assumed to be equal for all light flavors: $q_{\mathrm{sea}}(x) = \bar{u}(x) = \bar{d}(x) = s(x) = \bar{s}(x)$. Note that u, d and s are the quark distribution functions of up, down and strange quark. Due to the argument of the isospin symmetry between proton and neutron:

$$u(x) = u^{\mathrm{p}}(x) = d^{\mathrm{n}}(x), \tag{2.64}$$

$$d(x) = d^{\mathrm{p}}(x) = u^{\mathrm{n}}(x), \tag{2.65}$$

the spin-independent structure function of the neutron is written similarly:

$$\frac{1}{x}F_2^{\mathrm{n}}(x) = \frac{1}{9}u_{\mathrm{v}}(x) + \frac{4}{9}d_{\mathrm{v}}(x) + \frac{12}{9}q_{\mathrm{sea}}(x). \tag{2.66}$$

The ration $F_2^{\mathrm{n}}/F_2^{\mathrm{p}}$ is obtained as:

$$\frac{F_2^{\mathrm{n}}(x)}{F_2^{\mathrm{p}}(x)} = \frac{u_{\mathrm{v}}(x) + 4d_{\mathrm{v}}(x) + 12q_{\mathrm{sea}}(x)}{4u_{\mathrm{v}}(x) + d_{\mathrm{v}}(x) + 12q_{\mathrm{sea}}(x)}. \tag{2.67}$$

The ratio were measured by NMC [29] and HERMES [30] and shows that the contribution of the sea quark is dominant at the region of lower x. The ratio approaches 1/4 at the region of high x [31], which is consistent with assumption that $u_{\mathrm{v}}(x)$ is dominant rather than $d_{\mathrm{v}}(x)$ and $q_{\mathrm{sea}}(x)$ in this region. It is assumed from recent measurements [32, 33, 34] that the sea quark distribution is flavor-asymmetric.

Polarized Quark Distribution Function

Similarly to the unpolarized quark distribution function, the polarized quark distribution function is defined as the subtraction of $q_f^+(x)$ and $q_f^-(x)$:

$$\Delta q_f(x) = q_f^+(x) - q_f^-(x). \tag{2.68}$$

The spin-dependent structure function $g_1(x)$ reflects the spin distribution of the quarks. The spin-dependent structure function $g_1(x)$ of the proton is:

$$g_1^{\mathrm{p}}(x) = \frac{1}{2}\left(\frac{1}{9}\Delta u(x) + \frac{4}{9}\Delta d(x) + \frac{1}{9}\Delta s(x)\right). \tag{2.69}$$

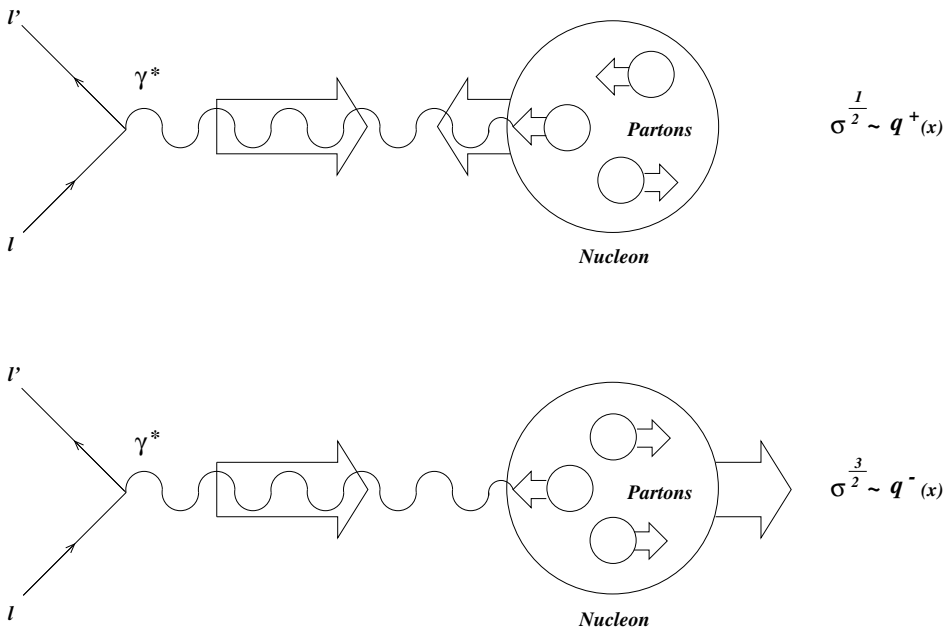

Figure 2.7: Schematic diagrams of the polarized deep-inelastic scattering in the level of QPM. The virtual photon emitted by the incoming lepton is absorbed only by a quark with spin 1/2 of the opposite direction to the direction of the photon spin. The spin of the nucleon and the virtual photon is 1/2 and 1 respectively.

$\Delta s(x)$ is the spin distribution function of the strange quark. Similarly to the unpolarized case the argument of the isospin symmetry yields $\Delta u(x) = \Delta u^{\mathrm{p}}(x) = \Delta d^{\mathrm{n}}(x)$ and $\Delta d(x) = \Delta d^{\mathrm{p}}(x) = \Delta u^{\mathrm{n}}(x)$. The spin-dependent structure function $g_1(x)$ of the neutron is then:

$$g_1^{\mathrm{n}}(x) = \frac{1}{2}\left(\frac{4}{9}\Delta u(x) + \frac{1}{9}\Delta d(x) + \frac{1}{9}\Delta s(x)\right). \tag{2.70}$$

Figure 2.7 allows the interpretation for the measurement of the spin structure of the nucleon by the polarized deep-inelastic scattering in the level of QPM. The circularly polarized virtual photon emitted by the incoming lepton has spin 1 and can be absorbed only by a quark with spin 1/2 of the opposite direction to the direction of the photon spin according to the helicity conservation law. Therefore the measurement of $\sigma^{\frac{1}{2}}$ and $\sigma^{\frac{3}{2}}$ proportionally lead to the measurement of the quark distributions with the spin of the same and the opposite direction to the nucleon spin respectively like:

$$\sigma^{\frac{1}{2}} \sim q^{+}(x), \tag{2.71}$$

$$\sigma^{\frac{3}{2}} \sim q^{-}(x). \tag{2.72}$$

This means that if equations (2.43) or (2.68) are positive the spin of a quark has the contribution to polarize the spin of the nucleon. Contrarily, if the equation is negative, the spin of the quark has the contribution to depolarize the spin of the nucleon.

2.2.3 Sum Rules

The nth moment for the integral of the structure function $f(x)$ is defined as:

$$M_n(f) = \int_0^1 x^{n-1} f(x)\, dx \tag{2.73}$$

For example, the first moment of the spin-independent quark distribution for the valence quarks $u_{\rm v}^{\rm p}(x)$ and $d_{\rm v}^{\rm p}(x)$ of proton gives the number of the up and down valence quarks in the proton:

$$\int_0^1 dx\; u_{\rm v}^{\rm p}(x) = 2 \quad \text{and} \quad \int_0^1 dx\; d_{\rm v}^{\rm p}(x) = 1. \tag{2.74}$$

The Gottfried sum rule $S_{\rm G}$ [35] is for the 0th integral of the spin independent structure functions $F_1(x)$ of proton and neutron. In the QPM, from equation (2.63) and (2.66):

$$S_{\rm G} = \int_0^1 \frac{dx}{x}\Big(F_1^{\rm p}(x) - F_1^{\rm n}(x)\Big) \tag{2.75}$$

$$= \frac{1}{3} + \frac{2}{3}\int_0^1 dx\, \Big(\bar{u}(x) - \bar{d}(x)\Big)\,. \tag{2.76}$$

$S_{\rm G} = 0.235 \pm 0.026$ was measured by NMC [33] and is far from 1/3. It implies a flavor asymmetry of the sea quark [34].

On the other hand several pieces of the information about the nucleon spin can be derived from the integral over the spin-dependent structure function g_1 of the proton and neutron. The first moments of g_1 of the proton and neutron are defined as:

$$\Gamma_1^{\rm p(n)}(Q^2) = \int_0^1 g_1^{\rm p(n)}(x, Q^2)\, dx. \tag{2.77}$$

In the QPM these can be expressed by equations (2.69) and (2.70) as [4, 36, 37]:

$$\Gamma_1^{\rm p(n)}(Q^2) = \frac{1}{12}\left(+(-)a_3 + \frac{a_8}{3}\right)\Delta C^{\rm NS}(Q^2) + \frac{1}{9}a_0 \Delta C^{\rm S}(Q^2), \tag{2.78}$$

where SU(3) flavor singlet (a_0), octet isotriplet (a_3) and octet isosinglet (a_8) combinations are the proton expectation values of the axial-vector current matrix elements [4], $\Delta C^{\rm S}(Q^2)$ and $\Delta C^{\rm NS}(Q^2)$ are the QCD corrections which are called the polarized singlet (S) and non-singlet (NS) coefficient functions [38, 39, 40]:

$$\Delta C^{\rm NS}(Q^2) = 1 - \frac{\alpha_{\rm s}(Q^2)}{\pi} - 3.5833\left(\frac{\alpha_{\rm s}(Q^2)}{\pi}\right)^2 - 20.2153\left(\frac{\alpha_{\rm s}(Q^2)}{\pi}\right)^3, \tag{2.79}$$

$$\Delta C^{\rm S}(Q^2) = 1 - \frac{\alpha_{\rm s}(Q^2)}{\pi} - 1.0959\left(\frac{\alpha_{\rm s}(Q^2)}{\pi}\right)^2. \tag{2.80}$$

Here $\Delta C^{\rm NS}(Q^2)$ is shown up to the third order, $\Delta C^{\rm S}(Q^2)$ up to the second order, when the number of the quark flavors is three. In the QPM a_0, a_3 and a_8 are related

to the first moments of the polarized quark distributions:

$$a_0 = \Delta\Sigma = (\Delta u + \Delta\bar{u}) + (\Delta d + \Delta\bar{d}) + (\Delta s + \Delta\bar{s}), \quad (2.81)$$

$$a_3 = \Delta q_3 = \left|\frac{g_{\rm A}}{g_{\rm V}}\right| = (\Delta u + \Delta\bar{u}) - (\Delta d + \Delta\bar{d}), \quad (2.82)$$

$$a_8 = \Delta q_8 = (\Delta u + \Delta\bar{u}) + (\Delta d + \Delta\bar{d}) - 2(\Delta s + \Delta\bar{s}), \quad (2.83)$$

where

$$\Delta q = \int_0^1 \Delta q(x)\ dx. \quad (2.84)$$

a_0 corresponds to the total fraction $\Delta\Sigma$ of the nucleon spin carried by the quark spin. a_3 is directly measured in the axial vector $g_{\rm A}$ and vector coupling constant $g_{\rm V}$ of the neutron β decay. Assuming the isospin symmetry, $|g_{\rm A}/g_{\rm V}| = 1.2573 \pm 0.0028$ was measured [5]. Assuming SU(3) flavor symmetry for the axial vector flavor octet current, a_3 and a_8 can be expressed in terms of the decay constants $F = 0.459 \pm 0.008$ and $D = 0.798 \pm 0.008$ [5] which are experimentally known from the neutron and hyperon β decays n $\rightarrow$ p and $\Sigma^- \rightarrow$ n:

$$a_3 = F + D = 1.2573 \pm 0.0028, \quad (2.85)$$

$$a_8 = 3F - D = 0.575 \pm 0.016. \quad (2.86)$$

Ellis-Jaffe Sum Rule

The Ellis-Jaffe sum rule [36] is defined by the individual integrals of $g_1^{\rm p}$ of the proton and $g_1^{\rm n}$ of the neutron. Assuming the total spin contribution of the strange quark is negligible:

$$\Delta s + \Delta\bar{s} = 0, \quad (2.87)$$

the Ellis-Jaffe sum rule is written as:

$$\Gamma_1^{\rm p} = \int_0^1 g_1^{\rm p}(x)dx = \frac{1}{18}(9F - D), \quad (2.88)$$

$$\Gamma_1^{\rm n} = \int_0^1 g_1^{\rm n}(x)dx = \frac{1}{18}(6F - D). \quad (2.89)$$

The Ellis-Jaffe sum rule corrected by the QCD for $\Delta s + \Delta\bar{s} = 0$ is:

$$\Gamma_1^{\rm p(n)} = \frac{1}{12}\left(+(-)(F - D) + F - \frac{D}{3}\right)\Delta C^{\rm NS}(Q^2) + \frac{1}{9}(3F - D)\Delta C^{\rm S}(Q^2). \quad (2.90)$$

At $Q^2 = 5$ GeV^2 and applying the strong coupling constant $\alpha_{\rm S} = 0.118 \pm 0.003$ scaled from the mass of the Z^0 boson the Ellis-Jaffe sum rule provides $\Gamma_1^{\rm p} = \int_0^1 g_1^{\rm p}(x)dx = 0.164 \pm 0.005$ and $\Gamma_1^{\rm n} = \int_0^1 g_1^{\rm n}(x)dx = -0.018 \pm 0.004$. In 1987, the g_1 integral was measured by EMC [1]. New results of the integral came from SLAC [19, 22, 41] and SMC [42, 43, 44]. Compared to $\Gamma_{1,\rm exp}^{\rm p} = 0.130 \pm 0.006$ and $\Gamma_{1,\rm exp}^{\rm n} = -0.040 \pm 0.008$, which were obtained from the average value of the experimental world data, it is obvious that the prediction is significantly violated.

Bjorken Sum Rule

The Bjorken sum rule [45] relates the difference between the first moments of g_1 of the proton and neutron to the coupling constants $|g_A/g_V|$:

$$\Gamma_1^p(Q^2) - \Gamma_1^n(Q^2) = \frac{1}{6}\left|\frac{g_A}{g_V}\right| C^{NS}(Q^2). \tag{2.91}$$

As the Bjorken sum rule is derived only from current algebra and SU(2) isospin symmetry, it provides us with a fundamental test of QCD, for example, to evaluate the value of $\alpha_s(Q^2)$. Different from the Ellis-Jaffe sum rule this sum rule requires no assumption on the contributions of the strange quark spin. At $Q^2 = 5$ GeV^2 with the strong coupling constant $\alpha_s = 0.118 \pm 0.003$ at the mass of Z^0 boson the Bjorken sum rule after the QCD correction is $\Gamma_1^p - \Gamma_1^n = 0.182 \pm 0.003$. The average value of the experimental world data is $(\Gamma_1^p - \Gamma_1^n)_{exp} = 0.170 \pm 0.012$ [41]. As a result up to now the Bjorken sum rule is valid in the level of the present experimental accuracy.

Spin Content of Nucleon

As the quark distribution functions $q_f^{\pm}(x)$ is related to the number of the quarks with a momentum fraction x, we firstly expect the total helicity s_z^N of the nucleon is carried by the quarks:

$$\begin{aligned} s_z^N/\hbar &= \frac{1}{2}\sum_f \int_0^1 dx \left(q_f^+(x) - q_f^-(x)\right) \\ &= \frac{1}{2}\sum_f \int_0^1 dx\ \Delta q_f(x) \\ &= \frac{1}{2}(\Delta u + \Delta\bar{u} + \Delta d + \Delta\bar{d} + \Delta s + \Delta\bar{s}) \\ &= \frac{1}{2}\Delta\Sigma. \end{aligned} \tag{2.92}$$

Namely,

$$s_z^N/\hbar = \frac{1}{2}\Delta\Sigma = \frac{1}{2} \tag{2.93}$$

because in the naive QPM the transverse component of the momentum of the quark are zero and all quarks have only longitudinal component of the momentum parallel to the momentum of the nucleon in the Breit frame. We now know that this naive picture of the spin structure of the nucleon, however, is far from the results obtained from the several experiments. For example, HERMES and SMC measured the spin contributions of each quark flavor to the nucleon spin [2, 44]. For example, for HERMES at $Q^2 = 2.5$ GeV^2 after the QCD corrections [46]:

$$\Delta\Sigma = 0.30 \pm 0.04 \pm 0.09, \tag{2.94}$$

$$\Delta u + \Delta\bar{u} = 0.57 \pm 0.02 \pm 0.03, \tag{2.95}$$

$$\Delta d + \Delta\bar{d} = -0.25 \pm 0.06 \pm 0.05, \tag{2.96}$$

$$\Delta s + \Delta\bar{s} = -0.01 \pm 0.03 \pm 0.04. \tag{2.97}$$

The value of equation (2.94) is known as the "*spin puzzle*". Equation (2.93) needs to be extended for the spin contributions of the gluon and/or the orbital angular momenta to generalize:

$$s_z^{\mathrm{N}}/\hbar = \frac{1}{2}\Delta\Sigma + \Delta g + L_q + L_g, \tag{2.98}$$

where Δg is the contribution of the gluon spin, and L_q and L_g are the orbital angular momenta of the quarks and gluons respectively. We don't have enough knowledge on Δg experimentally and theoretically although the HERMES measurements already implied that Δg might be positive and large [47]. Up to now there is no experimental technique to determine the value of the orbital angular momentum for gluons while the angular momentum for quarks may be accessed through the measurement of off-forward parton distributions (OFPD) extracted from deeply virtual Compton scattering (DVCS) [48]. The semi-inclusive measurement allows us to provide more detailed information on the spin contributions of each quark flavor.

2.3 Semi-inclusive Measurement

2.3.1 Spin Asymmetry for semi-inclusive Measurement

The semi-inclusive measurement of hadrons in the final state provides additional information to separate the spin contributions of each quark flavor to the nucleon spin, especially to isolate the spin contribution of the strange quark. In analogy to $A_{||}$ of the inclusive measurement the spin asymmetry $A_{||}$ for hadrons h of the semi-inclusive measurement is:

$$A_{||}^h = \frac{\sigma_h^{\frac{1}{2}} - \sigma_h^{\frac{3}{2}}}{\sigma_h^{\frac{1}{2}} + \sigma_h^{\frac{3}{2}}}, \tag{2.99}$$

where $\sigma_h^{\frac{1}{2}(\frac{3}{2})}$ is the cross section for hadrons when the projection of the total spin of the photon and nucleon along the direction of the photon momentum is $\frac{1}{2}(\frac{3}{2})$.

In the semi-inclusive measurement the production process of a hadron in the final state is understood as follows: (1) a quark in the nucleon with opposite direction of the spin to the direction of the virtual photon spin absorbs the photon; (2) the quark fragments into hadrons. Other hadrons produced by the fragments from the quarks which did not absorb the photon are generated at the same time. The former is called hadrons from the current fragments and the latter hadrons of the target remnants. We intend to study hadrons from the current fragments. The productions of hadron from the current fragments are expressed in the fragmentation functions $D_f^h(x, Q^2, z)$, which is the probability density of finding hadron h with the kinematical variable z which comes from the fragment of the quark flavor f at x and Q^2 [49, 50]. The differential cross section $d^3\sigma^h/dxdQ^2dz$ for the productions of hadron from the region of the current fragments is expressed with the fragmentation

functions:

$$\frac{d^3\sigma^h(x,Q^2,z)}{dx\ dQ^2\ dz} = \frac{\sum_f e_f^2 q_f(x,Q^2) D_f^h(x,Q^2,z)}{\sum_f e_f^2 q_f(x,Q^2)} \frac{d^2\sigma_{\mathrm{Incl}}(x,Q^2)}{dx\ dQ^2}, \tag{2.100}$$

where $\sigma_{\mathrm{Incl}}(x,Q^2)/dxdQ^2$ is the total inclusive DIS cross section. Equation (2.100) relies on the assumption that the scattering process of the quark and the fragmentation process are factorizing and depends on the fractional energy z [51, 52]. In analogy to the case of the inclusive measurement the spin-independent structure function $F_1^h(x,Q^2,z)$ for the semi-inclusive measurement is defined as:

$$F_1^h(x,Q^2,z) = \frac{1}{2}\sum_f e_f^2 q_f(x,Q^2) D_f^h(x,Q^2,z). \tag{2.101}$$

Similarly, the spin-dependent structure function $g_1^h(x,Q^2,z)$ can be defined as:

$$g_1^h(x,Q^2,z) = \frac{1}{2}\sum_f e_f^2 \Delta q_f(x,Q^2) D_f^h(x,Q^2,z). \tag{2.102}$$

The definition of g_1^h is reasonable because it is assumed that the fragmentation process into hadrons, which is represented in the fragmentation functions $D_f^h(x,Q^2,z)$, is independent of the relative orientations between the quark spin and nucleon spin. Assuming $g_2^h = 0$ like the case of the inclusive measurement one obtains the spin asymmetry A_1^h for the semi-inclusive measurement as:

$$\begin{aligned} A_1^h(x,Q^2) &\overset{g_2^h=0}{=} \frac{\int_{z_{\min}}^1 dz\ g_1^h(x,Q^2,z)}{\int_{z_{\min}}^1 dz\ F_1^h(x,Q^2,z)} \\ &= \frac{\sum_f e_f^2 \Delta q_f(x,Q^2) \int_{z_{\min}}^1 dz\ D_f^h(x,Q^2,z)}{\sum_f e_f^2 q_f(x,Q^2) \int_{z_{\min}}^1 dz\ D_f^h(x,Q^2,z)}, \end{aligned} \tag{2.103}$$

where above integrals are performed with the minimum z value cut, $z > z_{\min}$. The $z_{\min}$ cut is required in order to select hadrons from the region of the current fragments.

2.3.2 Fragmentation Functions

As the fragmentation function is the probability density of finding a hadron with the fractional energy z between 0 and 1:

$$\sum_h \int_0^1 dz\ z D_f^h(z) = 1. \tag{2.104}$$

The mean multiplicity n_h for the productions of hadrons of a type h is:

$$\sum_f \int_0^1 dz\ D_f^h(z) = n_h. \tag{2.105}$$

The fragmentation functions can be classified in favoured ($D_+(z)$), unfavoured ($D_-(z)$) and strange fragmentation functions ($D_s(z)$). For the charged pion the number of the fragmentation functions can be reduced using the charge conjugation symmetry like $D_u^{\pi^+}(z) = D_{\bar{u}}^{\pi^-}(z)$ and the isospin symmetry like $D_u^{\pi^+}(z) = D_{\bar{d}}^{\pi^-}(z)$:

$$\begin{array}{rclclclcl} D_+(z) & = & D_u^{\pi^+}(z) & = & D_{\bar{u}}^{\pi^-}(z) & = & D_{\bar{d}}^{\pi^+}(z) & = & D_d^{\pi^-}(z), \\ D_-(z) & = & D_u^{\pi^-}(z) & = & D_{\bar{u}}^{\pi^+}(z) & = & D_{\bar{d}}^{\pi^-}(z) & = & D_d^{\pi^+}(z), \\ D_s(z) & = & D_s^{\pi^+}(z) & = & D_{\bar{s}}^{\pi^-}(z) & = & D_{\bar{s}}^{\pi^+}(z) & = & D_s^{\pi^-}(z). \end{array}$$

The ratio $\frac{D_-(z)}{D_+(z)}$ between the favoured and unfavoured fragmentation functions was measured by EMC [53] and HERMES [54] and it was shown that the ratio approaches 1 as z is decreasing. This means that in the region of low z hadrons from the region of the current fragments and the hadrons of the target remnants are intermingled in the same degree. In the region of higher z hadrons of the target remnants decrease compared to hadrons from the region of the current fragments. As hadrons of the target remnants do not relate to hadrons produced from the quark which interacted with the virtual photon, z can be used as a cut to select hadrons of the current fragments, which we are interested in.

Chapter 3

The HERMES Experiment

The HERMES experiment [55] has been performed at DESY in Hamburg, Germany. The main aim of the experiment is to investigate the spin structure of the nucleon. It uses a longitudinally polarized beam and a longitudinally polarized internal gas target in a storage cell installed into the ring of HERA [56]. The experiment started in 1995. The produced hadrons are detected, which we call the semi-inclusive measurement. The Ring Imaging Čerenkov (RICH) detector for the hadron identification is one of the characteristic detectors of the HERMES spectrometer.

3.1 Overview of HERA

HERA is a synchrotron for electrons and protons. In the HERA ring the nominal energy is 27.5 GeV for electrons and 820 GeV for protons. The center of mass energy of the electron-proton collider is 314 GeV. The circumference of the electron and the proton storage rings is 6335 m, which has straight lines of 360 m and four interaction regions. In figure 3.1 the four experiments HERMES, ZEUS, HERA-B and H1 are schematically shown in the ring. HERMES is located in the East area and uses only electron beam of HERA. ZEUS and H1 use both electron and proton beams and HERA-B the proton beam only. HERA has 220 bunch buckets in the storage ring, a crossing time of 96 ns apart, a bunch length of 27 ps and 3.65×10^{10} electrons per bunch. The luminosity of the collider is 1.5×10^{31} cm^{-2}s^{-1}. The current of the electron beam after the injection is typically 35 - 45 mA and decreases as time goes by because the beam has interactions with the residual gas in the vacuum of the ring. Finally the beam is dumped around the current of 10 mA and then is started to be injected for a new fill. The typical life time for the electron beam in the data taking is about 8 - 12 hours. HERA has been operated with positrons from 1995 to 1997 and with electrons in 1998 and first four months of 1999. Since July of 1999 HERA has been running with positrons again for the data taking.

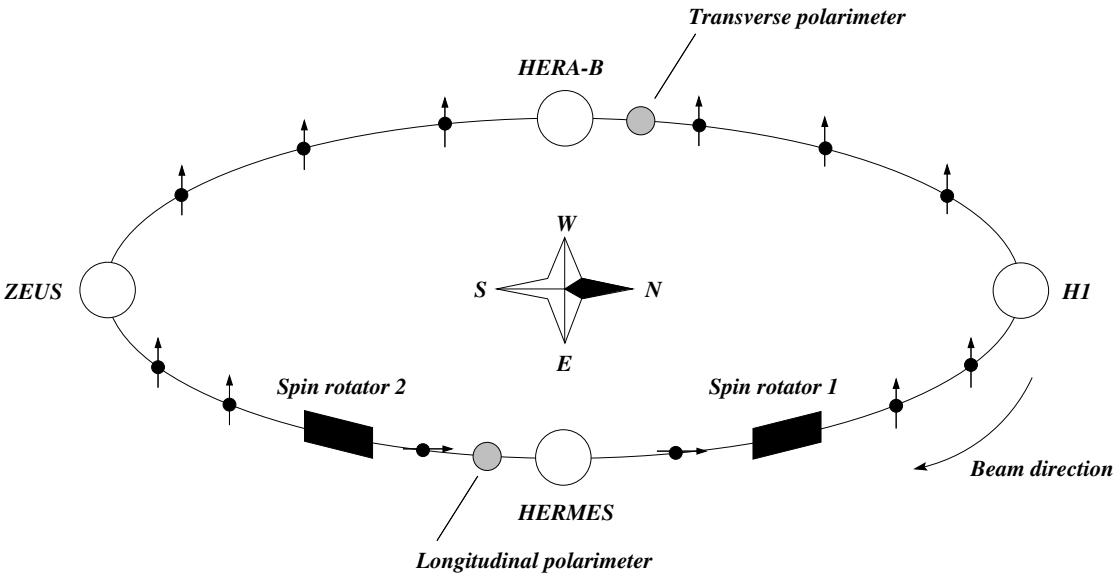

Figure 3.1: Schematic picture of the HERA storage ring, which indicates the locations of the four sites of the experiments, the spin rotators and the beam polarimeters. The solid arrows indicate the orientations of the polarization of electrons.

3.2 Polarized Beam of HERA

Electrons in the storage ring [57] are naturally transversely polarized by the emission of the synchrotron radiation, which is known as the Sokolov-Ternov effect [58]. The process is generated by a small asymmetric spin-flip amplitude which causes electrons to enhance the polarization state anti-parallel to the magnetic field of the bending magnet. The transverse polarization reaches its maximum value asymptotically with the exponential law as [59]:

$$P(t) = P_{\max}(1 - e^{-t/\tau}), \tag{3.1}$$

where t is the time, τ the polarization build-up time and $P_{\max} = 92.38$ % the equilibrium of the polarization. The polarimeter can be calibrated from the measurement of the build-up time τ, which is called the method of the rise time calibration.

HERMES requires the longitudinally polarized beam to study the spin structure of the nucleon. The longitudinally polarized beam is achieved by two spin rotators [60] to change the transverse direction of the polarization to the longitudinal direction of the polarization. The spin rotators are located in front of the experimental section and behind the section in the straight line of the HERA ring. Figure 3.2 shows the schematic diagrams of the one of the spin rotators. The most upper and middle ones show the effect on the orbit of the beam by the horizontal and vertical bending magnets of the mini-rotators. The most lower one shows how the spin rotators change the direction of the polarization. The size of the vertical bump is about 22 cm. The orbit is shifted in both horizontal and vertical deflections and finally comes back to the nominal position and slope when the longitudinal direction of

the beam polarization is achieved. The system of the spin rotators has a length of about 70 m.

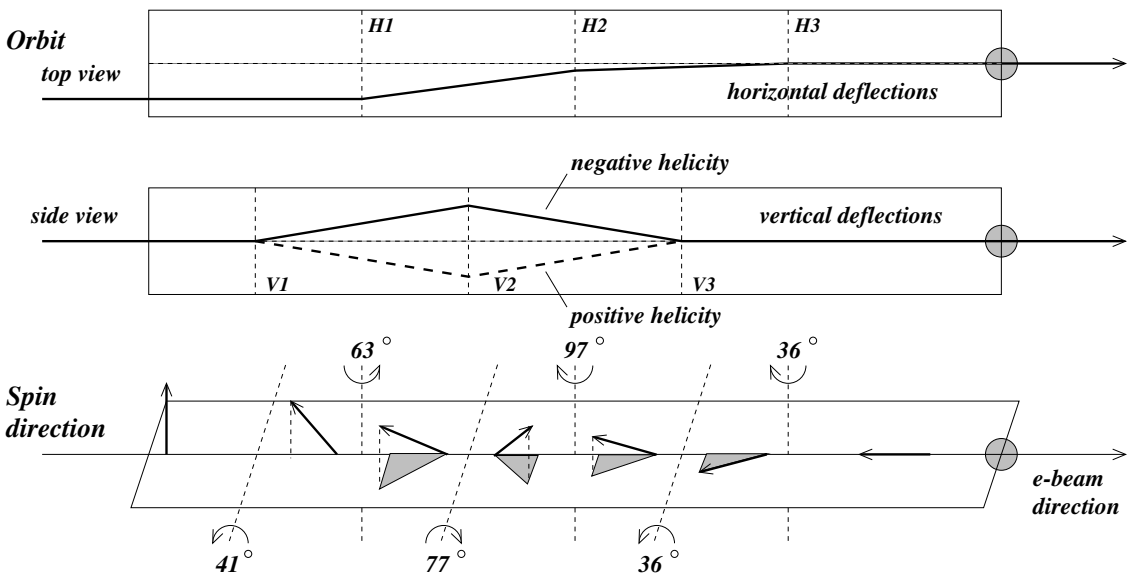

Figure 3.2: Schematic diagrams of a spin rotator. The most upper and middle ones show the effect on the orbit of the beam by the horizontal and vertical bending magnets of the mini-rotators. The most lower one shows how the spin rotators change the direction of the polarization.

The polarization of the beam is measured by two Compton polarimeters. One is the transverse polarimeter [61] which measures the transverse polarization and is located in the West area of the HERA ring. Another one is the longitudinal polarimeter which measures the longitudinal polarization and is located roughly 50 m downstream of the HERMES internal gas target, between two spin rotators. The transverse polarimeter uses an Argon-ion laser which has 514.5 nm of a wavelength to provide the continuous beam of 2.41 eV photons at 10 W. Energy and vertical position of the backscattering Compton photons are measured with a calorimeter which has a position sensitivity. The up-down spatial asymmetry of the position distribution is used to determine the polarization of the beam. The sign of the asymmetry can be changed between the left and right circularly polarized laser photon. The longitudinal polarimeter uses a pulsed Nd:YAG laser with a wavelength of 532 nm which provides the circular polarization. The total energy deposit of the backscattering Compton photons per bunch of the beam in a calorimeter is measured and the asymmetry in the energy spectrum is extracted to determine the longitudinal polarization of the beam. Figure 3.3 shows the rise of the longitudinal polarization of the beam of HERA. The build-up time of the beam is about 40 minutes and the typical polarization is about 55 % as shown in figure 3.4.

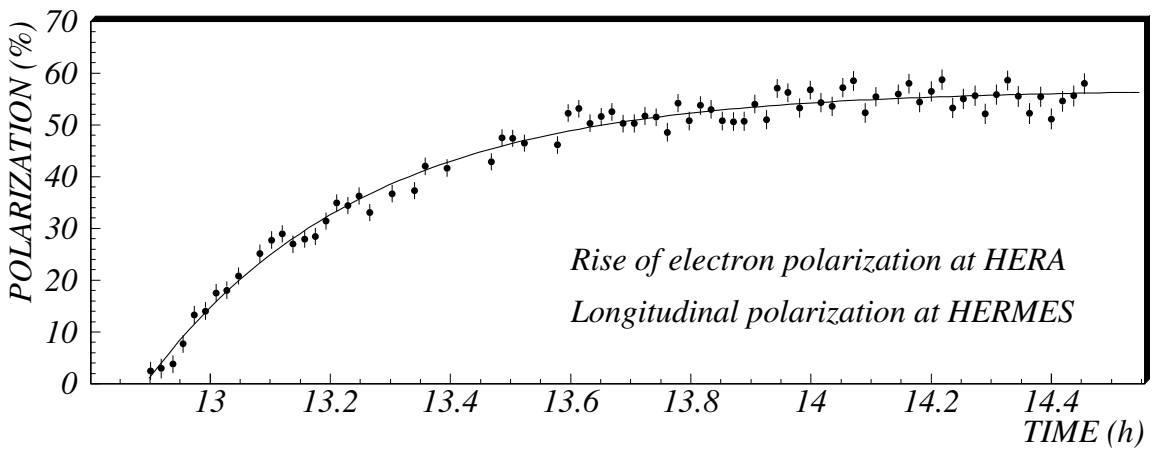

Figure 3.3: Rise of the longitudinal polarization in the beam of HERA. The solid line is a fit of the expected exponential curve in equation (3.1).

3.3 Polarized Deuterium Target

One of the most characteristic techniques in the HERMES experiment is the polarized internal gas target. Using pure gas as a target is advantageous because it requires no correction due to a dilution factor. If one uses NH_3, which is one of the materials for the solid polarized target, only three protons out of 17 nucleons are polarized. In the HERMES experiment the Atomic Beam Source (ABS) [62, 63] is used to polarize the deuterium. The ABS is based on the Stern-Gerlach separation of the atomic deuterium. The atoms of the deuterium are generated by dissociating the molecules of the deuterium with the radio frequency discharge at low pressure. The unpolarized beam of the atom with a thermal velocity is formed by a cooled nozzle and skimmers. The atomic beam is delivered into the sequential region of the sextupole magnetic fields in the system. By the Stern-Gerlach separation of the different states of the electron spin in the atom the sextupole magnetic fields focus the atoms with the same spin direction as the electron spin along the direction of the local magnetic field. On the other hand other atoms with opposite spin direction to the electron spin are defocused and pumped away. As a result the selected atomic beam by the Stern-Gerlach separation can be polarized. Using the high radio frequency transitions by the Weak Field Transition (WFS) and Strong Field Transition (SFT), the polarization of the electron spin transfers to the nuclear spin. The polarized atomic beam is injected through the injection tube to the storage cell in the HERA ring.

The high density of the gas is achieved by the target cell. The cell has T shape, a length of 40 cm installed along the direction of the beam pipe, and an elliptically open ended cross section of 29.0×9.8 mm^2 in 1998 and 19.0×8.0 mm^2 from January 1999. It consists of the ultra-pure aluminium of 0.99999 purity with 75 μm thickness in 1998 and 1999. The cell is coated with Drifilm to minimize the depolarization and recombination by the collisions on the inside wall of the cell. The nominal

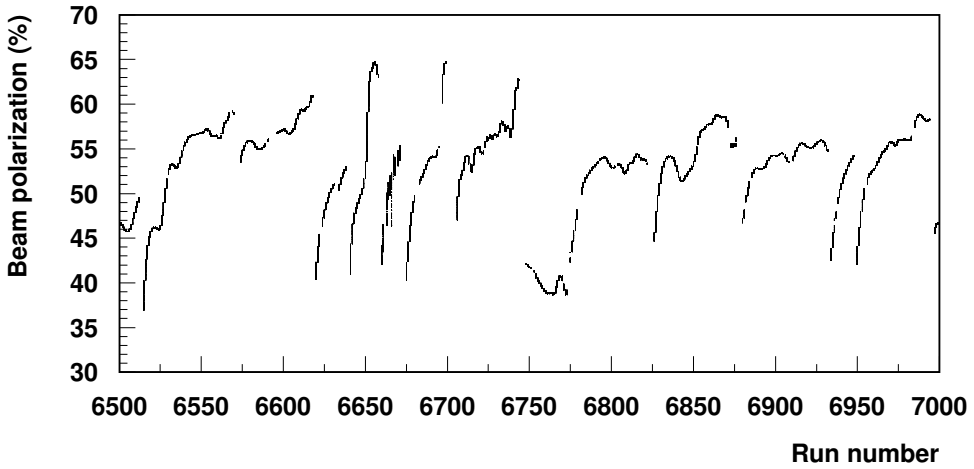

Figure 3.4: Beam polarization versus run number for the data taking in the experiment. The curves of the polarization represent the structure per fill of the beam.

temperature to cool the cell is chosen to be 85 K to increase the density of the gas by suppressing the movement of the target atoms. The gas in the cell leaks from both ends of the cell and is pumped away by a high speed differential pumping system. The density of the target gas has maximum value at the center of the cell and forms a triangle shaped distribution along the beam pipe. The thickness of the polarized deuterium target is about 1.2×10^{14} nucleons/cm^2 when viewed from the beam direction. The orientation of the nuclear spin is reversed every 45 seconds to decrease the systematical uncertainty on the measured quantities of the experiment.

The polarization of the deuterium atoms in the target cell is measured by the Breit-Rabi Polarimeter (BRP). In analogy to the ABS, a small fraction of the deuterium atoms is sampled through a tube mounted on the target cell. The radio frequency transitions and sextupole magnets isolate the single state of the nuclear spin. The occupancy number of the selected state of the target atoms is counted in the mass spectroscopy to determine the polarization of the target atom.

The Target Gas Analyser (TGA) measures the fraction of the dissociation of the target atoms in the cell. As the target atoms recombine to the molecules in the cell, the value of the polarization measured by the BRP and TGA has a correction as:

$$P_{\mathrm{T}} = \alpha_0 \cdot [\alpha_r + (1 - \alpha_r) \cdot \beta] \cdot P_a, \tag{3.2}$$

$$\alpha_r = c_\alpha \cdot \alpha_r^{\mathrm{TGA}}, \tag{3.3}$$

$$P_a = c_{\mathrm{P}} \cdot P^{\mathrm{BRP}}, \tag{3.4}$$

where α_0 is the initial fraction in the TAG before the injection of the atoms into the target cell, $(1 - \alpha_r)$ the fraction of the molecules which are generated from the recombination of the atoms in the cell, β the ratio of the polarization of the molecules produced by the recombination to the polarization of the atoms, c_α and c_{P} the sampling corrections, P_a the polarization of the atoms in the cell, P^{BRP} and

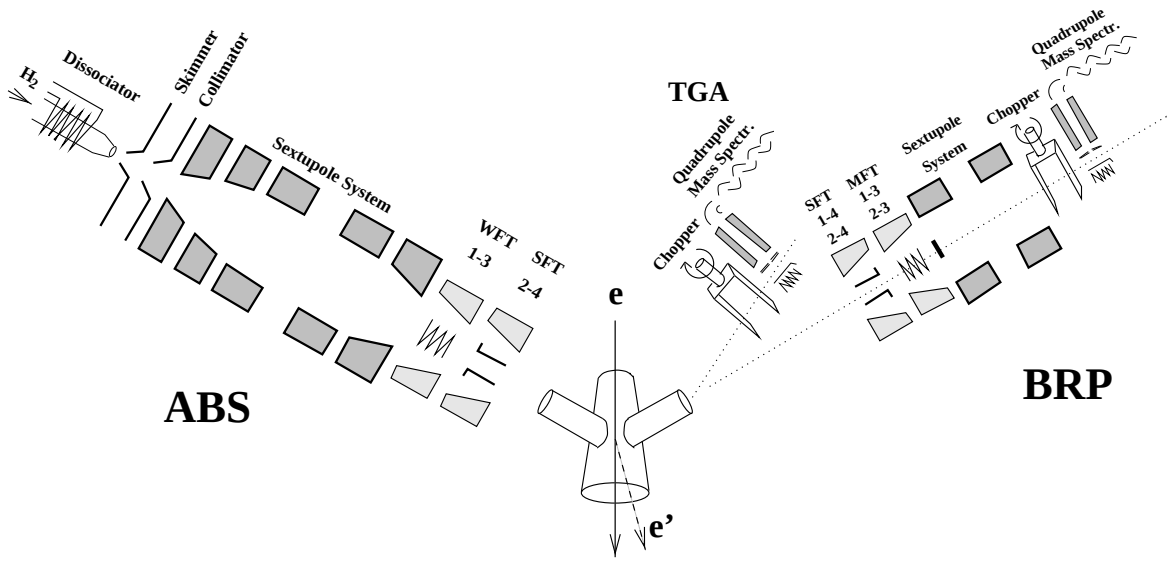

Figure 3.5: Schematic picture of the target system. The left side one is the Atomic Beam Source (ABS) and the right side one the Breit-Rabi Polarimeter (BRP). The Target Gas Analyser (TGA) is nearby the BRP. The target cell is seen between the ABS and BRP.

α_r^{TGA} are the calibrated values of the nuclear polarization measured by the BRP and TGA respectively. Equation (3.2) is used to determine the correct target polarization in the analysis. The effective target polarization on the deuterium target reaches about 90 % as shown in figure 3.6.

3.4 The HERMES Spectrometer

The HERMES spectrometer is a forward detector which consists of the symmetrical detector in the upper and lower halves with regard to the horizontal plane including the beam line. The acceptance is limited at the small angle by an iron plate (septum plate) of 11 cm thickness placed in the beam plane, which shields the beam particles from the magnetic field of the spectrometer with the integrated field of 1.3 T·m. The acceptance of the spectrometer for the scattering angle is from -170 mrad to 170 mrad in the horizontal direction and between $+(-)40$ mrad to $+(-)140$ mrad in the vertical direction. Therefore, the spectrometer has acceptance from 40 mrad to 220 mrad. Figure 3.7 schematically shows the side view of the HERMES spectrometer. In the figure the beam particles go from left to right passing through the target cell. The center of the target cell is defined as the origin in the HERMES coordinate system. The right-handed coordinate system is used. The beam direction is the Z axis. The X axis is horizontal and the Y axis is upward in the picture of figure 3.7. In front of and behind the spectrometer magnet, several tracking detectors are installed. The particle identification (PID) is realized with four detectors: a lead glass calorimeter, a pre-shower counter which consists of a lead wall of two radiation

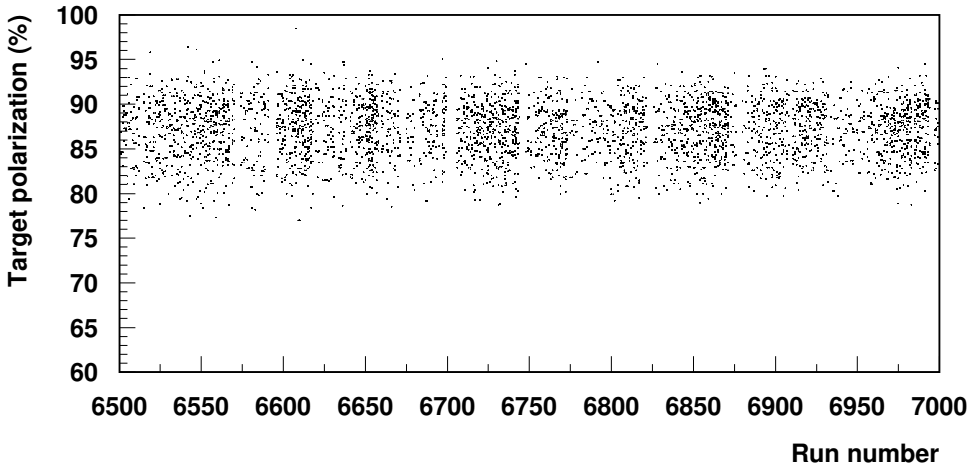

Figure 3.6: Effective target polarization versus run number for the data taking in the experiment.

lengths and a plastic scintillator hodoscope (H2), a transition radiation detector (TRD) and a Ring Imaging Čerenkov (RICH) detector. For the detailed description of the spectrometer the reference is published in [64]. The detector half (up for down) will be described below as two halves are identical.

3.4.1 Tracking System

The tracking system of the HERMES spectrometer is described below. The microstrip gas chambers (VC1/2) and drift chambers (DVC, FC1/2) in front of the spectrometer magnet are used to determine the scattering angle and the initial trajectory of the particles. The drift chambers (BC1/2 and BC3/4) behind the magnet are used to measure the momentum of the particles. Additionally three proportional chambers (MC1 - 3) are installed in the magnet gap to help connect the tracks between the front and back ones and to track the particles with low momentum which do not reach the rear section of the spectrometer. All planes of the tracking chambers are one of three types with wires oriented either in the vertical directions for the measurement of the X coordinate or in the tilted directions of $+30^\circ$ or -30° for the measurement of the Y coordinate (U and V planes). The properties of the tracking chambers are listed in table 3.1.

Tracking in front of the Magnet

The VCs are located just behind the target cell to provide the highly precise measurements of the scattering angle and reaction vertex position of the particles. The VC1 and VC2 consist of the microstrip gas counter. The microstrip gas counter uses the aluminium strips etched on the thin substrate of the glass so that it provides higher drift fields and much smaller pitch than in a conventional drift chamber. The cathode plane supplies the electric field for the drift of the charged particle. Ionized

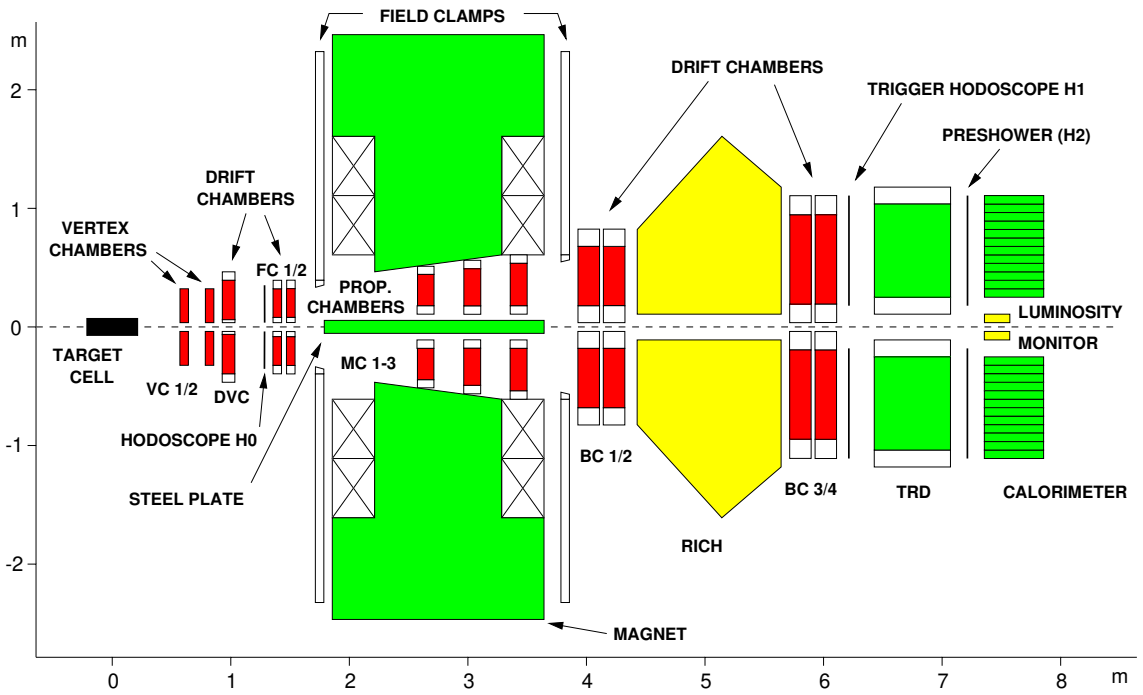

Figure 3.7: Schematic side view of the HERMES spectrometer.

electrons created by a traversing particle in a 3 mm thick gap volume move in a drift field of about 5 kV/cm directly away from a planar cathode and towards a 200 μm thick glass substrate that carries a pattern of fine etched aluminium strips. The anode strip is 7 μm wide separated by 193 μm long and the cathode strip 85 μm wide on the glass substrate of 200 μm thickness. The plane configuration of each module is VUX for the VC1 and XVU for the VC2. The resolution of the plane is 65 μm.

The FC1 and FC2 are conventional type drift chambers. The FCs consist of six sense wire planes of UU'XX'VV'. The X', U' and V' planes are staggered with respect to their partners by half the cell size in order to help resolve left-right ambiguities. To maximize the tolerance of the background of the charged particles a drift cell size of only 7 mm was chosen. The performance of the FC planes closest to the magnet was not severely influenced by the field of the magnet at the position of these planes. The resolution of the plane is 225 μm.

The DVC is used to enhance the efficiency of the tracking and to provide muon detection beyond the standard acceptance. The DVC consists of six planes of XX'UU'VV' with the resolution of 220 μm.

Tracking in the Magnet Region

The MCs are the proportional chamber located in the gap of the spectrometer magnet to help track the particles with low momentum, which are deflected by the strong field of the magnet. It allows to analyse, for example, decay particles from the

Λ baryon. The MCs can be operated in the magnetic field with sufficient resolution of $\pm$ 1 mm. The planes consist of UXV. The LeCroy PCOS IV system is used for the read out.

Tracking behind the Magnet

The BC1 and BC2 are located just behind the magnet and the BC3 and BC4 between the RICH and hodoscope H1 to provide the tracking of the charged particles between the magnet and the calorimeter. They measure the magnetic deflection, which is used to calculate the momentum of the particle track. The active area of 1880 $\times$ 520 mm^2 for the BC1 and BC2 and 2890 $\times$ 710 mm^2 for the BC3 and BC4 were chosen according to their positions of Z and acceptance of the spectrometer. The BCs consist of six planes of UU'XX'VV'. The resolution of the plane is 275 μm for the BC1 and BC2 and 300 μm for the BC3 and BC4.

Chamber	Vertex		Drift Vertex	Front		Magnet			Back	
Detector name	VC1	VC2	DVC	FC1	FC2	MC1	MC2	MC3	BC1/2	BC3/4
Cell design	microstrip gas	←	horizontal drift	←	←	MWPC	←	←	horizontal drift	←
Distance from target (mm)	731	965	1100	1530	1650	2725	3047	3369	4055	5800
Active area:										
Horizontal (mm)	323	393	474	660	←	996	1210	1424	1880	2890
Vertical (mm)	137	←	290	180	←	263	306	347	520	710
Cell width (mm)	0.193	←	6	7	←	2	←	←	15	←
Anode (A) wire diameter (μm)	7	←	30	20	←	25	←	←	←	←
Cathode (C) thickness (μm)	200	←	34	6.4	←	90	←	←	25.4	←
A-C plane gap (μm)	3	←	←	4	←	←	←	←	8	←
Potential wire diameter (μm)	85	←	50	←	←	-	-	-	127	←
Gas composition	DME/Ne	←	$Ar/CO_2/CF_4$	←	←	←	←	←	←	←
Gas composition ratio (%)	50/50	←	90/5/5	←	←	65/30/5	←	←	90/5/5	←
Wires in X plane	1674	2046	80	96	←	496	608	720	128	192
Wires in U, V plane	2170	←	96	←	←	512	608	720	128	192
U, V stereo angle (degree)	+5, −90	←	±30	←	←	←	←	←	←	←
Module configuration	VUX	XVU	XX'UU'VV'	UU'XX'VV'	←	UXV	←	←	UU'XX'VV'	←
Resolution per plane (σ) (μm)	65	←	220	225	←	700	←	←	275	300
Number of modules	1	←	←	←	←	←	←	←	2	←
Radiation length/module (%) (upper or lower)	0.8	←	0.25	0.075	←	0.29	←	←	0.26	←
Channel per module	6014	6386	544	576	←	1520	1824	2160	768	1152
Total channels	24800		1088	2304		11008			7680	

Table 3.1: Properties of the tracking chambers.

3.4.2 Particle Identification Detectors

The HERMES particle identification (PID) detectors can discriminate between leptons and hadrons with high efficiency and with low contamination. This allows more detailed studies on the spin structure of the nucleon. One of the most characteristic detectors for PID in the HERMES experiment is the RICH detector. The RICH detector identifies kaons as well as pions and protons in a wide momentum range. The RICH detector is described in more detail in chapter 4.

Calorimeter

Each half of the calorimeter [65] consists of the radiation resistant F101 lead glass blocks [66] of 42×10. The size of a block is 9×9 cm^2, the length is 50 cm with about 18 radiation lengths. Each block is coupled to a 7.62 cm photomultiplier (PMT) by a silicone glue with the index of refraction of 1.41. In order to prevent the radiation damage of the lead glass, both parts of the upper and lower calorimeter are vertically moved away from the electron and proton beam pipes by 50 cm during the beam injection. The status of the PMTs is monitored by the Gain Monitoring System (GMS). The GMS sends the light pulse of a dyelaser with a wavelength of 500 nm at different intensities to every PMT of the calorimeter and to a reference photodiode via glass fibers. As the gain of the photodiode is stable, the ratio of the response of the PMT to the one of the photodiode signal is used to monitor the relative change of the gain of the PMTs. The calorimeter has an energy resolution of:

$$\frac{\sigma(E)}{E}(\%) = \frac{5.1 \pm 1.1}{\sqrt{E(\mathrm{GeV})}} + (1.5 \pm 0.5) \tag{3.5}$$

with an energy response to electrons linear within 1 % over the range from 1 GeV to 30 GeV.

The calorimeter is used as the first level trigger for the scattered electrons. With a signal at least 1.4 GeV energy deposit in a localized spatial region is required. By this way pions are suppressed. The calorimeter measures the energy of electrons and photons from the radiative process or from decay of π^0 and η. The first level trigger is required to initiate the digitization of the readout electronics.

Preshower Counter

The preshower counter provides the first level trigger combined with the calorimeter. The counter consists of the lead wall of 11 mm thickness with 2 radiation lengths sandwiched between two stainless steel sheet of 1.3 mm thickness, which is followed by the plastic scintillator hodoscope called H2. The H2 consists of the vertical plastic scintillator modules of 42. Each module has a size of 9.3 cm width, 91 cm length and 1 cm thickness and covers one vertical column of the lead glass blocks of the calorimeter. To prevent the acceptance gap between the modules, two adjacent modules are overlapped by 1.5 mm. The modules are connected to PMT tubes

with a diameter of 5.2 cm. As the profile of the longitudinal shower is different for electrons and pions, the relative amplitude of the preshower signal compared to the signal from the calorimeter can be used to improve the separation between electrons and pions to 4000 : 1 in the first level trigger.

Transition Radiation Detector

The Transition Radiation Detector (TRD) is used to separate between electrons and hadrons with high efficiency. When a ultra-relativistic charged particle passes through the boundary of the materials with different dielectric constants, the transition radiation is emitted in the forward direction. The angle between the transition radiation and the charged particle is proportional to $1/\gamma$. γ is the Lorentz factor of $E/(mc^2)$, where E is the energy of the particle, m the mass of the particle and c the speed of light. Therefore, measuring γ makes it possible to provide information on the type of the particle. The transition radiation from the ultra-relativistic charged particles with $\gamma > 1000$ is within the range of X-ray which has several keV. On the other hand the charged particles with smaller γ factor emit softer photons with lower energy. Since an electron with the energy of 5 GeV emits the transition radiation in a certain γ of 10^2 compared to γ of 36 for pion, the TRD is suited to distinguish between electrons and pions.

In HERMES the TRD is located between the hodoscope H1 and preshower counter H2. The TRD consists of 6 modules which contain a radiator and proportional chamber. The polypropylene fiber with a diameter of 17 - 20 μm, a density of 0.059 g/cm^3 was chosen as a radiator. The thickness of the radiator is 6.5 cm, which corresponds to an average of 267 dielectric layers. The detectors are conventional proportional chambers filled with Xe/CH_4 gas which absorbs X-ray efficiently. The HERMES TRD can separate between electrons and pions with a ratio of 1 : 100 at least.

Čerenkov Detector

The HERMES Čerenkov detector is a ring imaging type with the dual-radiator of silica aerogel and C_4F_{10} gas. The Čerenkov detector is described in detail in the next chapter.

3.4.3 Luminosity Monitor

The luminosity is measured by detecting the elastic scattering of the beam electrons from electrons of the target atoms like $e^+e^- \rightarrow e^+e^-$ (Bhabha scattering) and the annihilation into photon pairs into $e^+e^- \rightarrow \gamma\gamma$. The scattered particles are detected in coincidence by two small calorimeters located 7.2 m away from the center of the target cell. The cross sections of both processes are known and are integrated over the acceptance of the calorimeters with a horizontal acceptance of 4.6 mrad to 8.9 mrad. For a beam energy of 27.5 GeV, the symmetric scattering angle of

both particles is 6.1 mrad with respect to the beam axis and the scattered particles have a half of the beam energy. The calorimeter consists of Čerenkov crystals of $NaBi(WO_4)_2$ with a very high radiation tolerance. In order to minimize the radiation damage, the calorimeters are moved away from the beam pipe exit window by about 20 cm in the horizontal direction during the beam injection and dumping. The calorimeter consists of 12 crystals with each size of 22 $\times$ 22 $\times$ 200 mm^3 in a 3 $\times$ 4 array. This size of the crystal corresponds to 19.4 radiation lengths along the longitudinal direction. The crystals are coupled to the PMTs of 1.9 cm diameter with optical grease. An energy resolution of the calorimeter is $[\sigma(E)/E](\%) \simeq (9.3 \pm 0.1)/\sqrt{E(\mathrm{GeV})}$ for electron energy of 1 - 6 GeV.

3.4.4 Trigger System

The purpose of the trigger system is to distinguish interesting events from the background with high efficiency, and to initate the digitization and readout of the signals from the detectors. For the physics trigger, the DIS trigger requires the hits in the three hodoscopes H0, H1 and H2 together with the energy deposit of 1.4 GeV at two adjacent columns of the calorimeter in both parts of the upper and lower detector in coincidence with the bunch signal of HERA. The threshold setting of 1.4 GeV of the calorimeter was determined so as to improve the acceptance of the semi-inclusive events with low x and Q^2. The requirement of H0, H1, H2 and BC1 without the calorimeter makes a trigger for the hadron tracks. In the case the BC1 is required to eliminate the shower originating in the upstream of the collimators. Unlike the wire chamber, the hodoscopes are not well shielded from the shower by the magnet steel. The rate of the DIS trigger is 60 Hz or less at the density 1.2 $\times$ 10^{14} nucleons/cm^2 for the polarized deuterium target at about 25 mA of the electron current.

3.4.5 Laser Alignment System

The Laser Alignment System (LAS) [67] has been developed to align the tracking detectors in order to improve the momentum resolution of the particle tracks. The position of the wires on the metallic frame of the tracking detector can be shifted by the influence of the change of temperature. The LAS continuously monitors the relative position of each tracking detector online during the experiment. The LAS consists of the 5 mW He-Ne laser light source with a wavelength of 633 nm, Fresnel zone plates, moving mechanisms of the Fresnel zone plates, CCD cameras with the effective imaging area of 6 $\times$ 8 mm^2, a few optical devices for the transportation of the laser beam and electronics to read out the image from the Fresnel zone plate. The laser beam with a head of 8 mm radius is expanded to 50 mm radius by a beam expander and is arranged to achieve the parallel beam by a beam collimator. The Fresnel zone plate mounted on the VC, FC1/2, BC1/2, BC3/4 and TRD is inserted into the beam line by remote control, and the focused image on the plate is transported to the CCD camera to capture the image with the VME electronics. Figure 3.8 shows one of the Fresnel zone plates, which is mounted on the BC1/2.

The Fresnel zone plate acts as a focusing lens to image the plate position on the CCD camera. All plates are placed at (X, Y) = (0 mm, ±450 mm) in the HERMES coordinate system. In total 30 Fresnel zone plates are mounted on the detectors. It takes about 30 minutes to survey all the Fresnel zone plates. LAS provides the information of the relative position of each tracking detector in the direction perpendicular to the beam axes, X and Y. The focusing image from the Fresnel zone plate has high intensity in its central area. The image is projected to the X and Y directions to determine the peak position of the image. Figure 3.9 shows the three prominent peaks in the central area. As the shape of these histograms remains unchanged as long as the intensity of the laser beam is not changed during the monitoring the movement of the peak allows to evaluate the relative position of each detector. The relative position is the most important quantity to monitor as it can dominate the determination of the momentum for the particle tracks. The precision for the monitoring of the relative position of the tracking detectors in the system is 60 μm in 1σ.

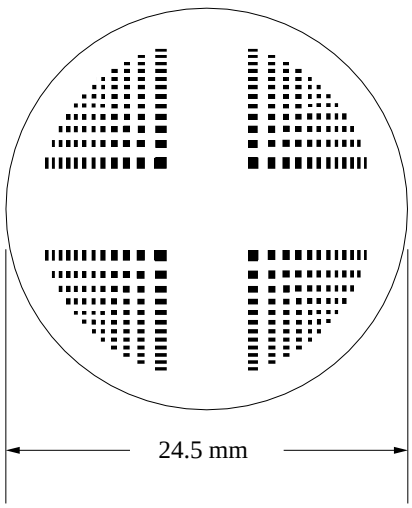

Figure 3.8: Fresnel zone plate mounted on the BC1/2. Diameter of all plates is 24.5 mm, thickness 13 μm. The black squares in the figure are the slit pattern on the plate.

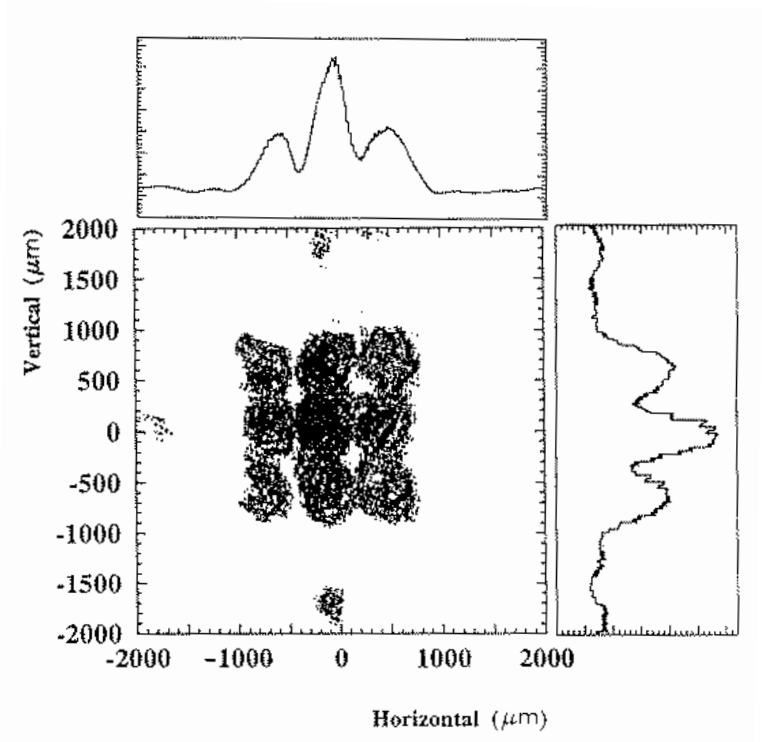

Figure 3.9: Focusing image of the Fresnel zone plate in the central area and projected images to the X and Y directions of the HERMES coordinate system.

Chapter 4

Dual-Radiator Ring Imaging Čerenkov Detector

The dual-radiator Ring Imaging Čerenkov (RICH) detector provides the information for the particle identification (PID) of pions, kaons and protons in a wide range of momentum, so that the RICH detector makes it possible to study the flavor dependence of the polarization by completely decomposing the contributions from the strange quark as well as from the up and down flavors and the sea quarks. It was accomplished by using two radiators, a silica aerogel with excellent optical properties and a heavy C_4F_{10} gas. A lightweight mirror was constructed using a newly perfected technique. The RICH system with clear aerogel in combination with a gas was used for the first time in the actual high energy physics experiment by HERMES.

4.1 Introduction

The HERMES experiment investigates the polarization which depends on each flavor of the quarks by the identification of hadrons in coincidence with scattered electrons, the so-called 'flavor tagging' method. To decompose and determine with high precision the quark polarization for each flavor the various types of hadrons need to be identified at the wide range of the HERMES kinematics.

From 1995 to 1997 HERMES had a threshold type Čerenkov detector. It used heavy gas radiator at atmospheric pressure to mainly identify pions. The momentum threshold for the charged particles was 0.015, 3.99, 14.13 and 26.83 GeV for electron, pion, kaon and proton respectively. The range of the momentum to obtain the clean sample of pions was limited from 4.9 to 13.5 GeV. The threshold Čerenkov detector was replaced by the RICH detector in 1998. The RICH detector allows to identify pions, kaons and protons with high efficiencies and low contaminations. Both upper and lower limits of the momentum were extended: from 2 GeV to 15 GeV for the PID. The momentum of most of all the hadrons produced in HERMES [68, 69] lies between 2 and 15 GeV. The RICH detector consists of the wall of the silica aerogel

tiles and heavy C_4F_{10} gas as radiators, mirror with resin-coated carbon-fiber surface of optically high quality and photon detector of 1934 PMTs per detector half.

4.1.1 Detector Design

Design required for HERMES

The RICH detector of HERMES is located between BC1/2 and BC3/4 behind the spectrometer magnet. The RICH detector has two symmetric halves for above and below modules with respect to the horizontal plane of the electron beam. About 95 % of the hadrons produced at HERMES are within the momentum range from 2 to 15 GeV. The low end of the momentum, 2 GeV, requires the index of refraction for aerogel to be $n = 1.03$ at the wavelength of $\lambda = 633$ nm. This index of refraction corresponds to the momentum threshold of 2 GeV for kaons. Momenta of all pions within the acceptance of the spectrometer are above the momentum threshold of pions for the aerogel, 0.6 GeV, while 90 % of kaons and 78 % of protons are above the momentum threshold for kaons (2 GeV). In table 4.1 the threshold of the Čerenkov radiation for pions, kaons and protons are listed.

	Aerogel	C_4F_{10}
n	1.0304	1.00137
$\beta_t\gamma_t$	4.03	19.10
π	0.6 GeV	2.7 GeV
K	2.0 GeV	9.4 GeV
p	3.8 GeV	17.9 GeV

Table 4.1: Thresholds of the Čerenkov radiation for pions, kaons and protons. The index of the refraction n is given at the wavelength of 633 nm. $\beta_t = 1/n$ is the velocity at the threshold and $\gamma_t = 1/\sqrt{1-\beta_t^2}$.

Figure 4.1 shows the Čerenkov angle as a function of momentum. As seen in figure 4.1, the aerogel radiator plays an efficient role at the region of the low momentum, while the gas radiator plays an important role in the region of the high momentum. The momentum of the threshold for kaons is between the one of pions and protons for both aerogel and gas.

At the high end of the momentum, 15 GeV, the number of the photons that must be detected for full separation of hadrons is fixed. The capability of the particle identification of the RICH detector can be qualified [70] for a given design through the computation of the maximum value of the separation momentum $p_{\max}$. This is defined as the maximum momentum at which the average emission angles of the Čerenkov photons for the two particle types with masses m_1 and m_2 are separated

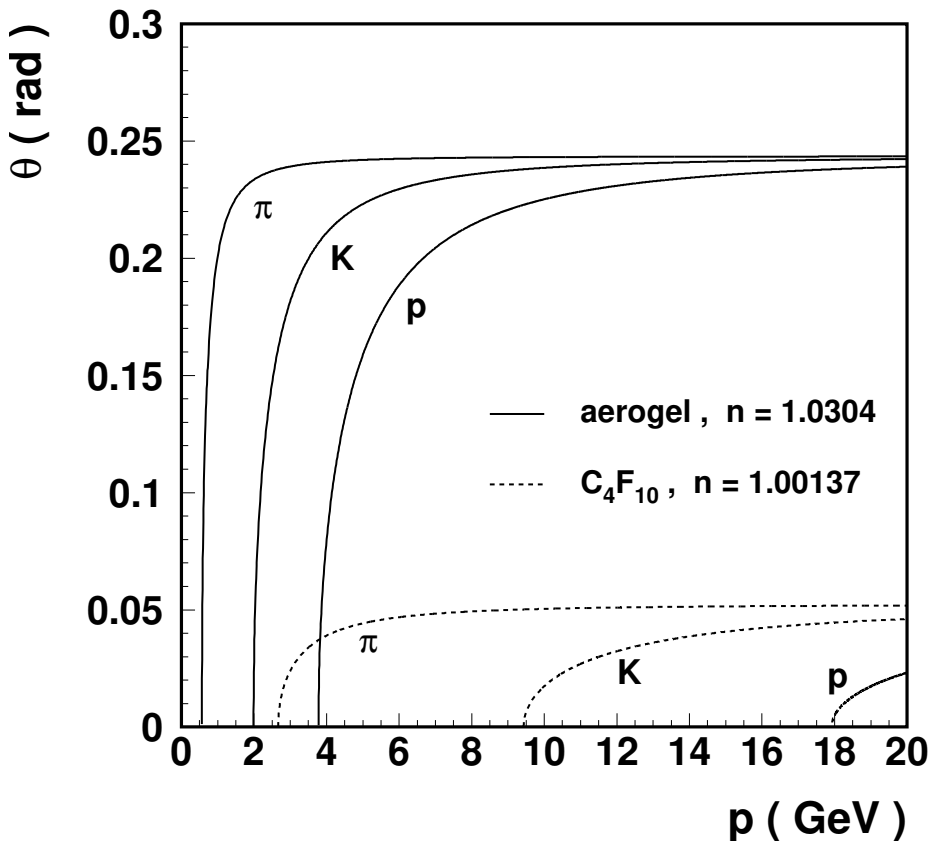

Figure 4.1: Čerenkov angle as a function of momentum for the aerogel (solid curves) and C_4F_{10} gas (dashed curves) radiators.

by the number of standard deviations n_σ:

$$p_{\max} = \sqrt{\frac{m_2^2 - m_1^2}{2k_f n_\sigma}}, \tag{4.1}$$

where $k_f = \tan\theta \cdot \sigma_\theta / \sqrt{N}$ is the constant for the RICH detector, N the number of the separately detected photons, θ the Čerenkov angle and σ_θ the standard deviation of the distribution for the reconstructed photon angles, the so-called single photon resolution. In the design, $n_\sigma = 4.652$ was chosen, as it corresponds to a misidentification of the particle of 1 % when the fluxes of the two particles are equal. The design values of $p_{\max}$ is listed in table 4.2. In this estimate it was assumed that the number of the separately detected photons from aerogel and gas radiators is 10 and 12 respectively. Figure 4.2 shows the range of momentum for the PID for both aerogel and C_4F_{10} gas. The region of the lightly shaded band indicates where the particle can be identified just based on whether a Čerenkov ring is emitted or not. In this region the detector has a behavior like a threshold type Čerenkov detector. The darkly shaded band indicates where they can be identified based on the average reconstructed angles.

	Aerogel	C_4F_{10}
k_f	5.46×10^{-4}	1.07×10^{-4}
$p_{\max}(\pi/\mathrm{K})$	6.7 GeV	15.0 GeV
$p_{\max}(\mathrm{K/p})$	11.2 GeV	25.3 GeV

Table 4.2: Maximum separation momenta $p_{\max}$. For example, $p_{\max}(\pi/\mathrm{K})$ means the maximum momenta for the separation between pions and kaons. $k_f = \tan\theta \cdot \sigma_\theta / \sqrt{N}$.

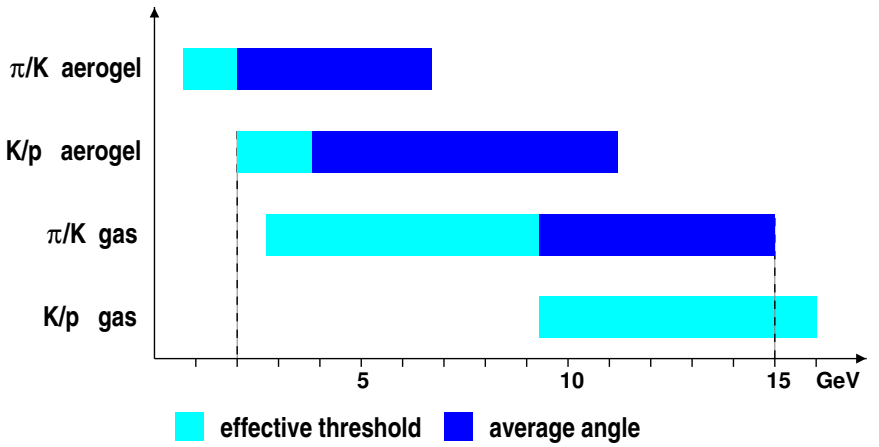

Figure 4.2: Ranges of momentum for the separation of pions, kaons and protons in aerogel and C_4F_{10} gas. The dashed line represents the range where the hadrons can be identified.

RICH of HERMES

The threshold type Čerenkov detector of the HERMES spectrometer, which had been used in the data taking period from 1995 to 1997, was converted to the RICH detector in 1998. The RICH detector was constructed by using the container of the threshold type Čerenkov detector. Figure 4.3 shows the schematic view of the RICH detector for the upper half of the HERMES detector. The material of the container is aluminium with an entrance window of 187.7 cm $\times$ 46.4 cm and an exit window of 257.0 cm $\times$ 59.0 cm. The entrance and exit windows are made of aluminium of 1 mm thickness. The volume of each half is 4000 ℓ. The gas control system recirculates the C_4F_{10} gas to the main volume of the RICH detector with a slight overpressure compared to the atomospheric pressure. The aerogel tiles are stacked to form the wall of 17 tiles in the X direction and 5 tiles in the Y direction. A layer of 5 tiles, total 5.5 cm thickness, was formed in the Z direction. The volume of the RICH detector behind the aerogel radiator is filled with the gas radiator C_4F_{10}. The Čerenkov light cones from the two radiators are reflected on a spherical mirror located at the rear end of the radiator box and are focused onto the PMT plane. The mirror array has a radius of 2.20 m. The PMT plane of 60 $\times$ 120 cm^2 has a matrix of 1934 PMTs for each half of the detector. The diameter of the PMT is

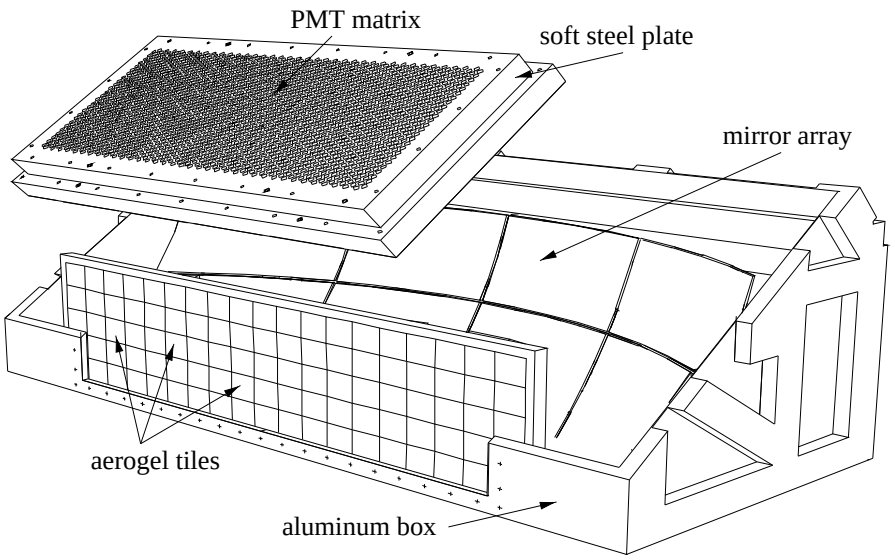

Figure 4.3: Schematic view of the RICH detector for the upper half of the HERMES detector.

3/4 inch. The pixel size of the PMT matrix is 23.3 mm. Figure 4.4 shows the inner structure of the RICH detector. From Monte Carlo (MC) simulation it is known that 95 % of the center of the rings and 90 % of all the photons arrive at the PMT plane. The inner wall of the detector box are painted in black to reduce the wall reflection of the light.

One photon resolution has three different contributions, $\Delta\theta_{\rm em}$, $\Delta\theta_{\rm pix}$ and $\Delta\theta_{\rm chr}$, where $\Delta\theta_{\rm em}$ comes from the uncertainty in the vertex position of emission along the track in the radiator. $\Delta\theta_{\rm pix}$ accounts for the finite granularity of the pixel size. These two contribute to the uncertainties of the Čerenkov angles for both aerogel and gas. The uncertainty $\Delta\theta_{\rm chr}$ for the chromatic aberration arises from the variation of the index of refraction as a function of wavelength. It has an important contribution to the Čerenkov angles for the aerogel. Each contribution is analytically calculated based on some simple assumptions and listed in table 4.3 in comparison with the estimate by MC. The main contribution to the resolution comes from the size of the PMT.

	Aerogel	C_4F_{10}
$\Delta\theta_{\rm em}$	1.8 mrad	2.2 mrad
$\Delta\theta_{\rm pix}$	5.6 mrad	5.2 mrad
$\Delta\theta_{\rm chr}$	2.5 mrad	-
$\Delta\theta_{\rm MC}$	7.1 mrad	7.2 mrad

Table 4.3: Individual contributions to the single photon resolution in aerogel and C_4F_{10} gas.

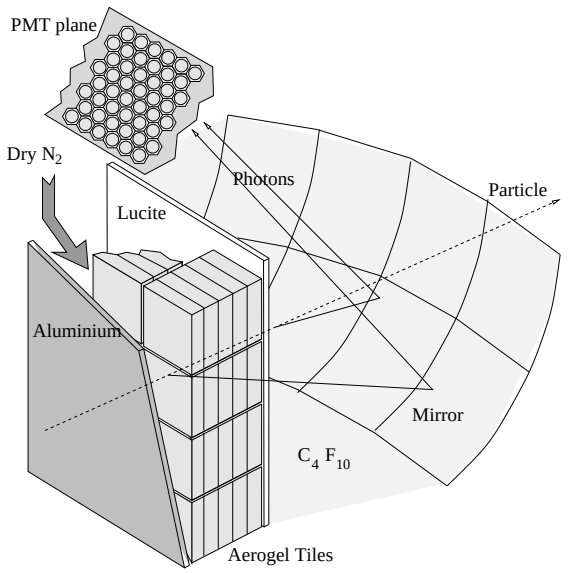

Figure 4.4: Schematic view of the inner structure of the RICH detector in HERMES.

Silica Aerogel Radiator

The aerogel with uniform and small colloidal SiO_2 particle structure has been developed recently [71, 72]. The uniform granular structure suppresses the Rayleigh scattering of the visible light and greatly enhances its transmission. Material with the index of refraction in the range 1.01 - 1.10, suitable for use in the momentum range of interest in HERMES, is now available. The mass production was done by Matsushita Electric Works in Japan. The form of the tile with average dimensions of $114 \times 114 \times 11.3$ mm^3 was produced for HERMES. The transmittance of each tile was measured for the range from 200 mm to 900 mm. The typical values of the transmittance for the wavelength of 400 mm are around 0.67.

The details of the optical properties of the aerogel tile are described in [73, 74, 75, 76]. The 425 tiles per detector half are stacked in a container consisting of the aluminium entrance window and a 3.2 mm UVT-lucite exit window. The average index of refraction of tiles for use is 1.03040, with a spread of 3.6×10^{-4}. To avoide possible degradation of the aerogel by the C_4F_{10} gas radiator, the tile container is tightly sealed from the gas radiator. Additionally the dry N_2 gas is continuously circulated through the aerogel box at a slow rate. The black plastic spacers of appropriate thickness were inserted between the aluminium frame and tile to prevent the tiles from shifting while the RICH detector is moved for the installation. The thickness of the aerogel wall was optimally determined so as to maximize the yield of the unscattered photons relative to the scattered background photons. The tiles were stacked according to their measured index of refraction, thickness, and quality of the surface when the wall was built. To achieve the best resolution for the Čerenkov ring the tiles with similar indicies of refraction are placed

together in the same stack, so that the particles passing through the aerogel emit the photons with very similar Čerenkov angles. The black sheets of tedlar surrounding the periphery of the edge of the tile absorb the photons that cross the stack boundary and reduce the distortion of the angle.

The material for the exit window was chosen considering its property of the transmission. The Čerenkov light produced in the aerogel suffers Rayleigh scattering. As the cross section of Rayleigh scattering is proportional to λ^{-4} (λ: photon wavelength), the low wavelength is dominated by the rescattered photons. Since such photons only contribute to the background, an exit window of ultraviolet-transmitting (UVT) lucite was chosen so as to absorb most of the background photons. The UVT lucite has an absorption cutoff at the wavelength of 290 nm. The thickness of the UVT window is 3.2 mm. The Čerenkov light generated in the lucite itself is emitted at such large angles that it is effectively trapped by the total internal reflection for most forward tracks.

Gas Radiator

The other radiator is heavy fluorocarbon gas, C_4F_{10}, at a slightly overpressure with respect to atmosphere. The C_4F_{10} gas has a Čerenkov threshold of $\beta_t\gamma_t = 19.10$. The depth of the radiator volume is about 1.2 m.

Mirror Array

The mirror array for each half of the RICH detector has eight segments: two rows and four columns as it is seen in figure 4.3. Both the mirror and the mounting frame were fabricated by Composite Mirror Applications in the USA. The backing of the segments is fabricated from a graphite fiber composite [77] coated with an epoxy film yielding an optically smooth surface. The surface roughness was specified to be less than 5 mm. The surface is aluminized to provide a reflectivity above 85 % for light in the range of the wavelength of 300 - 600 nm. The dimension of each array is 252.4 cm $\times$ 79.4 cm. The weight of each array is less than 13 kg.

The simple alignment procedure was performed at the period of installation of the mirrors. A point light source at the nominal radius of the curvature of the array was imaged on a screen. Then mirror segments were adjusted to minimize the size of the reflected image on the screen. Moreover their mounting was finely tuned by adjusting additional pressure points where necessary. The actual mirror alignment was determined from the data itself, which is described in section 4.2.2.

Photon Detector

The useful photons emitted in the aerogel radiator are mostly limited to the visible region of wavelength. The photons emitted in the gas radiator have a component extending to the UV region of wavelength. However, since the photon yield from the gas is sufficiently high, the detector response in the UV region is not crucial.

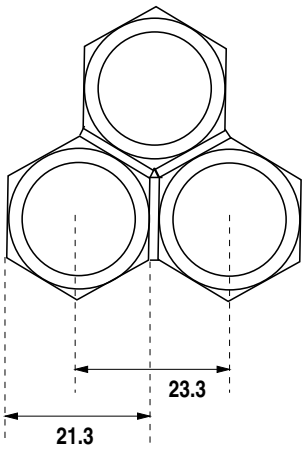

Figure 4.5: Schematic view of the hexagonal close packed matrix with the photomultiplier at the center of the cell. The picture is not scaled. The unit of the numbers in the picture are in mm.

The Philips XP1911 photomultiplier with a diameter of 3/4 inch (18.6 mm) was chosen for the RICH detector of HERMES. The XP1911 PMT guarantees the minimum active photocathod diameter of 15 mm. This led to a pixel size of 23.3 mm.

The XP1991/UV PMT was chosen for its broad quantum efficiency curve that matches the spectrum of the Čerenkov light in the aerogel well. Since the efficiency extends to the UV region, it is good choice for the photons from the gas. After the installation of the RICH detector in the HERMES spectrometer a noise rate of the PMT reached about 1 kHz. It corresponds to 1 PMT firing per detector half every five events. The PMTs were sorted according to their gain characteristics and noise level. With an especially developed low current (0.040 mA at 1300 V) high voltage divider it was possible to supply 32 PMTs from a single HV channel.

The photomultipliers were arranged in a hexagonal close packed matrix of 120 $\times$ 60 cm^2, centered on the focal point of the mirror. This configuration of the matrix was firstly used by the E781-SELEX experiment at FNAL [78]. The elementary cell of the array is hexagon with the photomultiplier at the center of the cell. Figure 4.5 shows the schematic view of the hexagonal close packed matrix. A light-gathering cone is attached in front of the photocathode plane to increase the photon collection efficiency by reducing the dead space between the photocathodes. The distance between two adjacent cell centers is 23.3 mm, yielding an elementary cell surface of 426 mm^2. The 1934 PMTs in each detector half are arranged in 73 columns of alternately 26 and 27 PMTs each. The matrix plate provides the gas seal for the C_4F_{10} volume. The gas seal for the individual PMT cavities was provided by the thin quartz windows which were glued to soft steel cone-shaped inserts that in turn were glued into the inner face of the PMT matrix plate.

Only 38 % of the area of the focal plane is covered by the PMT photocathodes. An aluminized plastic foil funnel was inserted into each steel entrance cone to increase the coverage to 91 % of the photon detector surface and also to improve the

reflectivity of the cone surface. The stray fields from the spectrometer magnet at the location of the photon detector matrix can reach up to 90 G perpendicular to the detector plane. It requires a careful magnetic shielding of the PMTs. Each PMT was wrapped with a μ-metal sheet of 100 μm thickness. Furthermore, the matrix plate holding the PMTs were constructed from the high permeability (C-1008) steel. The soft steel matrix, combined with the μ-metal shielding and the soft steel insert, reduces the magnetic fields to the negligible level.

Readout and Event Format

For the readout of the photon detector, the commercial LeCroy PCOS4 is used. The LeCroy PCOS4 is upgraded for the HERMES application. Each detector half is read out by a set of 8 symmetric backplane sections, each housing 15 or 16 PCOS4 cards. This reduces the number of the cables needed to 10 twisted piars cables. Only digital information is recorded when the pulse exceeds the threshold of 0.1 photoelectrons. The PCOS4 system generates a data stream on an event-by-event basis. The data from the RICH detector consists of a hit table for the PMT for each detector half, where a PMT hit simply referes to the PMT that fired during the event time window. A RICH mapping file is used to link the data channel numbers computed in the decoding process to the PMT location in the detector matrix. This information can be used to generate the spatial hit coordinates and the hit pattern in the focal plane.

4.2 Online Monitoring

The status of the RICH detector during the data taking is monitored online using a client-server based system [79, 80]. The information of high and low voltages, gas pressure and composition, and the temperatures at the photon detector is available in the form of Tcl/Tk based displays [81]. Additionally the performance of the PMTs, the high voltage and the electronics are monitored in the tubemaps.

Figure 4.6 shows the two-dimensional tubemap for the lower half of the RICH detector, which is used to monitor the performance of the PMTs, the high voltage and the electronics. The data from the RICH detector have been integrated into the online event display system for HERMES to allow the online analysis of the events. Figure 4.7 shows an event of a clean single electron from the data on the online event display.

As the electrons and positrons that are detected in the RICH detector always have momenta above the thresholds for both aerogel and C_4F_{10} gas, they emit Čerenkov photons in the radiators. Therefore such Čerenkov photons are useful to check the quality of the data. The average number of PMT hits for single electron events in a run is used to monitor the quality. Usually the hits for single electron events is around 20. Figure 4.8 shows the typical online plot for the data quality monitoring.

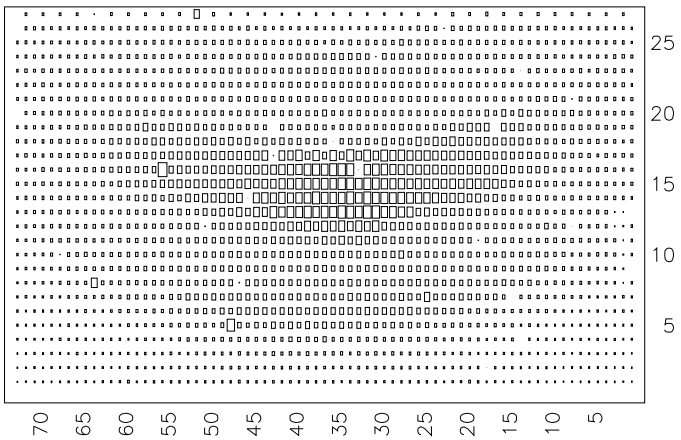

Figure 4.6: Two-dimensional tubemap for the lower half of the RICH detector. The axes indicate the position number of each PMT.

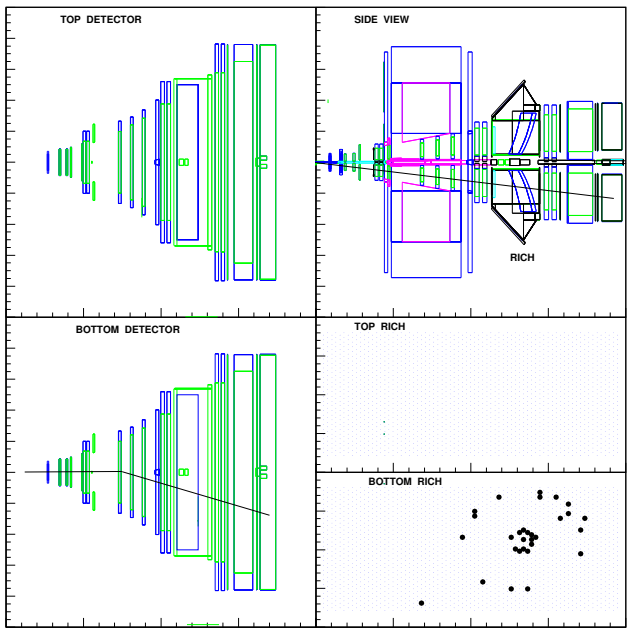

Figure 4.7: Online display of a single electron event from the data. The upper and lower left parts show the top and bottom detector halves of the HERMES spectrometer. The most upper right part shows both top and bottom detector halves of the side view. The lower parts show the photon detectors in the top and bottom parts of the RICH detector respectively. The dots represent each position of 1934 PMTs. The fired PMTs are marked by the solid circles.

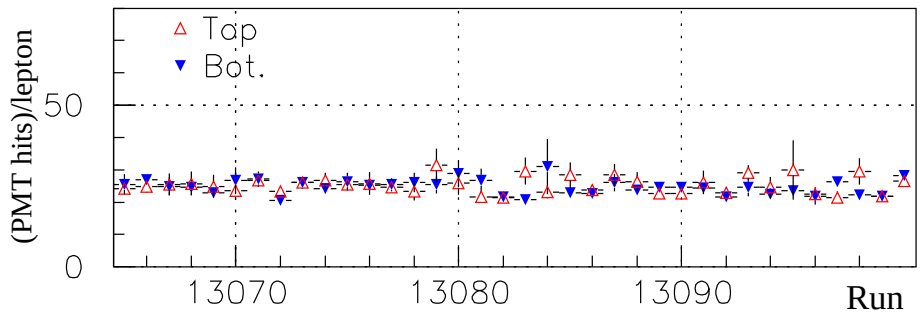

Figure 4.8: Average number of PMT hits for single electron events for the online data quality monitoring. The horizontal axis represents the run number for the data taking in the experiment.

4.2.1 Reconstruction and Particle Identification

Principle of Reconstruction

The detected Čerenkov rings are not circles, but in general asymmetrically distorted ellipse because the photon detector is on the flat plane. The raw data that provide the input for any procedure of the reconstruction of the ring are the list of PMT hits per event and the parameters of the particle tracks determined by the tracking detectors [64].

In the case of the aerogel ring only about 10 % of the PMTs that lie on the aerogel ring will be hit on average. This means that the multiple hits are rare case and each PMT hit is due to one photon. The average number of PMT hits for the aerogel ring with an ultra-relativistic ($\beta \simeq 1$) particle is about 10 when the particle gets no effects of the acceptance by the shape of the aerogel tiles and the mirror. The number of PMT hits for the aerogel ring is small. It makes the detection of this ring susceptible to the background, noise and acceptance problems. Contrary to the aerogel rings, the average multiplicity of the photons for each PMT that lie on the gas ring is about 2 based on the MC simulations. On average about 23 PMTs are concerned with the photons of the gas ring of an ultra-relativistic particle, but only 12 of those PMTs are actually fired.

The task of the pattern recognition algorithm is to associate the various hits in the photon detector of the RICH detector with a ring assigned to a certain track with a certain momentum. The separation between leptons and hadrons is performed by other detectors of the HERMES spectrometer. The average efficiency for the identification of electron is 99 %. The hadron contamination to electrons reaches below 1 % [64].

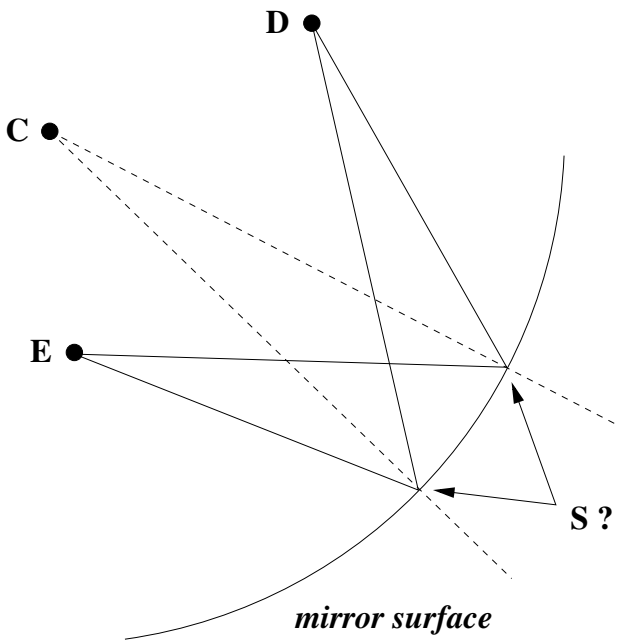

Figure 4.9: Problem of the inverse ray tracing.

Inverse Ray Tracing

For the analysis of the hit patterns in the RICH detector, a method, so-called inverse ray tracing (IRT) was developed and studied [82, 83, 84, 85, 86]. In this method the Čerenkov angle corresponding to each PMT is reconstructed from the track parameters and the position of the PMT.

The problem of the IRT method is to determine the angle with which the photon was emitted, given a track and a hit in the plane of the photon detector. Assume that the photon emission point can be estimated. This assumption will be discussed as follows. Figure 4.9 expresses the geometrical problem. Given point E is the likely emission point of photon, point D the detection point on the photon detector and point C the center of the spherical mirror, find the point S on the surface of the mirror where the photon is reflected. The point S can be expressed in the notation of the vector:

$$\overrightarrow{\mathrm{CS}} \text{ is coplanar with } \overrightarrow{\mathrm{CE}} \text{ and } \overrightarrow{\mathrm{CD}}, \tag{4.2}$$

$$| \overrightarrow{\mathrm{CS}} | = R, \tag{4.3}$$

$$\angle(\overrightarrow{\mathrm{ES}}, \overrightarrow{\mathrm{CS}}) = \angle(\overrightarrow{\mathrm{CS}}, \overrightarrow{\mathrm{DS}}). \tag{4.4}$$

Here R is the radius of the spherical mirror. For the mathematical formulation of the problem it is convenient to use an Euclidean coordinate system with the C as the origin (figure 4.10). The u axis is defined along $\overrightarrow{\mathrm{CE}}$. The v axis is coplanar with $\overrightarrow{\mathrm{CE}}$ and $\overrightarrow{\mathrm{CD}}$, and $\hat{\mathrm{v}} \cdot \overrightarrow{\mathrm{CD}} > 0$. The expression like $\hat{\mathrm{v}}$ means the unit vector. The third axis w is defined as an axis in the right-handed coordinate system. Then the vectors

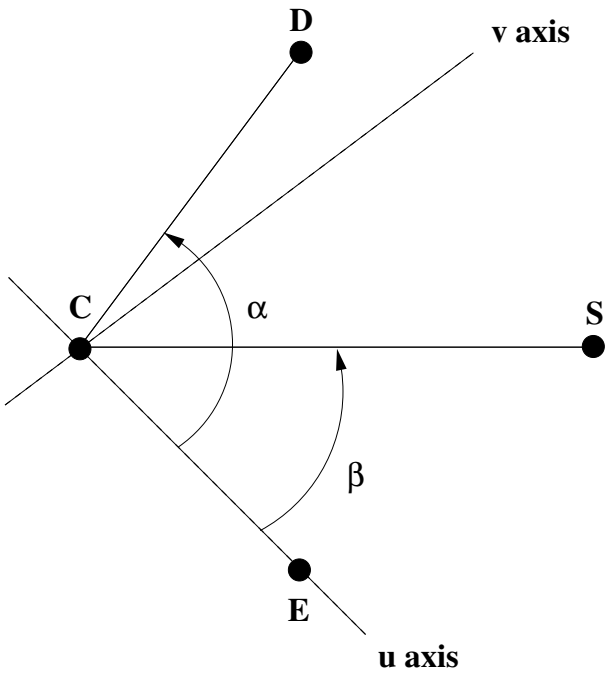

Figure 4.10: Definition of the u and v axes and the angles in the Euclidean coordinate system.

have the components:

$$\overrightarrow{\mathrm{CE}} = (a \quad , 0 \quad , 0), \tag{4.5}$$

$$\overrightarrow{\mathrm{CD}} = (d\cos\alpha \, , d\sin\alpha \, , 0), \tag{4.6}$$

$$\overrightarrow{\mathrm{CS}} = (R\cos\beta, R\sin\beta, 0). \tag{4.7}$$

Here $a = \mid \overrightarrow{\mathrm{CE}} \mid$ and $d = \mid \overrightarrow{\mathrm{CD}} \mid$. The angles of α and β are defined in figure 4.10. Clearly the following holds:

$$a, d, R > 0, \tag{4.8}$$

$$0 < \alpha < \pi, \tag{4.9}$$

$$0 < \beta < 0. \tag{4.10}$$

The parameter β must be determined from the equations of the relation between the incident and reflected angles:

$$\hat{\mathrm{SC}} \cdot \hat{\mathrm{SE}} = \hat{\mathrm{SD}} \cdot \hat{\mathrm{SC}}, \tag{4.11}$$

$$\hat{\mathrm{SC}} \times \hat{\mathrm{SE}} = \hat{\mathrm{SD}} \times \hat{\mathrm{SC}}. \tag{4.12}$$

The essential vectors in the two equations can be written in the Euclidean coordinate system as:

$$\overrightarrow{\mathrm{SC}} = (-R\cos\beta \quad , -R\sin\beta \quad , 0), \tag{4.13}$$

$$\overrightarrow{\mathrm{SE}} = (a - R\cos\beta \quad , -R\sin\beta \quad , 0), \tag{4.14}$$

$$\overrightarrow{\mathrm{SD}} = (d\cos\alpha - R\cos\beta, d - R\sin\beta, 0). \tag{4.15}$$

The equation (4.11) reduces to:

$$\frac{|\overrightarrow{\mathrm{SD}}|}{|\overrightarrow{\mathrm{SE}}|} = \frac{d(\cos\alpha\cos\beta + \sin\alpha\sin\beta) - R}{a\cos\beta - R} \tag{4.16}$$

The equation (4.12) reduces to:

$$\frac{|\overrightarrow{\mathrm{SD}}|}{|\overrightarrow{\mathrm{SE}}|} = \frac{d(-\cos\alpha\sin\beta + \sin\alpha\cos\beta) - R}{a\sin\beta}. \tag{4.17}$$

Combining the equations of (4.16) and (4.17) leads to:

$$ad\sin(\alpha - 2\beta) + R[a\sin\beta - d\sin(\alpha - \beta)] = 0. \tag{4.18}$$

The solution of this equation (4.18) can now be found from the Newton-Raphson iterations. Since the result will be the angle β, no further work is necessary. Using a half of the angle α as the starting point, the reflection point on the mirror can then be found as:

$$\overrightarrow{\mathrm{S}} = \overrightarrow{\mathrm{C}} + \left(\frac{R\cos\beta}{a} - \frac{R\sin\beta\cos\alpha}{a\sin\alpha}\right)\cdot\overrightarrow{\mathrm{CE}} + \frac{R\sin\beta}{d\sin\alpha}\cdot\overrightarrow{\mathrm{CD}}\ . \tag{4.19}$$

The IRT method reconstructs the emission angle for each hit, provided the emission vertex is known. For the hypothesis of each radiator, the emission angle is reconstructed. Figure 4.11 shows the results of spectra for the reconstructed angles. It clearly shows the reconstructed angles depend on the radiator hypothesis. Due to the very different index of refraction, a problem rarely can happen to distinguish which of the two radiators was the real emitter of the photon. The uncertainty of the emission vertex due to the finite length of the radiator is unavoidable and results of the contribution $\Delta\theta_{\mathrm{em}}$ to the resolution are shown in table 4.3. For the actual reconstruction of the angles in the radiators on the assumption that the photons are emitted in the center of the aerogel layer and the center of the path length of the track in the gas the emission vertices are given.

A different treatment between the reconstructed angle of the aerogel and gas is required because of the refraction of the aerogel photons at the boundaries between aerogel and gas. This is approximately corrected under the assumption of a flat boundary between aerogel and gas and the coplanar refraction [87].

Likelihood

The particle identification is largely based on the average value of the reconstructed angles. The theoretically expected angles θ_{th} are calculated for each particle type hypothesis i from the track momenta. For each particle type hypothesis a window is imposed on the spectrum of the reconstructed angles around the θ_{th}. The width of the window σ_{w} is set to 2 times of the single photon resolution σ_θ. This, however, is in principle a free parameter that can be adjusted to optimize the performance

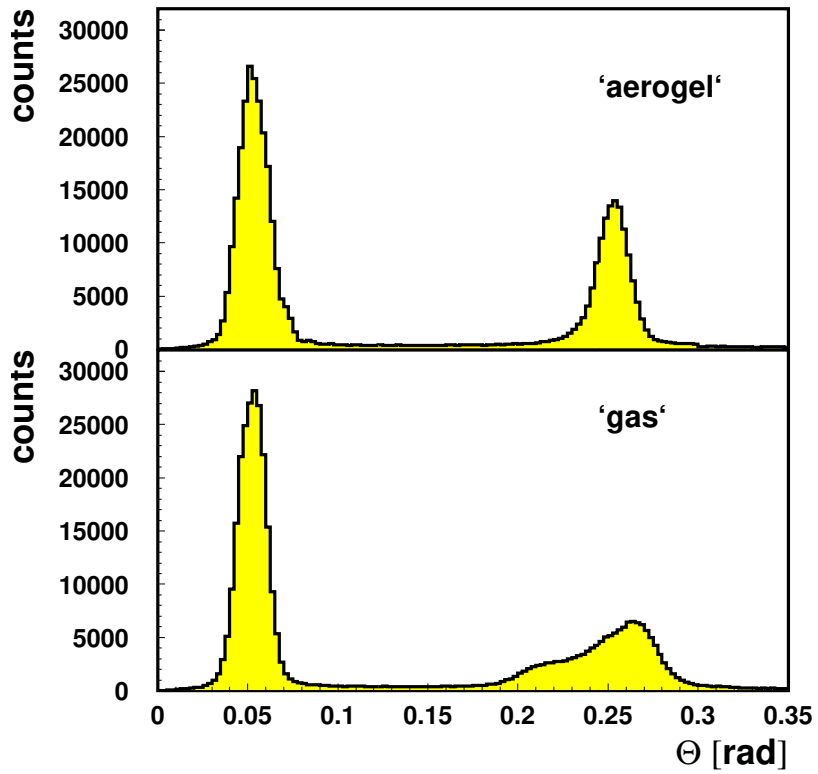

Figure 4.11: Spectra of the reconstructed Čerenkov angles for assumption that the photon was emitted in the aerogel (upper figure) or in the C_4F_{10} gas (lower figure). The results are for the events of single electron track with momentum greater than 5 GeV in the low background.

of algorithm for the particle identification. The average value of the reconstructed angles is determined from each reconstructed angle within the window of $[\theta_{\rm th} - \sigma_{\rm w}, \theta_{\rm th} + \sigma_{\rm w}]$.

With a Gaussian distribution of the average angle the likelihood L is calculated as:

$$L(\langle\theta\rangle) = \exp\left[-\frac{(\theta_{\rm th} - \langle\theta\rangle)^2}{2\sigma^2_{\langle\theta\rangle}}\right], \tag{4.20}$$

where $\sigma_{\langle\theta\rangle}$ is the standard deviation of the average angle, which is calculated from the single photon resolution as:

$$\sigma_{\langle\theta\rangle} = \frac{\sigma_\theta}{\sqrt{N}}. \tag{4.21}$$

Here N is the number of the photons within the window. The likelihood for each radiator are combined to an overall likelihood by multiplying each other. For a particle hypothesis if the momentum of the track is under the momentum threshold and the number of PMT hits is smaller than the number of background PMT hits, the likelihood is set to a constant value, which is 0.5 for aerogel and gas. This is called the sub-threshold likelihood [84, 85, 86]. The number of background PMT

hits is set to 0 (1) for aerogel and 2 (3) for gas in low (high) background case [86]. If the momentum of the track is above the momentum threshold and the PMT hits are smaller than the background PMT hits or if the momentum of the track is under the momentum threshold and the PMT hits are larger than the background PMT hits, the likelihood is set to a constant minimum value, which is about 10^{-4} for aerogel and 10^{-8} for gas [86].

4.2.2 Mirror Alignment

The mirror array was aligned by using the data in the three steps of so-called global, individual and local alignment [84].

In the global mirror alignment, the mirror array of each half of the RICH detector was regarded as one unit. A three-dimensional scan of the assumed position of the center of the spherical mirror was carried out in the software level and the influence on the reconstructed rings for aerogel and gas was studied using a set of single electron tracks with high energy. A careful study derived a small range of the acceptable value for the position of the center of the mirror.

For the individual alignment the eight individual mirrors were aligned relative to one another and each mirror was individually adjusted.

Moreover, the local alignment was performed by artificially dividing the individual mirrors into small segment of 3×3 parts, which was treated as one of the locally individual mirrors. The local mirror alignment allows for a better approximation of the real surface of the mirrors.

The individual and local mirror alignment are based on a large sample of pions with momenta between 4.5 and 5.5 GeV. They were selected to cover as much as possible of the surface of the mirror. The pions with such momenta have well defined rings from the gas.

4.2.3 Detector Performance

The detector performance is evaluated by the number of fired PMTs and the Čerenkov angle for aerogel and gas as well as the single photon resolution. Complications arise from overlapping rings and background hits.

Photon Yields

Figure 4.12 shows the number of PMT hits for aerogel N(aero) and gas N(gas) as a function of momentum of the particle for the ideal tracks of pions which do not suffer from the acceptance or effects of overlapping rings. These two plots show the rise towards the asymptotic values of 10 for PMT hits for the aerogel and 12 for the gas. Due to the acceptance effects, the asymptotic number of PMT hits for all tracks goes down to about 8 for the aerogel.

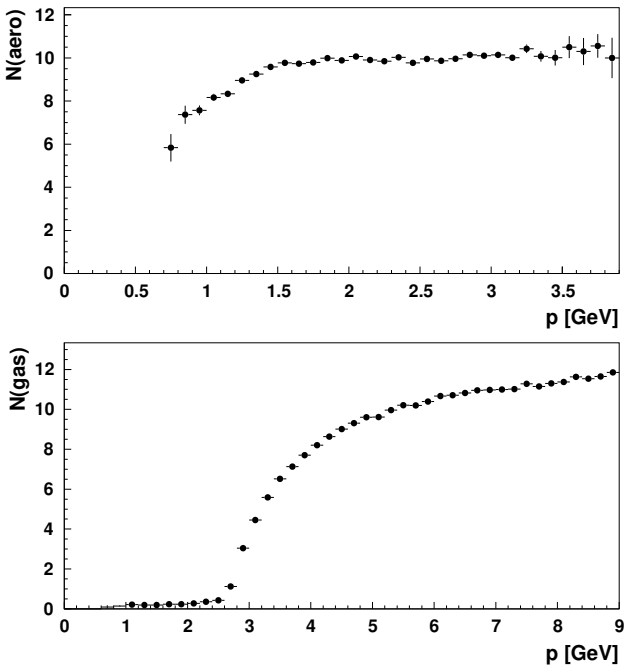

Figure 4.12: Number of fired PMTs for aerogel (upper) and gas (lower) as a function of momentum for the ideal tracks of pions.

Background

An inspection of all events from a single run with 1861 events showed that roughly one third of all particles that produce clear rings in the detector do not have a full reconstructed track. Such tracks come from the particles with low momentum that do not pass through the overall spectrometer of HERMES. These trackless rings contribute as background to the rings that are associated with tracked particles. In the events with more than one track in one detector half of the RICH detector the rings from the tracked particles are background for one another. In addition to the trackless rings, there are several sources of the photons which can be background, for example, Rayleigh scattering photons, Čerenkov photons produced in the lucite window, proton beam correlated background showers that directly hit the PMT matrix and scintillation in the gas. The effects of the electronic and PMT noise in the detector is very small, amounting to only about 1 fired PMT every 5 events.

Average Angles and Resolution

Figures 4.13 and 4.14 show the average angle for pions in the aerogel and gas respectively. The data were fit with a theoretical curve with the index of refraction of 1.0304 for the aerogel and 1.00137 for the gas. The result of figure 4.13 reproduces the theoretical expectation and the optically measured index of refraction well. The systematic difference between the data and the theoretical curve at the region of the

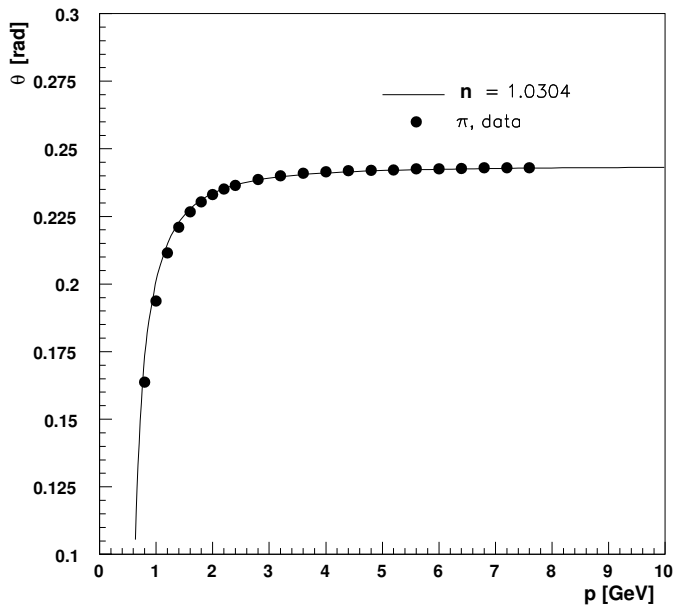

Figure 4.13: Reconstructed average angle (closed circles) for pions in the aerogel as a function of momentum. The solid curve represents a theoretical fit to the data. The resulting index of refraction is $n = 1.0304$.

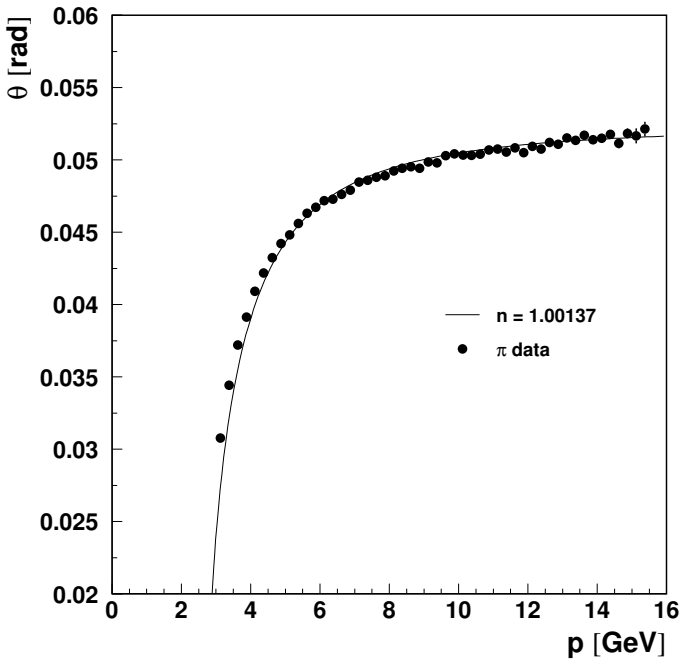

Figure 4.14: Reconstructed average angle (closed circles) for pions in the gas as a function of momentum. The solid curve represents a theoretical fit to the data. The resulting index of refraction is $n = 1.00137$.

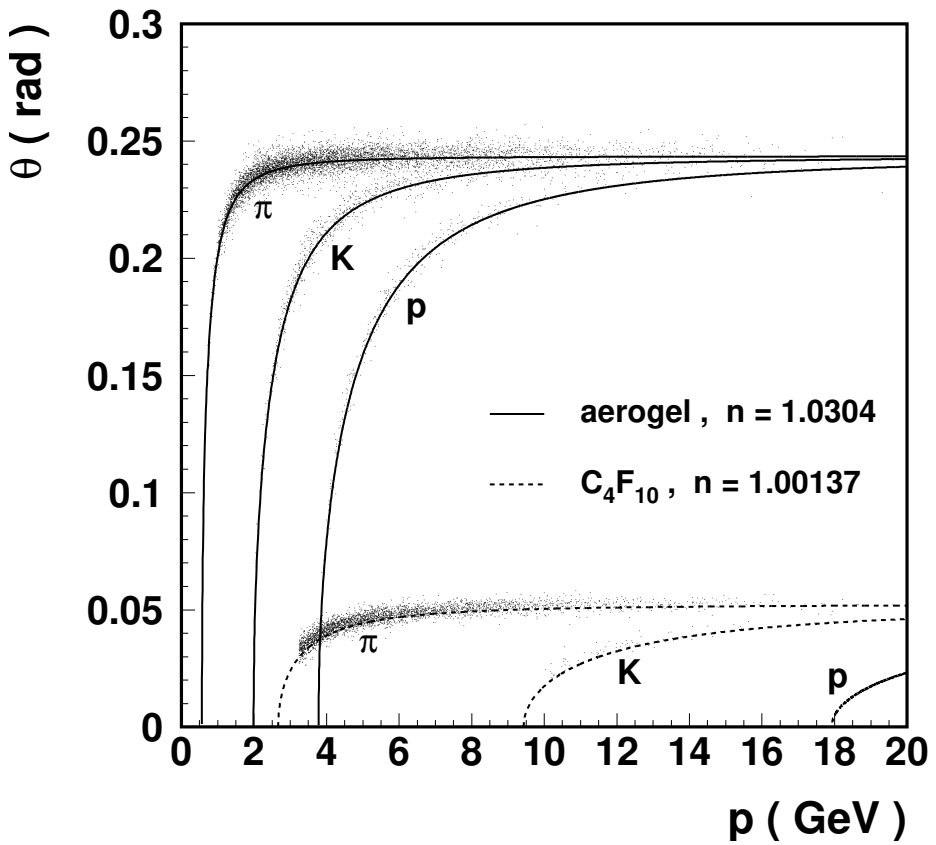

Figure 4.15: Reconstructed average angles in aerogel and gas from the experimental data as a function of momentum. The solid and dashed curves represent the theoretical curves in aerogel and gas respectively. For the angle in the gas there are no entries of data for proton here. The Čerenkov angle for the gas is reconstructed from the region of 0.6 GeV higher than the momentum threshold due to the small size of the Čerenkov ring for the gas.

low momentum is due to the finite size of the PMTs. Figure 4.15 shows the reconstructed average angles in aerogel and gas from the experimental data as a function of momentum with the theoretical curves from the index of refraction of 1.0304 for the aerogel and 1.00137 for the gas. As the size of the Čerenkov rings from the gas is small, the Čerenkov angle for the gas is reconstructed from the region of 0.6 GeV higher than the momentum threshold.

Figure 4.16 shows the squared mass of hadrons which is calculated based on the reconstructed Čerenkov angles for aerogel and gas. Each squared mass of 0.018 GeV^2, 0.25 GeV^2 and 0.9 GeV^2 corresponds to pion, kaon and proton. As clearly visible, the separation between pions and kaons in the aerogel is possible up to about 3 GeV. In the region more than 3 GeV the Čerenkov angles from the gas are available for the particle identification of pions and kaons.

Table 4.4 shows the additional contributions to the resolution of the Čerenkov

angle. The large contribution comes from the effect of the sharply curved surface near the edge of the aerogel tiles. This leads to unpredictable refraction of the photons, which contributes to the rise of the resolution $\Delta\theta_{\rm tile}$. Additionally this effect can create background. $\Delta\theta_{\rm tile}$ was estimated by comparing the resolution between the tracks which are not affected by the edge of the tiles and those which are affected. $\Delta\theta_{\rm nvar}$ is the contribution for the variation of the index of refraction between the aerogel tiles. This was estimated from the measured indices of refraction. $\Delta\theta_{\rm fw}$ represents the contribution for the forward scattering. This contribution is not included into the Monte Carlo simulation.

For the gas radiator, the fluctuations of the pressure and temperature of the gas change the density of the gas, so that this leads to a change of the index of refraction for the gas. This contribution, $\Delta\theta_{\rm press}$, was estimated from the fluctuations of the observed maximum pressure.

The experimental contribution $\Delta\theta_{\rm exp}$ was determined by using the tracks of single electron with high energy that are not affected by any effects of the tile edge or mirror acceptance. The events with a large background were excluded. This means that $\Delta\theta_{\rm tile}$ does not contribute and the effect of the background is minimized. Since the data were taken in a period of the stable atmospheric pressure, $\Delta\theta_{\rm press}$ is negligible.

The contribution which comes from the inperfection of the mirror surface $\Delta\theta_{\rm mirr}$ was calculated from the difference between the experimental resolution and the quadratic sum of the relevant resolutions to each contribution.

	Aerogel	C_4F_{10}
$\Delta\theta_{\rm tile}$	$\sim$ 3.0 mrad	-
$\Delta\theta_{\rm nvar}$	$\sim$ 1.1 mrad	-
$\Delta\theta_{\rm fw}$	$\sim$ 0.9 mrad	-
$\Delta\theta_{\rm press}$	-	$\sim$ 1.0 mrad
$\Delta\theta_{\rm exp}$	7.6 mrad	7.5 mrad
$\Delta\theta_{\rm mirr}$	$\sim$ 2.3 mrad	$\sim$ 2.2 mrad

Table 4.4: Additional contributions to the single photon resolution in aerogel and C_4F_{10} gas.

4.2.4 Efficiencies and Contaminations

It is important to estimate the performance of the particle identification of the RICH detector for the physics analyses. The performance was studied by using the technique of the Monte Carlo simulation. This studies is described in detail in chapter 5.

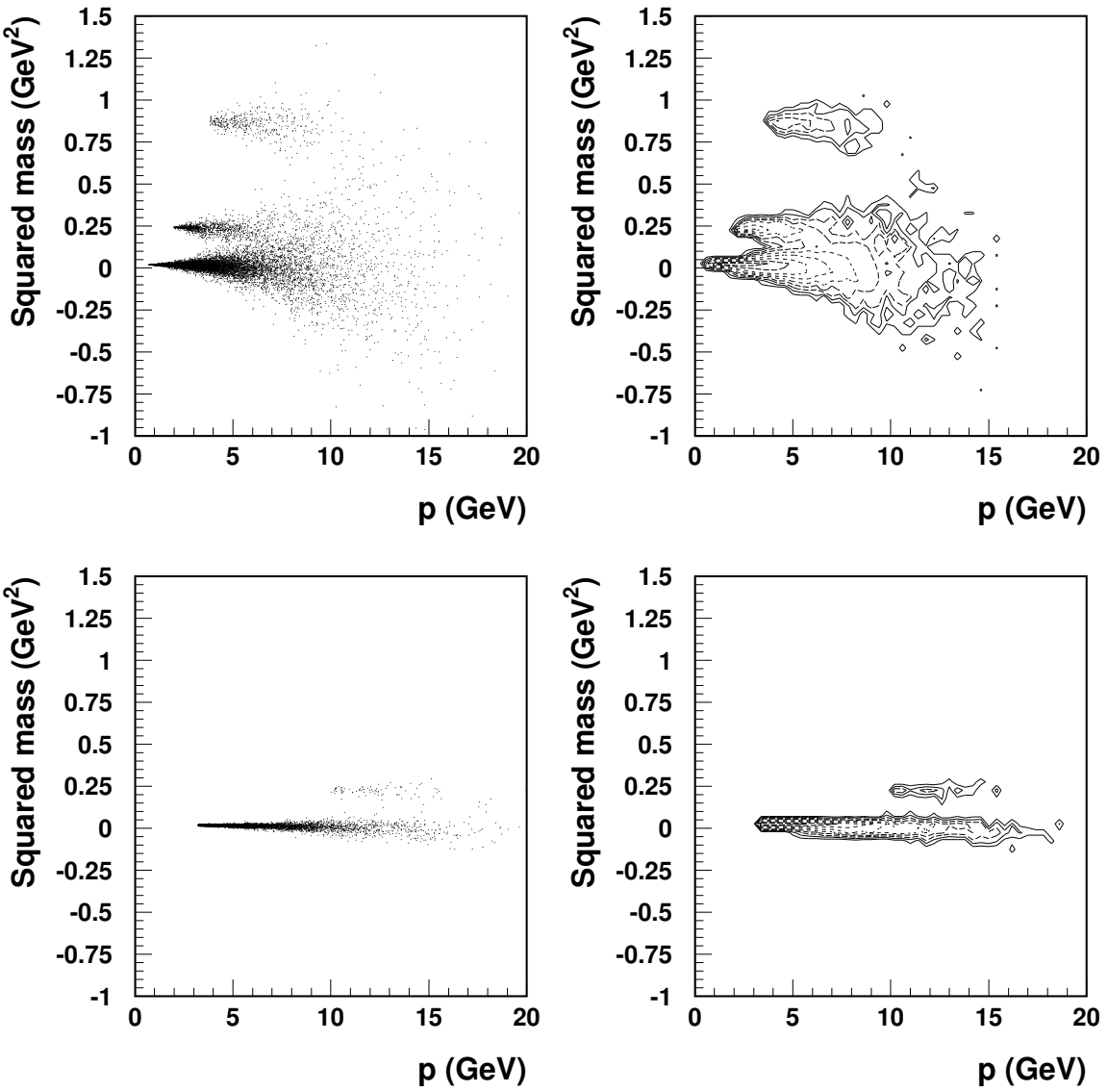

Figure 4.16: Squared mass of hadrons calculated from the Čerenkov angles for aerogel (upper) and gas (lower) from the experimental data as a function of momentum. The left side is a scatter plot and the right side a contour plot for the left figures.

Chapter 5

PID Performance of RICH Detector

The most important performance of the RICH detector is how exactly and efficiently the RICH detector can identify hadrons. The performance is unambiguously estimated by Monte Carlo simulations. Detailed Monte Carlo simulation allows to determine the performance of the RICH detector well.

5.1 Monte Carlo Programs

The Monte Carlo simulation of the RICH detector is performed using the programs of PEPSI [88], JETSET [89] and GEANT [90].

For the simulation, the PEPSI (version 4.21) Monte Carlo event generator, which was developed for HERMES to simulate the longitudinally polarized leptoproduction, is used. PEPSI is based on the program LEPTO (version 6.5.1) [91]. LEPTO is the Monte Carlo event generator for the unpolarized case to simulate the complete events of the deep-inelastic scattering in the electron-nucleon interaction processes like e-p collisions of HERA. For the parton level interaction, LEPTO is based on the standard model of the electroweak cross sections in the leading order for any electron of arbitrary polarization. The program JETSET (version 7.4.10) is included into PEPSI to simulate the hadronization processes, following the LUND string model [92]. The LUND string model was successfully developed to describe the dynamics of the hadronization processes of the quark and gluon jets as well as the properties of the quark flavors. The GEANT program provides the system of the detector description and response and the simulation tools for the tracking of the particles passing through the matter and detector, secondary interactions in the matter like Bremsstrahlung, multiple scattering, bending of the tracks in the magnetic field, particle decays and so on. GEANT (version 3.21) was developed at CERN and used in the field of the high energy physics.

5.2 Optimization of RICH Detector in Software

Some optimizations are performed at the level of software to describe well the properties and behaviors of the RICH detector.

5.2.1 Level of MC Program

Aerogel Tiles

The geometry of the 850 aerogel tiles for both halves of the RICH detector is defined and added into the program. Each tile is described with the individually measured index of refraction and thickness. The shape of the surface of all tiles is approximately expressed in the program by a function, which was derived from the measurement of the shape. Figure 5.1 shows the geometry of the aerogel tiles in the Monte Carlo simulation.

Reflectivities of Mirrors

The problem of the default Monte Carlo simulation of the RICH detector was to overestimate the number of fired PMTs for both aerogel and gas compared to the experimental data. The solution of this problem was approached as follows [93]: If the reflectivities of the mirrors of the RICH detector is artificially degraded in the Monte Carlo simulation, the number of fired PMTs in the Monte Carlo simulation can be brought close up to the level of the experimental data.

It is assumed that the 16 individual mirrors of the mirror arrays in both detector halves have different reflectivities. Their difference has impact on the number of fired PMTs in the photon detector, therefore on the identification of hadrons. The artificial reflectivity of each mirror can be estimated by comparing the number of fired PMTs between the experimental data and the Monte Carlo data if in the Monte Carlo simulation the reflectivities of all mirrors are set to 100 %. Since the radius of the gas ring is smaller than the one of the aerogel ring at the same momentum of the same type of the particle, it is convenient for this estimate to use the number of fired PMTs for the gas because the Čerenkov photons emitted in the gas can go in one mirror unlike the photons emitted in the aerogel. For this study the pions with the momentum from 4.5 GeV to 8.5 GeV are used because the pion tracks in this range of momentum are well identified as true pions and spread over the large area of the mirror array. The number of fired PMTs for such pions was compared between the experimental data and Monte Carlo data to derive the reflectivities of each mirror. As a result the values of the reflectivity from 42 % to 78 % was determined and added into the Monte Carlo program. Although the values are not real reflectivities but artificial ones of the mirrors, the number of fired PMTs in the Monte Carlo simulation is improved and approaches the real one of the experiment for both aerogel and gas.

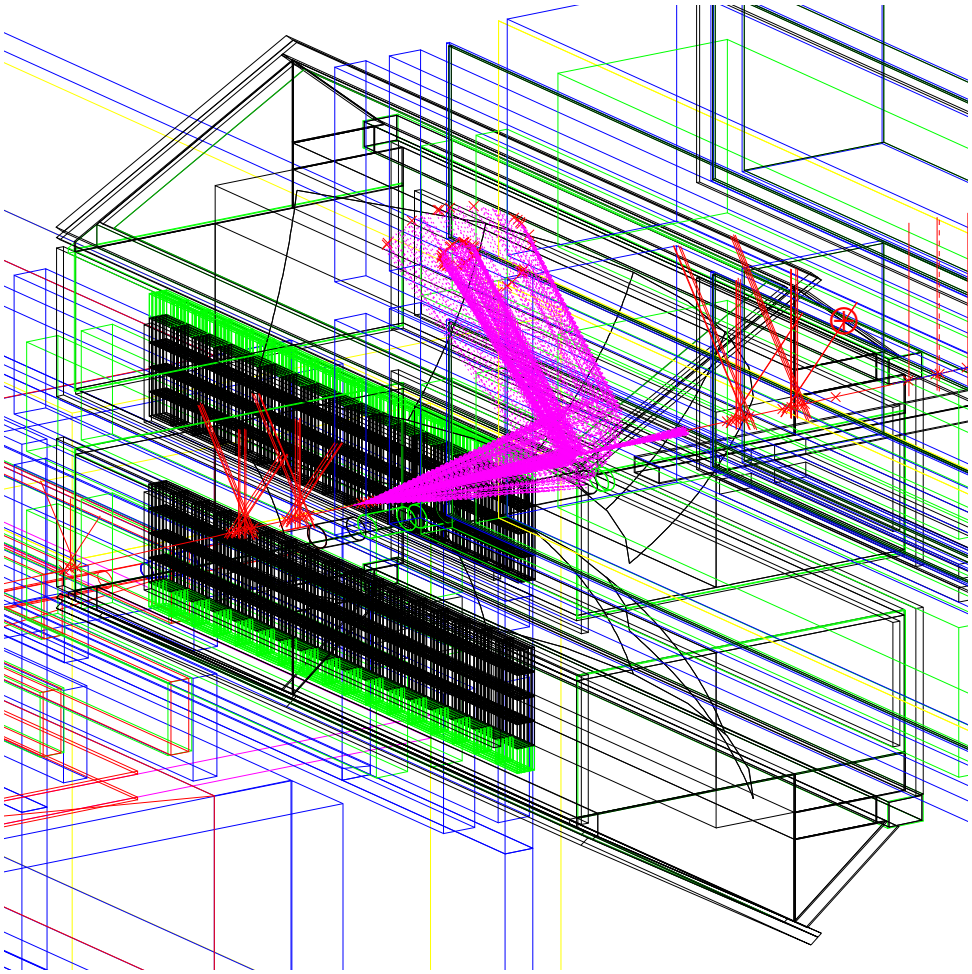

Figure 5.1: Schematic view of the geometry of the aerogel tiles in the RICH detector realized on the Monte Carlo program. In the picture the particle passing through the aerogel tiles at the entrance window and the gas in the main volume in the upper part of the RICH detector emits the Čerenkov light. The light is reflected on the mirror array in the box and detected on the photon detector. In the plane of the photon detector the larger ring comes from the aerogel and smaller ring from the gas.

5.2.2 Level of Reconstruction

Reconstructed Angle for Aerogel

The Čerenkov photons for the aerogel is refracted at the boundary between aerogel and C_4F_{10} gas radiators, so that the angles for the aerogel are reconstructed at larger angles, which are, however, not real angles, if this effect is not taken into account.

The refractions between the aerogel and dry N_2 gas cancels out in the sequential refractions of themselves. In the experiment one does not know the emission point of the Čerenkov photons in the radiators, while the Monte Carlo simulation gives the point. From the requirement to treat the Monte Carlo data with the same approach as the experimental data the Čerenkov photons are assumed to be emitted in the middle of the aerogel layer in both data of the experiment and Monte Carlo. The IRT method does not take care of the conditions between the emission point and mirror surface. Therefore the angles for the aerogel are corrected for the reconstruction of the angles by the IRT method. The code [87] of the correction is added into the reconstruction program in the IRT method. Figure 4.13 in the previous chapter is for the result of the correction. The result reproduces the measured index of refraction $n = 1.0304$ for the aerogel well.

Background

As mentioned in chapter 4, several sources of the background photons exist. The background photons are hard to simulate in the Monte Carlo. One of the sources of the background in the experimental data are the trackless rings. They contribute as the background photons. The background photons of the trackless rings are extracted from the experimental data in the deuterium target and added into the Monte Carlo data to realize a more realistic structure of the data [85].

5.3 Event Generation and Performance in Monte Carlo

5.3.1 Event Generation

The event generation of the Monte Carlo with the geometry of the aerogel tiles was performed in the mode of the deep-inelastic scattering taking into account all effects mentioned above. Additionally both deuterium target and HERA electron beam with the energy of 27.5 GeV have different modes of their polarizations. The number of the produced events is 2.52 millions. Out of this number of events 1.73 millions tracks have been reconstructed. Finally about 842 k hadron tracks are available to study the performance for the particle identification of the RICH detector after the separation of the tracks between hadrons and electrons. The separation of hadrons and leptons will be described in section 6.3.1.

5.3.2 Performance

In the Monte Carlo simulation all types of the generated hadrons are defined and already known, which is called the GEANT particle type [90]. Figure 5.2 shows the momentum distributions for pions, kaons and protons in the GEANT particle type as well as all hadrons. Almost all tracks are with momenta below 15 GeV. Of all hadron

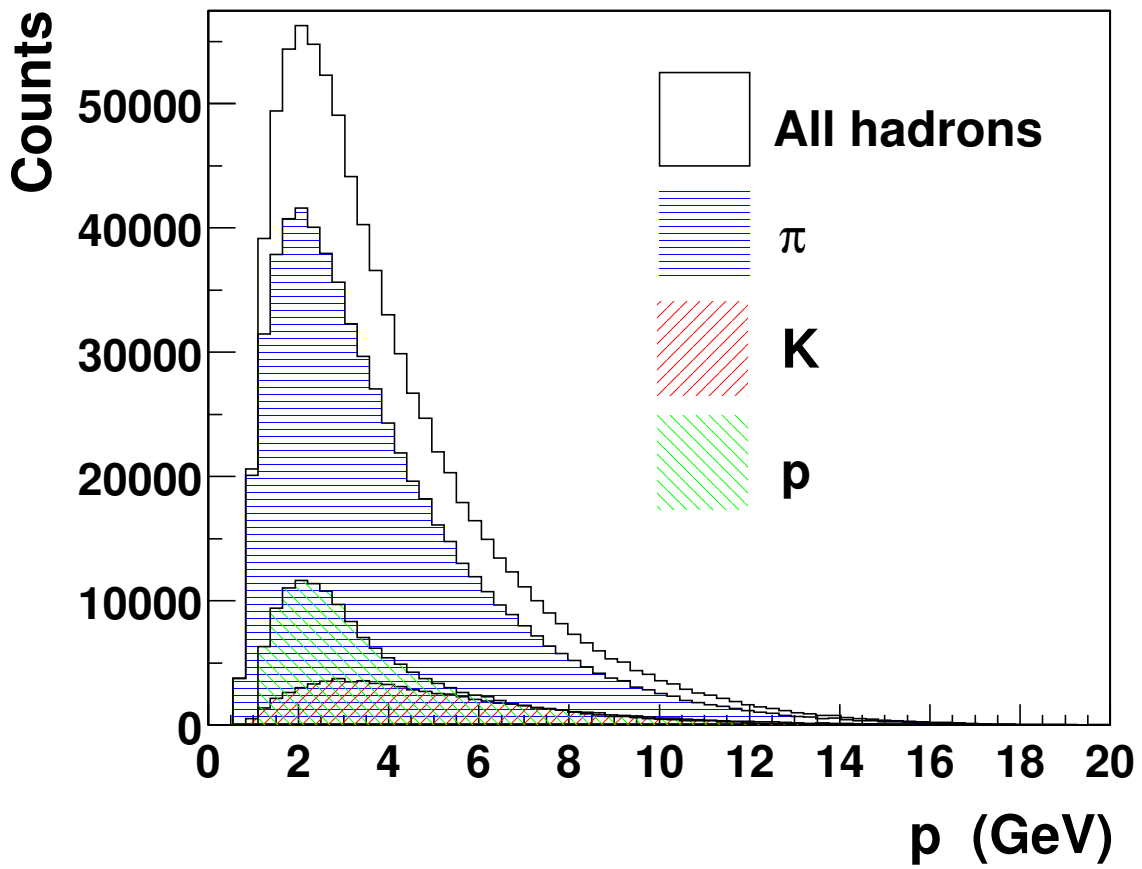

Figure 5.2: Momentum distributions for pions, kaons and protons in the GEANT particle type as well as all hadrons. The number of the tracks for all hadrons is about 842 k.

tracks pions occupy large number of the tracks over the whole range of momentum. The number of tracks for protons is larger than that of kaons, especially at the range from 2 to 6 GeV. The tracks of kaons and protons are very few above 12 GeV. Both the Čerenkov angle and the number of fired PMTs for aerogel and gas in the single tracks of electrons are compared between the experimental and Monte Carlo data in figures 5.3 and 5.4. In figure 5.3 the mean value of the Čerenkov angle for the aerogel is in good agreement between the experiment and Monte Carlo simulation. The difference is seen in the width of the tail. The wider tail in the Monte Carlo simulation mainly comes from the contribution of the sharply curved surfaces near the edge of the aerogel tiles, which is presented in table 4.4. For the Čerenkov angle for the gas the mean value does not completely agree between both. In figure 5.4 the number of fired PMTs in the Monte Carlo simulation is still overestimated for the aerogel compared to the experimental one though the reflectivities of the mirrors of the RICH detector are artificially degraded in the Monte Carlo simulation [93].

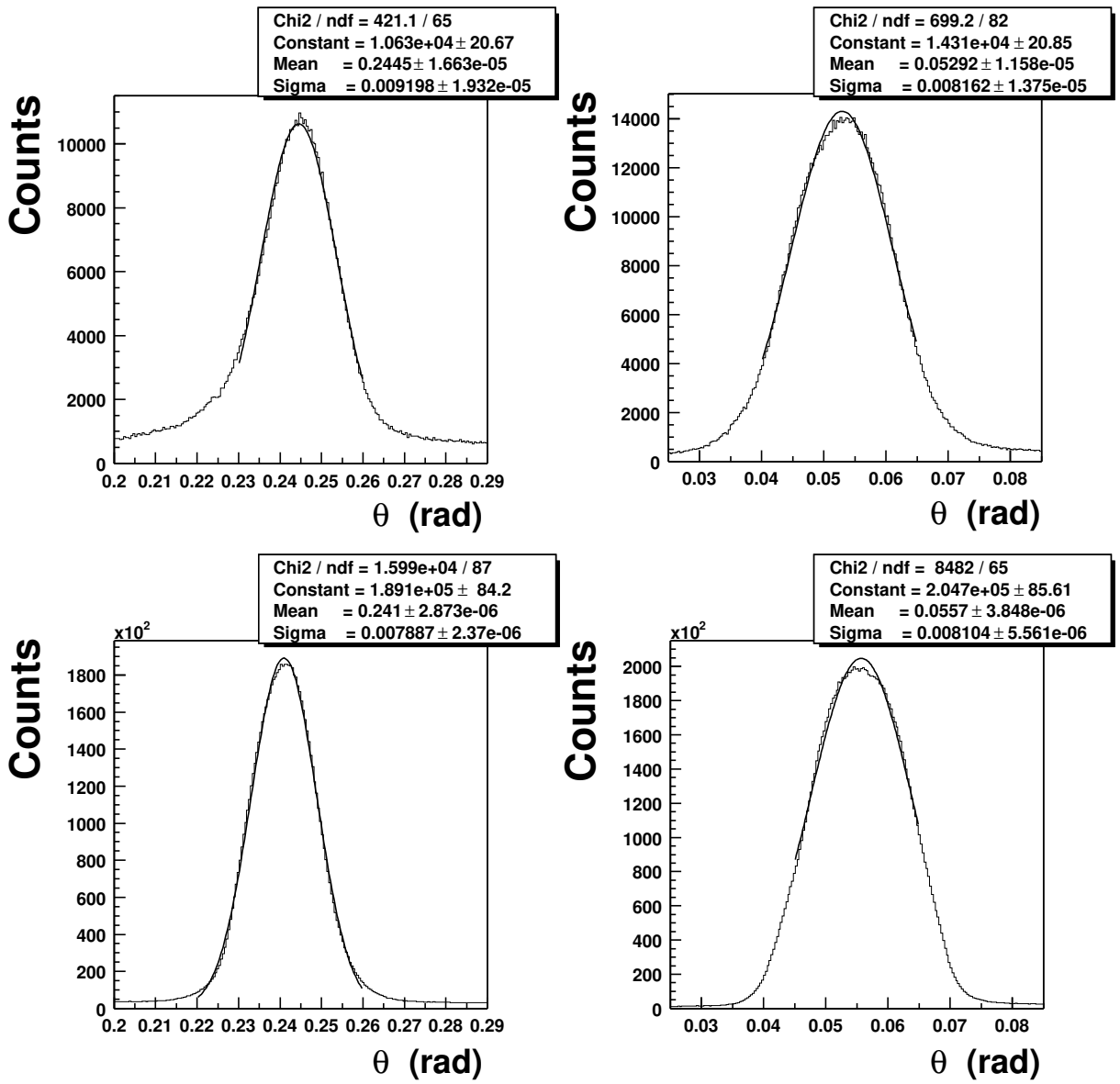

Figure 5.3: Histograms of the Čerenkov angle for aerogel (left) and gas (right) for the single tracks of electrons compared between the experimental (upper) and Monte Carlo data (lower). The distributions are fitted with the Gaussian. The numerical tables represent the values of the Gaussian fit.

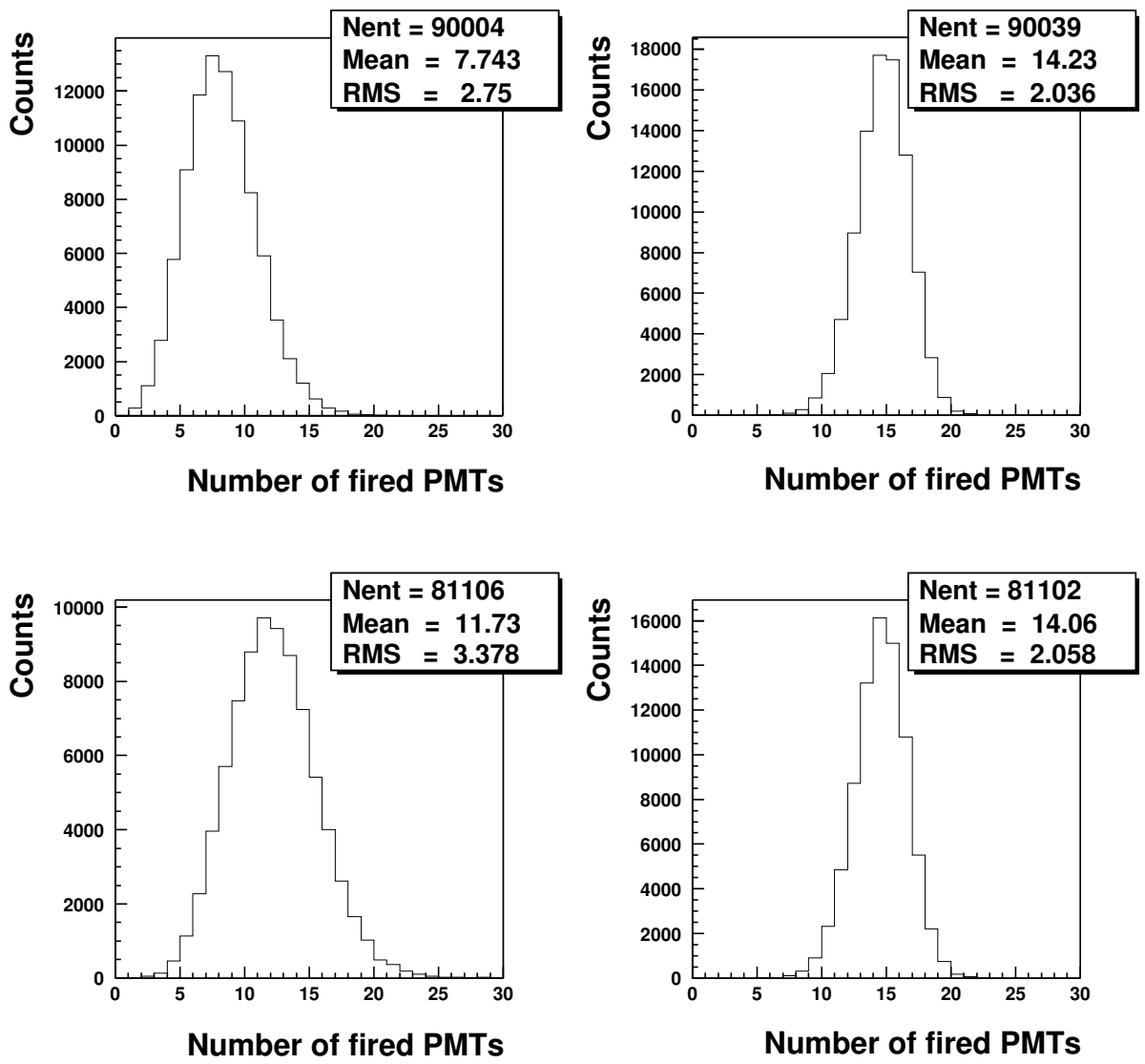

Figure 5.4: Histograms of the number of fired PMTs for aerogel (left) and gas (right) for the single tracks of electrons compared between the experimental (upper) and Monte Carlo data (lower).

5.4 Definitions of Identification Efficiencies and Probabilities

The identification efficiency and probability are the most important and fundamental properties for the estimate of the performance of the RICH detector. As mentioned above the 842 k tracks of hadrons in the MC data are used to study for the estimate. The identification efficiency and probability are defined below.

5.4.1 Definitions

When one tries to know the type of a particle (π, K, p) in the experiment by using a certain detector with the ability of the particle identification like the RICH detector the type of the particle can be determined with a certain efficiency and a certain probability unless a perfect system for the particle identification exists. To know the efficiency and probability the technique of the Monte Carlo simulation is well used because in the simulation all types of the particles are already known and labeled. Each particle has a true type labeled by the Monte Carlo simulation, which corresponds to the so-called GEANT particle type. Additionally each particle is assigned to the identified type of the particle by the detector of the experiment or of the Monte Carlo simulation. Now for the estimate of the performance of the particle identification it is convenient that a certain observable A with two indices is defined as follows:

$$\begin{array}{ll} A_t^i & \begin{array}{l} \leftarrow \text{identified particle type} \\ \leftarrow \text{true particle type} \end{array} \end{array} \tag{5.1}$$

This means that:

> A is a certain observable of the true particle type t labeled with the Monte Carlo simulation and that is identified as the particle type i by the detector of the experiment or Monte Carlo simulation.

If the observable is the number of the particle N like N_π^{K}, this means the number of the true pions labeled with the Monte Carlo simulation and that is identified as kaons with the detector of the experiment or of the Monte Carlo simulation.

Identification Efficiencies

Now the observable A is interpreted as the number of the particle type N_t^i. Then the identification efficiencies P_t^i are defined as:

$$P_t^i = \frac{N_t^i}{\sum_j N_t^j}. \tag{5.2}$$

The superscript j runs over all identified particle types. It means that the ratio of the number of an identified particle type i to the total number of all identified particle types for a certain true particle type t. As the RICH detector identifies pions (π), kaons (K) and protons (p), the matrix P is written as:

$$\mathsf{P} = \mathsf{P}(\pi, \mathrm{K}, \mathrm{p}, \mathrm{X}) = \begin{pmatrix} P_\pi^\pi & P_\mathrm{K}^\pi & P_\mathrm{p}^\pi \\ P_\pi^\mathrm{K} & P_\mathrm{K}^\mathrm{K} & P_\mathrm{p}^\mathrm{K} \\ P_\pi^\mathrm{p} & P_\mathrm{K}^\mathrm{p} & P_\mathrm{p}^\mathrm{p} \\ P_\pi^\mathrm{X} & P_\mathrm{K}^\mathrm{X} & P_\mathrm{p}^\mathrm{X} \end{pmatrix}, \tag{5.3}$$

where X is the unidentified particle type. In equation (5.3) the diagonal elements of P_π^π, P_K^K and P_p^p are the identification efficiencies for pions, kaons and protons

respectively. Other elements represent the probabilities of the misidentification. The matrix P with 3×3 elements can be formed if the particle type of X is not taken into account:

$$\mathsf{P} = \mathsf{P}(\pi, \mathrm{K}, \mathrm{p}) = \begin{pmatrix} P_\pi^\pi & P_\mathrm{K}^\pi & P_\mathrm{p}^\pi \\ P_\pi^\mathrm{K} & P_\mathrm{K}^\mathrm{K} & P_\mathrm{p}^\mathrm{K} \\ P_\pi^\mathrm{p} & P_\mathrm{K}^\mathrm{p} & P_\mathrm{p}^\mathrm{p} \end{pmatrix}. \tag{5.4}$$

After this the particle type of X is disregarded. By the definition of equation (5.2) the sum of the elements of each column should be one:

$$\sum_i P_t^i = 1. \tag{5.5}$$

Identification Probabilities

The identification probabilities are defined as:

$$Q_t^i = \frac{N_t^i}{\sum_s N_s^i}. \tag{5.6}$$

The subscript s runs over all true particle types. Above equation means the ratio of the number of a true particle type t to the total number of all true particle types for a certain identified particle type i. The matrix of Q_t^i for pions, kaons and protons can be formed as:

$$\mathsf{Q} = \mathsf{Q}(\pi, \mathrm{K}, \mathrm{p}) = \begin{pmatrix} Q_\pi^\pi & Q_\pi^\mathrm{K} & Q_\pi^\mathrm{p} \\ Q_\mathrm{K}^\pi & Q_\mathrm{K}^\mathrm{K} & Q_\mathrm{K}^\mathrm{p} \\ Q_\mathrm{p}^\pi & Q_\mathrm{p}^\mathrm{K} & Q_\mathrm{p}^\mathrm{p} \end{pmatrix}. \tag{5.7}$$

In equation (5.7) the diagonal elements of Q_π^π, Q_K^K and Q_p^p are the identification probabilities, which mean the purities of a true particle type to all particle types identified. The off-diagonal elements in equation (5.7) correspond to the identification contaminations. Similarly to the identification efficiencies, by the definition of equation (5.6) the sum of the elements of each column should be one:

$$\sum_t Q_t^i = 1. \tag{5.8}$$

It is convenient that the off-diagonal elements are written in the different expressions of Q_t^i:

$$c_t^i = Q_t^i, \qquad \text{where } t \neq i. \tag{5.9}$$

Then it follows:

$$Q_i^i = 1 - \sum_{\substack{t \\ (t \neq i)}} c_t^i. \tag{5.10}$$

From now the Q_t^t is called the identification purities and the c_t^i $(t \neq i)$ the identification contaminations.

When the total number of all particles $N_{\rm total}$ is written as:

$$N_{\rm total} = \sum_t \sum_i N_t^i, \tag{5.11}$$

the flux factor ϕ_t is expressed as:

$$\phi_t = \frac{\sum_i N_t^i}{N_{\rm total}}. \tag{5.12}$$

ϕ_t means the ratio of the total number of a true particle to the total number of all particles. Then another expression of Q_t^i is written as:

$$Q_t^i = \frac{P_t^i \cdot \phi_t}{\sum_s P_s^i \cdot \phi_s}. \tag{5.13}$$

When the numbers of the identified particles I^i for pions, kaons and protons are written as:

$$\vec{\mathsf{I}} = (I^\pi, I^{\rm K}, I^{\rm p}) \tag{5.14}$$

and the numbers of the true particles N_t as:

$$\vec{\mathsf{N}} = (N_\pi, N_{\rm K}, N_{\rm p}), \tag{5.15}$$

the relationships are given:

$$\vec{\mathsf{I}} = \mathsf{P} \cdot \vec{\mathsf{N}}, \tag{5.16}$$

$$\vec{\mathsf{N}} = \mathsf{Q} \cdot \vec{\mathsf{I}}. \tag{5.17}$$

This does not necessarily mean $\mathsf{P}^{-1} = \mathsf{Q}$. This relationship is expressed in a determinant as follows:

$$\left| \mathsf{P} \cdot \mathsf{Q} - 1 \right| = 0. \tag{5.18}$$

5.4.2 Quality Parameters

The likelihood [84, 85, 86] from the IRT method is available to judge the confidence of the identified particle type by the RICH detector. As the index of the confidence the quality parameter rQp, which has a real number, is defined as:

$$rQp = \log_{10}\left(\frac{L_1}{L_2}\right), \tag{5.19}$$

where L_1 and L_2 are the likelihoods of the most likely particle type hypothesis and of the second likely particle type hypothesis. If $L_1 = L_2$, rQp is set to be zero and then X of the unidentified particle type by the RICH detector is assigned. Figure 5.5 shows the distributions of rQp for pions, kaons and protons in the experimental data as a function of momentum. As it is known from the figures the value of

rQp for pions is higher in the region from 3 GeV, which corresponds to the pion momentum threshold for gas, to about 12 GeV where kaons can produce enough Čerenkov photons in gas because in this region the information of Čerenkov angles for both aerogel and gas is available for pions. The value of rQp for kaons is generally higher in the region from 10 GeV to 13.5 GeV, where the information of the kaon identification in both aerogel and gas is available. For protons rQp in the region lower than 3.5 GeV is due to the sub-threshold likelihood [84, 85, 86] of protons below the momentum threshold. The value of rQp for protons in the region more than about 9.5 GeV to 16.5 GeV goes up because in the region protons do not emit Čerenkov photons in gas and pions and kaons are distinguished from protons by the information of Čerenkov angle for pions and kaons in gas.

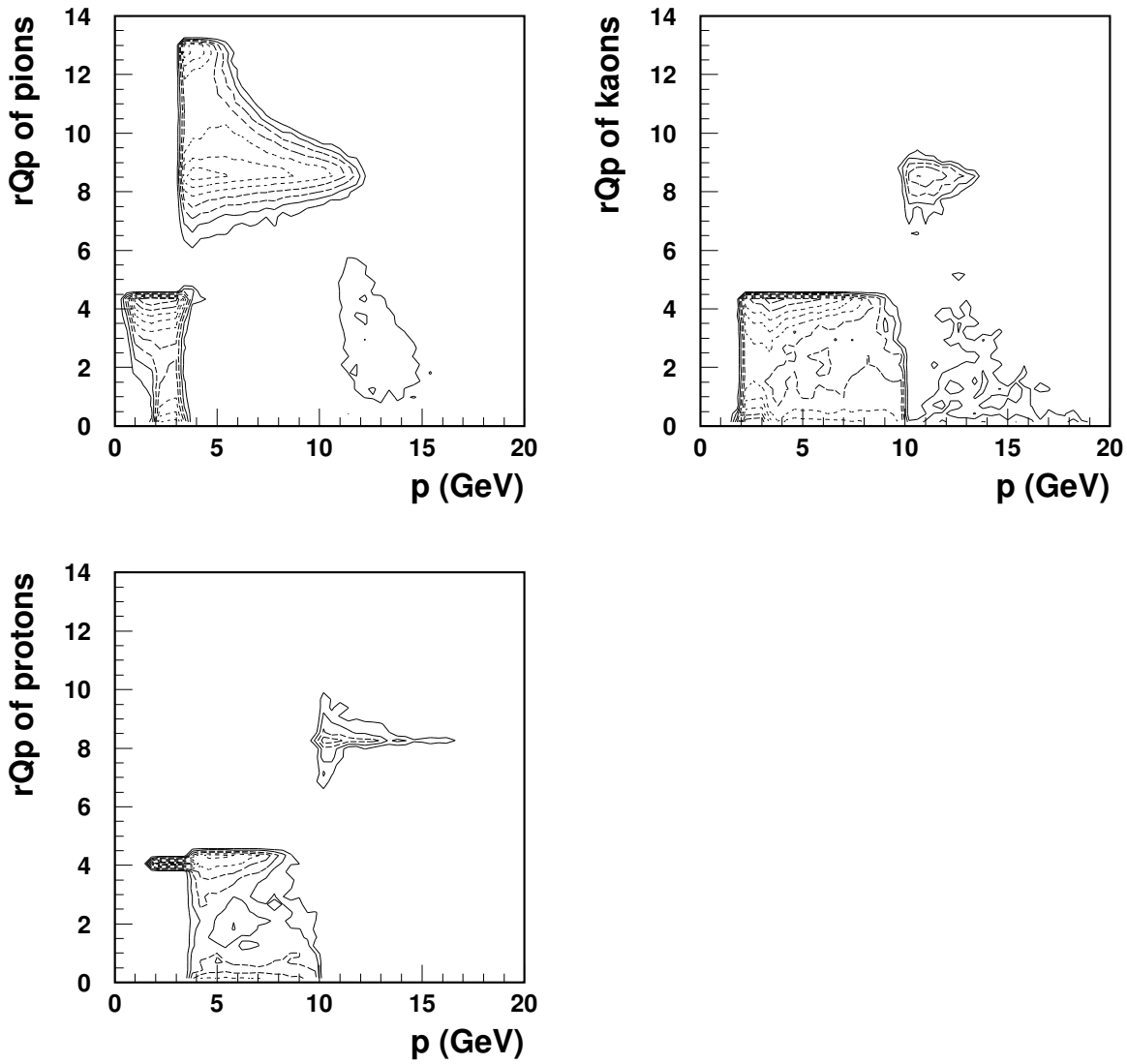

Figure 5.5: rQp distributions for particles identified as pions, kaons and protons as a function of momentum. The results of each distribution are obtained from the experimental data.

5.5 Results of Identification Efficiencies, Purities and Contaminations

5.5.1 Conditions

The analysis of the identification efficiencies, purities and contaminations takes some conditions into account:

- The momentum of the particle tracks because the particle type hypothesis based on the likelihood analysis depends on the reconstructed angles, which depend on the momentum of the tracks,
- the quality parameter rQp because it depends on the likelihoods,
- and the number of the tracks per detector half of the RICH detector because the multiple rings by the multiple tracks in the detector half contribute as background for one another and as a result affect the efficiencies, purities and contaminations.

For the first item the momenta of the tracks are divided into bins taking statistics of hadrons into account. According to the distributions in figure 5.2 the ranges of the momentum with large statistics are more finely divided than the other ranges. Table 5.1 shows the width of each bin in the different momentum regions.

Momentum range	Width of bin
0 - 2 GeV	per 0.5 GeV
2 - 6 GeV	per 0.25 GeV
6 - 10 GeV	per 0.5 GeV
10 - 15 GeV	per 1 GeV
15 GeV -	defined as one bin

Table 5.1: Width of each bin in the different momentum regions. For momenta greater than 15 GeV one bin is assigned.

For the second item the identification efficiencies, purities and contaminations are studied in $rQp > 0.0$, > 0.5 and > 1.0. The analyses in these values of rQp mean that the unidentified particle type X by the RICH detector is excluded.

For the third item the numbers of the tracks $N_{\text{tracks}} = 1$, $= 2$ and > 2 per detector half of the RICH detector are taken into account. $N_{\text{tracks}} = 1$ occupies most of the numbers of the tracks. $N_{\text{tracks}} \leq 2$ meets most of the cases.

5.5.2 Comparison of Charge Dependence

The identification efficiencies in $rQp > 0.0$ are compared between the positively and negatively charged particles taking into account the number of the tracks per

detector half of the RICH detector. The results in figures 5.6, 5.7 and 5.8 show the comparison of the identification efficiencies between the positively and negatively charged particles. The identification efficiencies between both types for the charged particles are in agreement within the statistical uncertainties and have no charge dependence in almost the whole range of momentum. Finally the identification probabilities as well as the identification efficiencies are studied combining both statistics of the positively and negatively charged particles to determine their values with higher precision.

5.5.3 Results available for Analysis of Asymmetry

The identification efficiencies and probabilities of all charged particles are studied with different quality parameters of $rQp > 0.0$, > 0.5 and > 1.0. To survey the identification efficiencies and probabilities the results of both efficiencies in $rQp > 0.0$ are shown here for the different numbers of tracks per detector half of the RICH detector. The numerical values of the efficiencies in other rQp are given in appendix D. Figures 5.9, 5.10 and 5.11 show the identification efficiencies for the different numbers of the tracks. For $N_{\text{tracks}} = 1$, 2 and ≥ 2 the identification efficiencies for pions are very close to 1 in the whole range of momentum except for the region from 2 GeV to 3 GeV. In this region the identification efficiencies for pions drop 25 % at maximum in $N_{\text{tracks}} \geq 2$ because kaons emit the Čerenkov photons from 2 GeV. The identification efficiencies for kaons reach more than 80 % in almost the whole momentum region for $N_{\text{tracks}} = 1$ and about 80 % in the region from 3 GeV to 12 GeV for $N_{\text{tracks}} = 2$. The dip of the efficiencies around 10 GeV is due to the threshold of kaons for the gas. The identification efficiencies for protons are more than about 80 % in almost the whole range of momentum for $N_{\text{tracks}} = 1$ and fall as the number of the tracks increases. Figures 5.12, 5.13 and 5.14 show the identification probabilities for each N_{tracks}. The identification probabilities for pions are almost 1 in almost the whole range of momentum for $N_{\text{tracks}} = 1$. The main contamination of pions is due to protons in the region from 1.5 GeV to 3 GeV, where protons have sub-threshold likelihood. In the region higher than 12 GeV kaons contaminate pions. For $N_{\text{tracks}} = 1$ the identification probabilities for kaons reach more than 70 % in the region higher than 3.25 GeV and increase as the momentum is higher. The kaons are contaminated by both pions and protons in the region lower than about 3 GeV. In the region higher than 3 GeV the main contamination of kaons is due to protons. The identification probabilities for protons is more than 65 % in almost the whole range of momentum for each N_{tracks}. The results of the identification efficiencies and probabilities in the different rQp are available for the corrections of the contaminations between hadrons, therefore of the spin asymmetry.

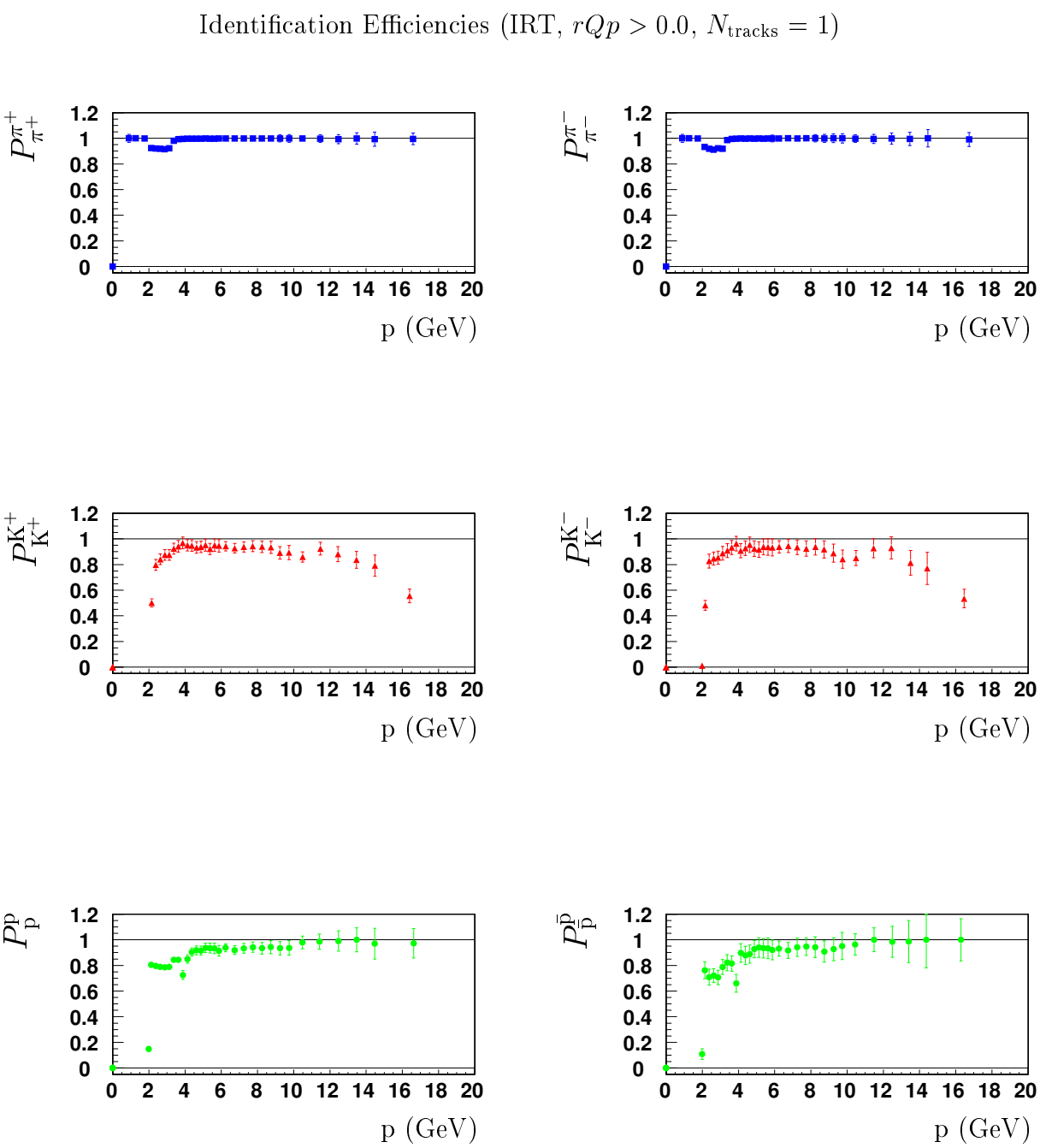

Figure 5.6: Comparison of the identification efficiencies between positively and negatively charged particles in $N_{\mathrm{tracks}} = 1$ at $rQp > 0.0$. The left and right sides are the results for the positively and negatively charged particles respectively. From upper to lower figures the results for pions, kaons and protons are shown.

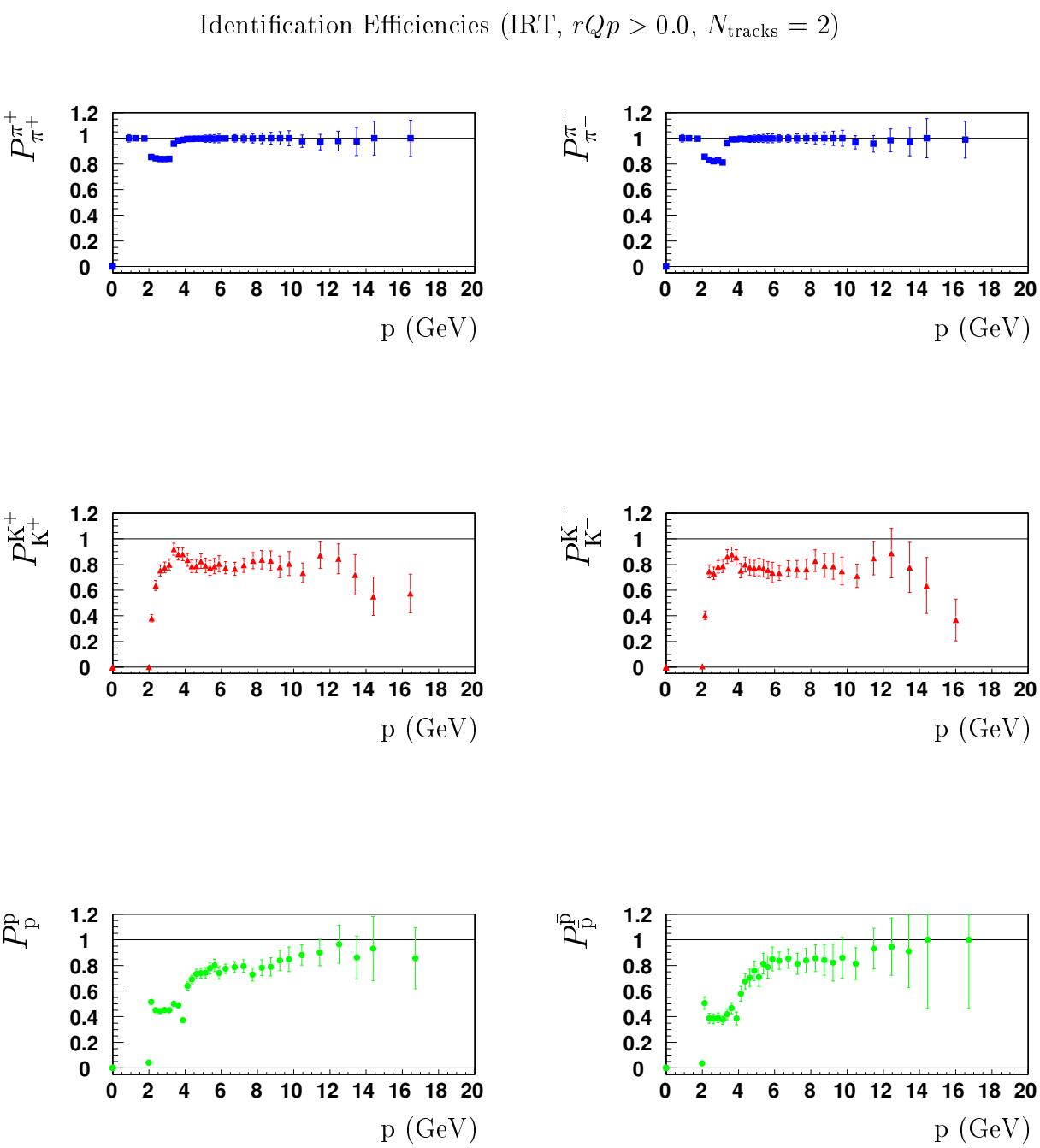

Figure 5.7: Comparison of the identification efficiencies between positively and negatively charged particles in $N_{\text{tracks}} = 2$ at $rQp > 0.0$. The left and right sides are the results for the positively and negatively charged particles respectively. From upper to lower figures the results for pions, kaons and protons are shown.

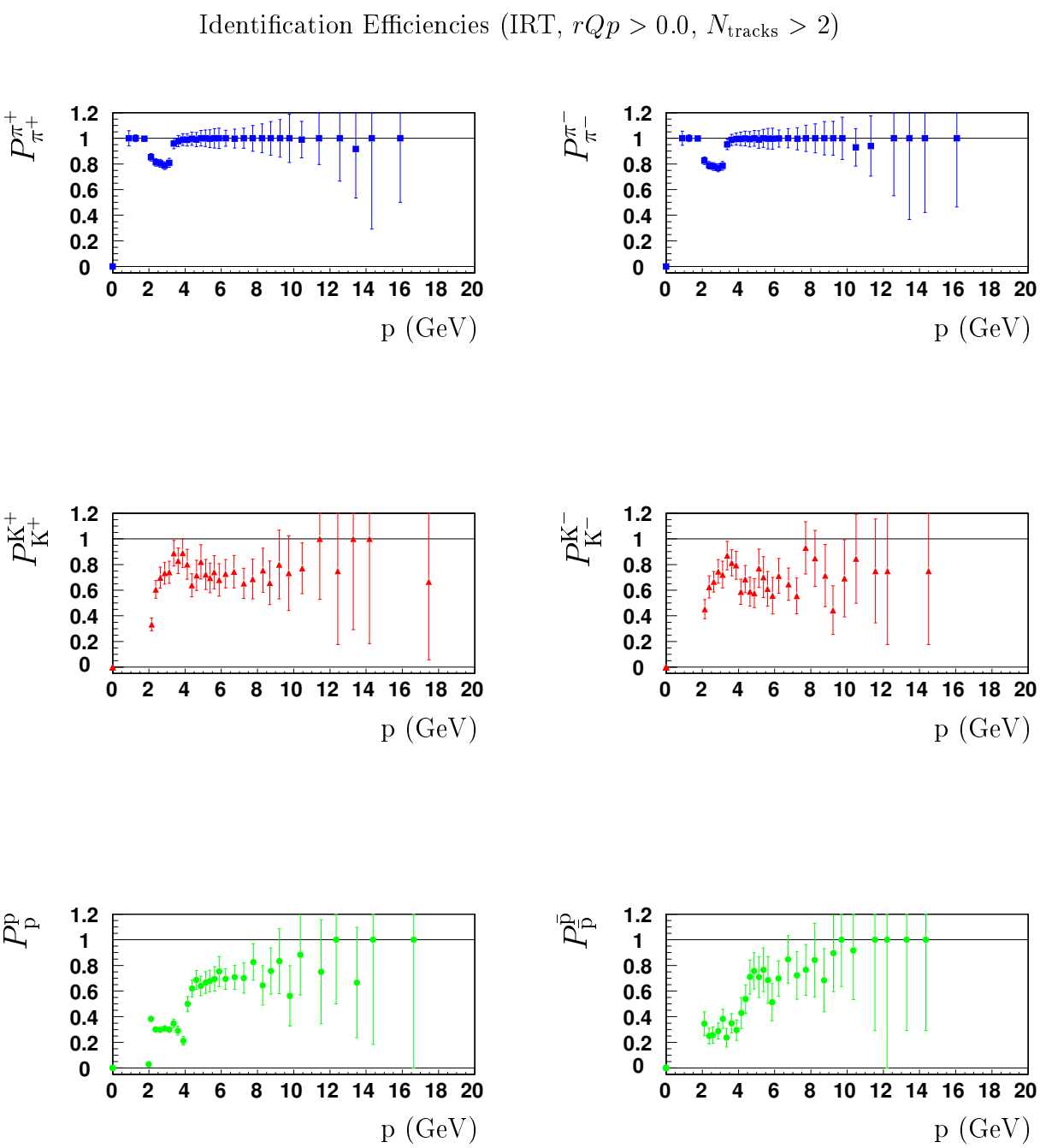

Figure 5.8: Comparison of the identification efficiencies between positively and negatively charged particles in $N_{\text{tracks}} > 2$ at $rQp > 0.0$. The left and right sides are the results for the positively and negatively charged particles respectively. From upper to lower figures the results for pions, kaons and protons are shown.

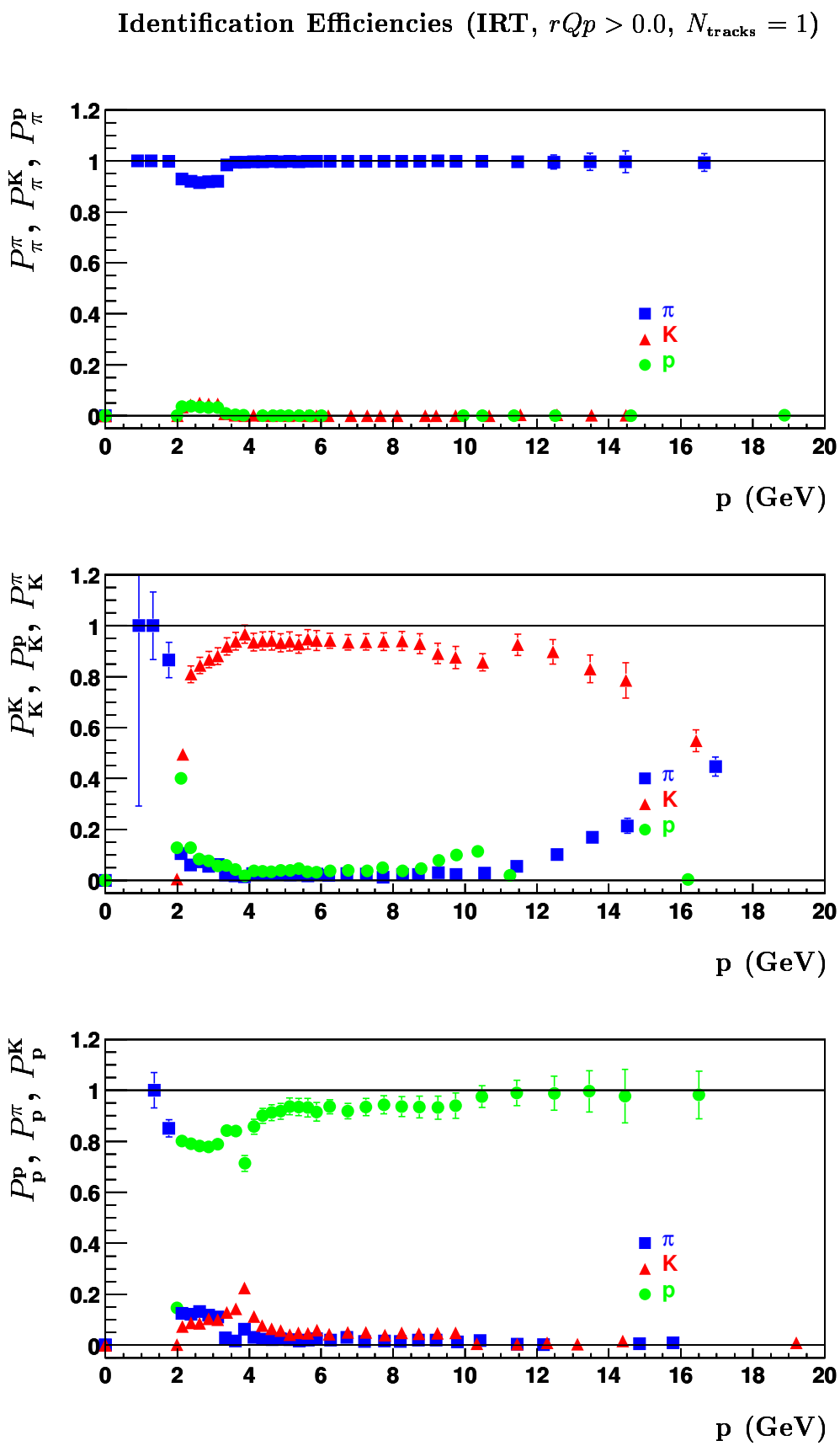

Figure 5.9: Identification efficiencies for pions (P^i_π, squares), kaons (P^i_{K}, triangles) and protons (P^i_{p}, circles) in $N_{\mathrm{tracks}} = 1$ at $rQp > 0.0$, where $i = \pi$, K, p.

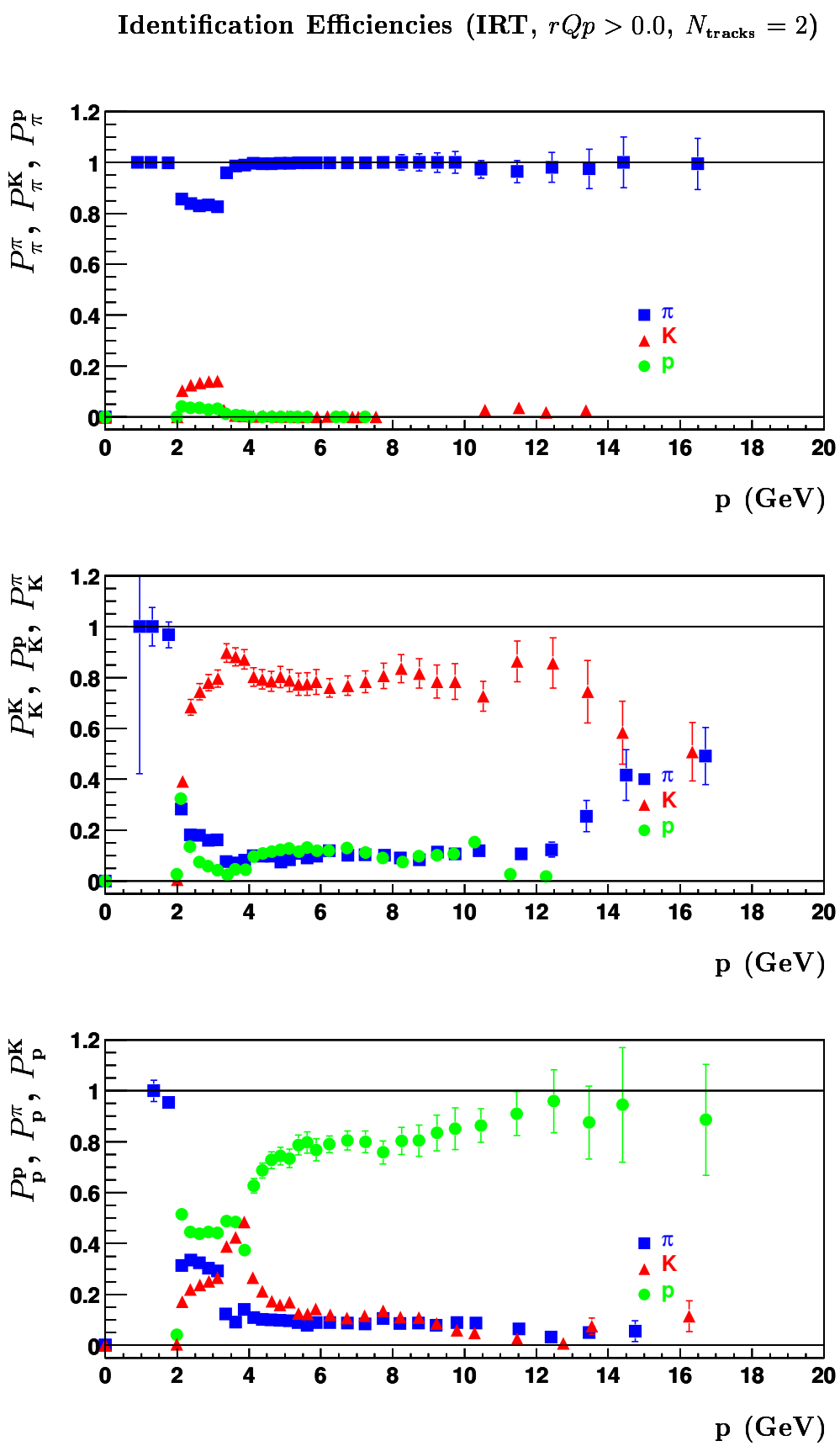

Figure 5.10: Identification efficiencies for pions (P^i_π, squares), kaons (P^i_{K}, triangles) and protons (P^i_{p}, circles) in $N_{\text{tracks}} = 2$ at $rQp > 0.0$, where $i = \pi$, K, p.

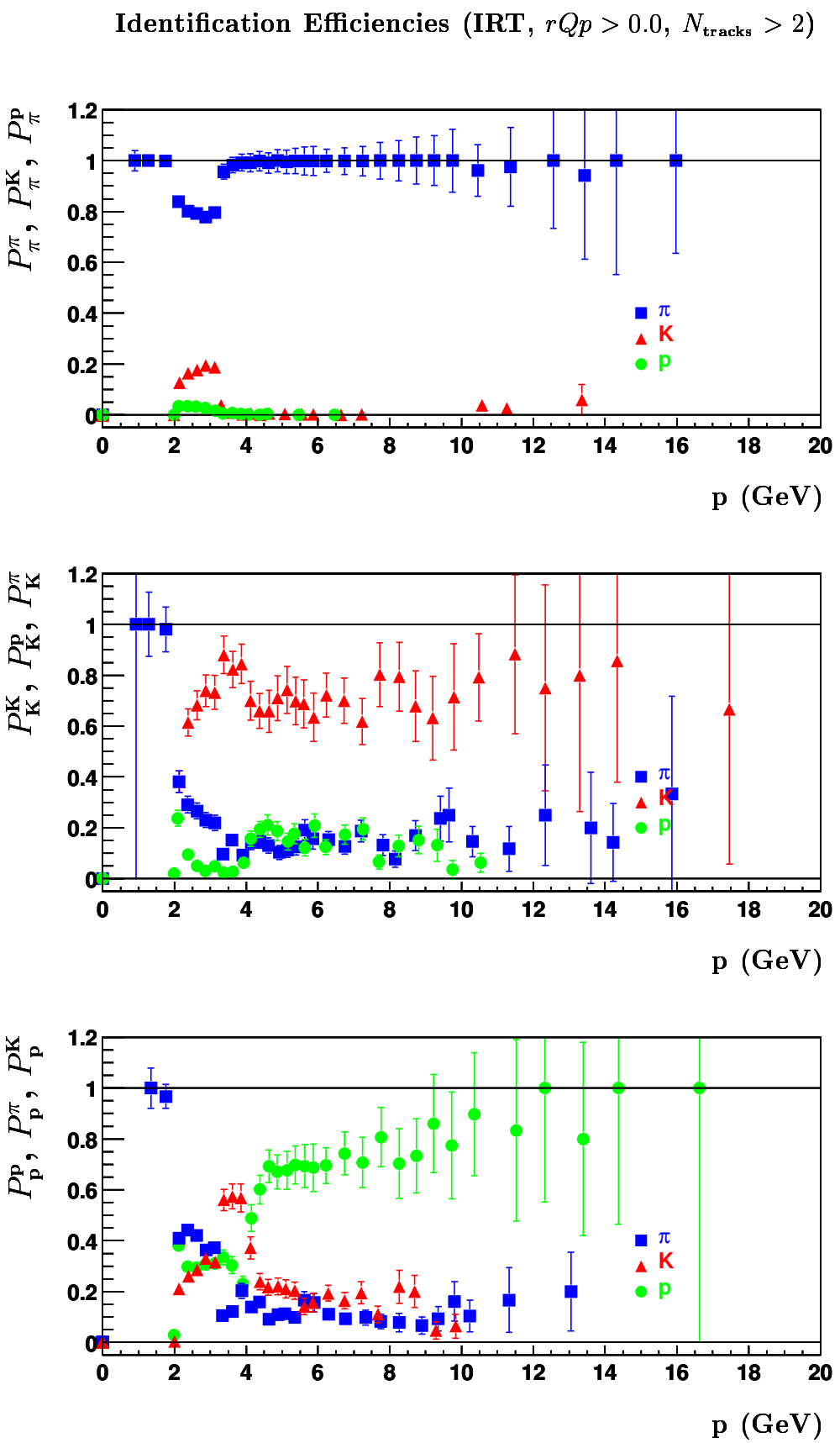

Figure 5.11: Identification efficiencies for pions (P^i_π, squares), kaons (P^i_{K}, triangles) and protons (P^i_{p}, circles) in $N_{\text{tracks}} > 2$ at $rQp > 0.0$, where $i = \pi$, K, p.

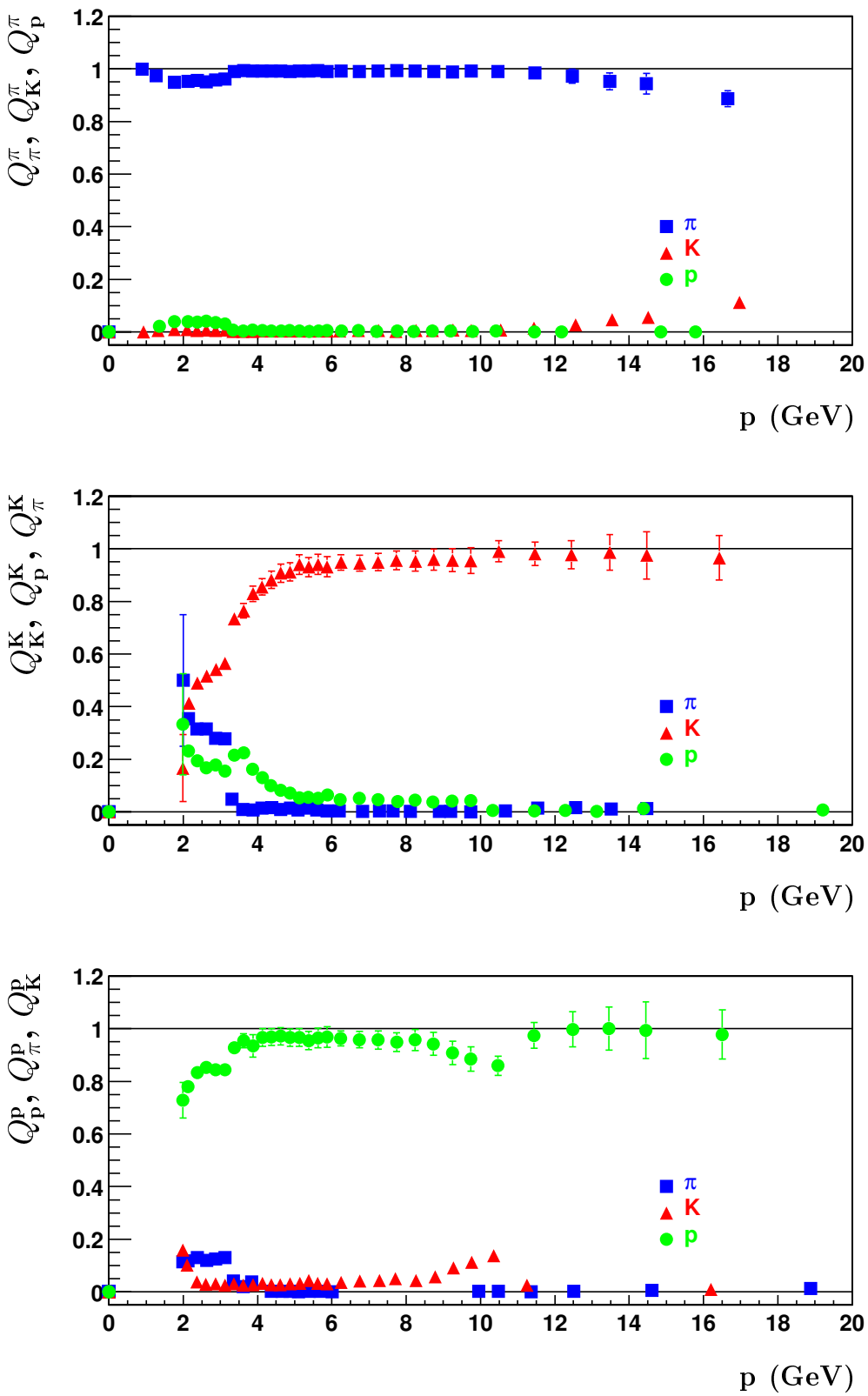

Figure 5.12: Identification purities and contaminations for pions (Q^{π}_{t}, squares), kaons (Q^{K}_{t}, triangles) and protons (Q^{p}_{t}, circles) in $N_{\text{tracks}} = 1$ at $rQp > 0.0$, where $t = \pi$, K, p.

Identification Purities and Contaminations (IRT, $rQp > 0.0$, $N_{\mathrm{tracks}} = 2$)

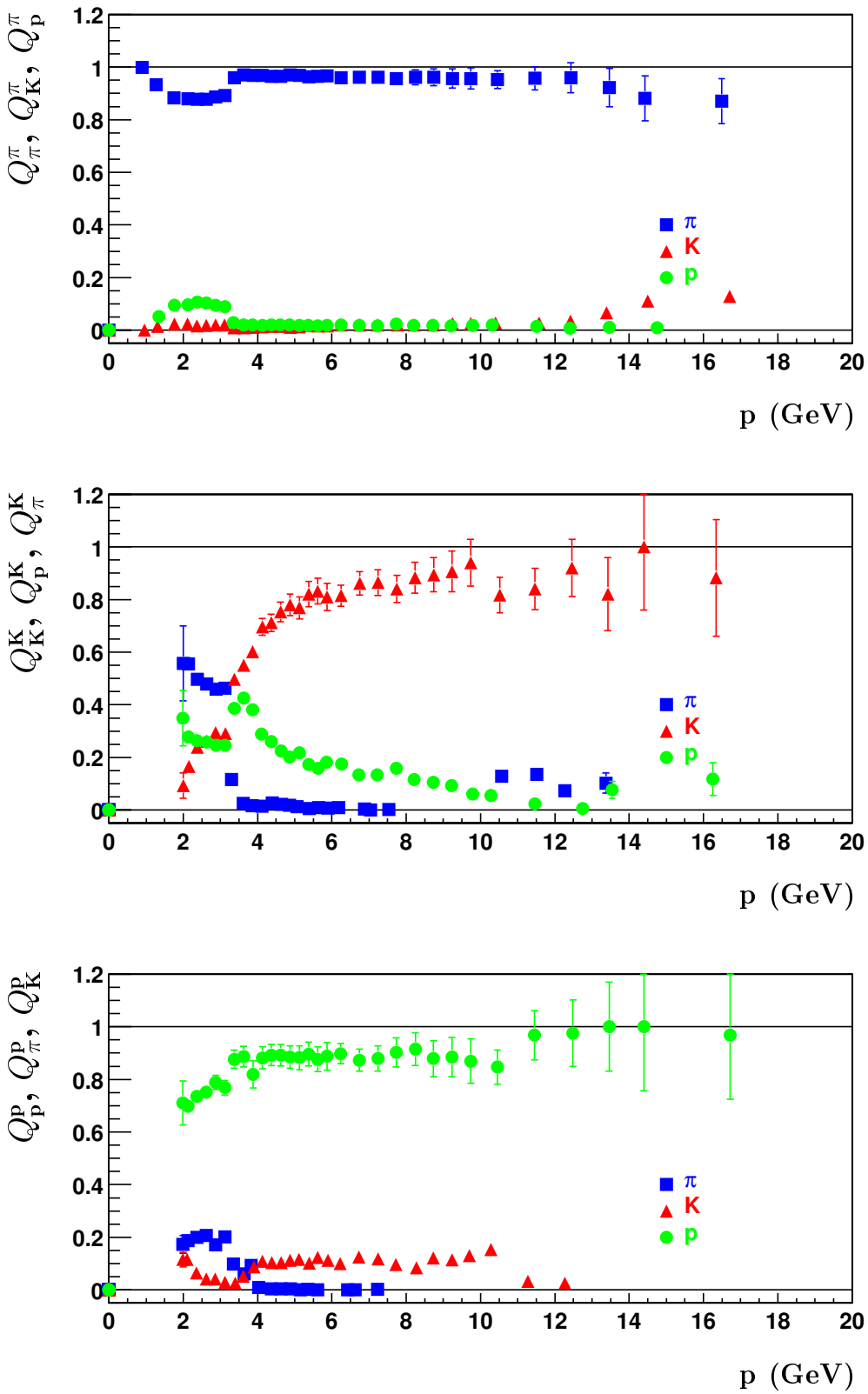

Figure 5.13: Identification purities and contaminations for pions (Q^{π}_{t}, squares), kaons (Q^{K}_{t}, triangles) and protons (Q^{p}_{t}, circles) in $N_{\mathrm{tracks}} = 2$ at $rQp > 0.0$, where $t = \pi$, K, p.

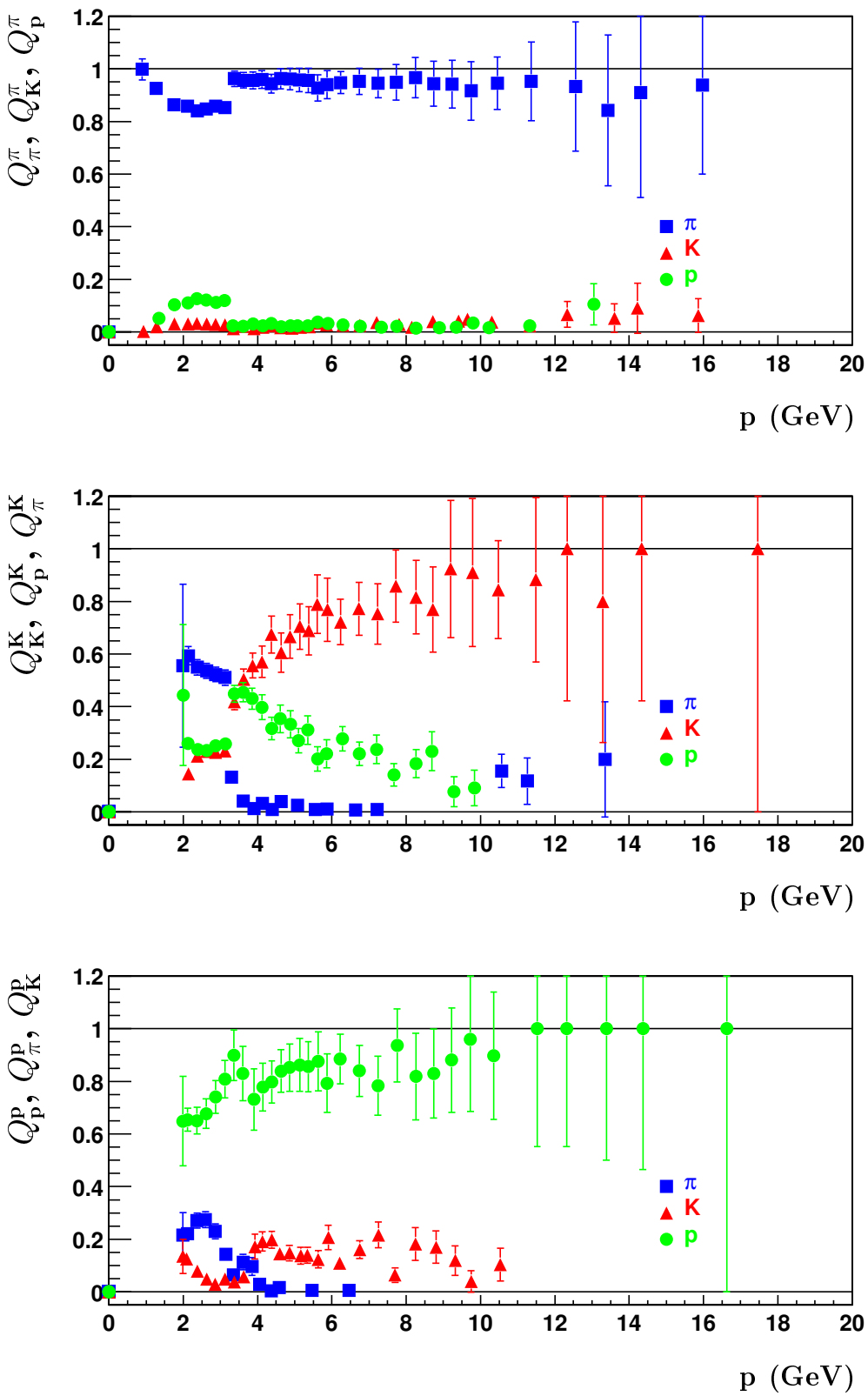

Figure 5.14: Identification purities and contaminations for pions (Q^{π}_{t}, squares), kaons (Q^{K}_{t}, triangles) and protons (Q^{p}_{t}, circles) in $N_{\text{tracks}} > 2$ at $rQp > 0.0$, where $t = \pi$, K, p.

Chapter 6

Extraction of Spin Asymmetries on Deuterium Target

The spin asymmetries extracted from the data of the deuterium target taken in the HERMES experiment are shown in this chapter following the descriptions of the data structure and quality selection of the data. In the analysis using the RICH detector the asymmetries can be extracted for each type of hadrons, namely, pions, kaons and protons. The asymmetries have some corrections. The identification purities and contaminations of hadrons for the particle identification of the RICH detector were estimated in the previous chapter. The corrections except for the correction for the contaminations between hadrons are applied here. The corrections for the contaminations are described in the next chapter.

6.1 Data Production

In the first stage the raw data, which contain the outputs of the detectors, in an EPIO [94] format in the stream of the data acquisition (DAQ) system are decoded, reconstructed [95], calibrated and then stored on the tapes in the ADAMO [96] format. ADAMO provides a database for the physics analyses by so-called entity-relationship. Another stream of DAQ for the slow control data in the ADAMO format, which contain the information related to the high voltage of the detectors and so on, are merged for the data production. The slow control data are used to monitor the online status of the experiment. The slow control data are collected in the DAD [80] servers. DAD provides the distributed database of an extended client-server. The data production is performed in DST (data summary tape) to provide the summary of the data necessary for the analyzers with the compact format. The different productions for the sets of so-called micro-DST (μDST) in the HERMES experiment are labeled basically according to the version of the event file production (A - E) and the DST production (1 - 5). The μDST is in the final stage of the production stream which is available for the physics analyses. The structure of the data have three levels to be characterized as follows:

- *fill* is defined as one quality which corresponds to the life time of the electron beam in HERA, which is typically about 8 hours,
- *run* is defined as a time interval of about 10 minutes,
- *burst* is defined as every 10 seconds which is determined from the smallest timescale of the DAQ system on which the slow control data are available. The polarization states of beam and target may or may not be changed per burst.

Each *event* which is grouped into the burst contain the information for the reconstructed *track* of the particles. In this thesis the data taken from 1998 to spring 1999 on the polarized deuterium target (μDST version 98b4) are used for the analysis of the spin asymmetries.

6.2 Data Quality Selection

The quality of the data is important for the analysis to insure the reliability of the extracted results of the physics. The criteria to put the reliability on the data quality in the burst level are described. The descriptions for the selection of the interesting tracks and events follow it.

6.2.1 Burst Level Criteria

To extract the asymmetries from the data the tracks in the interesting events should be counted in the event level, while the luminosity and different polarization states between beam and target have to be measured on the burst level. Each detector of the HERMES spectrometer is independently operated as well as in the upper and lower halves of the spectrometer. The condition of each detector may not be the same during one fill and between fills. Moreover, not all data collected in the period of the data taking have good quality. The criteria of the data quality selection are applied in the burst level imposing the pre-condition that both upper and lower halves of the spectrometer are fully operational and have the good quality of data after the removal of the problematic runs for analysis or the special runs like the ones for the alignment of the spectrometer or the measurement of Bhabha events. The criteria of the data quality selection in the burst level are summarized in table 6.1. The complete list of data quality criteria is shown by [97]. The selected bursts by the criteria for the data with the good quality are used for extraction of the asymmetries in the inclusive and semi-inclusive analyses.

Beam Quality

The beam polarization of smoothed values is used to decrease the fluctuation of statistics for the determination of the polarization and to cover the values in the

Parameter	Burst quality criterion
Beam	
Beam polarization P_{B}	$30 < P_{\mathrm{B}} < 80$ %
Beam current I_{e^+}	$5 \leq I_{\mathrm{e}^+} \leq 50$ mA
Target	
Target type	Deuterium
Spin state	Defined parallel or anti-parallel
Target polarization P_{T}	Within reasonable polarization
Luminosity	
Luminosity rate R_{Lumi}	$5 \leq R_{\mathrm{Lumi}} \leq 60$ Hz
Data acquisition	
Trigger lifetime T_{DAQ}	$50 \leq T_{\mathrm{DAQ}} < 100$ %
Burst length T_{Burst}	$0 < T_{\mathrm{Burst}} \leq 11$ sec

Table 6.1: List of criteria for the burst level quality.

short time scale of the data taking period for which the longitudinal or transverse polarimeter fails to function. The beam current is measured every minute.

Target Quality

The direction of the target polarization is flipped every 45 seconds for the deuterium target during the data taking to reduce the systematic uncertainty. The bursts with the undefined direction of the polarization during flipping from one direction to another are removed from the analysis of the spin asymmetry.

Luminosity Quality

The fitted values to the detector coincidence rate in the measurement of the luminosity are used for the analysis.

Data Acquisition Quality

The lifetime in the trigger and the length of the burst are selected within the reasonable range.

6.3 Particle Identification and Event Selection

6.3.1 Particle Identification

It is necessary to separate between electrons and hadrons for the inclusive and semi-inclusive analyses. In the HERMES experiment the separation between electrons and hadrons is achieved by the efficient method which uses the combined responses

from the particle identification detectors of the calorimeter, preshower counter and TRD [98]. Figure 6.1 shows the distributions of the responses for each detector in the experimental data.

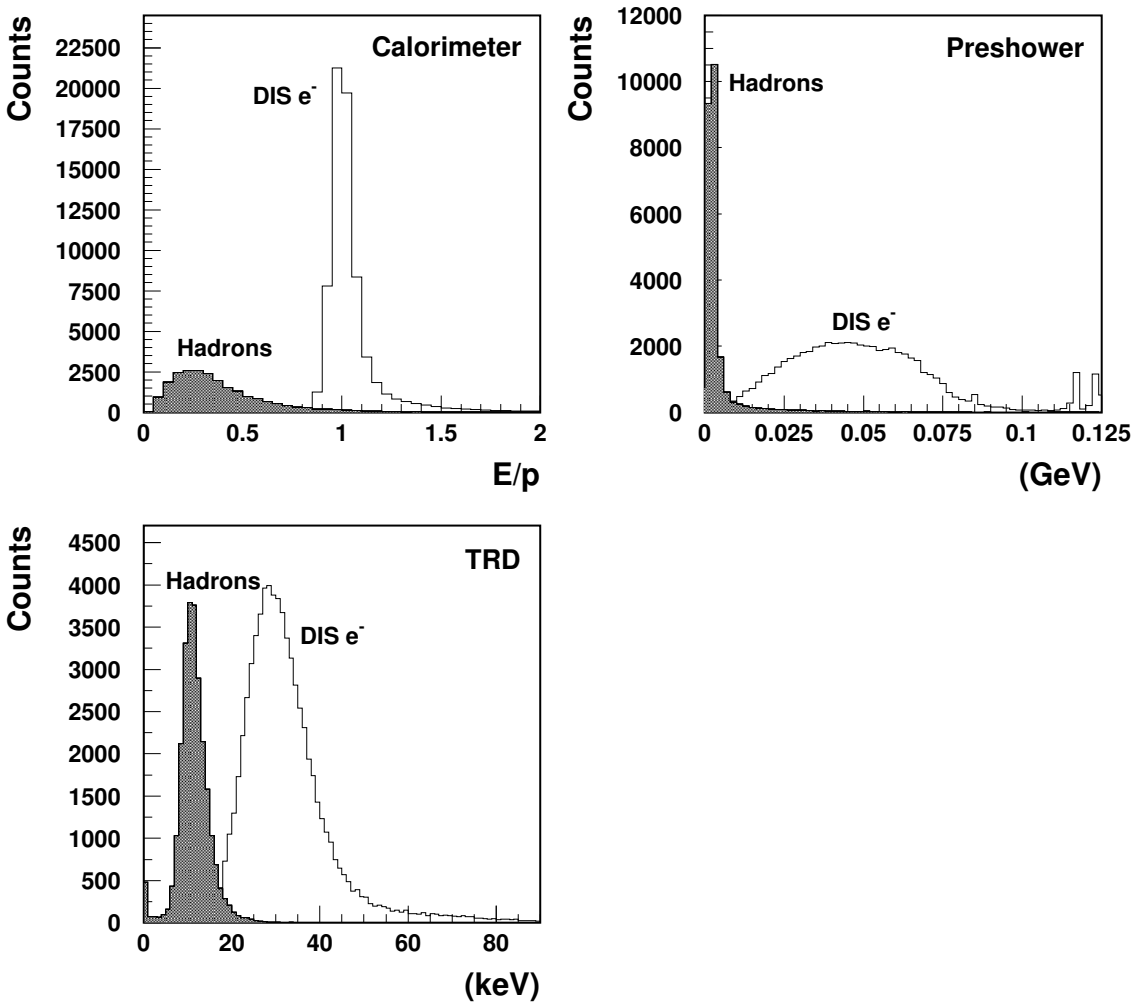

Figure 6.1: Responses of the particle identification detectors for the calorimeter, preshower counter and TRD in the experimental data. The open hatches are the responses of electrons in the DIS events and the closed ones the responses of hadrons with the DIS events.

The responses of each particle identification detector are translated into the conditional probabilities $\mathcal{L}_{\mathrm{D}}^{j}$ which is defined as the probability that a track is identified as a particle of type j under the assumption that the detector signal was generated by this type of the particle when the track of the particle passed through the detector D. The conditional probabilities from a number of n detectors can be combined

into an overall conditional probability like:

$$\mathcal{L}^j = \prod_{\mathrm{D}=1}^{n} \mathcal{L}^j_{\mathrm{D}}. \tag{6.1}$$

The conditional probabilities $\mathcal{L}^j$ are related to the probabilities $\mathcal{P}^j$ by the fluxes Φ_j of the true particle incident to the detectors as:

$$\mathcal{P}^j = \frac{\Phi_j \mathcal{L}^j}{\sum_k \Phi_k \mathcal{L}^k}, \tag{6.2}$$

where k runs over all types of the true particle. The fluxes Φ_j of the true particle are estimated in the Monte Carlo simulation. To separate between electrons ($j = l$) and hadrons ($j = h$) a quantity PID is defined in the logarithmic ratio of $\mathcal{L}^l$ to the $\mathcal{L}^h$ as:

$$\mathrm{PID} = \log_{10} \frac{\mathcal{L}^l}{\mathcal{L}^h} = \log_{10} \frac{\mathcal{P}^l}{\mathcal{P}^h} + \log_{10} \frac{\Phi_h}{\Phi_l}. \tag{6.3}$$

If the flux ratio Φ_h/Φ_l weakly depends on the kinematics of momentum p and scattering angle θ the second term of equation (6.3) becomes the constant offset and then the logarithm of the ratio of the probabilities provides an efficient information of the particle identification. The responses of the two particle identification detectors, calorimeter and preshower counter of HERMES are combined into the quality of so-called PID_2:

$$\mathrm{PID}_2 = \log_{10} \frac{\mathcal{L}^l_{\mathrm{Pre}} \cdot \mathcal{L}^l_{\mathrm{Cal}}}{\mathcal{L}^h_{\mathrm{Pre}} \cdot \mathcal{L}^h_{\mathrm{Cal}}}. \tag{6.4}$$

The PID_5 is defined from the six individual modules of the TRD as:

$$\mathrm{PID}_5 = \log_{10} \frac{\prod_{m=1}^{6} \mathcal{L}^l_{\mathrm{TRD},m}}{\prod_{m=1}^{6} \mathcal{L}^h_{\mathrm{TRD},m}}. \tag{6.5}$$

The values of $\mathrm{PID}_2 + \mathrm{PID}_5$ provide the separation between electrons and hadrons:

$$\mathrm{PID}_2 + \mathrm{PID}_5 > 2 \quad \text{for electrons,} \tag{6.6}$$

$$\mathrm{PID}_2 + \mathrm{PID}_5 < 0 \quad \text{for hadrons.} \tag{6.7}$$

Figures 6.2 and 6.3 show the results of the PID likelihoods. When the cut of equation (6.6) is applied for the separation of electron tracks from hadron tracks the efficiency of the identification for electrons is higher than 97 % with contamination of hadrons lower than 1 % in the whole range of x.

The information of the identification between hadrons is independently provided by the RICH detector apart from other particle identification detectors.

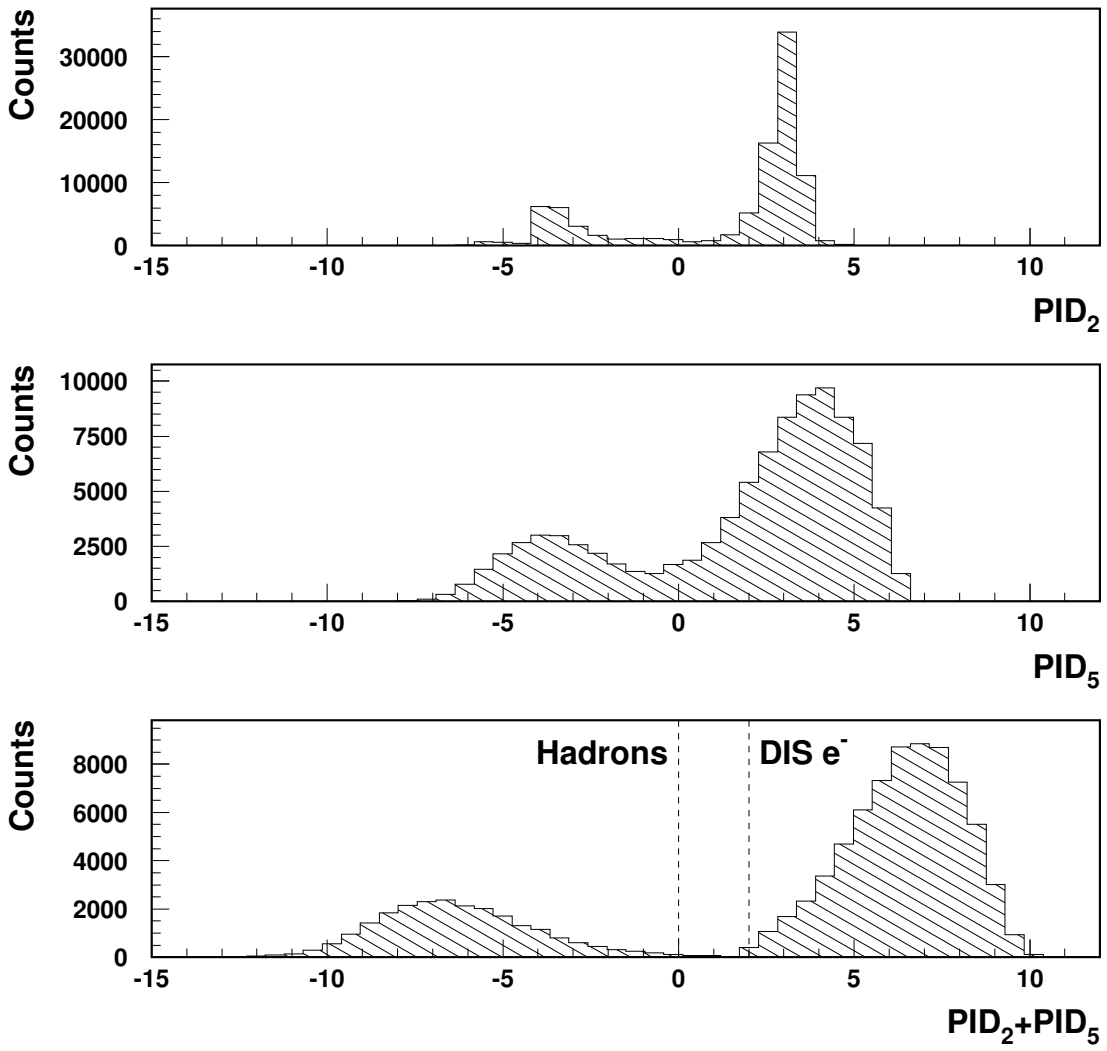

Figure 6.2: Distributions of PID likelihoods. For the top and middle figures show the distributions of PID_2 and PID_5 respectively. As seen in the bottom figure finally the summation of distributions of PID_2 and PID_5 separates between electrons and hadrons. The dashed lines in the bottom figure indicate the boundaries of cut for the separation: $PID_2 + PID_5 > 2$ is the cut for electrons, $PID_2 + PID_5 < 0$ for hadrons.

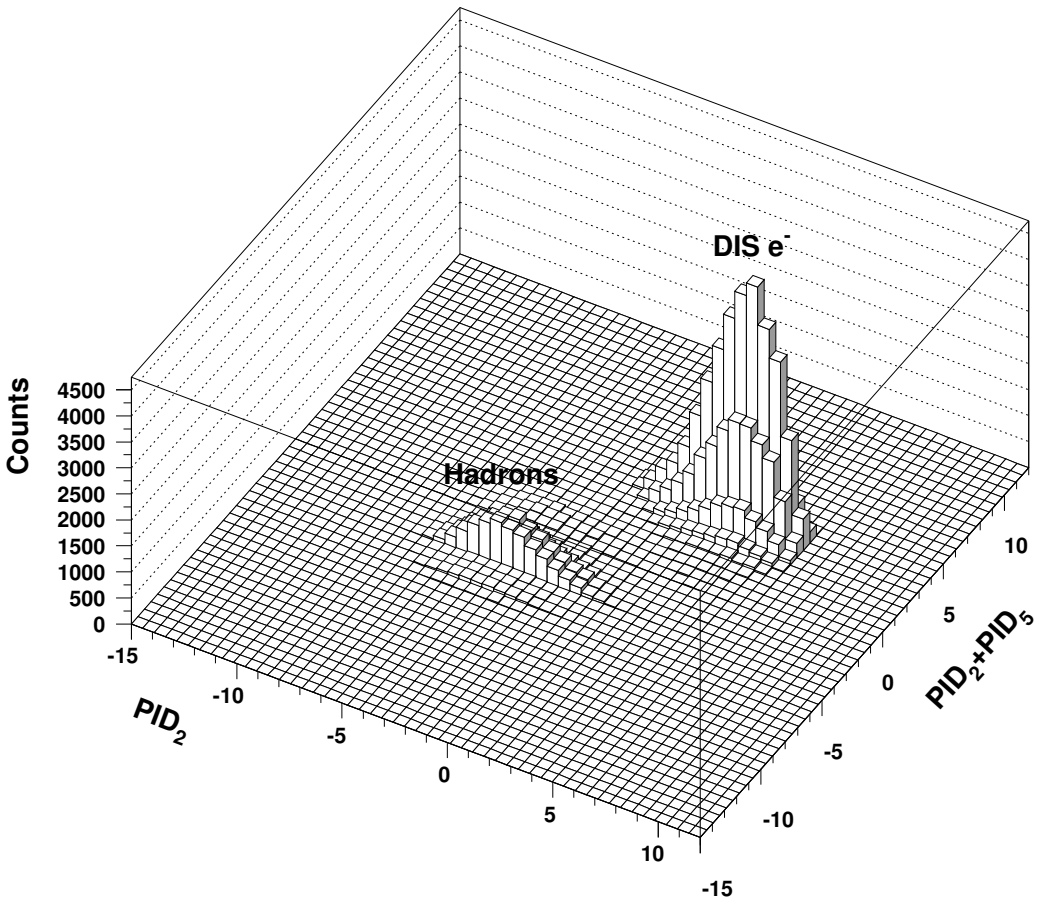

Figure 6.3: Distributions of PID likelihoods for PID_2 and $\mathrm{PID}_2 + \mathrm{PID}_5$ shown in the two-dimensional plot.

6.3.2 Event Selection

Kinematical Cuts

The scattering electron off the target nucleon in the target cell can be identified as the electron track with the highest momentum in an event. Firstly the geometrical cuts are imposed to the electrons in an event. If the electron with the highest momentum is found, the cut criteria for the event of the DIS are imposed to the electrons which passed through the geometrical cuts in the event. These procedures are applied to the inclusive analysis. For the semi-inclusive analysis the hadron tracks in the DIS events which passed through both the geometrical cuts and the reliable cuts for z and x_{F} to make sure of the quark-hadron correlation are counted.

The cuts criteria of the event selection are listed in table 6.2.

To make sure that the tracks come from the inside of the target cell the cuts on the longitudinal and lateral vertex positions at the target cell are imposed. Especially the regions of the distorted distribution at the ends of the target cell are rejected by the cut of the longitudinal vertex position:

$$|z_{\mathrm{vertex}}| \leq 18.0 \text{ cm}, \quad r_{\mathrm{vertex}} \leq 0.75 \text{ cm}. \tag{6.8}$$

The acceptance cuts for the horizontal and vertical projections of the scattering angle are imposed on the tracks:

$$-170 \leq |\theta_x| \leq 170 \text{ mrad}, \quad 40 \leq |\theta_y| \leq 140 \text{ mrad}. \tag{6.9}$$

To make sure that the tracks passed though all the detectors the fiducial cuts at the positions of the calorimeter are imposed:

$$|x_{\mathrm{Calo}}| \leq 175 \text{ cm}, \quad 30 \leq |y_{\mathrm{Calo}}| \leq 100 \text{ cm}. \tag{6.10}$$

The additional cut for the momentum of the tracks is imposed:

$$p \geq 0.5 \text{ GeV}. \tag{6.11}$$

Especially the cuts for the momentum of the kaon and proton tracks are chosen according to the performance of the particle identification of the RICH detector to reject the region of the momentum with the low identification purities:

$$\begin{aligned} p &> 3.25 \text{ GeV for kaons}, \\ p &> 2.0 \text{ GeV for protons}. \end{aligned}$$

The effect of the different cuts of the momentum threshold on the asymmetry is studied in the section 6.6.2.

Figure 6.4 shows the distributions z_{vertex}, r_{vertex}, θ_x, θ_y, horizontal and vertical positions at the calorimeter for electrons before and after the track selection criteria applied.

For the DIS events $Q^2 \geq 1$ GeV^2 for the scale of the deep-inelastic scattering process, $W^2 \geq 4$ GeV^2 for the rejection of the resonance region in the hadronic final state and $y \leq 0.85$ for the rejection of the radiative region are imposed. Additionally the cluster energy deposit more than 3.5 GeV in the localized spatial region at the calorimeter is required to increase the reliability for the higher threshold energy of the calorimeter. For the hadrons with the DIS events, the higher cut of $W^2 \geq 10$ GeV^2 than the one of the inclusive case is imposed to improve the separation of hadrons of the current fragments from those of the target remnants. Figure 6.5 shows the distributions of Q^2, W^2, y and calorimeter cluster energy for electrons before and after the DIS kinematical criteria applied. The cuts of $z \geq 0.2$ and $x_{\mathrm{F}} \geq 0.1$ are also required to increase the probability of hadrons which come from the current fragments.

Track selection	
Parameter	**Range**
Vertex inside target cell	
Longitudinal vertex position	$\lvert z_{\text{vertex}}\rvert \leq 18.0$ cm
Lateral vertex position	$r_{\text{vertex}} \leq 0.75$ cm
Acceptance	
Horizontal angular acceptance	$\lvert\theta_x\rvert \leq 170$ mrad
Vertical angular acceptance	40 mrad $\leq \lvert\theta_y\rvert \leq 140$ mrad
Horizontal position at the calorimeter	$\lvert x_{\text{Calo}}\rvert \leq 175$ cm
Vertical position at the calorimeter	30 cm $\leq \lvert y_{\text{Calo}}\rvert \leq 100$ cm
Kinematics	
Momentum	$p \geq 0.5$ GeV
DIS kinematical criterion	
Parameter	**Range**
Kinematics	
Scaling region	$Q^2 \geq 1$ GeV^2
Reject resonance region	$W^2 \geq 4$ GeV^2
Reject radiative region	$y \leq 0.85$
Calorimeter cluster energy	$E'_{\text{Calo}} \geq 3.5$ GeV
Hadron with DIS kinematical criterion	
Parameter	**Range**
Kinematics	
Reject resonance region	$W^2 \geq 10$ GeV^2
Hadron momentum ratio	$z \geq 0.2$
x Feynman	$x_{\text{F}} \geq 0.1$
RICH PID	
Kaon momentum	$p > 3.25$ GeV
Proton momentum	$p > 2.0$ GeV

Table 6.2: List of criteria for the event selection. The count rates of the tracks passed through all cuts criteria above are used to extract the spin asymmetries.

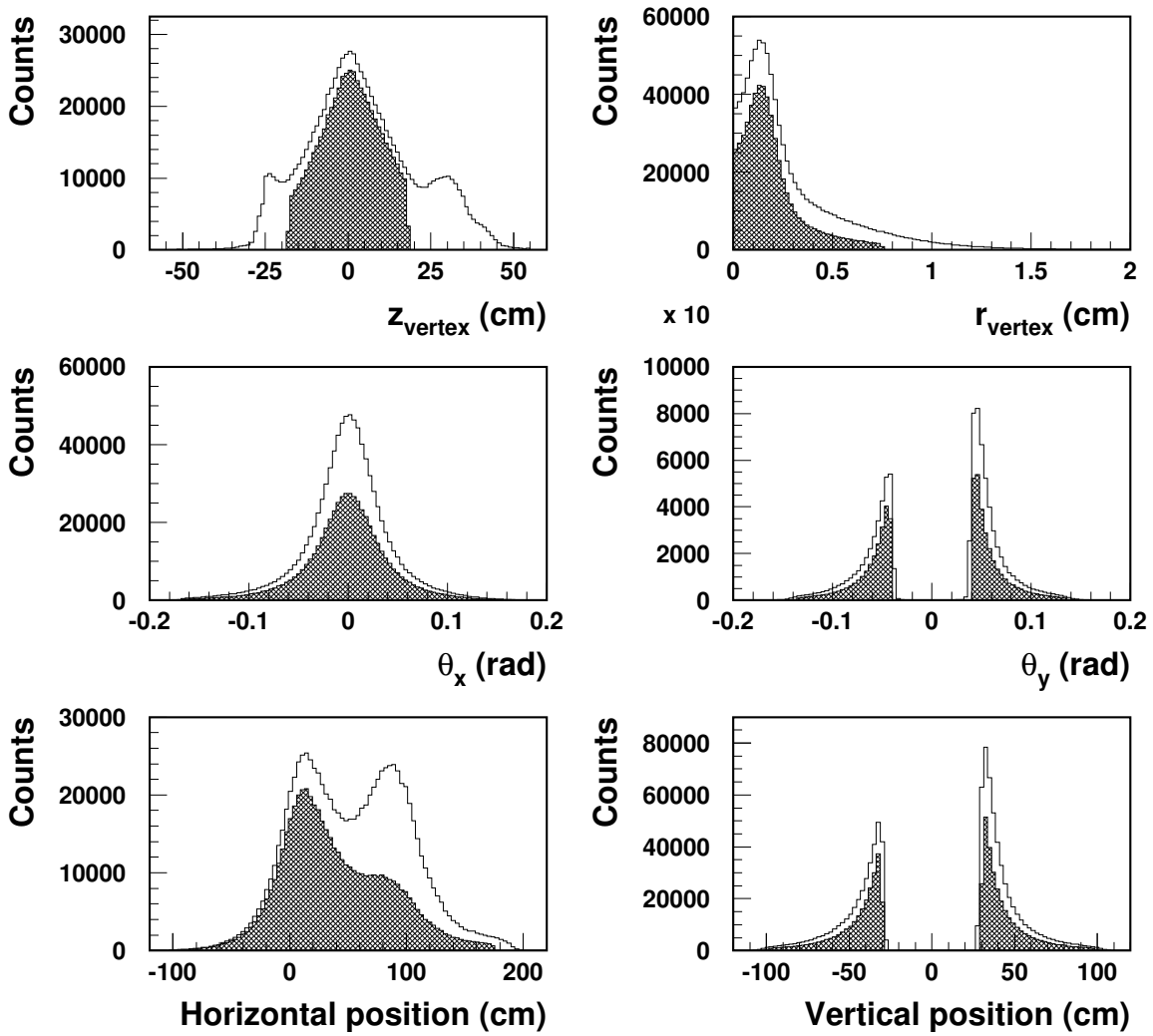

Figure 6.4: Distributions of $z_{\rm vertex}$, $r_{\rm vertex}$, θ_x, θ_y, horizontal and vertical positions at the calorimeter for electrons before (open histograms) and after (hatched histograms) the track selection criteria in table 6.2 applied.

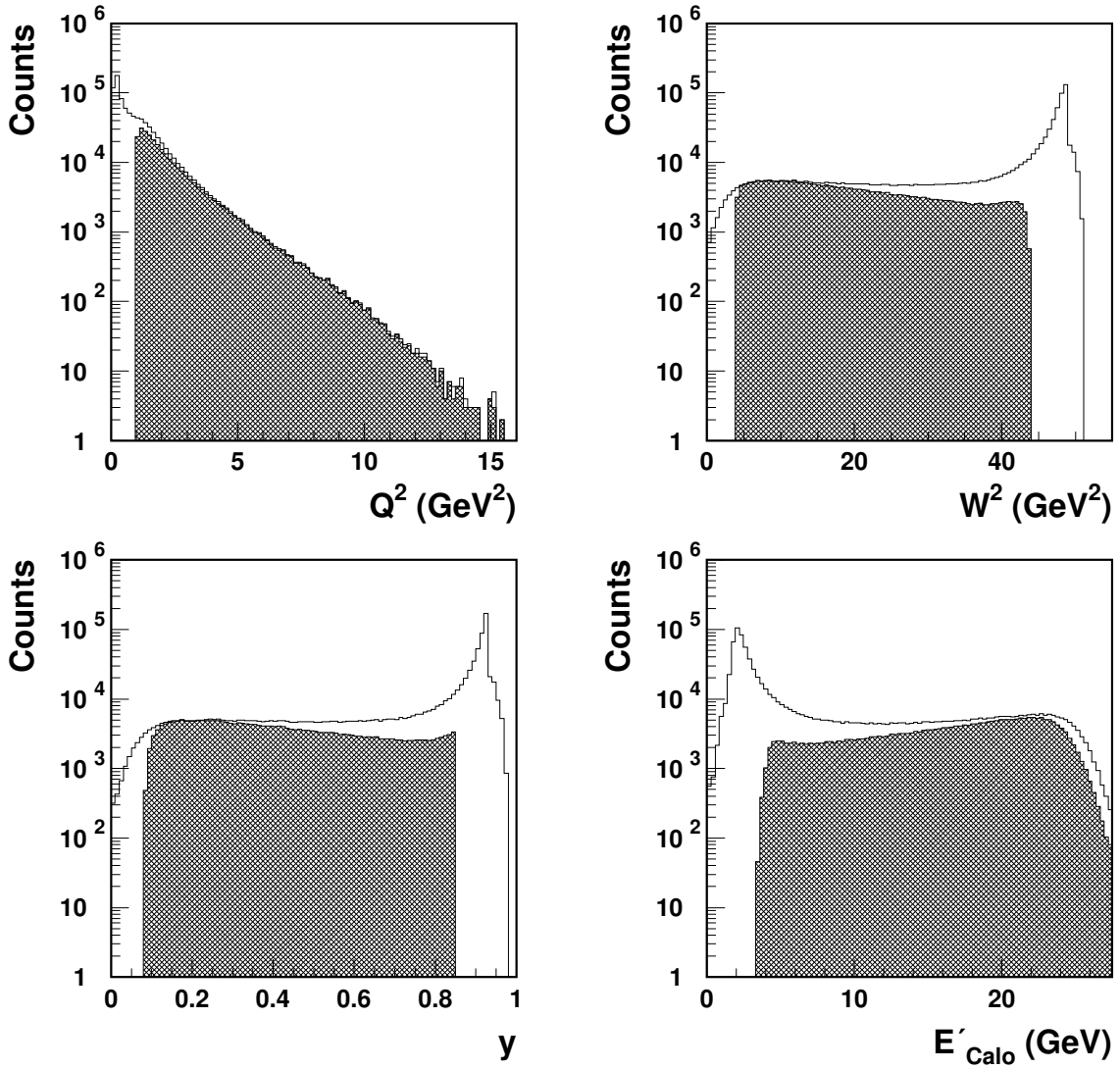

Figure 6.5: Distributions of Q^2, W^2, y and calorimeter cluster energy E'_{Calo} for electrons before (open histograms) and after (hatched histograms) the DIS kinematical criteria in table 6.2 applied.

6.4 Extraction of Spin Asymmetry

The spin asymmetry of the virtual photon-nucleon interaction is extracted from the measurement of the count rates, $N^{\vec{\Leftarrow}}$ and $N^{\vec{\Rightarrow}}$, for the different states of the spin

between the beam and the target nucleon:

$$N^{\overrightarrow{\Leftarrow}}(x,Q^2) = \sigma(x,Q^2)\int_{\overrightarrow{\Leftarrow}} dt\ \mathcal{A}(t,x,Q^2)\ \mathcal{E}(t,x,Q^2)\ \mathcal{L}(t) \left(1 + A_1(x,Q^2)\ D(x,Q^2)\ P_{\rm B}(t)\ P_{\rm T}(t)\right), \quad (6.12)$$

$$N^{\overrightarrow{\Rightarrow}}(x,Q^2) = \sigma(x,Q^2)\int_{\overrightarrow{\Rightarrow}} dt\ \mathcal{A}(t,x,Q^2)\ \mathcal{E}(t,x,Q^2)\ \mathcal{L}(t) \left(1 - A_1(x,Q^2)\ D(x,Q^2)\ P_{\rm B}(t)\ P_{\rm T}(t)\right), \quad (6.13)$$

where $\overrightarrow{\Leftarrow}$ and $\overrightarrow{\Rightarrow}$ are spin states between beam and target parallel and anti-parallel respectively, $\mathcal{A}$ and $\mathcal{E}$ the acceptance and efficiency of the detector, $\mathcal{L}$ the luminosity, $P_{\rm B}$ and $P_{\rm T}$ the beam and target polarizations and D the virtual photon depolarization factor which describes the degree of the depolarization at the transfer from the polarized lepton to the virtual photon. σ is the unpolarized cross-section integrated over the kinematical region of interest. When it can be assumed that the acceptance $\mathcal{A}$ and detector efficiency $\mathcal{E}$ are constant over the time period of data taking, equation (6.12) and (6.13) are expressed as:

$$N^{\overrightarrow{\Leftarrow}}(x,Q^2) = \sigma(x,Q^2)\ \mathcal{A}(x,Q^2)\ \mathcal{E}(x,Q^2) \int_{\overrightarrow{\Leftarrow}} dt\ \mathcal{L}(t)\ \left(1 - A_1(x,Q^2)\ \langle D^{\overrightarrow{\Leftarrow}}(x,Q^2)\rangle\ P_{\rm B}(t)\ P_{\rm T}(t)\right), \quad (6.14)$$

$$N^{\overrightarrow{\Rightarrow}}(x,Q^2) = \sigma(x,Q^2)\ \mathcal{A}(x,Q^2)\ \mathcal{E}(x,Q^2) \int_{\overrightarrow{\Rightarrow}} dt\ \mathcal{L}(t)\ \left(1 + A_1(x,Q^2)\ \langle D^{\overrightarrow{\Rightarrow}}(x,Q^2)\rangle\ P_{\rm B}(t)\ P_{\rm T}(t)\right), \quad (6.15)$$

where $\langle D\rangle$ is given by averaging the depolarization factor which obtained in event-by-event over all events. Assuming that the beam and target polarizations are constant for the burst, as a result the count rate n_i for the burst number i can be written as:

$$n_i^{\overrightarrow{\Rightarrow}(\overrightarrow{\Leftarrow})} = \mathcal{A}\ \mathcal{E}\ \sigma\ L_i^{\overrightarrow{\Rightarrow}(\overrightarrow{\Leftarrow})} \left(1 - (+)\ A_1\ \langle D_i^{\overrightarrow{\Rightarrow}(\overrightarrow{\Leftarrow})}\rangle\ P_{{\rm B},i}^{\overrightarrow{\Rightarrow}(\overrightarrow{\Leftarrow})}\ P_{{\rm T},i}^{\overrightarrow{\Rightarrow}(\overrightarrow{\Leftarrow})}\right), \quad (6.16)$$

where L_i is the measured luminosity, $P_{{\rm B},i}$ and $P_{{\rm T},i}$ the measured polarization. The notations are defined as follows:

$$N^{\overrightarrow{\Rightarrow}(\overrightarrow{\Leftarrow})} = \sum_i n_i^{\overrightarrow{\Rightarrow}(\overrightarrow{\Leftarrow})}, \quad (6.17)$$

$$L^{\overrightarrow{\Rightarrow}(\overrightarrow{\Leftarrow})} = \sum_i L_i^{\overrightarrow{\Rightarrow}(\overrightarrow{\Leftarrow})}, \quad (6.18)$$

$$L_{\rm P}^{\overrightarrow{\Rightarrow}(\overrightarrow{\Leftarrow})} = \sum_i (L_i \cdot P_{{\rm B},i} \cdot P_{{\rm T},i})^{\overrightarrow{\Rightarrow}(\overrightarrow{\Leftarrow})}. \quad (6.19)$$

The experimentally measured asymmetry $A_{||}$ is expressed as:

$$A_{||} = \frac{N^{\overrightarrow{\Leftarrow}}/L_{\rm P}^{\overrightarrow{\Leftarrow}} - N^{\overrightarrow{\Rightarrow}}/L_{\rm P}^{\overrightarrow{\Rightarrow}}}{N^{\overrightarrow{\Leftarrow}}/L^{\overrightarrow{\Leftarrow}} + N^{\overrightarrow{\Rightarrow}}/L^{\overrightarrow{\Rightarrow}}}. \quad (6.20)$$

The spin asymmetry A_1 is expressed with the virtual photon depolarization factor neglecting the spin dependent structure function g_2:

$$A_1 = \frac{1}{1+\eta\gamma} \cdot \frac{N^{\vec{\Leftarrow}} L^{\vec{\Rightarrow}} - N^{\vec{\Rightarrow}} L^{\vec{\Leftarrow}}}{N^{\vec{\Leftarrow}} \langle D^{\vec{\Rightarrow}} \rangle L_{\mathrm{P}}^{\vec{\Rightarrow}} + N^{\vec{\Rightarrow}} \langle D^{\vec{\Leftarrow}} \rangle L_{\mathrm{P}}^{\vec{\Leftarrow}}}. \tag{6.21}$$

The statistical uncertainty δA_1 of A_1 is given by the law of the error propagation:

$$\begin{aligned}
(\delta A_1)^2 &= \left(\frac{1}{1+\eta\gamma}\right)^2 \cdot \left[\left(\delta N^{\vec{\Leftarrow}} \cdot \frac{\partial}{\partial N^{\vec{\Leftarrow}}} \frac{N^{\vec{\Leftarrow}} L^{\vec{\Rightarrow}} - N^{\vec{\Rightarrow}} L^{\vec{\Leftarrow}}}{N^{\vec{\Leftarrow}} \langle D^{\vec{\Rightarrow}} \rangle L_{\mathrm{P}}^{\vec{\Rightarrow}} + N^{\vec{\Rightarrow}} \langle D^{\vec{\Leftarrow}} \rangle L_{\mathrm{P}}^{\vec{\Leftarrow}}} \right)^2 \right. \\
&\quad + \left. \left(\delta N^{\vec{\Rightarrow}} \cdot \frac{\partial}{\partial N^{\vec{\Rightarrow}}} \frac{N^{\vec{\Leftarrow}} L_{\vec{\Rightarrow}} - N^{\vec{\Rightarrow}} L^{\vec{\Leftarrow}}}{N^{\vec{\Leftarrow}} \langle D^{\vec{\Rightarrow}} \rangle L_{\mathrm{P}}^{\vec{\Rightarrow}} + N^{\vec{\Rightarrow}} \langle D^{\vec{\Leftarrow}} \rangle L_{\mathrm{P}}^{\vec{\Leftarrow}}} \right)^2 \right] \\
&= \left(\frac{1}{1+\eta\gamma}\right)^2 \cdot \left[\left(\sqrt{N^{\vec{\Leftarrow}}} \cdot \frac{YL^{\vec{\Rightarrow}} - X \langle D^{\vec{\Rightarrow}} \rangle L_{\mathrm{P}}^{\vec{\Rightarrow}}}{Y^2} \right)^2 \right. \\
&\quad + \left. \left(\sqrt{N^{\vec{\Rightarrow}}} \cdot \frac{-YL^{\vec{\Leftarrow}} - X \langle D^{\vec{\Leftarrow}} \rangle L_{\mathrm{P}}^{\vec{\Leftarrow}}}{Y^2} \right)^2 \right].
\end{aligned} \tag{6.22}$$

Here

$$X = N^{\vec{\Leftarrow}} L^{\vec{\Rightarrow}} - N^{\vec{\Rightarrow}} L^{\vec{\Leftarrow}}, \tag{6.23}$$

$$Y = N^{\vec{\Leftarrow}} \langle D^{\vec{\Rightarrow}} \rangle L_{\mathrm{P}}^{\vec{\Rightarrow}} + N^{\vec{\Rightarrow}} \langle D^{\vec{\Leftarrow}} \rangle L_{\mathrm{P}}^{\vec{\Leftarrow}}, \tag{6.24}$$

and $\delta N^{\vec{\Leftarrow}(\vec{\Rightarrow})}$ is given by $\sqrt{N^{\vec{\Leftarrow}(\vec{\Rightarrow})}}$. The spin asymmetry A_1 is extracted in each bin of x. The bins of x are determined so as to obtain almost the same number of counts in each bin. Table 6.3 shows the range of each bin in x. In the semi-inclusive case the spin asymmetry A_1^h and its uncertainty δA_1^h for hadrons are extracted in the same formulae as the ones in the inclusive case if the count rates of the interesting hadrons are given. Equation (3.2) for the target polarization is applied to the above formulae of the asymmetry.

Bin	Range of x
1	$0.023 - 0.040$
2	$0.040 - 0.055$
3	$0.055 - 0.075$
4	$0.075 - 0.100$
5	$0.100 - 0.140$
6	$0.140 - 0.200$
7	$0.200 - 0.300$
8	$0.300 - 0.400$
9	$0.400 - 0.600$

Table 6.3: Definition of the binning in x. This binning is commonly used for the extraction of the spin asymmetry in both inclusive and semi-inclusive case.

6.5 Corrections to Asymmetry

The corrections to the measured asymmetry are described in this section. The correction for the contaminations between hadrons to the spin asymmetry of hadron, especially kaon, is described in detail in the next chapter. The spin asymmetries of DIS events and hadrons with the DIS events are shown at the end of this section after the application of all corrections except the corrections for the contaminations.

6.5.1 Background Corrections

The asymmetry is extracted from the count rate for the DIS events. The asymmetry can be biased if the events of uninterest are included in the count rate. The count rate for the extraction of the asymmetry is corrected for the misidentified electrons from the charge-symmetric process like e^+e^- pair production. Such e^+ can contribute as the background to the count rate. The photoproduction is a source of the background to the DIS process. In this process the electron of the beam particle will generally be scattered in the small angle and will escape into the acceptance gap of the spectrometer. On the other hand e^- from the production of π^0 and its subsequent decay through $\pi^0 \rightarrow \gamma\gamma$, $\gamma \rightarrow e^+e^+$ may be included into the count rate of the DIS events. e^- from a high energy bremsstrahlung photons, which are converted into e^+e^-, can be another source of the background.

Assuming the equal probabilities of identifying electron and positron from the charge symmetric processes, electron and positron have mirrored relationship. Therefore, they are considered as a tag of the above background processes and are available to correct the count rate of the DIS electron by detecting the positron of uninterest together with the electron of interest in an event. The procedures of the corrections for the above background processes were performed as follows. If a positron track with the highest momentum was found in all positron tracks in an event in coincidence with the DIS electron and if the positron which passed through the DIS kinematical criteria listed in table 6.2 and if the positron has higher momentum than that of the DIS electron in the event, such event was rejected and was not counted for the extraction of the asymmetry. By above procedures it was found that such background positrons mainly contributed in the region of low x and the degree of the contribution was very small. The contribution rapidly decreases as x increases.

Since the hadron asymmetries are extracted from the count rate of hadrons with the DIS events, the degree of the background corrections on the hadron asymmetries are much smaller.

6.5.2 Alignment Corrections

The alignment of the tracking chambers is performed in two steps: an internal alignment for each plane of the tracking chambers with respect to one another within each half of the spectrometer, followed by an external alignment of the entire half of the spectrometer with respect to the reference frame of the spectrometer.

The tracks are reconstructed from the information for each position of the tracking chambers. The information is stored on the geometry data base in advance. The difference of the positions of the spectrometer from the data base leads to the wrongly reconstructed tracks. It directly affects the scattering angle θ and acceptance of the spectrometer and therefore the kinematical variables, for example, Q^2. By comparing the vertex positions of the tracks of the DIS leptons at the target cell which are obtained from the Monte Carlo simulation and the data, a significant shifts of the slope and offset for the tracks were observed. The offset of the external alignment is compensated by correcting the parameters which define the position of the tracks using an algorithm which is given in [99]. This algorithm takes into account the position and the slope of the HERA beam at the interaction point at the target cell and determines the longitudinal vertex positions of the scattering particles at the target cell. In this thesis the correction for the longitudinal vertex positions at the target cell was applied to the tracks of the data.

6.6 Results of Asymmetries

After the burst level criteria, the event selection, the background and the alignment corrections are applied the DIS events of 1.14×10^6 were collected. After the application of all cuts for hadrons in coincident with the DIS events statistics of positively and negatively charged hadrons identified by the particle identification detectors were 1.39×10^5 and 9.29×10^4 respectively. Out of the hadrons the numbers of positively and negatively charged kaons identified by the RICH detector were 1.64×10^4 and 6.61×10^3 respectively. These statistics are used to measure the asymmetries.

In this section the result of the inclusive asymmetry on the deuterium target is shown. The spin asymmetry of kaon before the corrections for the contaminations between hadrons are studied for the effect of the momentum threshold and in the different quality parameters. The final results of the semi-inclusive asymmetries corrected for the contaminations are described in the next chapter. Moreover for the inclusive and semi-inclusive asymmetries the systematic uncertainties are discussed in the next chapter.

6.6.1 Result of inclusive Asymmetry

Figure 6.6 shows the result of the inclusive asymmetry on the deuterium target in comparison with the one measured in the E143 Collaboration [41]. The inclusive asymmetry on the deuteron is small in the range of $x < 0.1$ and increases to about 0.3 at maximum as x increases. In general the inclusive deuteron asymmetry has a tendency to be between the inclusive hydrogen and ^{3}He asymmetries [2]. Most of the asymmetry from ^{3}He is due to the neutron as the two protons in the ^{3}He nucleus pair to zero spin in the ground state, so that the spin of the ^{3}He nucleus is brought about by the spin of the neutron [100]. The result is in agreement with the one of the E143 Collaboration. The HERMES experiment, however, determined the

asymmetry more precisely. Here the result of the E143 Collaboration in the same kinematic range as the HERMES experiment is shown in the figure. The dominant sources of the systematic uncertainty mainly come from the uncertainties of the measurement of the target polarization and the spin-dependent structure function g_2 on the deuteron.

6.6.2 Kaon Asymmetry uncorrected for Contaminations

Effect of Momentum Threshold

Figures 6.7 and 6.8 show the effect of the momentum threshold on the kaon asymmetry. The momentum threshold is raised from 2 GeV to 3.25 GeV per 0.25 GeV. The analyses are performed in the quality parameter $rQp > 0.0$. The results between the different momentum thresholds are in agreement within their statistical uncertainties. As seen in figure 5.9 the identification efficiency for kaons rises up to more than 90 % at 3.25 GeV and it is kept up to 9 GeV. Especially from figure 5.12 when the momentum threshold is raised up to 3.25 GeV the identification purity for kaons stays at more than 70 % over the whole range of the momentum above 3.25 GeV, so that the low identification purity for kaons in the region of the momentum lower than 3.25 GeV can be rejected. Since statistics of kaons are larger in the region of the momentum from 2 GeV to 6 GeV, in this region it is important to yield a high kaon identification purity to extract the kaon asymmetry with higher reliability.

Studies for different Quality Parameters

Figure 6.9 shows the comparison of statistics between the different quality parameters for pions, kaons and protons. Figure 6.10 shows the distributions of the quality parameters for these. If the cut of the quality parameter $rQp > 0.5$ is imposed statistics of kaons decrease significantly, especially in the lower region of momentum compared to pions and protons. The reason can be attributed to that the curve of the kaon Čerenkov angle is between the curves of the pion and proton Čerenkov angles and the identification purity of kaon is low in the lower region of momentum, which means that kaons are contaminated by both pions and protons in lower region.

Figures 6.11 and 6.12 show the comparisons of the asymmetries between the different quality parameters. It is found that the results between the different quality parameters agree within their statistical uncertainties and do not significantly depend on the values of rQp. As a result it is assumed that using the cut of the quality parameter $rQp > 0.0$ is more advantageous statistically rather than imposing other values of the quality parameter to measure the asymmetry.

6.7 Summary of Kaon Asymmetry uncorrected for Contaminations

The kaon asymmetry before the corrections for the contaminations between hadrons was studied for the effect of the momentum threshold and the different quality parameters. It was found that for extraction of the kaon asymmetry:

- If the momentum threshold more than 3.25 GeV is imposed according to the higher identification purity for kaons the asymmetry can be measured with more reliability,
- the cut of the quality parameter $rQp > 0.0$ has statistical advantage.

When the corrections of the kaon asymmetry for the contaminations between hadrons are performed above two items are consistently imposed as the critera for the extraction of the kaon asymmetry.

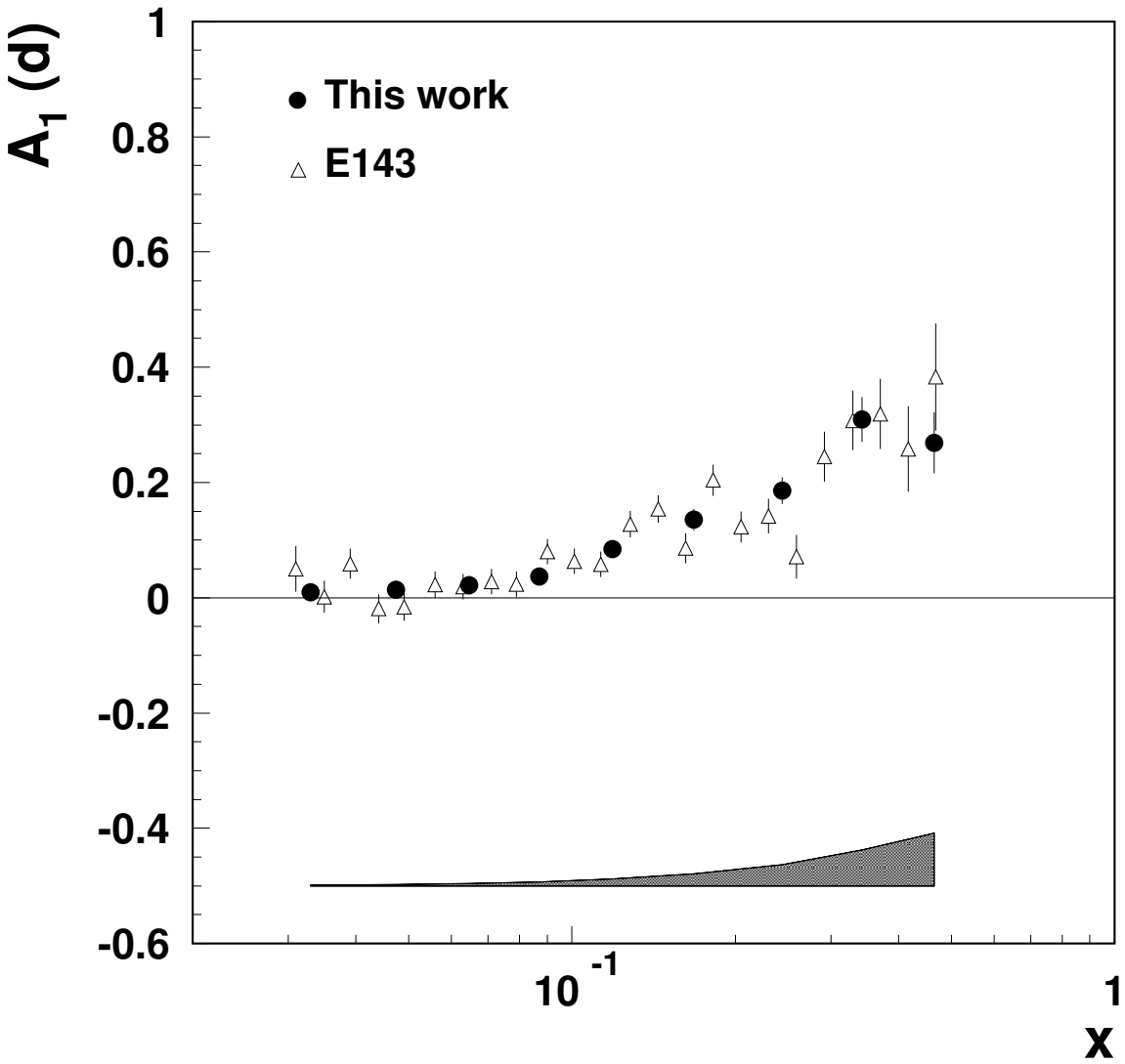

Figure 6.6: Result of the inclusive asymmetry (closed circles) on the deuterium target. The band represents the total systematic uncertainty of the experiment (see section 7.7.1). The open triangles are the result measured by the E143 Collaboration [41], which is shown in the kinematic range of the HERMES experiment. The error bar for the result of the E143 Collaboration includes the systematic uncertainty only.

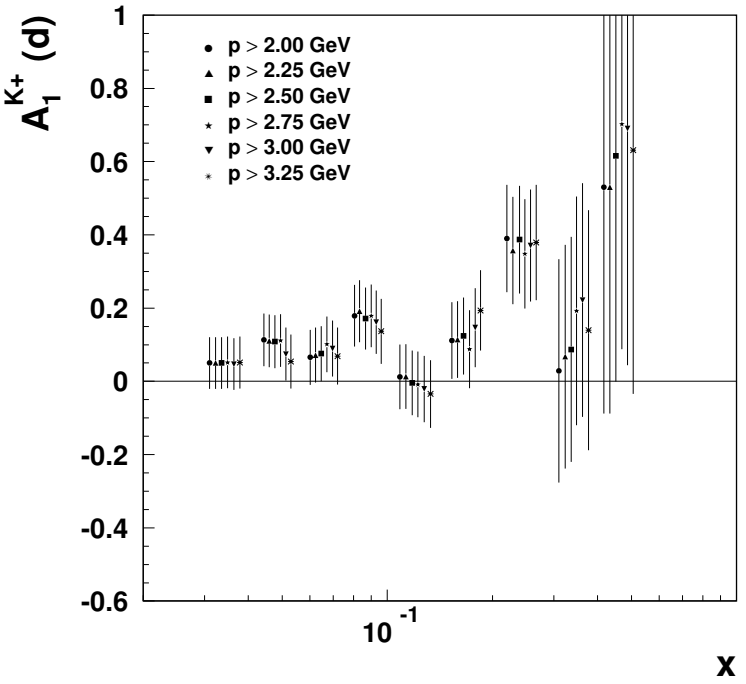

Figure 6.7: Effect of the momentum threshold on the K^+ asymmetry. The asymmetries are for the results before the corrections for the contaminations between hadrons. The analyses are consistently performed in $rQp > 0.0$.

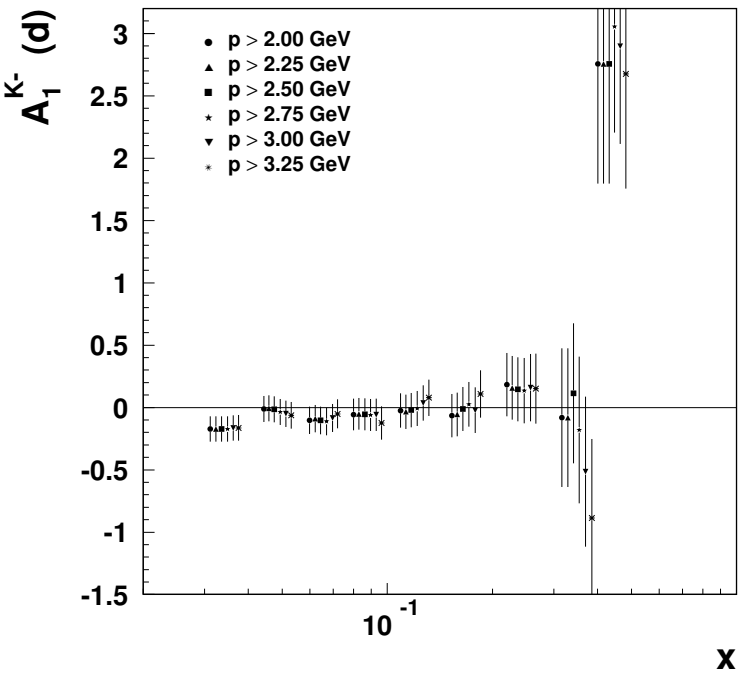

Figure 6.8: Effect of the momentum threshold on the K^- asymmetry. The asymmetries are for the results before the corrections for the contaminations between hadrons. The analyses are consistently performed in $rQp > 0.0$.

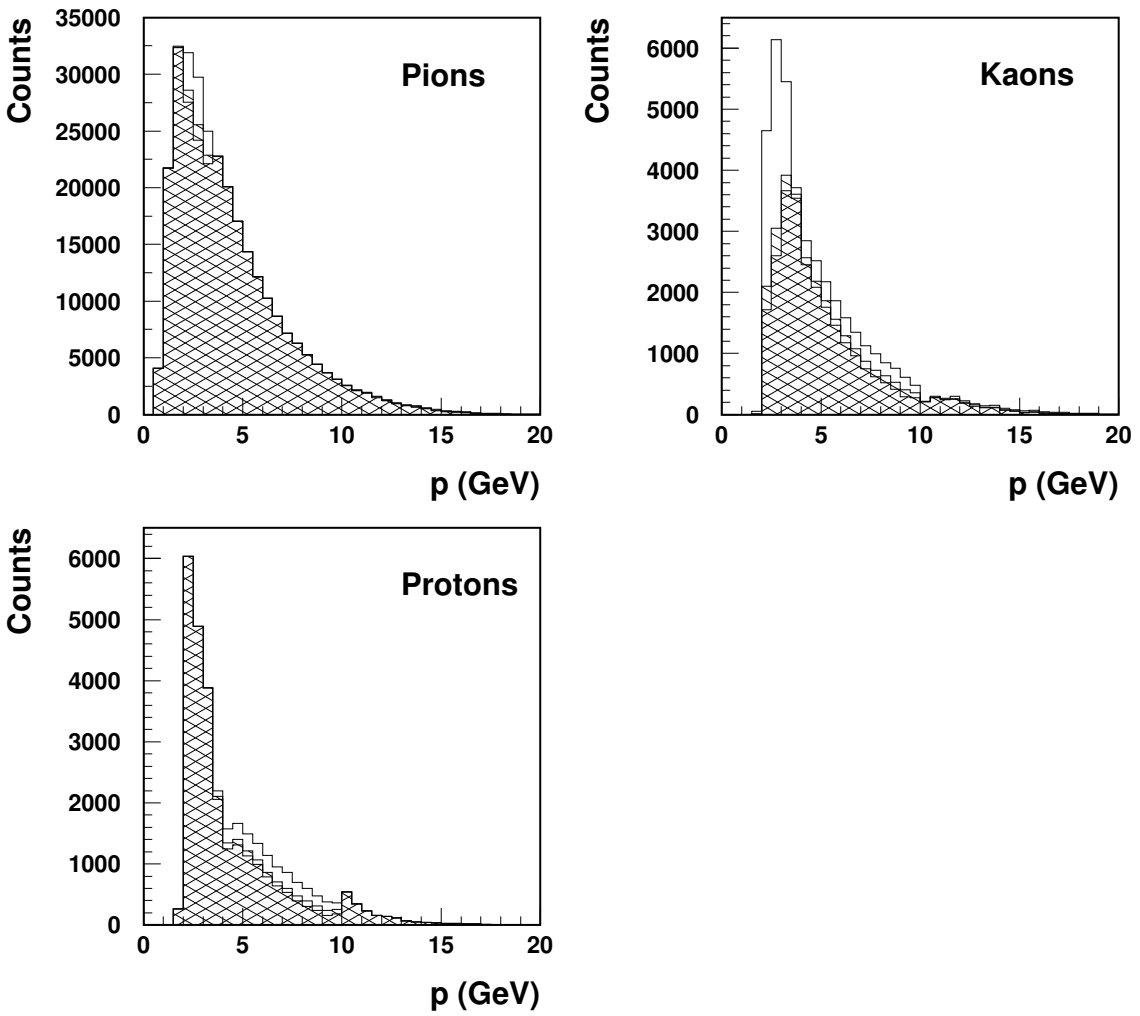

Figure 6.9: Comparison of statistics for pions, kaons and protons between the different quality parameters of $rQp > 0.0$, $rQp > 0.5$ and $rQp > 1.0$. The open hatch, right and left diagonal hatches represent the statistics for $rQp > 0.0$, $rQp > 0.5$ and $rQp > 1.0$ respectively.

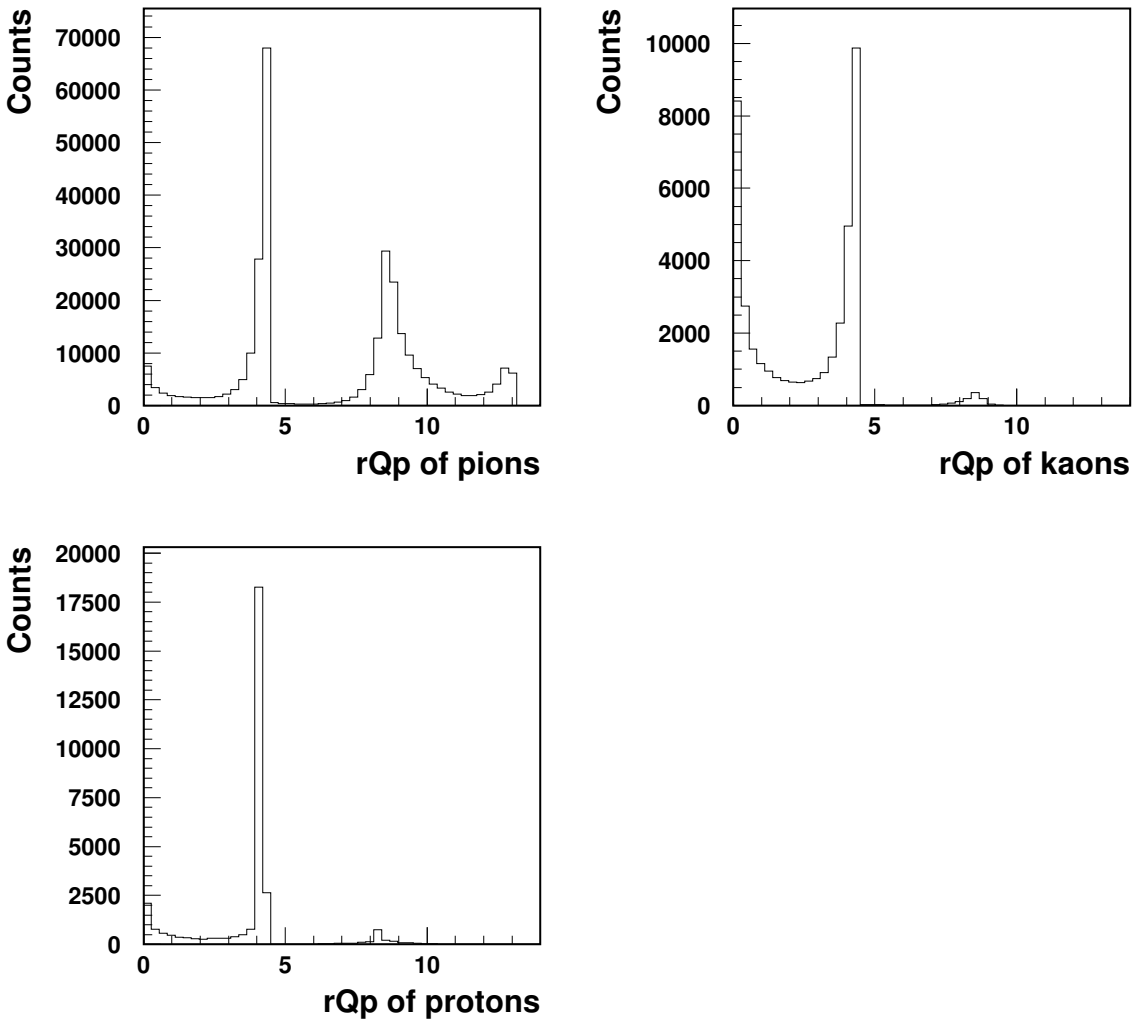

Figure 6.10: Distributions of the quality parameter for pions, kaons and protons.

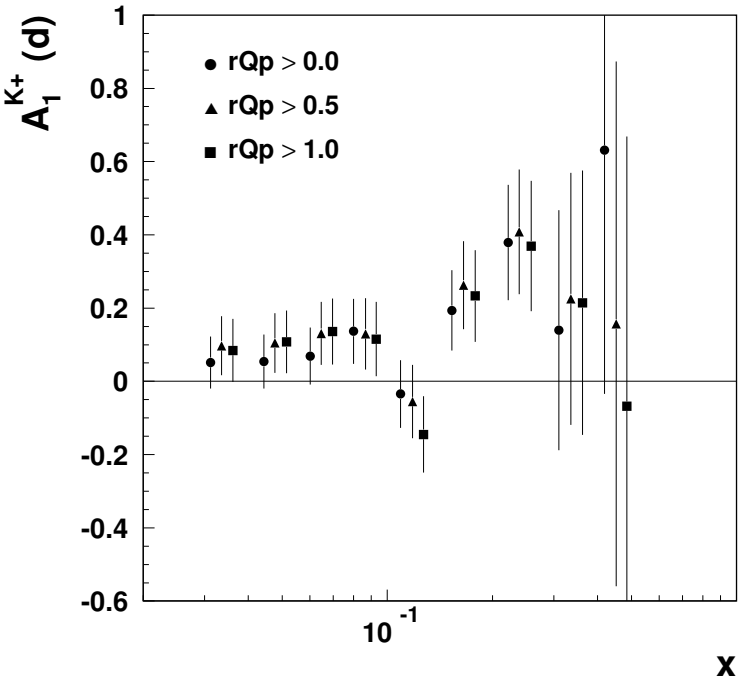

Figure 6.11: Comparison of the K^+ asymmetry between the different quality parameters. The asymmetries are for the results before the corrections for the contaminations between hadrons. The analyses are performed imposing the momentum threshold more than 3.25 GeV consistently .

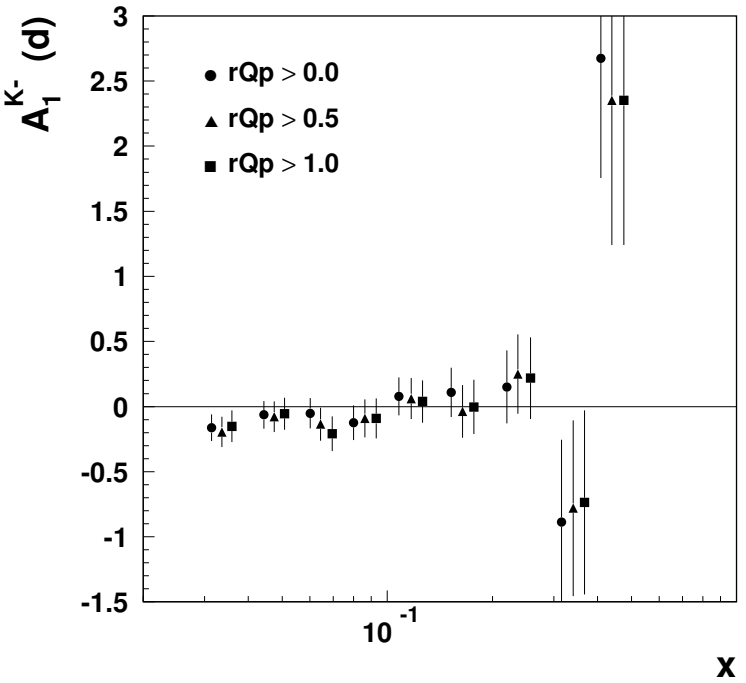

Figure 6.12: Comparison of the K^- asymmetry between the different quality parameters. The asymmetries are for the results before the corrections for the contaminations between hadrons. The analyses are performed imposing the momentum threshold more than 3.25 GeV consistently .

Chapter 7

Corrections of Asymmetries for Hadron Contaminations

The count rate for each type of hadrons for the extraction of the semi-inclusive asymmetries is generally contaminated by the tracks of uninteresting particles. The separation between leptons and hadrons by the particle identification detectors of HERMES experiment is excellent. The most contributions of the contaminations to the asymmetry of each type of hadrons is due to the uninteresting tracks of hadrons which are misidentified by the RICH detector. In this section the asymmetries of the hadrons are corrected for the contaminations between the hadrons by the identification probabilities presented in the previous chapter. At the end the results of the corrected asymmetry for each type of hadrons are shown together with the estimate of the systematic uncertainties.

7.1 Method of Corrections

The value of each element of the Q matrix in equation (5.7) corresponds to the probabilities for the particle hypothesis assigned to each type of hadrons. For example, when the cuts of the momentum more than 0.5 GeV for pions, more than 3.25 GeV for kaons and more than 2.0 GeV for protons are imposed the Q matrix averaged in the whole region of the momentum more than 0.5 GeV is formed like:

$$\mathsf{Q} = \begin{pmatrix} Q_\pi^\pi & Q_\pi^{\mathrm{K}} & Q_\pi^{\mathrm{p}} \\ Q_{\mathrm{K}}^\pi & Q_{\mathrm{K}}^{\mathrm{K}} & Q_{\mathrm{K}}^{\mathrm{p}} \\ Q_{\mathrm{p}}^\pi & Q_{\mathrm{p}}^{\mathrm{K}} & Q_{\mathrm{p}}^{\mathrm{p}} \end{pmatrix} \tag{7.1}$$

$$= \begin{pmatrix} 0.975 & 0.012 & 0.047 \\ 0.007 & 0.898 & 0.041 \\ 0.018 & 0.090 & 0.912 \end{pmatrix}. \tag{7.2}$$

Then this means that a kaon track identified by the RICH detector has probabilities for each true type of hadron like 89.8 % for kaon, 0.90 % for proton and 1.2 % for pion. Similarly, a pion track identified by the RICH detector has probabilities for

each true type like 97.5 % for pion, 0.7 % for kaon and 1.8 % for proton and also a proton track identified by the RICH detector 91.2 % for proton, 4.7 % for pion and 4.1 % for kaon. Since the elements of the Q matrix depend on the momentum of the tracks, in the real procedure for a hadron track identified by the RICH detector the true type of hadron has to be assigned by the corresponding elements of the Q matrix per momentum bin. Moreover as the elements of the Q matrix mean the probabilities, the corrections from the identified type of hadron to the true type of hadron are achieved by iterating this many times. If the assignment of the true type of hadron per track for the total statistics of hadrons identified by the RICH detector is performed many times by the generation of the random number, it will form the Gaussian distribution according to the theorem of the central limit distribution (CLD). The random number is generated in the range from 0 to 1. Figure 7.1 shows the procedures of the CLD method. In the figure as an example for an identified pion track the true type of hadron according to the corresponding elements of the Q matrix is assigned. Concretely, at first the group of hadrons identified by the RICH detector is yielded. Secondly for the identified type of hadron in the group the true type is assigned according to the corresponding elements of the Q matrix taking the momentum of each track into account. Then one obtains the corrected group for statistics of hadrons and in this first assignment one can measure the asymmetry of each type of hadrons from statistics of each true type in the group. When this procedure is performed many times, one obtains the results of many asymmetries by the measurements of the many times. The results of the many asymmetries will form the Gaussian distribution. Finally the corrected asymmetry can be determined from the mean value of the distribution.

7.2 Corrected Kinematics

Since the Q matrix represents the probabilities for the true type of hadron it is impossible to see the distributions of the kinematical variables like momentum, z, x Feynman and so on related to hadrons when the CLD method was performed. It, however, is assumed that it is interesting to see the distributions beforehand when the procedure for the assignment of the true type of hadron to the identified type of hadron by the RICH detector is performed once. Especially since z and x Feynman are original kinematical variables related to hadrons and the mass of each type of hadrons is required in their calculations, it makes sense to see the distributions.

7.2.1 Momentum Distributions

Figure 7.2 shows the momentum distributions for pions, kaons and protons. The left figures show the uncorrected distributions, which mean the distributions for the identified type by the RICH detector. The right figures show the corrected distributions when the procedure for the assignment of the true type to the identified type of hadron by the RICH detector was performed once according to the elements of the Q matrices. These mean the distributions for the true type of hadron. Here

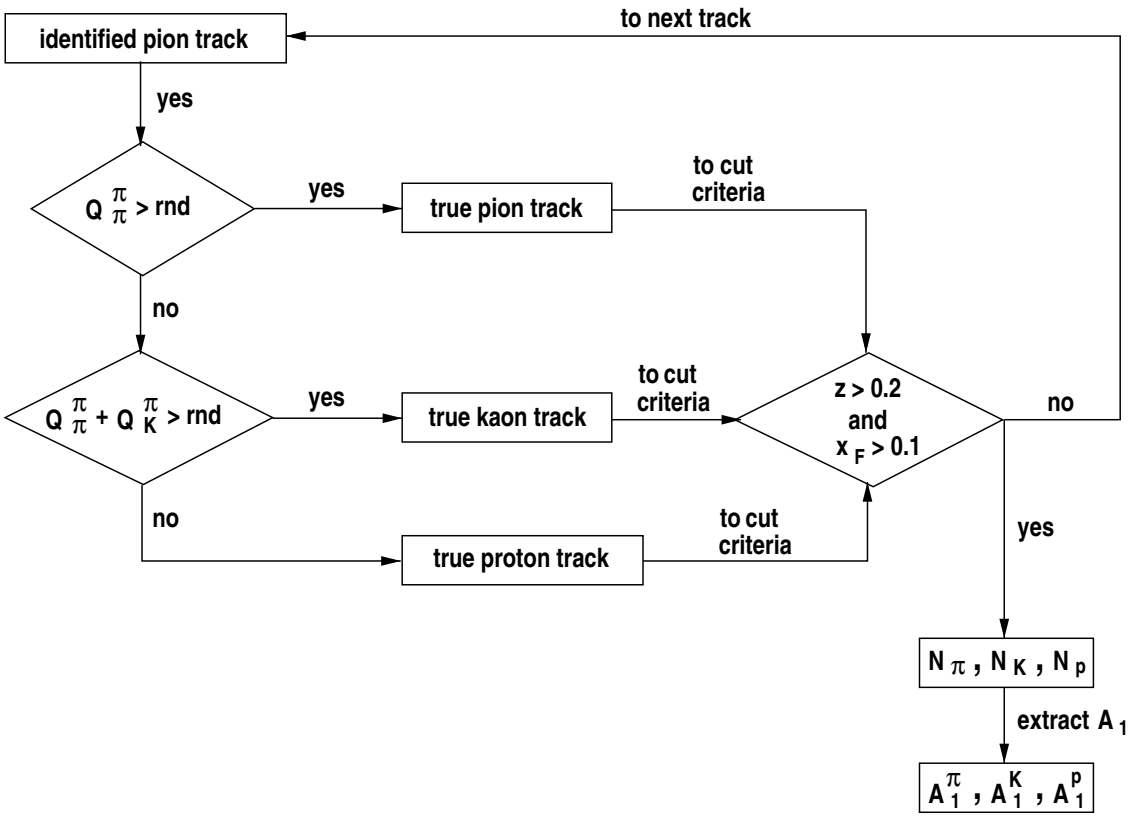

Figure 7.1: Procedures for the assignment of the true type of hadron to the identified type of hadron in the CLD method. rnd means the random number, which is generated in the range from 0 to 1. The corresponding elements of the Q matrix are compared with the random number to assign the true type of hadron. The numbers of the true type for pions, kaons and protons are counted after the imposition of the kinematical cuts like z and x_{F} and the asymmetries for pion, kaon and proton are extract from their numbers of each true type of hadron.

the Q matrices in $rQp > 0.0$ studied by the Monte Carlo simulation were used for the corrections. In the experiment since kaon and proton have heavier mass than pion and their tracks have low momenta, they are bent by the magnetic field of the spectrometer magnet and do not reach the RICH detector. In the left figures the distributions for kaons and protons identified by the RICH detector are truncated at the region of the momentum lower than 2 GeV. On the other hand in the right figures kaons and protons are distributed in the region lower than 2 GeV by the correction of the true type. The distributions of kaons and protons in the region lower than 2 GeV come from the converted pions with the momentum lower than 2 GeV by correction of the true type according to the Q matrices. As the original statistics of hadrons increases, it is assumed that more statistics of kaons and protons in the region of the momentum lower than 2 GeV will be accumulated and the distributions of kaons and protons will be closer to the ones of the GEANT type for kaons and protons shown in figure 5.2.

For the distribution of protons the dip at about 4 GeV in the left figure is due to the effect of the momentum threshold in the aerogel and to some extent is improved after the correction. It is assumed that if the original statistics increases more this distribution can be more smoothly corrected.

7.2.2 z Distributions

Similarly, figure 7.3 is the corrected distributions of z for all hadrons, pions, kaons and protons. It is found that the distribution for kaons has gentler hill compared to the shapes for pions and protons and has the maximum at $z \simeq 0.2$. The distribution for protons has sharper peak than others. The starting points of the distributions are higher in order of protons, kaons and pions according to their masses. Each distribution does not start from $z = 0$ because the tracks with low momenta are bent by the spectrometer magnet and are not detected by the HERMES spectrometer.

7.2.3 x_{F} Distributions

Figure 7.4 shows the corrected distributions of x_{F} for all hadrons, pions, kaons and protons. The variable of x_{F} has the values within the range from -1 to 1. x_{F} for pions is less distributed in the negative region. x_{F} for kaons has gentle shape and is clearly distributed in both positive and negative regions. It is found that x_{F} for proton distributes in the negative region much and greatly contributes to the negative region of the distribution for hadrons. If the asymmetries of pion, kaon and proton are extracted from statistics of these distributions it is found that it is reliable enough to impose the cut of $x_{\mathrm{F}} > 0.1$ to the tracks of hadrons in order to remove the possibility of the tracks of hadrons which come from the target remnants.

7.2.4 Relationship between kinematical Variables

Figure 7.5 shows the relationship between z and x_{F} for pions, kaons and protons. It is found that for pions and kaons z and x_{F} have correspondence of almost 1 to 1. It, namely, means that if the cut of $z \geq 0.2$ is required then the cut of $x_{\mathrm{F}} \geq 0.1$ for a criterion of the event selection listed in table 6.2 already meets, so that the cut of x_{F} can be neglected. For protons, as x_{F} greatly distributes in the negative region the correspondence between z and x_{F} is not rigidly 1 to 1. It, however, can be regarded that the cut of $z \geq 0.2$ is almost equal to the cut of $x_{\mathrm{F}} \geq 0.1$.

Figure 7.6 shows the relationship between momentum and z for pions, kaons and protons. The left side is a scatter plot and the right side corresponds to a contour plot for the left figures. As seen in the figures if the cut of $p > 5.0$ GeV for pions, kaons and protons is required the cut of $z \geq 0.2$ automatically is satisfied, so that the cut of z can be neglected. Then large statistics, however, is sacrificed to measure the asymmetry because most statistics of each hadron distribute in the region of the momentum from 2 GeV to 6 GeV.

7.3 Conclusion for kinematical Cuts

In conclusion to extract the asymmetry with more reliability both cuts of $z \geq 0.2$ and $x_{\mathrm{F}} \geq 0.1$ are required. Then each mass of pion, kaon and proton is applied to calculate z and x_{F} for their cut criteria. As mentioned in section 6.7 the momentum threshold of 3.25 GeV is imposed for kaons. For pions and protons the momentum thresholds of 0.5 GeV and 2 GeV are imposed respectively as listed in table 6.2. Then more statistics of each hadron can be kept to determine the asymmetry more precisely.

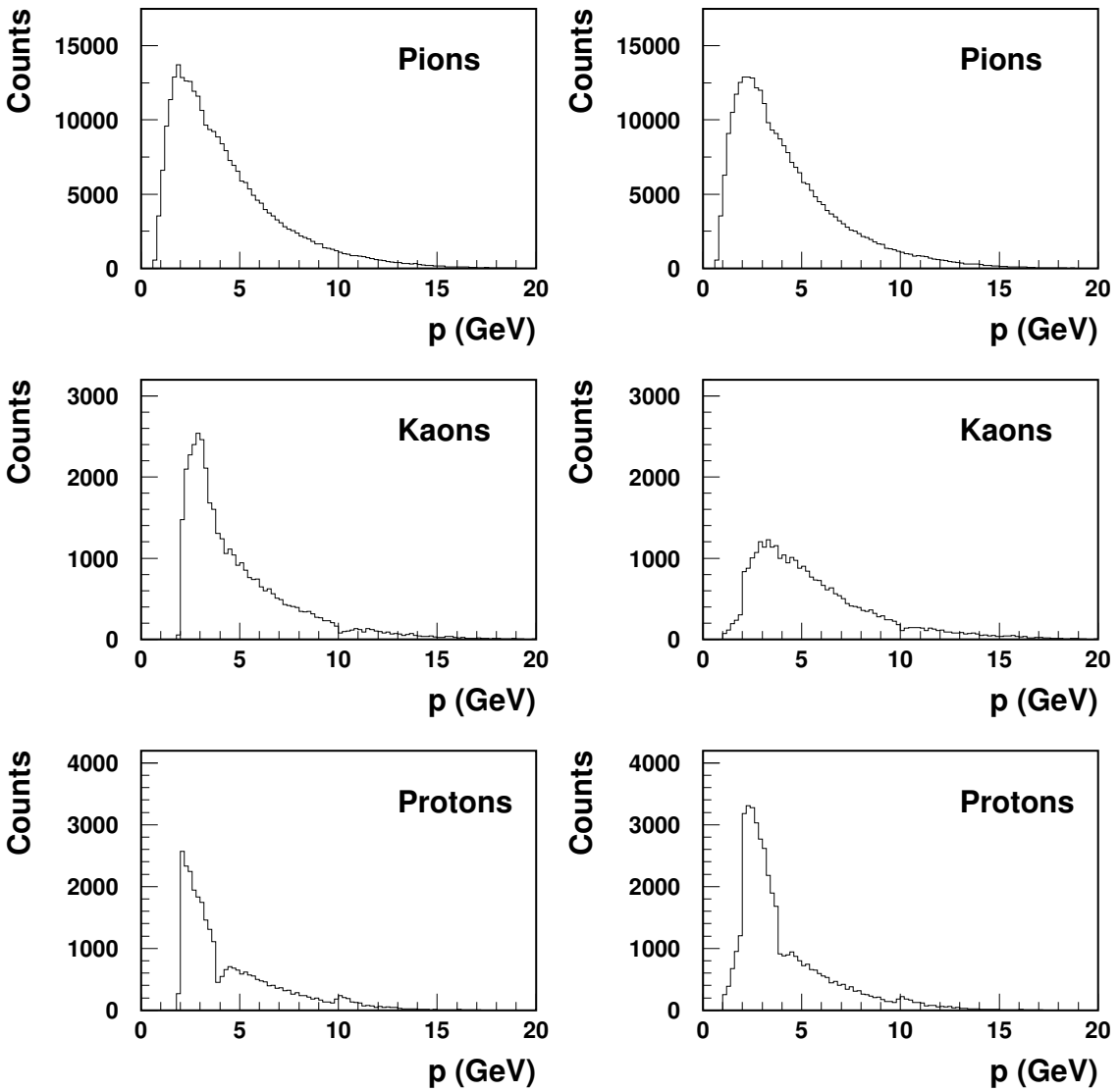

Figure 7.2: Momentum distributions for pions, kaons and protons. The left side figures show the uncorrected distributions, which mean the distributions for the identified type of hadron by the RICH detector. The right side figures show the corrected distributions when the procedure for the assignment of the true type to the identified type by the RICH detector was performed once according to the elements of the Q matrices in $rQp > 0.0$. These mean the distributions for the true type of hadron.

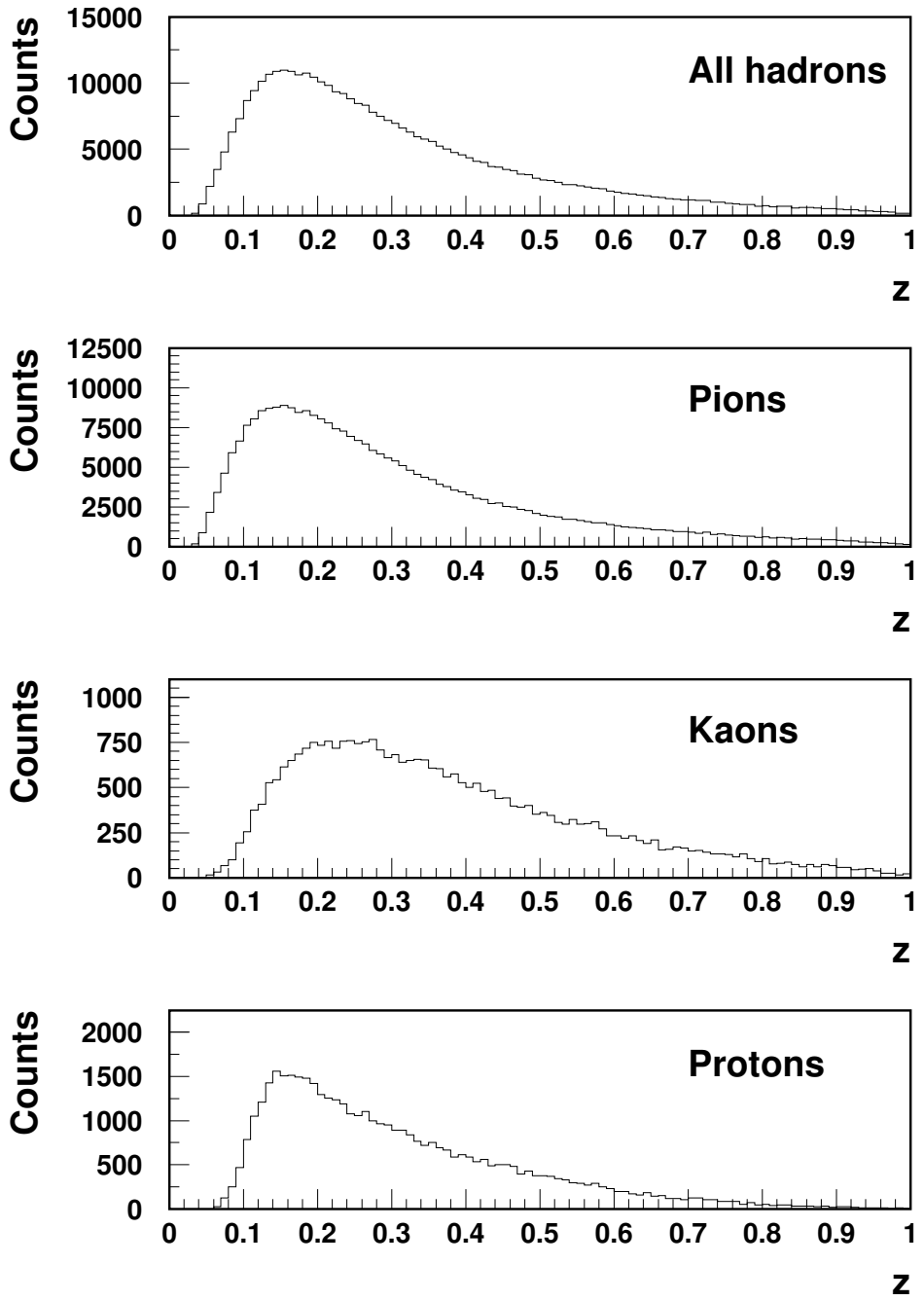

Figure 7.3: Corrected distributions of z for all hadrons, pions, kaons and protons when the procedure for the assignment of the true type to the identified type by the RICH detector was performed once according to the elements of the Q matrices in $rQp > 0.0$.

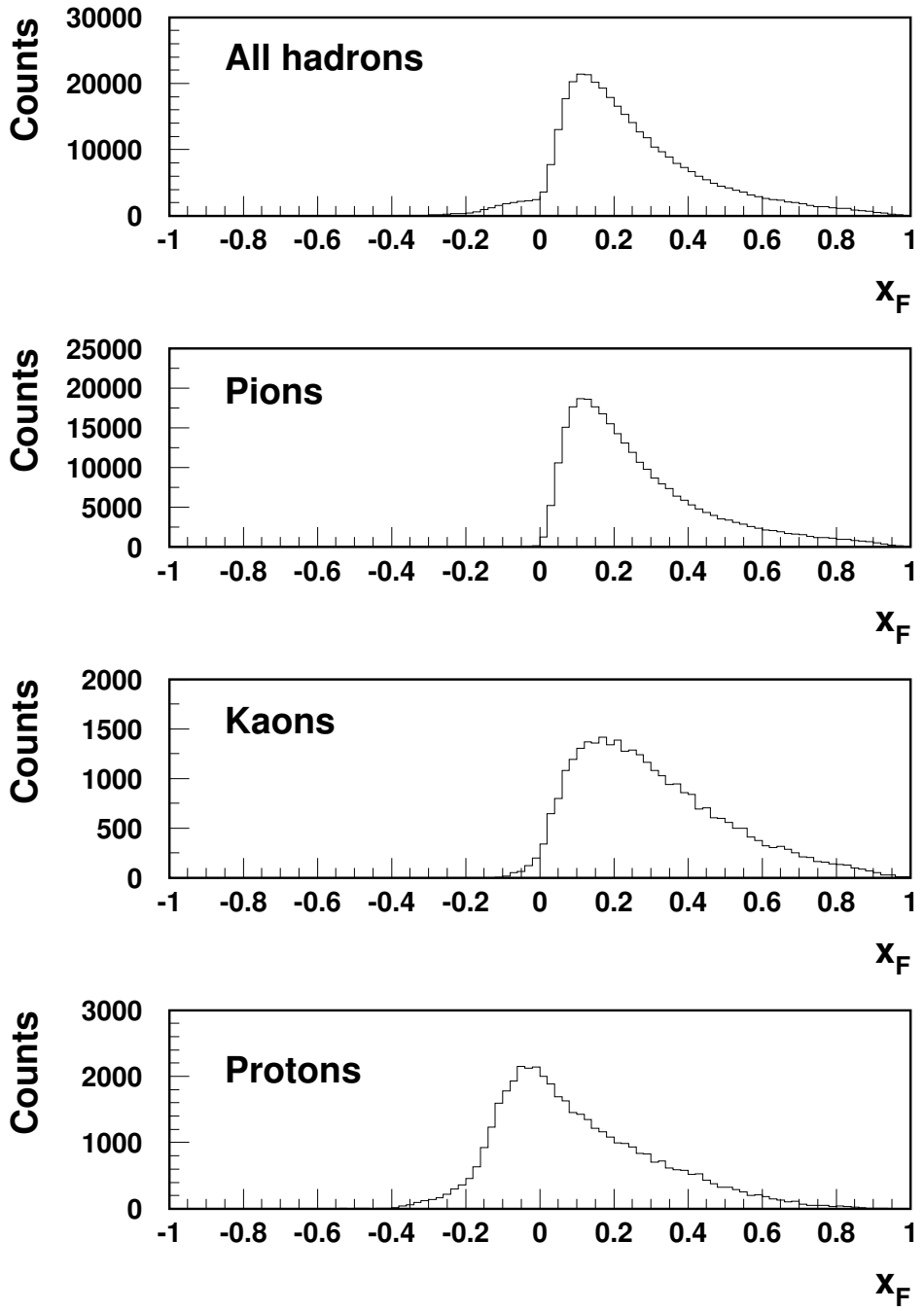

Figure 7.4: Corrected distributions of x_{F} for all hadrons, pions, kaons and protons when the procedure for the assignment of the true type to the identified type by the RICH detector was performed once according to the elements of the Q matrices in $rQp > 0.0$.

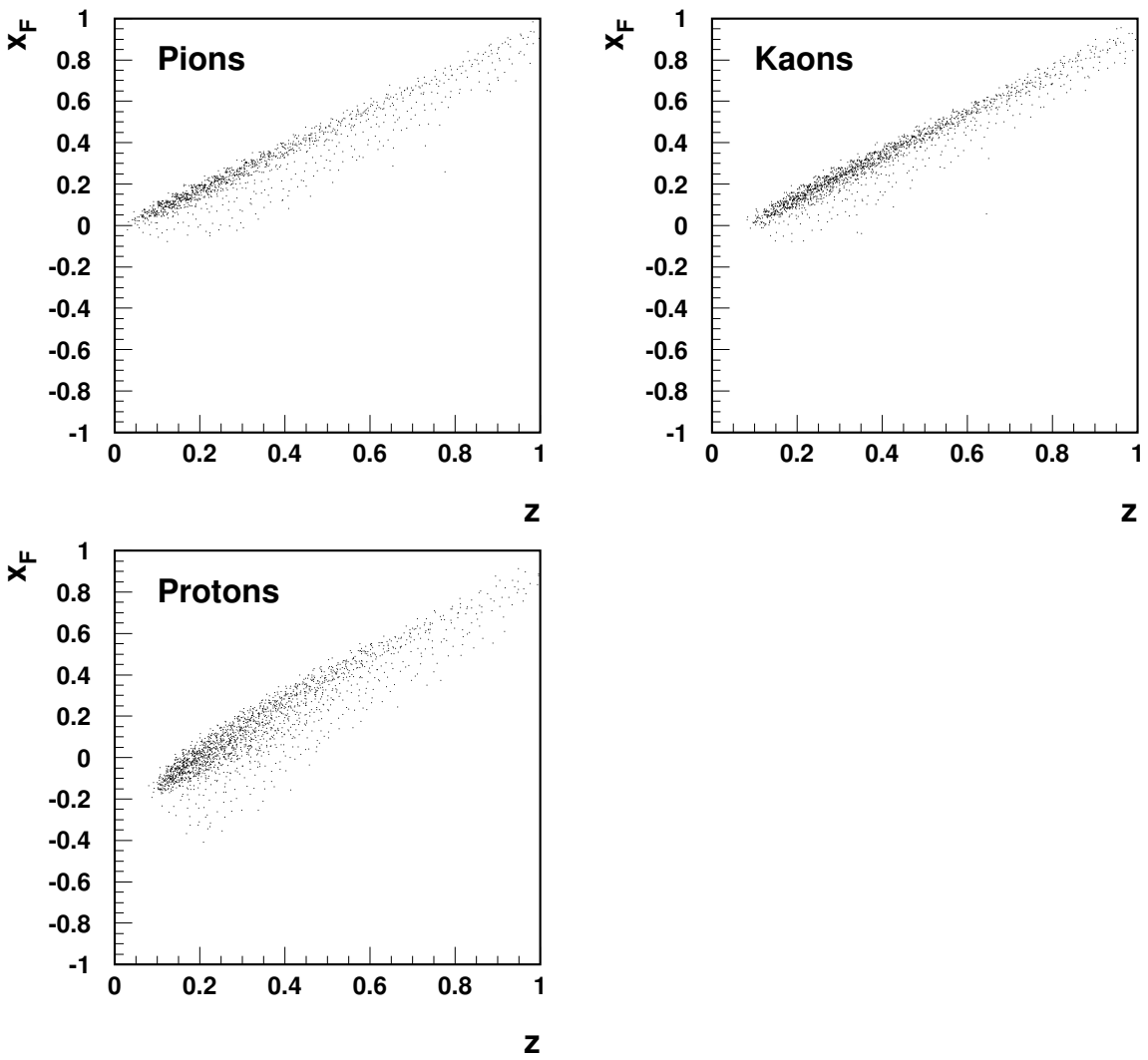

Figure 7.5: Relationship between z and x_{F} for pions, kaons and protons when the procedure for the assignment of the true type to the identified type by the RICH detector was performed once according to the elements of the Q matrices in $rQp > 0.0$.

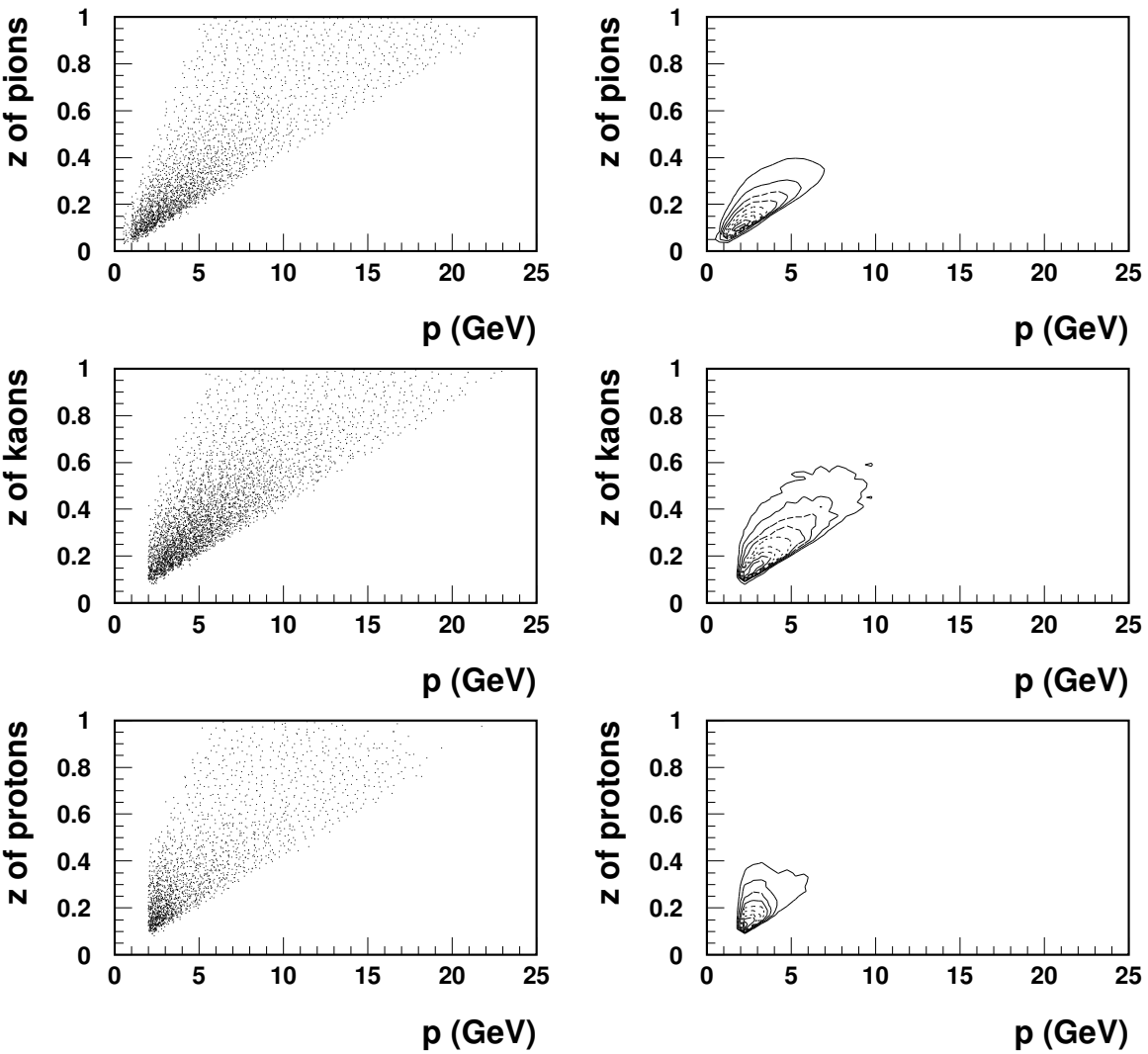

Figure 7.6: Relationship between momentum and z for pions, kaons and protons when the procedure for the assignment of the true type to the identified type by the RICH detector was performed once according to the elements of the Q matrices in $rQp > 0.0$. The left side is a scatter plot and the right side a contour plot for the left figures.

7.4 Test of central Limit Distribution Method

To test the central limit distribution (CLD) method, supposing that a simple Q matrix for only pions and kaons in a certain bin of momentum is defined as follows:

$$\mathsf{Q} = \begin{pmatrix} Q_\pi^\pi & Q_\pi^{\mathrm{K}} \\ Q_{\mathrm{K}}^\pi & Q_{\mathrm{K}}^{\mathrm{K}} \end{pmatrix} \tag{7.3}$$

$$= \begin{pmatrix} 0.7 & 0.3 \\ 0.3 & 0.7 \end{pmatrix}. \tag{7.4}$$

Moreover just supposing that the numbers $\vec{\mathsf{I}}$ of pions and kaons identified by the RICH detector in the different spin states between beam and target is obtained in the same bin of momentum in the experiment as follows:

$$(I^{\pi,\rightrightarrows}, I^{\mathrm{K},\rightrightarrows}) = (100, 900), \tag{7.5}$$

$$(I^{\pi,\rightleftarrows}, I^{\mathrm{K},\rightleftarrows}) = (900, 100). \tag{7.6}$$

One of the ways to obtain the numbers of the true type for pions and kaons is to simply multiply $\vec{\mathsf{I}}$ by the Q matrix according to equation (5.17). Then the numbers $\vec{\mathsf{N}}$ of the true type for pions and kaons per different spin states can be obtained below:

$$(N_\pi^{\rightrightarrows}, N_{\mathrm{K}}^{\rightrightarrows}) = (340, 660), \tag{7.7}$$

$$(N_\pi^{\rightleftarrows}, N_{\mathrm{K}}^{\rightleftarrows}) = (660, 340). \tag{7.8}$$

On the other hand in the CLD method each element of the Q matrix is regarded as the probability for the particle hypothesis of a hadron track identified by the RICH detector. Then the numbers $\vec{\mathsf{N}}$ can be determined by the central limit theorem. To perform the CLD method the random number generated in the range from 0 to 1 is compared to the Q matrix elements in column related to pion and kaon in order to assign the true type. Finally the numbers $\vec{\mathsf{N}}$ of the true type obtained in the former way and the CLD method should be close to each other if the assignment of the true type in the CLD method is executed many times.

Figure 7.7 shows the result obtained by the CLD method. The number of true type in each distribution can be determined as the mean value by the Gaussian fit to the distribution. The resulting numbers $N_\pi^{\rightrightarrows}$ and $N_{\mathrm{K}}^{\rightrightarrows}$, $N_\pi^{\rightleftarrows}$ and $N_{\mathrm{K}}^{\rightleftarrows}$ obtained by the CLD method is in good agreement with the ones of the former way. The width of each distribution is automatically determined by the Q matrix elements in column and this uncertainty cannot be avoided because this obeys the property of the binominal distribution. Therefore it is assumed that the precision of the determination for the elements of the Q matrix is sensitive to the resulting quantity. As the Q matrix depends on the flux of each hadron according to equation (5.13), this means that the flux of each hadron is the most important quantity to know though in general the real flux is difficult to estimate from the experiment. The

uncertainty of the flux on the asymmetry should be estimated and is discussed in section 7.7.3. Additionally it is assumed that the average value of the distribution can fluctuate due to the originally small statistics. This fluctuation is estimated as the systematic uncertainty in section 7.7.2.

The former way to obatin the number of the true type is approximate way to extract the semi-inclusive spin asymmetry A_1. In principle this way cannot take into account the cuts of z and x_{F} and does not allow to calculate the depolarization factor and the kinematical variables of η and γ related to the asymmetry A_1, which should be averaged per each bin of x. On the other hand the CLD method allows to take all above conditions into account, so that the asymmetry can be correctly extracted with the best reliability.

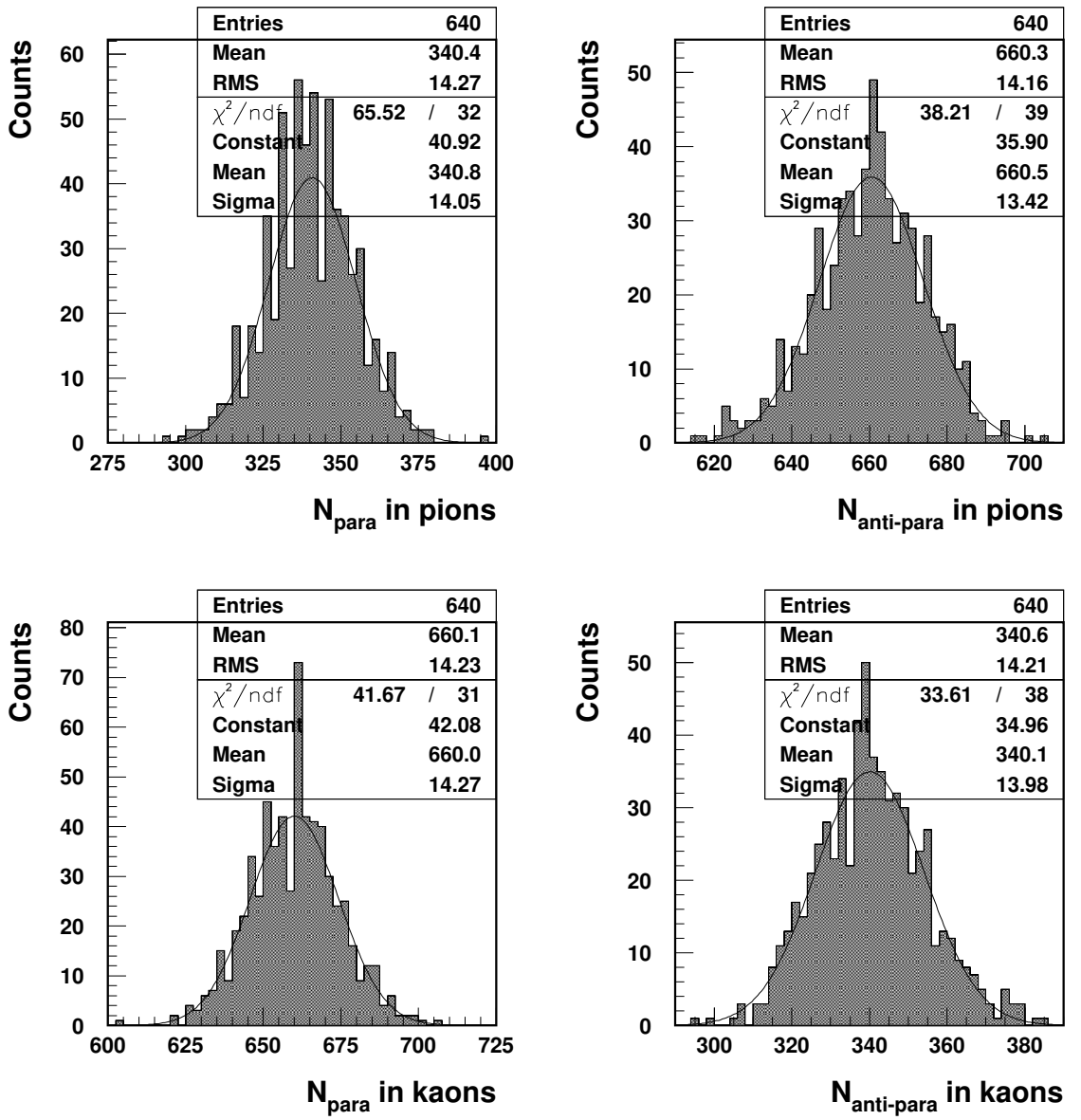

Figure 7.7: Distributions of statistics $N^{\rightrightarrows}$ (left) and $N^{\rightleftarrows}$ (right) for pions (upper) and kaons (lower) resulting from the execution more than 600 times for the assignment of the true type to the identified type. The average of the distribution was determined by the Gaussian fit in the solid curve. N_{para} and $N_{anti-para}$ in the figures mean $N^{\rightrightarrows}$ and $N^{\rightleftarrows}$ respectively.

7.5 Corrected Asymmetry

As the results of the execution of the CLD method the observable quantities like the mean value of the asymmetry, its statistical uncertainty, Bjorken x and so on related to the asymmetry are determined from the average value of the quantity for the extraction of the asymmetry in each bin of x. In the CLD method the assignment of the true type of hadron to the identified type of hadron by the RICH detector is performed more than 600 times. Statistics of the identified hadrons to assign the true type are 1.39×10^5 for the positively charged hadrons and 9.29×10^4 for the negatively charged hadrons as mentioned in section 6.6. The assignment of the true type of hadron to the identified type of hadron is performed per track for these statistics. The asymmetry is formed per an assignment of the true type for the whole statistics of hadrons. Therefore it means that the 600 asymmetries are formed if the assignments of 600 times are done. The average value of the distribution for the 600 asymmetries is taken as the final result of the asymmetry. The average value of the distribution is determined by the Gaussian fit to the distribution. In this section especially the corrections of the spin asymmetry for kaon is described. Not only the final result of the asymmetry for kaon but also the asymmetry for hadron, pion and proton are presented in section 7.8. The systematic uncertainties on the asymmetry are studied in section 7.7.

Figure 7.8 shows the distributions for the mean value of the K^+ asymmetry in each bin of x. In the ninth bin of x the standard deviation is larger than other bins and the result of the fit to the distribution is not good. In section 7.7.2 the error of the fit in the determination of the average values of the distribution is estimated as a systematic uncertainty on the corrected asymmetry. The average values by the fit are taken to form the asymmetry of the final result. Similarly figure 7.9 shows the distributions for the statistical uncertainty of the K^+ asymmetry in each bin of x. Their standard deviation in each bin is added as a systematic uncertainty on the corrected asymmetry as well. The average Bjorken x in each bin should be determined from the fit to the distribution for the mean Bjorken x. Figure 7.10 shows the distributions for the mean Bjorken x of the K^+ asymmetry in each bin of x and the fit to the distributions is performed. Not only for the K^+ asymmetry but also for the K^- and other hadron asymmetries the same procedures are performed to determine the final results of the asymmetries.

Figures 7.11 and 7.12 show the comparison between the uncorrected and corrected asymmetry for K^+ and K^- respectively. From each figure it is found that the correction is small. As a reason it is assumed that if the region of the momentum with the high identification purities is chosen, the degree of the assignment from the identified type of hadron to the true type of hadron is small even though the procedures for the assignment are performed many times. For kaons if the momentum threshold of 3.25 GeV is required the average identification purity in the region of the momentum more than 3.25 GeV reaches about 90 %. For the ninth bin of the K^- asymmetry the average value of the asymmetry are affected by the fluctuation of the distribution resulting from the assignment of the true type because of

the originally small statistics in this bin. Tables 7.1 and 7.2 are the comparison of statistics between before and after the corrections of the asymmetry. Statistics after the corrections of the asymmetry were determined from the average value by the Gaussian fit to the distribution for statistics obtained by the assignment of the true type to the identified type more than 600 times.

From the definition in equation (2.43) the value of the spin asymmetry should be from -1 to 1. As seen in figure 7.12 the mean value and its statistical error for the K^- asymmetry in the ninth bin exceed 1. The reason is attributed to that the measured asymmetry includes the virtual photon depolarization factor into the denominator of the formula in equation (6.21). The depolarization factor represents the degree of the polarization transfer from the polarized beam to the virtual photon. Therefore the depolarization factor has values from 0 to 1. Figure 7.13 shows the depolarization factor for the DIS events, positively and negatively charged kaons in coincidence with the DIS events. The depolarization factor for positively and negatively charged kaons slowly decreases to about 0.5 at minimum compared to the one of the DIS events. Furthermore the spin asymmetry has the kinematical factor of $1/(1+\eta\gamma)$ in the formula of itself, which is additionally shown in the bottom part of figure 7.13.

Statistics for $A_1^{K^+}$				
	Before		After	
Bin	$N^{\vec{\Rightarrow}}$	$N^{\vec{\Leftarrow}}$	$N^{\vec{\Rightarrow}}$	$N^{\vec{\Leftarrow}}$
1	1125	1137	1140	1152
2	1466	1476	1432	1437
3	1585	1603	1521	1526
4	1318	1371	1251	1304
5	1280	1236	1205	1172
6	845	901	792	837
7	386	447	366	419
8	96	100	90	95
9	21	27	20	26

Table 7.1: Comparison of statistics between before and after the corrections of the K^+ asymmetry. Statistics after the corrections of the asymmetry were determined from the average value by the Gaussian fit to the distribution for statistics obtained by the assignment of the true type of hadron more than 600 times. For the values of statistics after the corrections the fractions are rounded off to integral place.

Statistics for $A_1^{K^-}$				
	Before		After	
Bin	$N^{\vec{\Rightarrow}}$	$N^{\vec{\Leftarrow}}$	$N^{\vec{\Rightarrow}}$	$N^{\vec{\Leftarrow}}$
1	570	507	586	535
2	686	651	676	649
3	697	667	673	643
4	551	510	520	483
5	457	464	431	436
6	267	275	248	254
7	123	129	112	119
8	29	19	26	18
9	2	9	2	8

Table 7.2: Comparison of statistics between before and after the corrections of the K^- asymmetry. Statistics after the corrections of the asymmetry were determined from the average value by the Gaussian fit to the distribution for statistics obtained by the assignment of the true type of hadron more than 600 times. For the values of statistics after the corrections the fractions are rounded off to integral place.

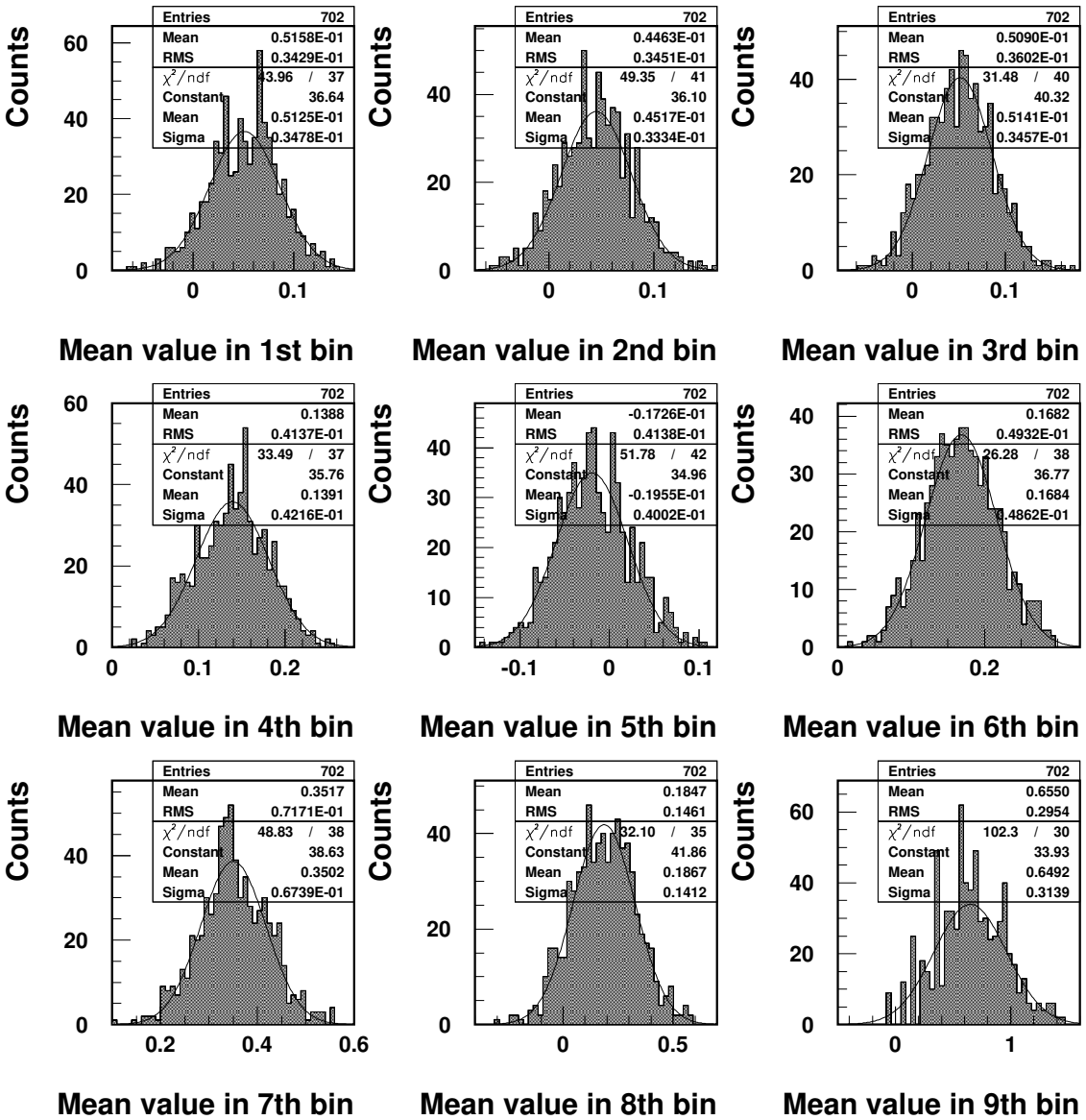

Figure 7.8: Distributions for the mean value of the K^+ asymmetry in each bin of x. The procedures for the assignment of the true type of hadron to the identified type of hadron were performed more than 600 times. The average value of the distribution was determined by the Gaussian fit in the solid curve.

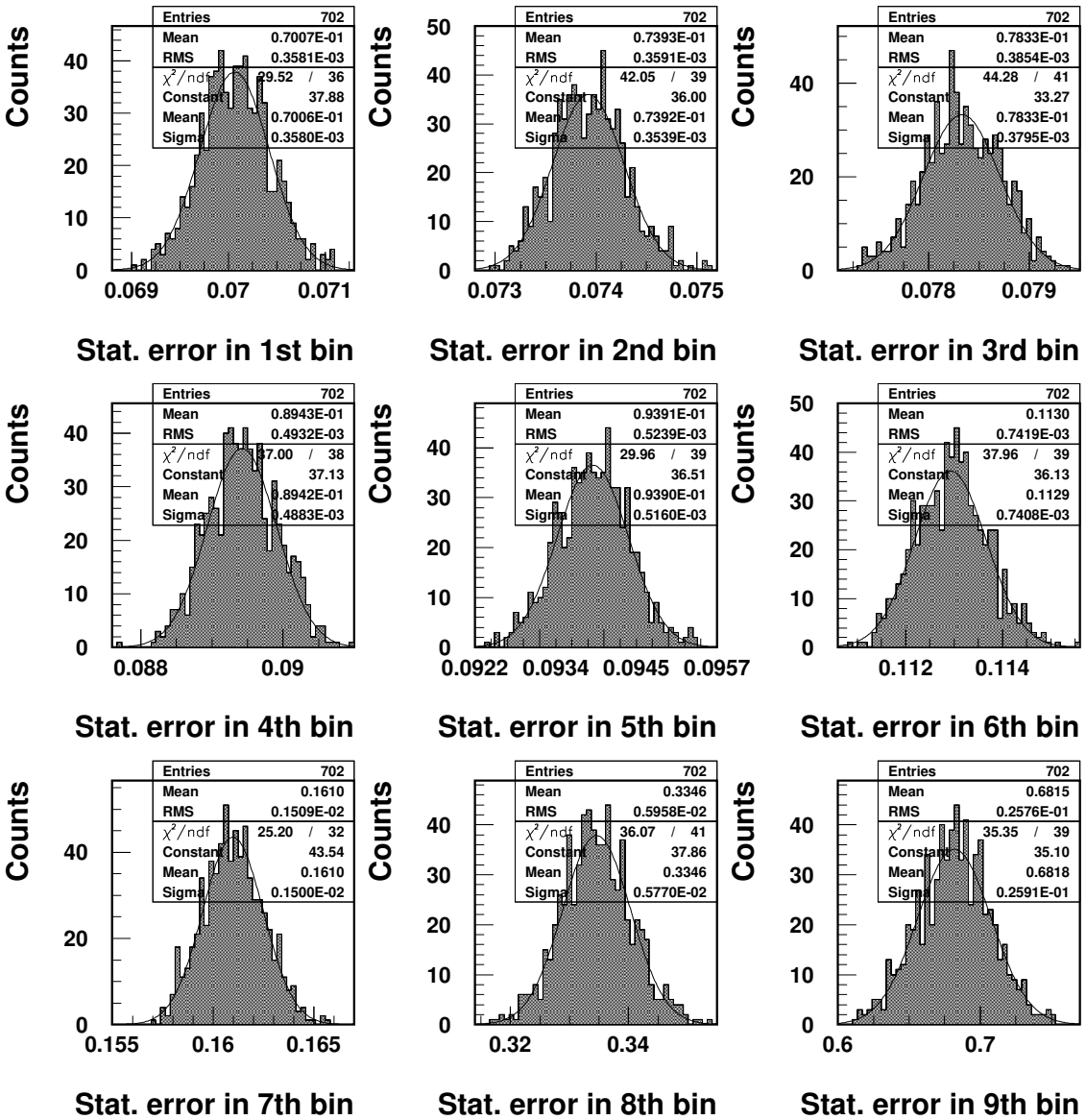

Figure 7.9: Distributions for the statistical uncertainty of the K^+ asymmetry in each bin of x. The procedures for the assignment of the true type of hadron to the identified type of hadron were performed more than 600 times. The average value of the distribution was determined by the Gaussian fit in the solid curve.

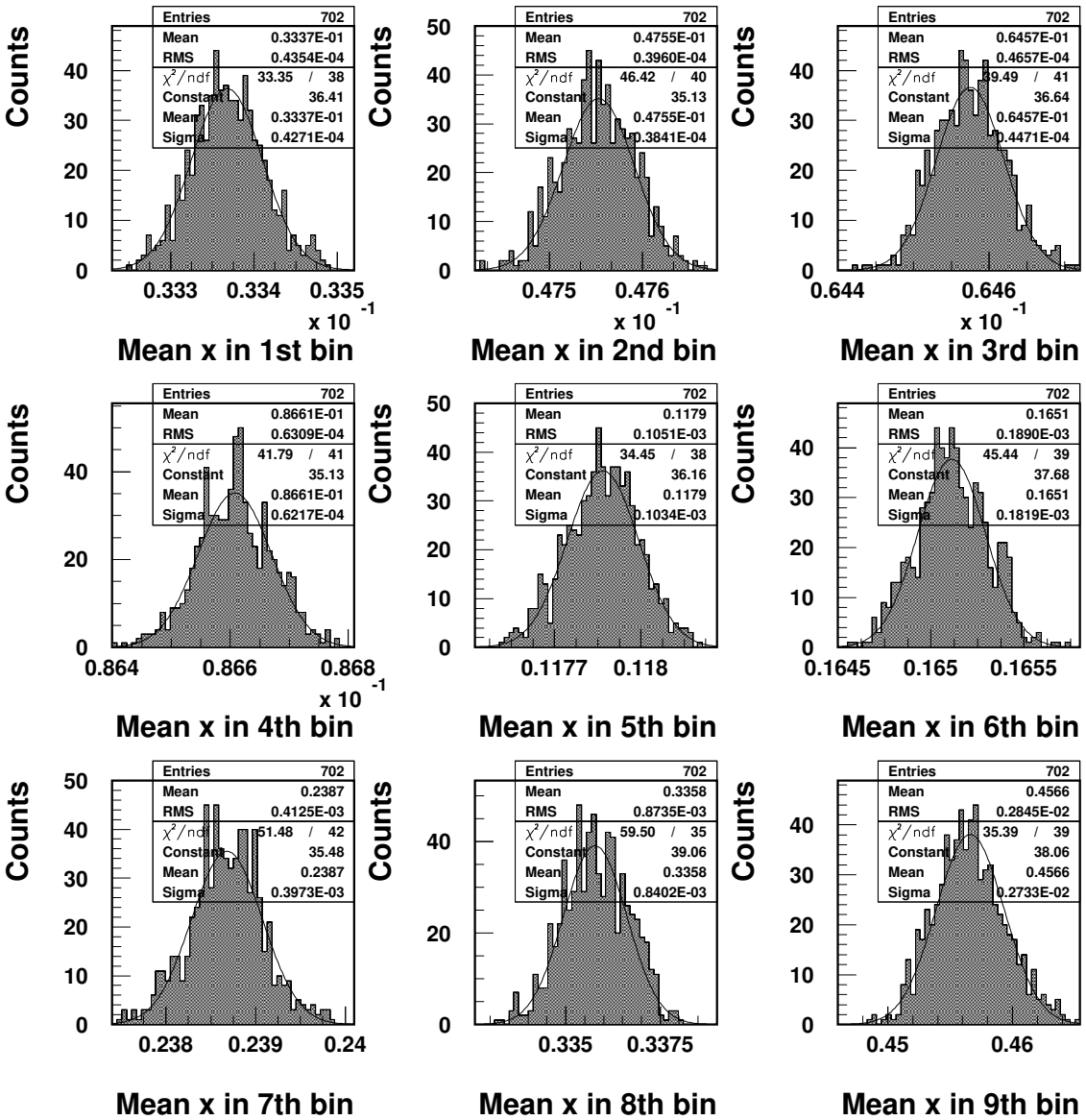

Figure 7.10: Distributions for the mean Bjorken x of the K^+ asymmetry in each bin of x. The procedures for the assignment of the true type of hadron to the identified type of hadron were performed more than 600 times. The average value of the distribution was determined by the Gaussian fit in the solid curve.

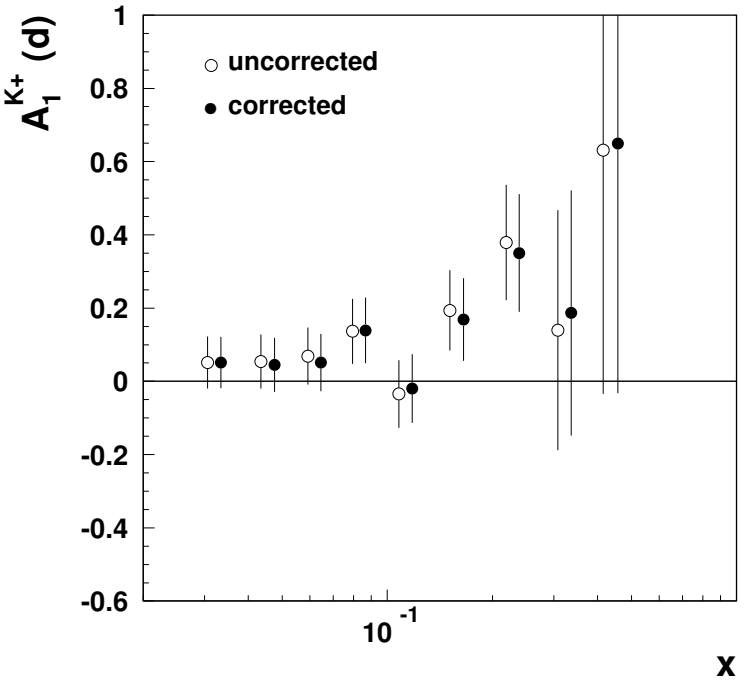

Figure 7.11: Comparison of the K^+ asymmetry between uncorrected (open circles) and corrected (closed circles) by the CLD method.

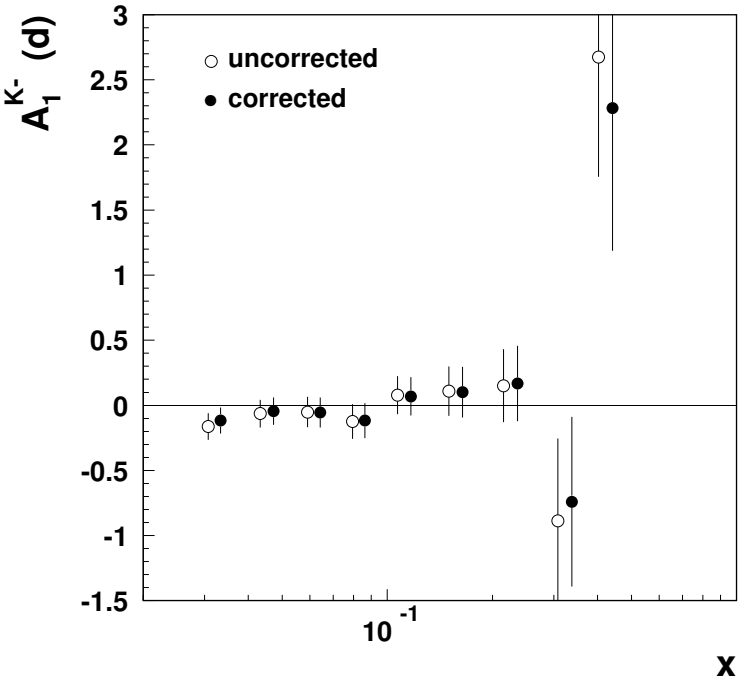

Figure 7.12: Comparison of the K^- asymmetry between uncorrected (open circles) and corrected (closed circles) by the CLD method.

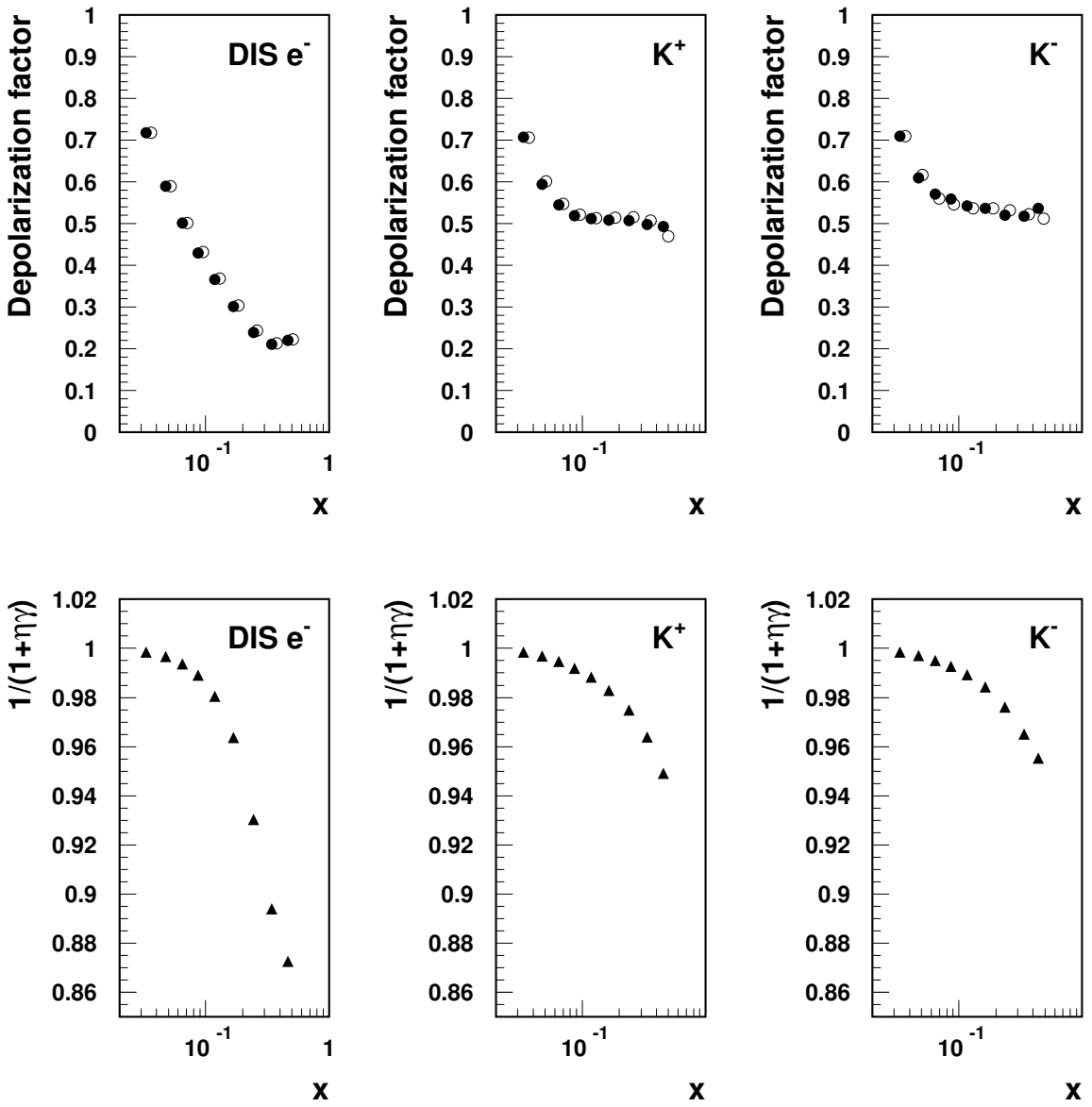

Figure 7.13: Distributions of the virtual photon depolarization factor (top) and kinematical factor $1/(1+\eta\gamma)$ (bottom) for the DIS events (left), positively (middle) and negatively (right) charged kaons in coincidence with the DIS events in each bin of x. For the depolarization factor in the top figures, the closed (open) circles are the averaged depolarization factor per bin of x when the spin state between beam and target is parallel (anti-parallel). The data points of the depolarization factor for the open circle are slightly shifted in x to make them clearly visible.

7.6 Test of Asymmetry formed by inverse P Matrix

More easily understandable way to correct the numbers $\vec{\mathsf{I}}$ of the identified type of hadron in order to obtain the numbers $\vec{\mathsf{N}}$ of the true type of hadron is to use the inverse P matrix from equation (5.16) like:

$$\vec{\mathsf{N}} = \mathsf{P}^{-1} \cdot \vec{\mathsf{I}} \ . \tag{7.9}$$

The P matrix does not need the flux of hadrons to form. It means that the usage of the inverse P matrix does not take into account the uncertainty of the flux unlike the Q matrix. Since the Q matrix includes the flux into the formula, the Q matrix automatically depends on the flux. The degree of the agreement between the asymmetry formed by $\vec{\mathsf{N}}$ from equation (7.9) and the asymmetry obtained from the CLD method is tested.

Figure 7.14 shows the comparison of the asymmetry formed by the number $\vec{\mathsf{N}}$ of the true type of hadron from equation (7.9) to the asymmetry obtained from the CLD method. The comparison is performed in the K^+ asymmetry. It is found that the asymmetry formed by using equation (7.9) is in agreement with the CLD method. Note that this is the approximate way to extract the asymmetry since in principle this way does not take into account the calculations for z and x_F per track of hadrons. Additionally this way cannot allow to give the virtual photon depolarization and the kinematical factors of η and γ, which are required to extract the asymmetry like equation (6.21) because these variables have to be calculated in each bin of x. The CLD method allows to take into account all above difficulties by using the Q matrix. In the extraction of the asymmetry by the CLD method the uncertainty of the flux on the asymmetry should be estimated and is discussed in section 7.7.3.

7.7 Systematic Uncertainties on Asymmetry

In this section the studies for the systematic uncertainties on the asymmetry are described. The estimates of the uncertainties are separated into three classes. The first one is related to the uncertainties of the experiment. The contributions of the systematic errors to the asymmetry are estimated through the uncertainties of the measurements of the beam and target polarizations, the the cross section ratio $R = \sigma_L/\sigma_T$ and the spin-dependent structure function g_2 on the deuteron. The second one is the uncertainties which come from the assignment of the true type of hadron to the identified type of hadron by the RICH detector in the CLD method. The last one is the uncertainty in the flux of pions, kaons and protons. The uncertainty in the flux can dominate the precision of the determination for the elements of the Q matrices. In the first one the procedures for the estimate of the systematic uncertainties on the asymmetry are common for the inclusive and semi-inclusive analyses. The second and third ones are original systematic uncertainties

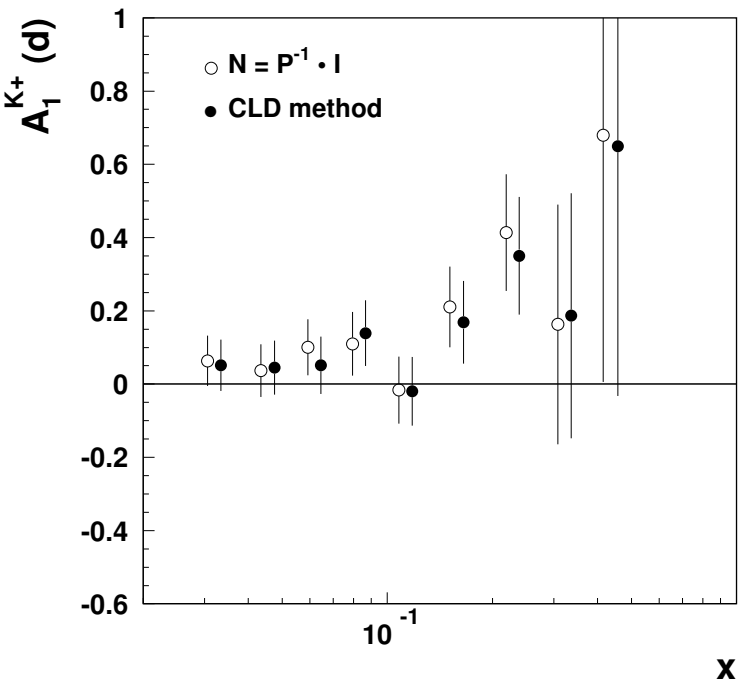

Figure 7.14: Comparison of the asymmetry (open circles) formed by the numbers $\vec{N}$ of the true type of hadron from equation (7.9) to the asymmetry (closed circles) obtained from the CLD method. The comparison is performed in the K^+ asymmetry.

in the analysis for the semi-inclusive asymmetry. The tables for the systematic uncertainties described here are given in chapter 8.

7.7.1 Uncertainties of Experiment

Beam Polarization

In the extraction of the asymmetry the count rates are scaled with the integrated luminosity corrected by the beam and target polarizations as it is not usually possible to obtain the perfect polarizations of 100 %. The main contribution of the beam polarization to the systematic uncertainty is attributed to the calibration by the rise time measurement of the polarization. The uncertainty of the rise time calibration of the beam polarimeters was evaluated at $(\delta P_B/P_B)_{\text{Rise}} = 3.3$ %. There is an additional systematic uncertainty of $(\delta P_B/P_B)_{\text{Point}}$, which arises from the point-to-point corrections to the polarimeter. The total uncertainty of the beam polarization is the square root of the quadratic sum of both uncertainties and was evaluated to $(\delta P_B/P_B) = 3.4$ %. Then the systematic uncertainty of the beam polarization measurement on the asymmetry is given by:

$$[\delta A_1]_{P_B} = \sqrt{\left(\frac{\delta A_1}{\delta P_B}\right)^2 (\delta P_B)^2} = \left| A_1 \cdot \frac{\delta P_B}{P_B} \right|. \tag{7.10}$$

Target Polarization

Similarly to the beam polarization, the target polarization has to be taken into account for the count rates for the asymmetry. The total uncertainty for the measurement of the target polarization on the deuterium was preliminarily evaluated to be about $(\delta P_{\mathrm{T}}/P_{\mathrm{T}}) = 8.0$ %. It was assumed that this large value of the uncertainty came from the unstable operation in the device of the atomic beam source on the deuterium target. Since the uncertainty for the measurement of the target polarization on the deuterium is under studies this value can be improved to the smaller value. For the present, of all systematic uncertainties this uncertainty gives the dominant contribution to the asymmetry. The systematic uncertainty of the target polarization measurement on the deuterium is given by:

$$[\delta A_1]_{P_{\mathrm{T}}} = \sqrt{\left(\frac{\delta A_1}{\delta P_{\mathrm{T}}}\right)^2 (\delta P_{\mathrm{T}})^2} = \left| A_1 \cdot \frac{\delta P_{\mathrm{T}}}{P_{\mathrm{T}}} \right|. \tag{7.11}$$

Cross Section Ratio R

The cross section ratio $R = \sigma_{\mathrm{L}}/\sigma_{\mathrm{T}}$ of the virtual photon absorption is necessary to calculate the virtual photon depolarization factor D. The depolarization factor is regarded as a correction factor to the spin asymmetry.

The cross section ratio R was measured by many experiments and was parameterized by [11] from the fit to the world data, which is known as $R1990$ parameterization valid in the region of $x > 0.07$. The systematic uncertainty of $R1990$ was also estimated in the parameters [11]. The E143 Collaboration made R measurements in the range $0.03 < x < 0.1$ and $1.3\ \mathrm{GeV}^2 < Q^2 < 2.7\ \mathrm{GeV}^2$ and determined the new parameterization with more confidence adding their data to the existing ones. This is called $R1998$ [10]. From the formula of the asymmetry $A_1 = A_{||}/[D(1+\eta\gamma)]$ and equation (2.49) the systematic uncertainty is given by:

$$[\delta A_1]_R = \left| \frac{\varepsilon}{1+\varepsilon R} \cdot A_1 \cdot \delta R \right|. \tag{7.12}$$

$R1998$ parameterization is consistently used in this thesis to extract the asymmetry.

Spin-dependent Structure Function g_2 on Deuteron

The extraction of the asymmetry is performed under the assumption that the spin-dependent structure function g_2 can be well approximated to be zero. As seen in equation (2.53), the asymmetry actually has the term related to g_2. When g_2 is neglected, the systematic uncertainty of g_2 measurement on the asymmetry has to be estimated.

g_2 of the deuteron was measured by the E143 Collaboration [41] in the range $0.03 \leq x \leq 0.8$ and $1.3\ \mathrm{GeV}^2 \leq Q^2 \leq 10\ \mathrm{GeV}^2$ and the E155 Collaboration [101] in the range $0.02 \leq x \leq 0.8$ and $1.0\ \mathrm{GeV}^2 \leq Q^2 \leq 30\ \mathrm{GeV}^2$. Figure 7.15 shows $x \cdot g_2^{\mathrm{d}}$ of the deuteron as a function of x together with the curves of the estimated limits for

the systematic uncertainty. The function form $x \cdot g_2^{\rm d}$ of the curves is expressed by $x \cdot g_2^{\rm d}(x) = \pm 0.065 \cdot x^{-1} \cdot (1-x)^{0.7}$. The measured $x \cdot g_2^{\rm d}$ by both experiments is small in the range of $x \geq 0.06$ within their statistical uncertainties. g_2 can be expressed as $g_2(x,Q^2) = g_2^{\rm WW}(x,Q^2) + \bar{g_2}(x,Q^2)$, where $g_2^{\rm WW}$ is twist-2 term derived by Wandzura and Wilczek [102] and depends on only g_1. $\bar{g_2}$ is twist-3 contribution [4] and may be non-zero according to bag model calculations [103]. The curves describe the behavior of the Wandzura-Wilczek term, which approaches zero as $x \to 1$, without the twist-3 contribution. When g_2 is assumed to be zero the systematic uncertainty on the asymmetry in equation (2.53) is estimated as:

$$[\delta A_1]_{g_2} = \left| \frac{\eta\gamma(1+\gamma^2)}{1+\eta\gamma} \cdot \frac{g_2(x)}{F_1(x)} \right| . \tag{7.13}$$

Here the spin-independent structure function $F_1(x)$ in equation (7.13) is derived from equation (2.31). For $F_1(x)$ of the deuteron the parameterization determined by NMC [29] is used.

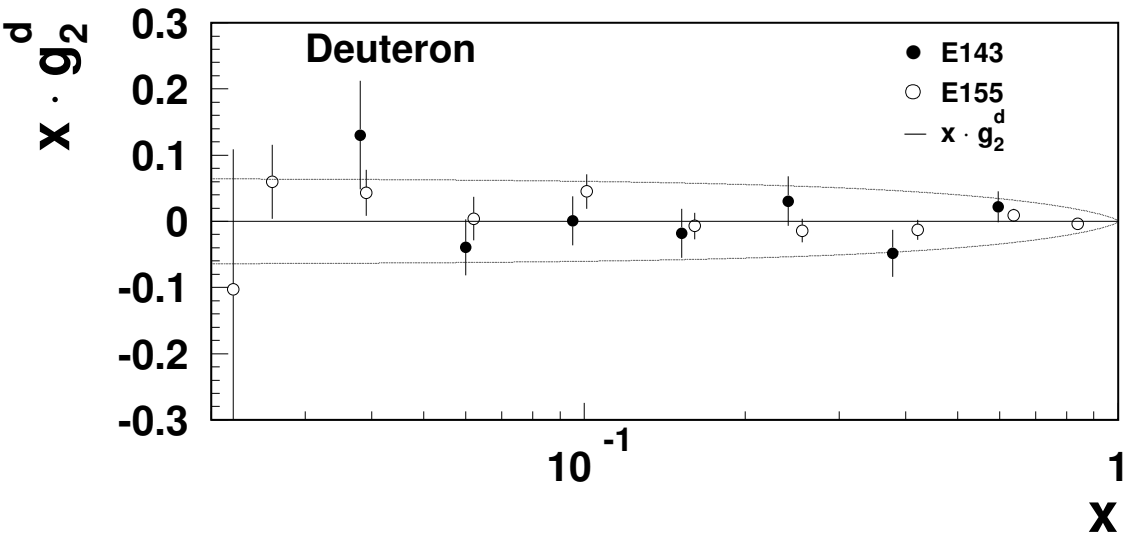

Figure 7.15: Spin-dependent structure function $x \cdot g_2^{\rm d}$ of the deuteron measured by the E143 Collaboration (closed circles) [41] in the range $0.03 \leq x \leq 0.8$ and 1.3 GeV$^2 \leq Q^2 \leq 10$ GeV^2 and the E155 Collaboration (open circles) [101] in the range $0.02 \leq x \leq 0.8$ and 1.0 GeV$^2 \leq Q^2 \leq 30$ GeV^2. The points are represented at the averaged values in the averaged Q^2 of each x bin. Two solid curves in the figure represents the upper and lower limits of the systematic uncertainty for $x \cdot g_2^{\rm d}$. They are estimated in the function form of $x \cdot g_2^{\rm d}(x) = \pm 0.065 \cdot x^{-1} \cdot (1-x)^{0.7}$.

Total systematic Uncertainty of Experiment

The total systematic error for the experiment is given by the square root of the quadratic sum of each element of above systematic uncertainties for the beam po-

larization, target polarization, cross section ratio R and spin-dependent structure function g_2:

$$\delta A_1^{\mathrm{Total}}(x_i) = \sqrt{([\delta A_1(x_i)]_{P_\mathrm{B}})^2 + ([\delta A_1(x_i)]_{P_\mathrm{T}})^2 + ([\delta A_1(x_i)]_R)^2 + ([\delta A_1(x_i)]_{g_2})^2}, \tag{7.14}$$

where the index i is the sequential integer from 1 to 9 which runs over the number of x bins. The treatment of the total systematic uncertainty for the experiment is common in both inclusive and semi-inclusive asymmetries.

7.7.2 Uncertainties of CLD Method

Error in Fit to Distributions

All semi-inclusive asymmetries are determined from the average values by the fit to the distributions which obtained in the procedures of the CLD method. The error $[\delta\sigma_{\mathrm{CLD}}]_{\mathrm{Fit\ Err}}$ of the fit to the distributions for the mean value of the asymmetry is added to the one of the systematic uncertainties which arises from the result of the CLD method. The values of the $[\delta\sigma_{\mathrm{CLD}}]_{\mathrm{Fit\ Err}}$ are generally within the order of 10^{-3} in the first bin to 10^{-2} in the ninth bin for both cases of K^+ and K^- asymmetries.

Uncertainty of statistical Error

The standard deviation $[\delta\sigma_{\mathrm{CLD}}]_{\mathrm{Stat}}$ of the distributions for the statistical uncertainty is added to the systematic uncertainty related to the CLD method as another source of the systematic uncertainties. The values of $[\delta\sigma_{\mathrm{CLD}}]_{\mathrm{Stat}}$ are generally within the order of 10^{-4} in the first bin to 10^{-2} in the ninth bin for the case of the K^+ asymmetry and from 10^{-4} in the first bin to 10^{-1} in the ninth bin for the case of the K^- asymmetry.

Total Uncertainty of CLD Method

The two sources of the systematic uncertainties $[\delta\sigma_{\mathrm{CLD}}]_{\mathrm{Fit\ Err}}$ and $[\delta\sigma_{\mathrm{CLD}}]_{\mathrm{Stat}}$ are quadratically summed to form the total systematic uncertainty for the CLD method as:

$$\delta\sigma_{\mathrm{CLD}}^{\mathrm{Total}}(x_i) = \sqrt{([\delta\sigma_{\mathrm{CLD}}(x_i)]_{\mathrm{Fit\ Err}})^2 + ([\delta\sigma_{\mathrm{CLD}}(x_i)]_{\mathrm{Stat}})^2}. \tag{7.15}$$

$\delta\sigma_{\mathrm{CLD}}^{\mathrm{Total}}$ is estimated in the semi-inclusive asymmetries not only for kaon but also for hadron, pion and proton.

7.7.3 Uncertainty of Flux

As the Q matrix depends on the flux of each type of hadrons like equation (5.13) the asymmetry corrected by the assignment of the true type of hadron to the identified type of hadron by the RICH detector using the elements of the Q matrices is

directly influenced by the flux. This influence on the asymmetry is estimated as the systematic uncertainty as follows.

Figure 7.16 shows the flux ratio of the experimental data to the Monte Carlo data for pions, kaons and protons. In both data the flux are taken from the identified type of hadron by the RICH detector. Obviously the flux ratio of each type of hadrons is far from 1, especially in the ratio for protons. For kaons the ratio decreases from 2 to 0.4 as momentum increases. To some extent, the ratio for pions seems to reproduce the flux of the experiment. Each ratio should be 1. When the flux ratios are averaged in the whole range of momentum the flux ratio $\phi(\mathrm{exp})/\phi(\mathrm{MC})$ for kaons is 1.5 and the flux ratio for protons 0.5. The Q matrix in $rQp > 0.0$ over the whole range of momentum estimated by the Monte Carlo simulation is given as:

$$\mathsf{Q} = \begin{pmatrix} Q_\pi^\pi & Q_\pi^\mathrm{K} & Q_\pi^\mathrm{p} \\ Q_\mathrm{K}^\pi & Q_\mathrm{K}^\mathrm{K} & Q_\mathrm{K}^\mathrm{p} \\ Q_\mathrm{p}^\pi & Q_\mathrm{p}^\mathrm{K} & Q_\mathrm{p}^\mathrm{p} \end{pmatrix} \tag{7.16}$$

$$= \begin{pmatrix} 0.977 & 0.007 & 0.017 \\ 0.086 & 0.809 & 0.106 \\ 0.053 & 0.044 & 0.903 \end{pmatrix}. \tag{7.17}$$

Note that in above the statistical uncertainty is neglected. Now the flux ratios for kaons and protons are uniformly moved further away from their current ratios to reconstruct the artificial Q matrix. The current ratio is shifted 1.5 times for kaons and 1/1.5 times for protons. As results the artificial flux ratio $\phi(\mathrm{exp})/\phi(\mathrm{MC})$ is 2.25 for kaons and for 0.33 for protons on the average in the whole range of momentum. Then the Q matrix can be reconstructed from these flux ratios. The artificial Q matrix over the whole range of momentum is given as:

$$\mathsf{Q}_{\mathsf{art}} = \begin{pmatrix} 0.970 & 0.005 & 0.025 \\ 0.101 & 0.713 & 0.186 \\ 0.037 & 0.023 & 0.940 \end{pmatrix}. \tag{7.18}$$

The identification purity for kaons decreases about 10 %. On the other hand the identification purity for protons increases 4 %. It is found that the flux of the hadrons significantly dominate the precision of the determination for the elements of the Q matrix.

Actually the artificial Q matrix is defined in each bin of momentum like table 5.1 taking into account the number of the tracks per detector half of the RICH detector. Then the false asymmetry can be measured by using the artificial Q matrix. As a result the false asymmetry is compared to the asymmetry resulting from the default Q matrix in $rQp > 0.0$ in order to estimate the systematic uncertainty of the flux on the asymmetry.

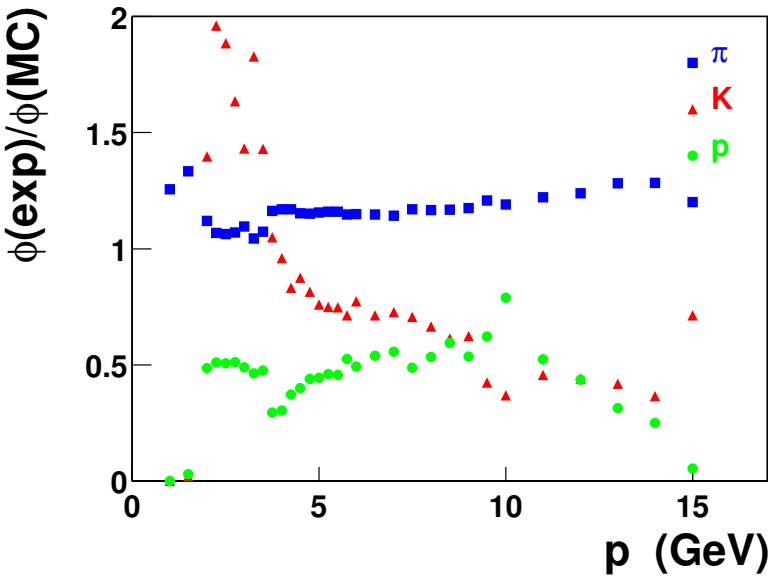

Figure 7.16: Flux ratios of the experimental data to the Monte Carlo data for pions (squares), kaons (triangles) and protons (circles). In both data the flux are taken from the identified type of hadron by the RICH detector.

7.8 Final Results of Asymmetries

The semi-inclusive asymmetries presented in figures 7.17 - 7.24 are obtained from the results by the assignment of the true type of hadron to the identified type of hadron by the RICH detector in the CLD method. The assignment is performed more than 600 times. In each figure the bands for the systematic uncertainties from top to bottom indicate the total uncertainty of the experiment, the total uncertainty of the CLD method and the uncertainty of the flux of hadrons.

K^+ shows positive asymmetry and reaches about 0.6 at $x \simeq 0.46$ at maximum. K^- shows small asymmetry and has values around zero in the region of $x < 0.24$. K^- asymmetry can provide the interesting information for the sea quarks because the components of K^-, $\bar{u}$ and s, are all sea objects. Though the K^- asymmetry is not determined precisely in the last two bins due to both smaller statistics and larger systematic uncertainties the most important region for the sea quarks is the lower region of x. It is known that the sea quarks contribute to the structure functions in the low range of x.

The π^+ asymmetry is compatible with zero in the region of $x < 0.09$ and reaches about 0.55 at about $x = 0.4$. The π^- asymmetry is small in the range of $x < 0.2$ because π^- is composed of $\bar{u}d$ and it is assumed that the interaction of the u sea with the incoming electron is dominant. The shape of the distribution approaches the one of the h^- asymmetry in figure 7.24.

The proton asymmetry is compatible with zero in the region of $x < 0.2$. Also the

anti-proton asymmetry is zero over all measured region of x. For the anti-proton asymmetry the value in the ninth bin of x is not represented because the fit to the distribution for the mean value of the asymmetry resulting from the procedures of the CLD method is not good due to the originally small statistics in this bin.

The h^+ asymmetry is small in the region of $x < 0.09$ and increases up to 0.55 at $x = 0.4$ at maximum. The result agrees with the one of SMC [104]. The h^- asymmetry is small in the range of $x < 0.2$ as well as the π^- asymmetry. For the h^- asymmetry the differences from the one of SMC [104] are seen in the range from the second to the fourth bin. The h^- asymmetry of this work is consistently similar with the π^- asymmetry in figure 7.19 because the most of the statistics in h^- is occupied by π^-. The HERMES experiment determined the h^+ and h^- asymmetries with much higher precision than the ones of SMC.

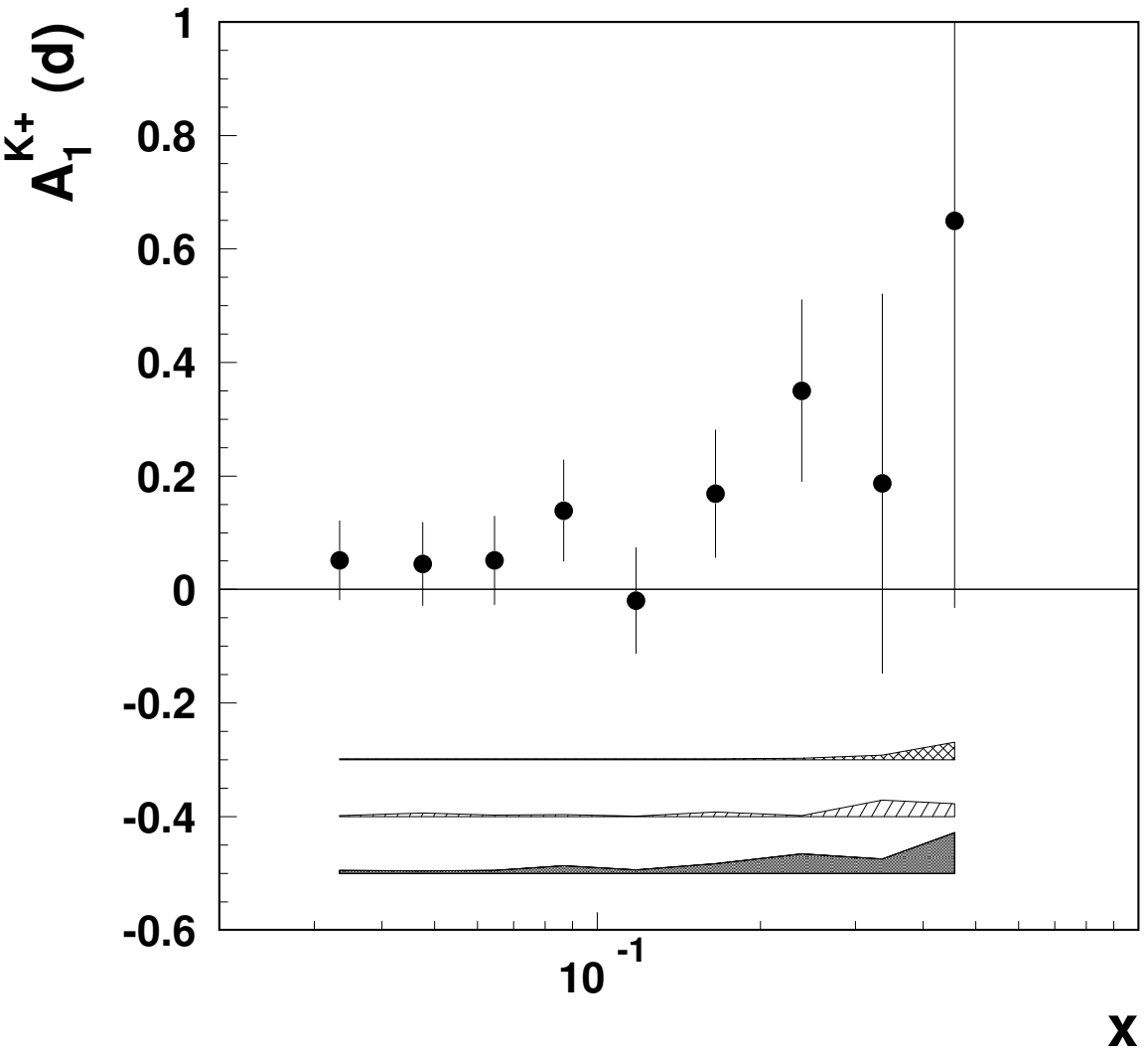

Figure 7.17: Result of the K^+ asymmetry on the deuterium target. The asymmetry was corrected by the assignment of the true type of hadron to the identified type of hadron by the RICH detector in the CLD method. The assignment was performed more than 600 times. The most upper band represents the total systematic uncertainty of the CLD method, the middle band the systematic uncertainty of the flux and the lowest band the total systematic uncertainty of the experiment.

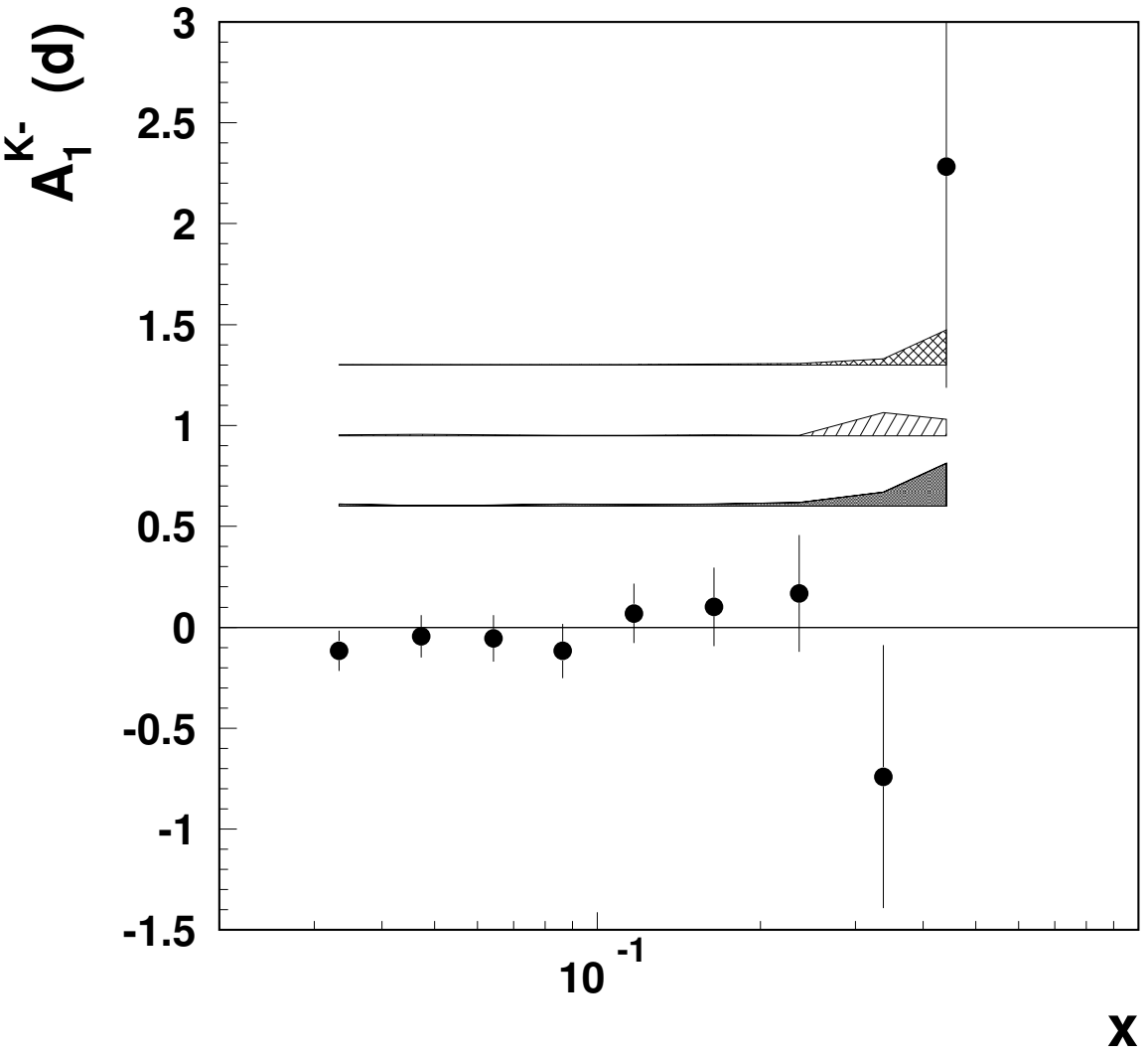

Figure 7.18: Result of the K^- asymmetry on the deuterium target. The asymmetry was corrected by the assignment of the true type of hadron to the identified type of hadron by the RICH detector in the CLD method. The assignment was performed more than 600 times. The most upper band represents the total systematic uncertainty of the CLD method, the middle band the systematic uncertainty of the flux and the lowest band the total systematic uncertainty of the experiment.

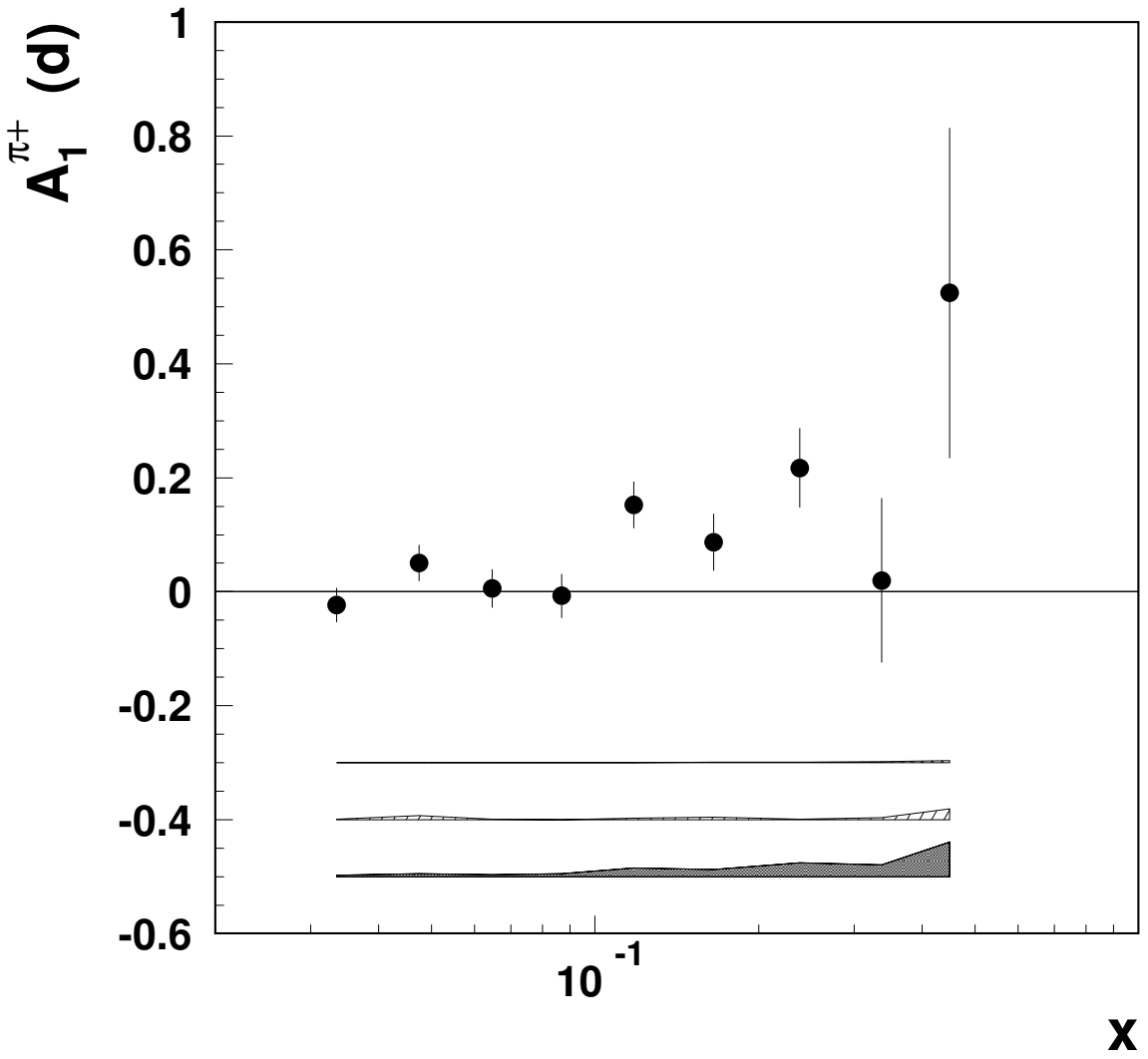

Figure 7.19: Result of the π^+ asymmetry on the deuterium target. The asymmetry was corrected by the assignment of the true type of hadron to the identified type of hadron by the RICH detector in the CLD method. The assignment was performed more than 600 times. The most upper band represents the total systematic uncertainty of the CLD method, the middle band the systematic uncertainty of the flux and the lowest band the total systematic uncertainty of the experiment.

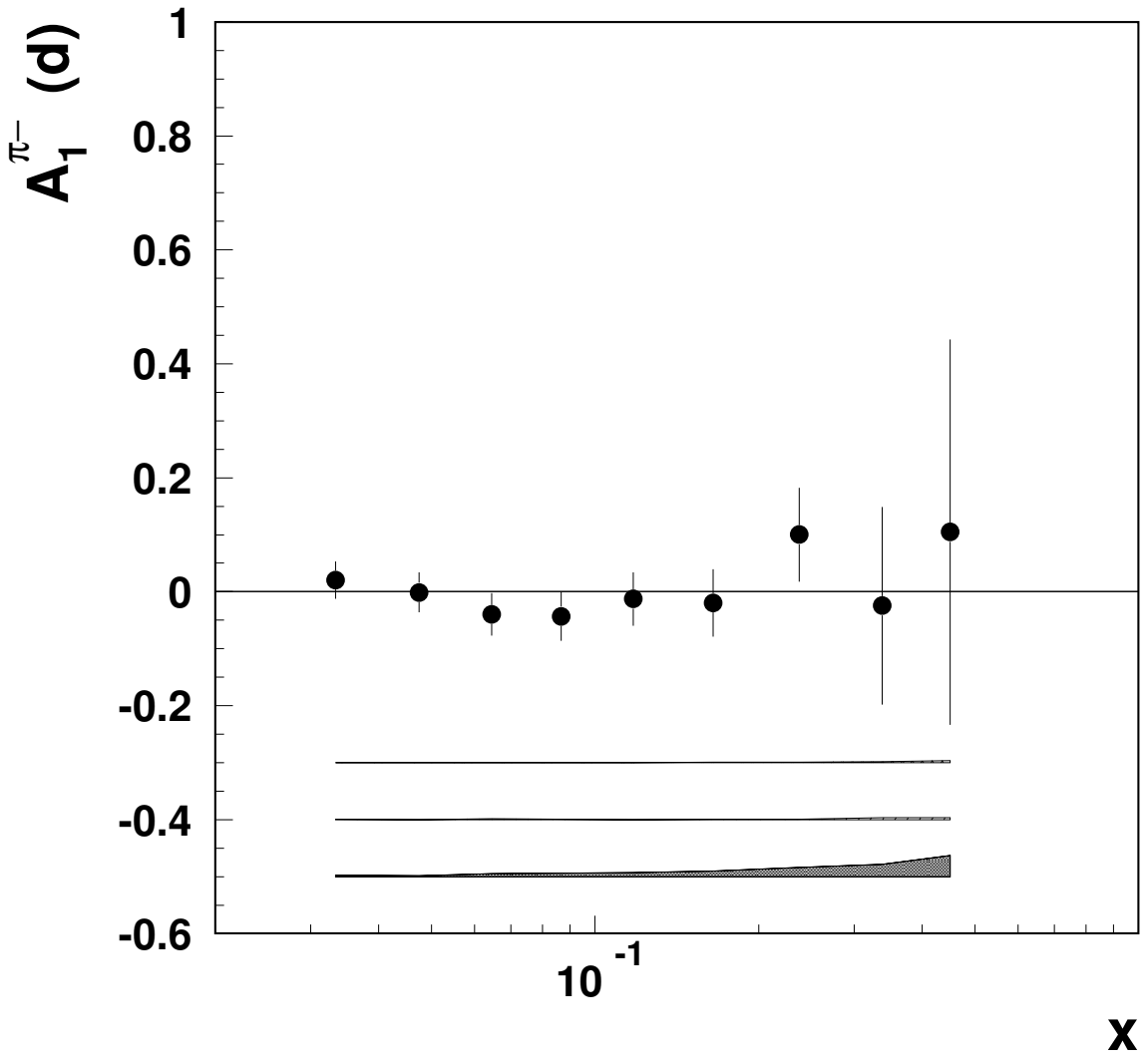

Figure 7.20: Result of the π^- asymmetry on the deuterium target. The asymmetry was corrected by the assignment of the true type of hadron to the identified type of hadron by the RICH detector in the CLD method. The assignment was performed more than 600 times. The most upper band represents the total systematic uncertainty of the CLD method, the middle band the systematic uncertainty of the flux and the lowest band the total systematic uncertainty of the experiment.

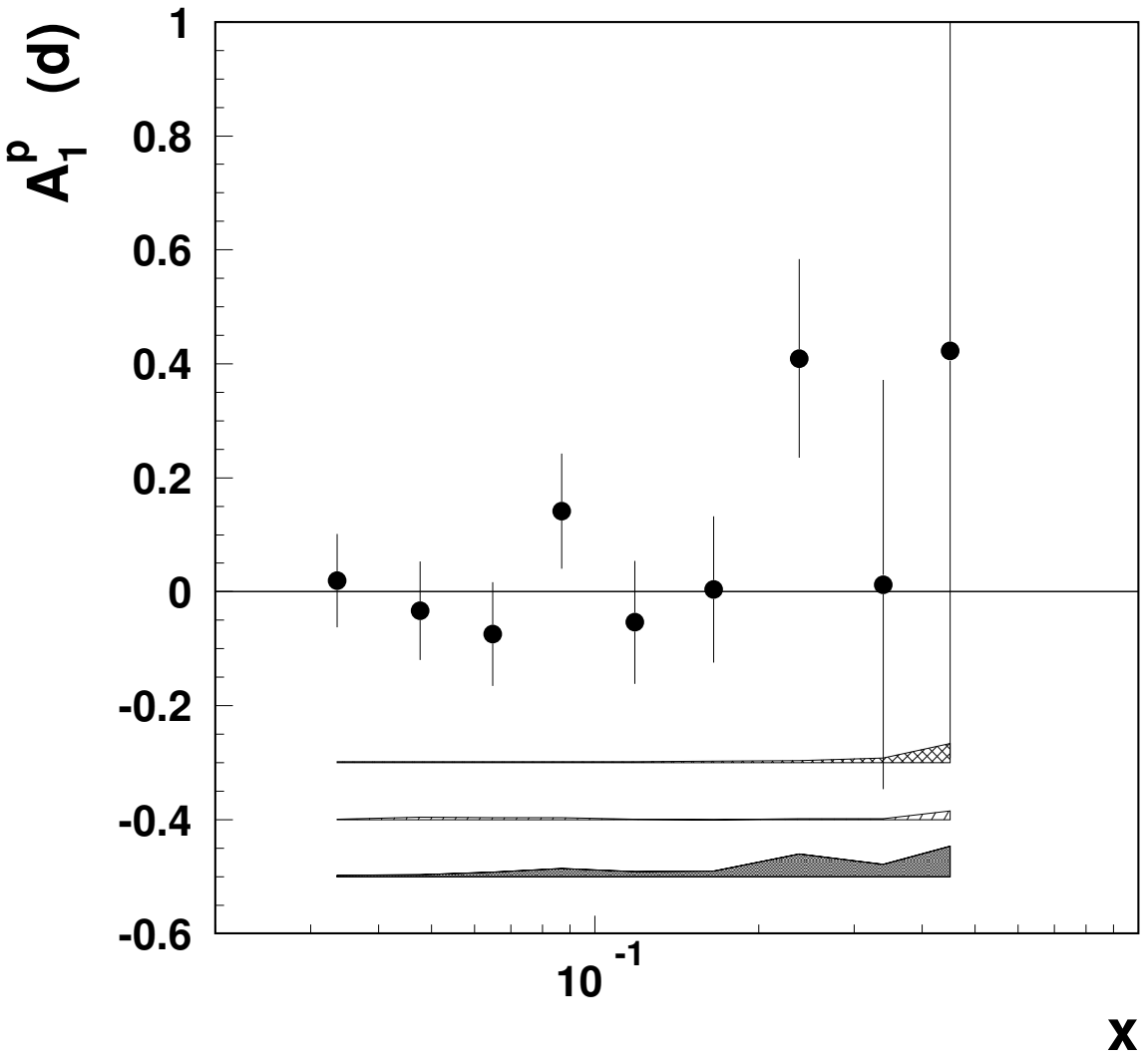

Figure 7.21: Result of the proton asymmetry on the deuterium target. The asymmetry was corrected by the assignment of the true type of hadron to the identified type of hadron by the RICH detector in the CLD method. The assignment was performed more than 600 times. The most upper band represents the total systematic uncertainty of the CLD method, the middle band the systematic uncertainty of the flux and the lowest band the total systematic uncertainty of the experiment.

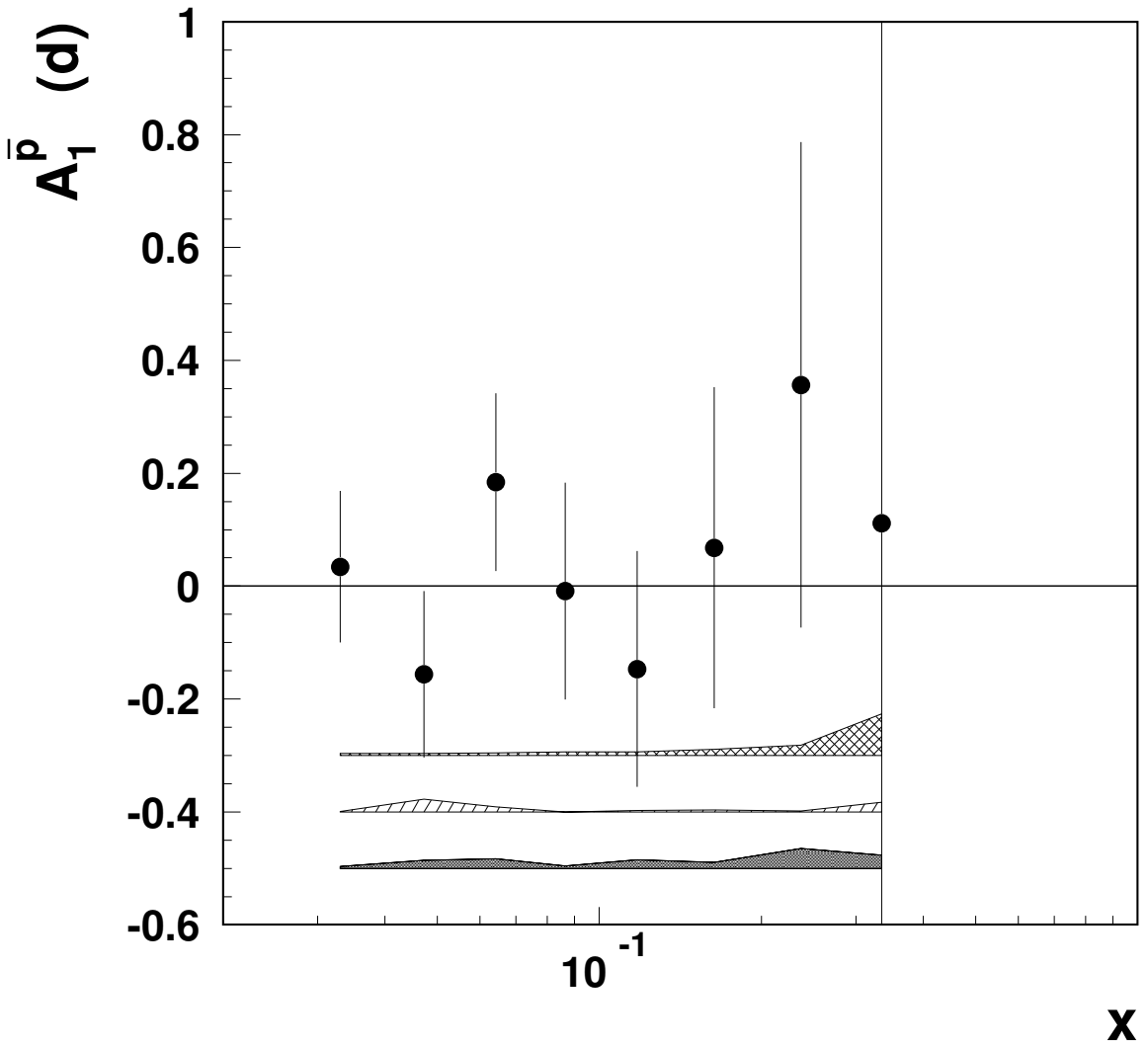

Figure 7.22: Result of the anti-proton asymmetry on the deuterium target. The asymmetry was corrected by the assignment of the true type of hadron to the identified type of hadron by the RICH detector in the CLD method. The assignment was performed more than 600 times. The most upper band represents the total systematic uncertainty of the CLD method, the middle band the systematic uncertainty of the flux and the lowest band the total systematic uncertainty of the experiment. The value in the ninth bin of x is not represented because that the fit to the distribution for the mean value of the asymmetry resulting from the CLD method is not good due to the small statistics.

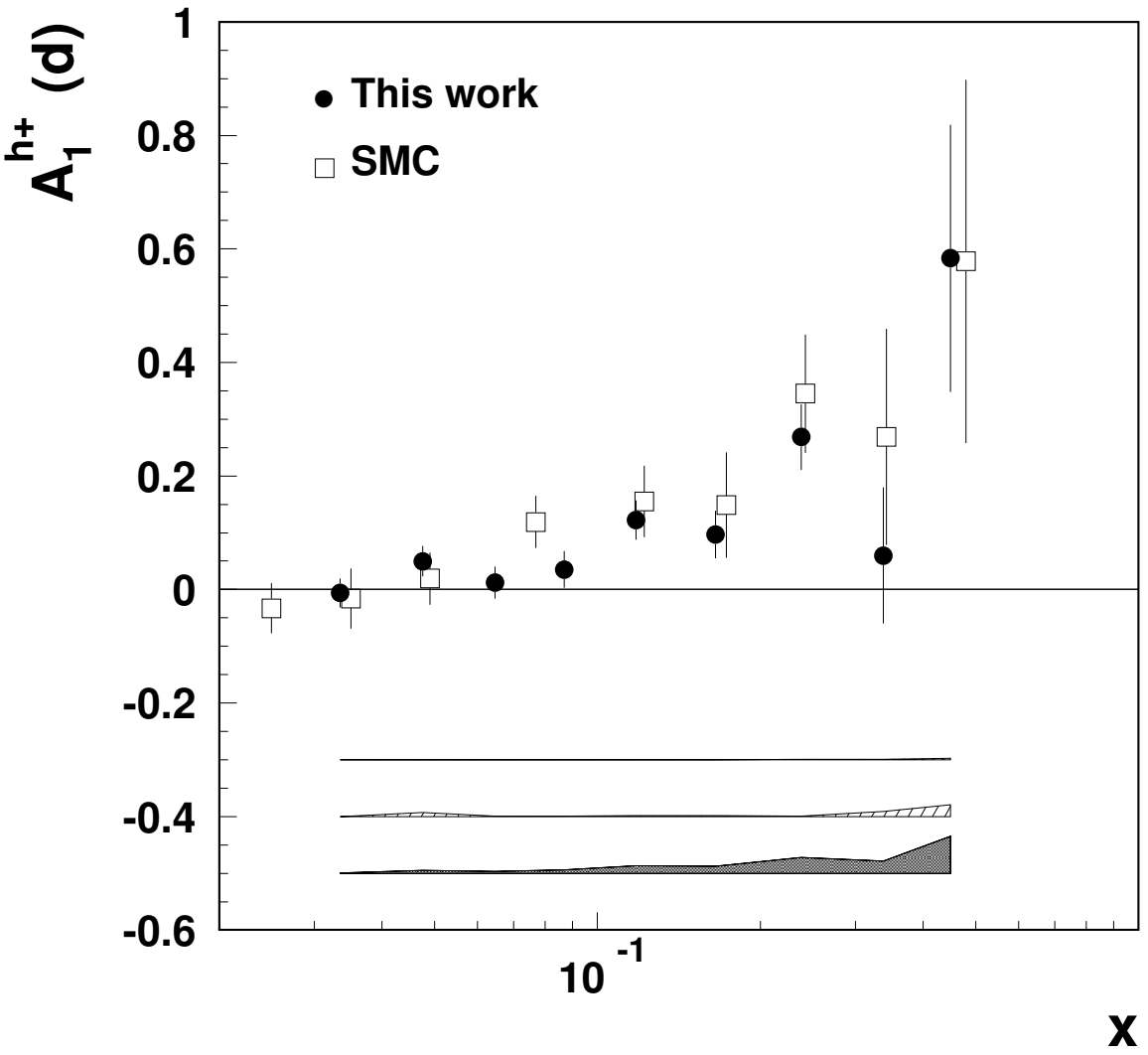

Figure 7.23: Result of the h^+ asymmetry (closed circles) on the deuterium target. The asymmetry was corrected by the assignment of the true type of hadron to the identified type of hadron by the RICH detector in the CLD method. The assignment was performed more than 600 times. The most upper band represents the total systematic uncertainty of the CLD method, the middle band the systematic uncertainty of the flux and the lowest band the total systematic uncertainty of the experiment. The open squares are the result measured by SMC [104], which is shown in the kinematic range of the HERMES experiment. The error bar for the result of SMC includes the statistical uncertainty only.

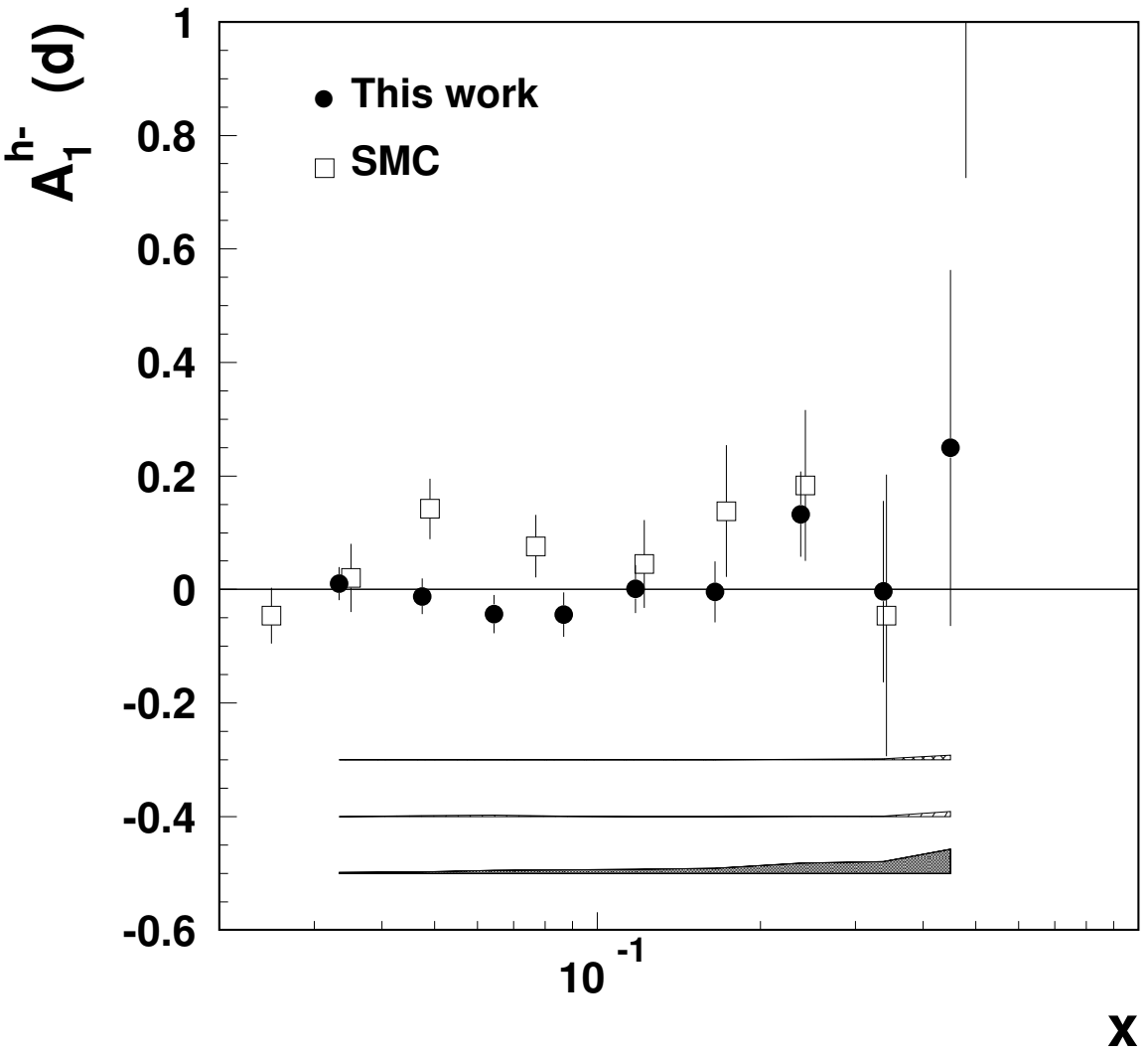

Figure 7.24: Result of the h^- asymmetry (closed circles) on the deuterium target. The asymmetry was corrected by the assignment of the true type of hadron to the identified type of hadron by the RICH detector in the CLD method. The assignment was performed more than 600 times. The most upper band represents the total systematic uncertainty of the CLD method, the middle band the systematic uncertainty of the flux and the lowest band the total systematic uncertainty of the experiment. The open squares are the result measured by SMC [104], which is shown in the kinematic range of the HERMES experiment. The error bar for the result of SMC includes the statistical uncertainty only. The error bar of the statistical uncertainty which is seen in the highest x belongs to the result of SMC.

Chapter 8

Conclusion

The HERMES experiment investigates the spin structure of the nucleon with a longitudinally polarized electron beam of 27.5 GeV and a longitudinally polarized target in the deep-inelastic scattering. The spectrometer was designed to detect the electron scattered off the target nucleon and the produced hadrons in coincidence by the particle identification detectors.

The threshold type Čerenkov detector was converted to the dual-radiator RICH detector in 1998. The RICH detector was successfully operated for the data taking. The usage of the radiators of the silica aerogel with a low index of refraction and C_4F_{10} gas at atmospheric pressure realized to identify pions, kaons and protons in the wide range of the momentum from 2 GeV to 15 GeV. Silica aerogel was used for the first time as a radiator of the RICH detector in the actual experiment by HERMES. The single photon resolution in aerogel and C_4F_{10} gas is 7.6 mrad and 7.5 mrad respectively. The algorithm of the IRT method for the particle identification was developed and excellently reconstructed the Čerenkov angle. The likelihood analysis based on the Čerenkov angle allowed to separate each type of hadrons for pions, kaons and protons. The performance of the particle identification of the RICH detector was studied in detail by the technique of the Monte Carlo simulation and the two kinds of the efficiencies for the performance were determined as the P and Q matrices. As a result the performance of the RICH detector indicates the successful particle identification in the large range of momentum when the different momentum thresholds for each type of hadrons are chosen. It was found that on the average the identification efficiency reaches 98 % for pions in the range of the momentum more than 0.5 GeV, 93 % for kaons in more than 3.25 GeV and 86 % for protons in more than 2 GeV. Similarly the identification purity is 98 % for pions in more than 0.5 GeV, 90 % for kaons in more than 3.25 GeV and 91 % for protons in more than 2 GeV on the average.

The spin asymmetries not only in the inclusive measurement but also in the semi-inclusive measurement are measured on the deuteron data collected from 1998 to spring 1999 by the polarized deep-inelastic scattering. The kinematic range of the data covers $0.023 < x < 0.6$ and $1\ \mathrm{GeV}^2 < Q^2 < 10\ \mathrm{GeV}^2$. The average value of Q^2 in the HERMES experiment is $\langle Q^2 \rangle \simeq 2.5\ \mathrm{GeV}^2$ in this range of x. After

applying the data quality and kinematical criteria the DIS events of 1.14×10^6 were collected. Statistics of positively and negatively charged hadrons in coincidence with the DIS events is 1.39×10^5 and 9.29×10^4 respectively. Out of all hadrons 1.64×10^4 positively and 6.61×10^3 negatively charged kaons were identified by the RICH detector when the momentum threshold of 3.25 GeV was imposed. In this thesis the spin asymmetries for kaons as well as for pions and protons were determined using the RICH detector. The asymmetries were corrected in the CLD method by using the Q matrix, which corresponds to the identification probabilities. It became clear that the correction was small due to the high probabilities of the identification.

The main results in the thesis are summarized as follows:

- The spin asymmetry of the virtual photon-nucleon reaction on the deuteron is small at the region of $x < 0.1$ and increases as x increases. The asymmetry reaches 0.3 at maximum.
- The spin asymmetry of kaon productions are extracted by using the RICH detector.
- K^+ showed positive asymmetry and reached about 0.6 at $x \simeq 0.46$.
- On the contrary K^- showed small asymmetry and has values around zero in the region of $x < 0.24$.
- It was shown for the first time that since K^- consists of the sea objects alone and the asymmetry is small the contribution of the sea quark spin to the nucleon spin is small.
- The spin asymmetry of kaon productions in polarized deep-inelastic scattering was measured for the first time in the world.

The numerical values of the results for the inclusive and semi-inclusive asymmetries are given together with their systematic uncertainties at the end of this chapter.

One of the most important aims in the HERMES experiment is to understand the contributions of the quark spin to the nucleon spin per quark flavor in detail. Especially it is interesting to know the spin contributions of the sea and strange quarks both in experiment and in theory. For example, for the side of the theory the Ellis-Jaffe sum rule assumes that the spin contribution of the strange quark is zero. The sum rule is known to be violated significantly [41]. It means that the polarization of the strange quark is not zero. It is assumed that K^- has good sensitivity to the sea quark, especially in the lower range of x. With more statistics of K^- not only the sea polarization but also the strange quark polarization can be studied. It can provide the models of the sea and strange polarizations to explain the violation of the Ellis-Jaffe sum rule.

The present work showed that the hadron identification with the RICH detector in polarized deep-inelastic scattering is a powerful tool to investigate the nucleon

spin. It also provided a firm basis for the further studies by HERMES in future: data taking with the proton target and the flavor decomposition of the spin-dependent quark distribution functions using all the data with the deuteron and the proton targets.

The direct measurement of the sea and strange quark polarizations has not ever been made before. The asymmetry of kaon productions can provide the mean of the ultimately and unambiguously direct measurement of them and lead to understanding of the spin structure of the nucleon. The ratio of the spin contributions of the valence quarks to $\Delta\Sigma$ is required to be completely understood before the investigations of other spin contributions to the nucleon spin such as gluon and orbital angular momenta of the quark and gluon.

Inclusive asymmetry A_1							
Bin	x	y	Q^2	$A_1 \pm$ stat.	$N^{\vec{\Rightarrow}}$	$N^{\vec{\Leftarrow}}$	$N^{\vec{\Rightarrow}} + N^{\vec{\Leftarrow}}$
1	0.033	0.719	1.22	0.0095±0.0097	57767	56951	114718
2	0.047	0.603	1.47	0.0137±0.0111	65734	64874	130608
3	0.065	0.518	1.73	0.0222±0.0121	75754	74959	150713
4	0.087	0.446	2.00	0.0366±0.0141	74808	74319	149127
5	0.119	0.378	2.32	0.0844±0.0153	85606	86175	171781
6	0.168	0.311	2.68	0.1355±0.0184	84000	85344	169344
7	0.244	0.246	3.09	0.1859±0.0230	78012	79638	157650
8	0.342	0.213	3.77	0.3092±0.0385	33172	34585	67757
9	0.464	0.216	5.22	0.2686±0.0525	15584	16178	31762

Table 8.1: Inclusive deuteron asymmetry A_1, x, y, Q^2, statistics in each spin state of beam and target, and their total.

Semi-inclusive asymmetry $A_1^{h^+}$							
Bin	x	y	Q^2	$A_1^{h^+}$ $\pm$ stat.	$N^{\vec{\Rightarrow}}$	$N^{\vec{\Leftarrow}}$	$N^{\vec{\Rightarrow}} + N^{\vec{\Leftarrow}}$
1	0.033	0.705	1.21	-0.0058 ± 0.0254	8953	8743	17695
2	0.048	0.597	1.46	0.0497 ± 0.0269	11391	11440	22829
3	0.065	0.533	1.78	0.0122 ± 0.0283	13042	12853	25897
4	0.087	0.486	2.18	0.0349 ± 0.0323	11725	11656	23383
5	0.118	0.452	2.75	0.1223 ± 0.0345	11130	11438	22572
6	0.165	0.437	3.74	0.0969 ± 0.0416	7617	7752	15370
7	0.238	0.425	5.22	0.2686 ± 0.0579	3660	3988	7645
8	0.337	0.418	7.30	0.0598 ± 0.1197	850	853	1702
9	0.449	0.427	9.94	0.5838 ± 0.2353	170	214	384

Table 8.2: Semi-inclusive deuteron asymmetry $A_1^{h^+}$, x, y, Q^2, statistics in each spin state of beam and target, and their total. After the corrections by the CLD method the sum of $N^{\vec{\Rightarrow}}$ and $N^{\vec{\Leftarrow}}$ does not become equal to $N^{\vec{\Rightarrow}} + N^{\vec{\Leftarrow}}$ as a matter of course because these numbers are determined from the average ones on the distributions. For the values of statistics the fractions are rounded off to integral place.

Semi-inclusive asymmetry $A_1^{h^-}$							
Bin	x	y	Q^2	$A_1^{h^-}$ $\pm$ stat.	$N^{\vec{\Rightarrow}}$	$N^{\vec{\Leftarrow}}$	$N^{\vec{\Rightarrow}} + N^{\vec{\Leftarrow}}$
1	0.033	0.707	1.21	0.0102 ± 0.0294	6581	6491	13070
2	0.047	0.601	1.47	-0.0122 ± 0.0314	8324	8110	16435
3	0.064	0.537	1.79	-0.0430 ± 0.0336	9185	8834	18021
4	0.087	0.491	2.20	-0.0444 ± 0.0394	7803	7511	15312
5	0.118	0.461	2.80	-0.0008 ± 0.0426	7154	7015	14170
6	0.165	0.441	3.76	-0.0045 ± 0.0539	4544	4447	8990
7	0.238	0.427	5.24	0.1328 ± 0.0754	2203	2276	4479
8	0.337	0.416	7.26	-0.0037 ± 0.1597	490	480	970
9	0.449	0.431	10.04	0.2493 ± 0.3132	104	113	218

Table 8.3: Semi-inclusive deuteron asymmetry $A_1^{h^-}$, x, y, Q^2, statistics in each spin state of beam and target, and their total. After the corrections by the CLD method the sum of $N^{\vec{\Rightarrow}}$ and $N^{\vec{\Leftarrow}}$ does not become equal to $N^{\vec{\Rightarrow}} + N^{\vec{\Leftarrow}}$ as a matter of course because these numbers are determined from the average ones on the distributions. For the values of statistics the fractions are rounded off to integral place.

Semi-inclusive asymmetry $A_1^{\pi^+}$							
Bin	x	y	Q^2	$A_1^{\pi^+} \pm$ stat.	$N^{\vec{\Rightarrow}}$	$N^{\vec{\Leftarrow}}$	$N^{\vec{\Rightarrow}} + N^{\vec{\Leftarrow}}$
1	0.033	0.705	1.21	-0.0233 ± 0.0301	6394	6180	12573
2	0.047	0.596	1.46	0.0502 ± 0.0319	8128	8166	16296
3	0.065	0.531	1.77	0.0060 ± 0.0336	9369	9207	18577
4	0.087	0.483	2.17	-0.0072 ± 0.0385	8416	8225	16643
5	0.118	0.450	2.74	0.1526 ± 0.0411	7834	8143	15974
6	0.165	0.437	3.73	0.0871 ± 0.0499	5298	5371	10669
7	0.238	0.423	5.19	0.2173 ± 0.0697	2585	2760	5344
8	0.337	0.417	7.27	0.0198 ± 0.1445	592	586	1177
9	0.449	0.430	9.99	0.5244 ± 0.2900	112	138	250

Table 8.4: Semi-inclusive deuteron asymmetry $A_1^{\pi^+}$, x, y, Q^2, statistics in each spin state of beam and target, and their total. After the corrections by the CLD method the sum of $N^{\vec{\Rightarrow}}$ and $N^{\vec{\Leftarrow}}$ does not become equal to $N^{\vec{\Rightarrow}} + N^{\vec{\Leftarrow}}$ as a matter of course because these numbers are determined from the average ones on the distributions. For the values of statistics the fractions are rounded off to integral place.

Semi-inclusive asymmetry $A_1^{\pi^-}$							
Bin	x	y	Q^2	$A_1^{\pi^-} \pm$ stat.	$N^{\vec{\Rightarrow}}$	$N^{\vec{\Leftarrow}}$	$N^{\vec{\Rightarrow}} + N^{\vec{\Leftarrow}}$
1	0.033	0.706	1.21	0.0202 ± 0.0328	5305	5263	10566
2	0.047	0.598	1.46	-0.1100 ± 0.0350	6776	6639	13417
3	0.064	0.533	1.77	-0.0395 ± 0.0373	7624	7346	14971
4	0.087	0.485	2.17	-0.0429 ± 0.0436	6554	6314	12870
5	0.118	0.456	2.77	-0.0128 ± 0.0470	6046	5898	11941
6	0.165	0.436	3.71	-0.0198 ± 0.0593	3867	3761	7627
7	0.237	0.422	5.19	0.1001 ± 0.0826	1895	1932	3828
8	0.337	0.413	7.21	-0.0246 ± 0.1735	423	411	834
9	0.450	0.430	10.01	0.1046 ± 0.3385	92	96	188

Table 8.5: Semi-inclusive deuteron asymmetry $A_1^{\pi^-}$, x, y, Q^2, statistics in each spin state of beam and target, and their total. After the corrections by the CLD method the sum of $N^{\vec{\Rightarrow}}$ and $N^{\vec{\Leftarrow}}$ does not become equal to $N^{\vec{\Rightarrow}} + N^{\vec{\Leftarrow}}$ as a matter of course because these numbers are determined from the average ones on the distributions. For the values of statistics the fractions are rounded off to integral place.

Semi-inclusive asymmetry $A_1^{K^+}$							
Bin	x	y	Q^2	$A_1^{K^+} \pm$ stat.	$N^{\vec{\Rightarrow}}$	$N^{\vec{\Leftarrow}}$	$N^{\vec{\Rightarrow}} + N^{\vec{\Leftarrow}}$
1	0.033	0.709	1.21	0.0512±0.0701	1140	1152	2293
2	0.048	0.610	1.50	0.0452±0.0739	1432	1437	2870
3	0.065	0.557	1.86	0.0514±0.0783	1521	1526	3046
4	0.087	0.523	2.34	0.1391±0.0894	1251	1304	2555
5	0.118	0.503	3.07	-0.0196±0.0939	1205	1172	2375
6	0.165	0.486	4.15	0.1684±0.1129	792	837	1630
7	0.239	0.470	5.80	0.3502±0.1610	366	419	785
8	0.336	0.450	7.82	0.1867±0.3346	90	95	185
9	0.457	0.425	10.06	0.649±0.6819	20	26	45

Table 8.6: Semi-inclusive deuteron asymmetry $A_1^{K^+}$, x, y, Q^2, statistics in each spin state of beam and target, and their total. After the corrections by the CLD method the sum of $N^{\vec{\Rightarrow}}$ and $N^{\vec{\Leftarrow}}$ does not become equal to $N^{\vec{\Rightarrow}} + N^{\vec{\Leftarrow}}$ as a matter of course because these numbers are determined from the average ones on the distributions. For the values of statistics the fractions are rounded off to integral place.

Semi-inclusive asymmetry $A_1^{K^-}$							
Bin	x	y	Q^2	$A_1^{K^-} \pm$ stat.	$N^{\vec{\Rightarrow}}$	$N^{\vec{\Leftarrow}}$	$N^{\vec{\Rightarrow}} + N^{\vec{\Leftarrow}}$
1	0.033	0.712	1.22	−0.1153±0.0998	586	535	1121
2	0.047	0.623	1.52	−0.0445±0.1061	676	649	1325
3	0.064	0.573	1.90	−0.0548±0.1153	673	643	1314
4	0.086	0.551	2.45	−0.1172±0.1348	520	483	1002
5	0.117	0.525	3.17	0.0691±0.1478	431	436	867
6	0.164	0.507	4.30	0.1017±0.1941	248	254	502
7	0.236	0.482	5.87	0.1684±0.2895	112	119	231
8	0.338	0.464	8.08	−0.7400±0.6522	26	18	45
9	0.442	0.456	10.44	2.2821±1.0961	2	8	10

Table 8.7: Semi-inclusive deuteron asymmetry $A_1^{K^-}$, x, y, Q^2, statistics in each spin state of beam and target, and their total. After the corrections by the CLD method the sum of $N^{\vec{\Rightarrow}}$ and $N^{\vec{\Leftarrow}}$ does not become equal to $N^{\vec{\Rightarrow}} + N^{\vec{\Leftarrow}}$ as a matter of course because these numbers are determined from the average ones on the distributions. For the values of statistics the fractions are rounded off to integral place.

Semi-inclusive asymmetry A_1^{p}							
Bin	x	y	Q^2	$A_1^{\mathrm{p}} \pm$ stat.	$N^{\vec{\Rightarrow}}$	$N^{\vec{\Leftarrow}}$	$N^{\vec{\Rightarrow}} + N^{\vec{\Leftarrow}}$
1	0.033	0.706	1.21	0.0195±0.0822	845	838	1682
2	0.048	0.596	1.46	−0.0335±0.0866	1125	1086	2213
3	0.065	0.532	1.78	−0.0745±0.0908	1294	1228	2523
4	0.087	0.480	2.15	0.1414±0.1010	1202	1246	2447
5	0.118	0.443	2.71	−0.0535±0.1080	1228	1180	2408
6	0.165	0.428	3.65	−0.0039±0.1283	857	840	1697
7	0.237	0.425	5.22	0.4094±0.1744	390	448	838
8	0.339	0.420	7.35	0.0126±0.3591	94	93	188
9	0.449	0.428	10.01	0.4223±0.7143	20	24	43

Table 8.8: Semi-inclusive deuteron asymmetry A_1^{p}, x, y, Q^2, statistics in each spin state of beam and target, and their total. After the corrections by the CLD method the sum of $N^{\vec{\Rightarrow}}$ and $N^{\vec{\Leftarrow}}$ does not become equal to $N^{\vec{\Rightarrow}} + N^{\vec{\Leftarrow}}$ as a matter of course because these numbers are determined from the average ones on the distributions. For the values of statistics the fractions are rounded off to integral place.

Semi-inclusive asymmetry $A_1^{\bar{\mathrm{p}}}$							
Bin	x	y	Q^2	$A_1^{\bar{\mathrm{p}}} \pm$ stat.	$N^{\vec{\Rightarrow}}$	$N^{\vec{\Leftarrow}}$	$N^{\vec{\Rightarrow}} + N^{\vec{\Leftarrow}}$
1	0.033	0.720	1.22	0.0345±0.1344	301	301	601
2	0.047	0.616	1.50	−0.1563±0.1474	370	336	705
3	0.064	0.560	1.86	0.1845±0.1576	357	380	737
4	0.086	0.513	2.29	−0.0088±0.1923	292	286	579
5	0.118	0.476	2.89	−0.1469±0.2091	283	262	544
6	0.163	0.454	3.84	0.0678±0.2845	150	152	301
7	0.237	0.448	5.46	0.3565±0.4301	57	65	121
8	0.334	0.424	7.34	0.1117±0.9908	12	12	24
9	0.447	0.462	10.71	1.2486±1.8681	1	3	4

Table 8.9: Semi-inclusive deuteron asymmetry $A_1^{\bar{\mathrm{p}}}$, x, y, Q^2, statistics in each spin state of beam and target, and their total. After the corrections by the CLD method the sum of $N^{\vec{\Rightarrow}}$ and $N^{\vec{\Leftarrow}}$ does not become equal to $N^{\vec{\Rightarrow}} + N^{\vec{\Leftarrow}}$ as a matter of course because these numbers are determined from the average ones on the distributions. For the values of statistics the fractions are rounded off to integral place.

Inclusive asymmetry A_1					
Bin	$[\delta A_1]_{P_B}$	$[\delta A_1]_{P_T}$	$[\delta A_1]_R$	$[\delta A_1]_{g_2}$	$\delta A_1^{\mathrm{Total}}$
1	0.0003	0.0008	0.0002	0.0008	0.0012
2	0.0005	0.0011	0.0004	0.0018	0.0022
3	0.0008	0.0018	0.0008	0.0032	0.0039
4	0.0012	0.0029	0.0013	0.0055	0.0065
5	0.0029	0.0068	0.0024	0.0094	0.0122
6	0.0046	0.0108	0.0039	0.0170	0.0211
7	0.0064	0.0149	0.0053	0.0331	0.0372
8	0.0106	0.0247	0.0089	0.0552	0.0620
9	0.0092	0.0215	0.0081	0.0883	0.0917

Table 8.10: Systematic uncertainties of the experiment for the inclusive deuteron asymmetry A_1. The sources of the systematic uncertainties are the measurements of the beam polarization ($[\delta A_1]_{P_B}$), the target polarization ($[\delta A_1]_{P_T}$), the cross section ratio R ($[\delta A_1]_R$) and the spin-dependent structure function g_2 ($[\delta A_1]_{g_2}$). Additionally the total uncertainty ($\delta A_1^{\mathrm{Total}}$) of the sources is shown in the table.

Semi-inclusive asymmetry $A_1^{h^+}$				
Bin	$[\delta\sigma_{\mathrm{CLD}}]_{\mathrm{Fit\ Err}}$	$[\delta\sigma_{\mathrm{CLD}}]_{\mathrm{Stat}}$	$\delta\sigma_{\mathrm{CLD}}^{\mathrm{Total}}$	$\delta A_1^{\mathrm{Flux}}$
1	0.00017	0.00002	0.00017	0.00014
2	0.00019	0.00002	0.00019	0.00709
3	0.00022	0.00002	0.00022	0.00060
4	0.00023	0.00002	0.00024	0.00027
5	0.00025	0.00002	0.00025	0.00201
6	0.00032	0.00003	0.00032	0.00204
7	0.00049	0.00007	0.00050	0.00094
8	0.00117	0.00034	0.00122	0.00928
9	0.00223	0.00136	0.00261	0.02069

Table 8.11: Systematic uncertainties of the CLD method and systematic uncertainty of the flux for hadrons for the semi-inclusive deuteron asymmetry $A_1^{h^+}$. The sources of the systematic uncertainties are the error ($[\delta\sigma_{\mathrm{CLD}}]_{\mathrm{Fit\ Err}}$) of the fit to the distributions for the mean value of the asymmetry and the standard deviation ($[\delta\sigma_{\mathrm{CLD}}]_{\mathrm{Stat}}$) in the distributions for the statistical uncertainty of the asymmetry. Additionally the total uncertainty ($\delta\sigma_{\mathrm{CLD}}^{\mathrm{Total}}$) of the sources is shown in the table. The uncertainty ($\delta A_1^{\mathrm{Flux}}$) of the flux for hadrons on the asymmetry is shown in the last column of the table.

Semi-inclusive asymmetry $A_1^{h^+}$					
Bin	$[\delta A_1]_{P_{\mathrm{B}}}$	$[\delta A_1]_{P_{\mathrm{T}}}$	$[\delta A_1]_R$	$[\delta A_1]_{g_2}$	$\delta A_1^{\mathrm{Total}}$
1	0.0002	0.0005	0.0001	0.0009	0.0010
2	0.0017	0.0040	0.0002	0.0018	0.0049
3	0.0004	0.0010	0.0004	0.0030	0.0032
4	0.0012	0.0028	0.0013	0.0047	0.0057
5	0.0042	0.0098	0.0035	0.0068	0.0131
6	0.0033	0.0078	0.0028	0.0093	0.0128
7	0.0092	0.0215	0.0080	0.0133	0.0280
8	0.0020	0.0048	0.0019	0.0208	0.0215
9	0.0200	0.0467	0.0194	0.0357	0.0650

Table 8.12: Systematic uncertainties of the experiment for the semi-inclusive deuteron asymmetry $A_1^{h^+}$. The sources of the systematic uncertainties are the measurements of the beam polarization ($[\delta A_1]_{P_{\mathrm{B}}}$), the target polarization ($[\delta A_1]_{P_{\mathrm{T}}}$), the cross section ratio R ($[\delta A_1]_R$) and the spin-dependent structure function g_2 ($[\delta A_1]_{g_2}$). Additionally the total uncertainty ($\delta A_1^{\mathrm{Total}}$) of the sources is shown in the table.

Semi-inclusive asymmetry $A_1^{h^-}$				
Bin	$[\delta\sigma_{\mathrm{CLD}}]_{\mathrm{Fit\ Err}}$	$[\delta\sigma_{\mathrm{CLD}}]_{\mathrm{Stat}}$	$\delta\sigma_{\mathrm{CLD}}^{\mathrm{Total}}$	$\delta A_1^{\mathrm{Flux}}$
1	0.00021	0.00002	0.00021	0.00024
2	0.00022	0.00002	0.00023	0.00173
3	0.00024	0.00002	0.00025	0.00212
4	0.00031	0.00004	0.00031	0.00098
5	0.00033	0.00004	0.00033	0.00001
6	0.00038	0.00006	0.00038	0.00022
7	0.00061	0.00012	0.00062	0.00046
8	0.00123	0.00050	0.00132	0.00057
9	0.00766	0.00231	0.00800	0.00884

Table 8.13: Systematic uncertainties of the CLD method and systematic uncertainty of the flux for hadrons for the semi-inclusive deuteron asymmetry $A_1^{h^-}$. The sources of the systematic uncertainties are the error ($[\delta\sigma_{\mathrm{CLD}}]_{\mathrm{Fit\ Err}}$) of the fit to the distributions for the mean value of the asymmetry and the standard deviation ($[\delta\sigma_{\mathrm{CLD}}]_{\mathrm{Stat}}$) in the distributions for the statistical uncertainty of the asymmetry. Additionally the total uncertainty ($\delta\sigma_{\mathrm{CLD}}^{\mathrm{Total}}$) of the sources is shown in the table. The uncertainty ($\delta A_1^{\mathrm{Flux}}$) of the flux for hadrons on the asymmetry is shown in the last column of the table.

Semi-inclusive asymmetry $A_1^{h^-}$					
Bin	$[\delta A_1]_{P_{\mathrm{B}}}$	$[\delta A_1]_{P_{\mathrm{T}}}$	$[\delta A_1]_R$	$[\delta A_1]_{g_2}$	$\delta A_1^{\mathrm{Total}}$
1	0.0004	0.0008	0.0003	0.0009	0.0013
2	0.0004	0.0010	0.0004	0.0018	0.0021
3	0.0015	0.0034	0.0015	0.0030	0.0050
4	0.0015	0.0036	0.0016	0.0046	0.0062
5	0.0000	0.0001	0.0000	0.0065	0.0065
6	0.0003	0.0004	0.0001	0.0091	0.0091
7	0.0045	0.0106	0.0039	0.0132	0.0179
8	0.0013	0.0029	0.0011	0.0210	0.0210
9	0.0085	0.0199	0.0083	0.0355	0.0424

Table 8.14: Systematic uncertainties of the experiment for the semi-inclusive deuteron asymmetry $A_1^{h^-}$. The sources of the systematic uncertainties are the measurements of the beam polarization ($[\delta A_1]_{P_{\mathrm{B}}}$), the target polarization ($[\delta A_1]_{P_{\mathrm{T}}}$), the cross section ratio R ($[\delta A_1]_R$) and the spin-dependent structure function g_2 ($[\delta A_1]_{g_2}$). Additionally the total uncertainty ($\delta A_1^{\mathrm{Total}}$) of the sources is shown in the table.

Semi-inclusive asymmetry $A_1^{\pi^+}$				
Bin	$[\delta\sigma_{\mathrm{CLD}}]_{\mathrm{Fit\ Err}}$	$[\delta\sigma_{\mathrm{CLD}}]_{\mathrm{Stat}}$	$\delta\sigma_{\mathrm{CLD}}^{\mathrm{Total}}$	$\delta A_1^{\mathrm{Flux}}$
1	0.00021	0.00002	0.00021	0.00055
2	0.00025	0.00002	0.00025	0.00715
3	0.00028	0.00002	0.00028	0.00029
4	0.00033	0.00003	0.00033	0.00016
5	0.00038	0.00004	0.00038	0.00251
6	0.00047	0.00005	0.00047	0.00428
7	0.00066	0.00011	0.00067	0.00076
8	0.00146	0.00046	0.00153	0.00307
9	0.00312	0.00223	0.00383	0.01858

Table 8.15: Systematic uncertainties of the CLD method and systematic uncertainty of the flux for hadrons for the semi-inclusive deuteron asymmetry $A_1^{\pi^+}$. The sources of the systematic uncertainties are the error ($[\delta\sigma_{\mathrm{CLD}}]_{\mathrm{Fit\ Err}}$) of the fit to the distributions for the mean value of the asymmetry and the standard deviation ($[\delta\sigma_{\mathrm{CLD}}]_{\mathrm{Stat}}$) in the distributions for the statistical uncertainty of the asymmetry. Additionally the total uncertainty ($\delta\sigma_{\mathrm{CLD}}^{\mathrm{Total}}$) of the sources is shown in the table. The uncertainty ($\delta A_1^{\mathrm{Flux}}$) of the flux for hadrons on the asymmetry is shown in the last column of the table.

Semi-inclusive asymmetry $A_1^{\pi^+}$					
Bin	$[\delta A_1]_{P_{\mathrm{B}}}$	$[\delta A_1]_{P_{\mathrm{T}}}$	$[\delta A_1]_R$	$[\delta A_1]_{g_2}$	$\delta A_1^{\mathrm{Total}}$
1	0.0008	0.0019	0.0006	0.0009	0.0023
2	0.0017	0.0040	0.0016	0.0018	0.0050
3	0.0002	0.0005	0.0002	0.0030	0.0031
4	0.0002	0.0006	0.0003	0.0047	0.0047
5	0.0052	0.0122	0.0044	0.0068	0.0155
6	0.0030	0.0070	0.0025	0.0092	0.0122
7	0.0074	0.0174	0.0064	0.0134	0.0240
8	0.0007	0.0016	0.0006	0.0208	0.0209
9	0.0179	0.0419	0.0174	0.0353	0.0603

Table 8.16: Systematic uncertainties of the experiment for the semi-inclusive deuteron asymmetry $A_1^{\pi^+}$. The sources of the systematic uncertainties are the measurements of the beam polarization ($[\delta A_1]_{P_{\mathrm{B}}}$), the target polarization ($[\delta A_1]_{P_{\mathrm{T}}}$), the cross section ratio R ($[\delta A_1]_R$) and the spin-dependent structure function g_2 ($[\delta A_1]_{g_2}$). Additionally the total uncertainty ($\delta A_1^{\mathrm{Total}}$) of the sources is shown in the table.

Semi-inclusive asymmetry $A_1^{\pi^-}$				
Bin	$[\delta\sigma_{\mathrm{CLD}}]_{\mathrm{Fit\ Err}}$	$[\delta\sigma_{\mathrm{CLD}}]_{\mathrm{Stat}}$	$\delta\sigma_{\mathrm{CLD}}^{\mathrm{Total}}$	$\delta A_1^{\mathrm{Flux}}$
1	0.00022	0.00003	0.00022	0.00048
2	0.00022	0.00003	0.00023	0.00016
3	0.00028	0.00003	0.00028	0.00194
4	0.00038	0.00004	0.00038	0.00095
5	0.00038	0.00004	0.00038	0.00021
6	0.00049	0.00007	0.00050	0.00097
7	0.00072	0.00015	0.00074	0.00035
8	0.00020	0.00062	0.00212	0.00382
9	0.00284	0.00228	0.00364	0.00371

Table 8.17: Systematic uncertainties of the CLD method and systematic uncertainty of the flux for hadrons for the semi-inclusive deuteron asymmetry $A_1^{\pi^-}$. The sources of the systematic uncertainties are the error ($[\delta\sigma_{\mathrm{CLD}}]_{\mathrm{Fit\ Err}}$) of the fit to the distributions for the mean value of the asymmetry and the standard deviation ($[\delta\sigma_{\mathrm{CLD}}]_{\mathrm{Stat}}$) in the distributions for the statistical uncertainty of the asymmetry. Additionally the total uncertainty ($\delta\sigma_{\mathrm{CLD}}^{\mathrm{Total}}$) of the sources is shown in the table. The uncertainty ($\delta A_1^{\mathrm{Flux}}$) of the flux for hadrons on the asymmetry is shown in the last column of the table.

Semi-inclusive asymmetry $A_1^{\pi^-}$					
Bin	$[\delta A_1]_{P_{\mathrm{B}}}$	$[\delta A_1]_{P_{\mathrm{T}}}$	$[\delta A_1]_R$	$[\delta A_1]_{g_2}$	$\delta A_1^{\mathrm{Total}}$
1	0.0007	0.0016	0.0005	0.0009	0.0020
2	0.0000	0.0001	0.0000	0.0018	0.0018
3	0.0014	0.0032	0.0014	0.0030	0.0048
4	0.0015	0.0034	0.0015	0.0047	0.0062
5	0.0004	0.0010	0.0004	0.0067	0.0068
6	0.0007	0.0016	0.0007	0.0093	0.0095
7	0.0034	0.0080	0.0029	0.0133	0.0162
8	0.0008	0.0020	0.0008	0.0211	0.0212
9	0.0036	0.0084	0.0035	0.0358	0.0371

Table 8.18: Systematic uncertainties of the experiment for the semi-inclusive deuteron asymmetry $A_1^{\pi^-}$. The sources of the systematic uncertainties are the measurements of the beam polarization ($[\delta A_1]_{P_{\mathrm{B}}}$), the target polarization ($[\delta A_1]_{P_{\mathrm{T}}}$), the cross section ratio R ($[\delta A_1]_R$) and the spin-dependent structure function g_2 ($[\delta A_1]_{g_2}$). Additionally the total uncertainty ($\delta A_1^{\mathrm{Total}}$) of the sources is shown in the table.

Semi-inclusive asymmetry $A_1^{K^+}$				
Bin	$[\delta\sigma_{\mathrm{CLD}}]_{\mathrm{Fit\ Err}}$	$[\delta\sigma_{\mathrm{CLD}}]_{\mathrm{Stat}}$	$\delta\sigma_{\mathrm{CLD}}^{\mathrm{Total}}$	$\delta A_1^{\mathrm{Flux}}$
1	0.00145	0.00036	0.00149	0.00122
2	0.00135	0.00035	0.00140	0.00644
3	0.00135	0.00038	0.00140	0.00253
4	0.00171	0.00049	0.00178	0.00307
5	0.00162	0.00052	0.00170	0.00032
6	0.00194	0.00074	0.00208	0.00827
7	0.00269	0.00150	0.00308	0.00122
8	0.00558	0.00577	0.00803	0.02897
9	0.01742	0.02591	0.03122	0.02301

Table 8.19: Systematic uncertainties of the CLD method and systematic uncertainty of the flux for hadrons for the semi-inclusive deuteron asymmetry $A_1^{K^+}$. The sources of the systematic uncertainties are the error ($[\delta\sigma_{\mathrm{CLD}}]_{\mathrm{Fit\ Err}}$) of the fit to the distributions for the mean value of the asymmetry and the standard deviation ($[\delta\sigma_{\mathrm{CLD}}]_{\mathrm{Stat}}$) in the distributions for the statistical uncertainty of the asymmetry. Additionally the total uncertainty ($\delta\sigma_{\mathrm{CLD}}^{\mathrm{Total}}$) of the sources is shown in the table. The uncertainty ($\delta A_1^{\mathrm{Flux}}$) of the flux for hadrons on the asymmetry is shown in the last column of the table.

Semi-inclusive asymmetry $A_1^{K^+}$					
Bin	$[\delta A_1]_{P_{\mathrm{B}}}$	$[\delta A_1]_{P_{\mathrm{T}}}$	$[\delta A_1]_R$	$[\delta A_1]_{g_2}$	$\delta A_1^{\mathrm{Total}}$
1	0.0018	0.0041	0.0013	0.0009	0.0047
2	0.0015	0.0036	0.0014	0.0017	0.0045
3	0.0018	0.0041	0.0017	0.0027	0.0055
4	0.0048	0.0111	0.0049	0.0040	0.0136
5	0.0007	0.0016	0.0005	0.0054	0.0057
6	0.0058	0.0135	0.0047	0.0075	0.0171
7	0.0120	0.0280	0.0101	0.0112	0.0340
8	0.0064	0.0150	0.0057	0.0185	0.0253
9	0.0222	0.0519	0.0217	0.0374	0.0712

Table 8.20: Systematic uncertainties of the experiment for the semi-inclusive deuteron asymmetry $A_1^{K^+}$. The sources of the systematic uncertainties are the measurements of the beam polarization ($[\delta A_1]_{P_{\mathrm{B}}}$), the target polarization ($[\delta A_1]_{P_{\mathrm{T}}}$), the cross section ratio R ($[\delta A_1]_R$) and the spin-dependent structure function g_2 ($[\delta A_1]_{g_2}$). Additionally the total uncertainty ($\delta A_1^{\mathrm{Total}}$) of the sources is shown in the table.

Semi-inclusive asymmetry $A_1^{\mathrm{K}^-}$				
Bin	$[\delta\sigma_{\mathrm{CLD}}]_{\mathrm{Fit\ Err}}$	$[\delta\sigma_{\mathrm{CLD}}]_{\mathrm{Stat}}$	$\delta\sigma_{\mathrm{CLD}}^{\mathrm{Total}}$	$\delta A_1^{\mathrm{Flux}}$
1	0.00205	0.00079	0.00220	0.00274
2	0.00218	0.00075	0.00230	0.00634
3	0.00215	0.00086	0.00231	0.00269
4	0.00260	0.00126	0.00289	0.00259
5	0.00301	0.00147	0.00335	0.00114
6	0.00406	0.00260	0.00482	0.00499
7	0.00552	0.00486	0.00736	0.00059
8	0.01422	0.02699	0.03051	0.11484
9	0.02554	0.17122	0.17311	0.08088

Table 8.21: Systematic uncertainties of the CLD method and systematic uncertainty of the flux for hadrons for the semi-inclusive deuteron asymmetry $A_1^{\mathrm{K}^-}$. The sources of the systematic uncertainties are the error ($[\delta\sigma_{\mathrm{CLD}}]_{\mathrm{Fit\ Err}}$) of the fit to the distributions for the mean value of the asymmetry and the standard deviation ($[\delta\sigma_{\mathrm{CLD}}]_{\mathrm{Stat}}$) in the distributions for the statistical uncertainty of the asymmetry. Additionally the total uncertainty ($\delta\sigma_{\mathrm{CLD}}^{\mathrm{Total}}$) of the sources is shown in the table. The uncertainty ($\delta A_1^{\mathrm{Flux}}$) of the flux for hadrons on the asymmetry is shown in the last column of the table.

Semi-inclusive asymmetry $A_1^{\mathrm{K}^-}$					
Bin	$[\delta A_1]_{P_{\mathrm{B}}}$	$[\delta A_1]_{P_{\mathrm{T}}}$	$[\delta A_1]_R$	$[\delta A_1]_{g_2}$	$\delta A_1^{\mathrm{Total}}$
1	0.0039	0.0092	0.0029	0.0009	0.0105
2	0.0015	0.0036	0.0014	0.0016	0.0044
3	0.0019	0.0044	0.0018	0.0025	0.0057
4	0.0040	0.0094	0.0040	0.0035	0.0115
5	0.0024	0.0055	0.0019	0.0049	0.0080
6	0.0035	0.0081	0.0028	0.0068	0.0115
7	0.0058	0.0135	0.0048	0.0106	0.0187
8	0.0253	0.0592	0.0225	0.0180	0.0705
9	0.0781	0.1826	0.0745	0.0307	0.2143

Table 8.22: Systematic uncertainties of the experiment for the semi-inclusive deuteron asymmetry $A_1^{\mathrm{K}^-}$. The sources of the systematic uncertainties are the measurements of the beam polarization ($[\delta A_1]_{P_{\mathrm{B}}}$), the target polarization ($[\delta A_1]_{P_{\mathrm{T}}}$), the cross section ratio R ($[\delta A_1]_R$) and the spin-dependent structure function g_2 ($[\delta A_1]_{g_2}$). Additionally the total uncertainty ($\delta A_1^{\mathrm{Total}}$) of the sources is shown in the table.

Semi-inclusive asymmetry A_1^{p}				
Bin	$[\delta\sigma_{\mathrm{CLD}}]_{\mathrm{Fit\ Err}}$	$[\delta\sigma_{\mathrm{CLD}}]_{\mathrm{Stat}}$	$\delta\sigma_{\mathrm{CLD}}^{\mathrm{Total}}$	$\delta A_1^{\mathrm{Flux}}$
1	0.00137	0.00046	0.00145	0.00046
2	0.00155	0.00047	0.00161	0.00477
3	0.00167	0.00048	0.00173	0.00366
4	0.00186	0.00055	0.00194	0.00312
5	0.00206	0.00060	0.00214	0.00088
6	0.00235	0.00084	0.00250	0.00019
7	0.00293	0.00147	0.00328	0.00143
8	0.00639	0.00567	0.00855	0.00195
9	0.02673	0.02673	0.03360	0.01497

Table 8.23: Systematic uncertainties of the CLD method and systematic uncertainty of the flux for hadrons for the semi-inclusive deuteron asymmetry A_1^{p}. The sources of the systematic uncertainties are the error ($[\delta\sigma_{\mathrm{CLD}}]_{\mathrm{Fit\ Err}}$) of the fit to the distributions for the mean value of the asymmetry and the standard deviation ($[\delta\sigma_{\mathrm{CLD}}]_{\mathrm{Stat}}$) in the distributions for the statistical uncertainty of the asymmetry. Additionally the total uncertainty ($\delta\sigma_{\mathrm{CLD}}^{\mathrm{Total}}$) of the sources is shown in the table. The uncertainty ($\delta A_1^{\mathrm{Flux}}$) of the flux for hadrons on the asymmetry is shown in the last column of the table.

Semi-inclusive asymmetry A_1^{p}					
Bin	$[\delta A_1]_{P_{\mathrm{B}}}$	$[\delta A_1]_{P_{\mathrm{T}}}$	$[\delta A_1]_R$	$[\delta A_1]_{g_2}$	$\delta A_1^{\mathrm{Total}}$
1	0.0007	0.0016	0.0005	0.0009	0.0020
2	0.0011	0.0027	0.0011	0.0018	0.0036
3	0.0025	0.0060	0.0026	0.0030	0.0076
4	0.0048	0.0113	0.0051	0.0048	0.0141
5	0.0018	0.0043	0.0015	0.0070	0.0086
6	0.0001	0.0003	0.0001	0.0097	0.0097
7	0.0140	0.0327	0.0120	0.0133	0.0399
8	0.0004	0.0010	0.0004	0.0211	0.0211
9	0.0144	0.0338	0.0140	0.0360	0.0533

Table 8.24: Systematic uncertainties of the experiment for the semi-inclusive deuteron asymmetry A_1^{p}. The sources of the systematic uncertainties are the measurements of the beam polarization ($[\delta A_1]_{P_{\mathrm{B}}}$), the target polarization ($[\delta A_1]_{P_{\mathrm{T}}}$), the cross section ratio R ($[\delta A_1]_R$) and the spin-dependent structure function g_2 ($[\delta A_1]_{g_2}$). Additionally the total uncertainty ($\delta A_1^{\mathrm{Total}}$) of the sources is shown in the table.

Semi-inclusive asymmetry $A_1^{\bar{p}}$				
Bin	$[\delta\sigma_{\mathrm{CLD}}]_{\mathrm{Fit\ Err}}$	$[\delta\sigma_{\mathrm{CLD}}]_{\mathrm{Stat}}$	$\delta\sigma_{\mathrm{CLD}}^{\mathrm{Total}}$	$\delta A_1^{\mathrm{Flux}}$
1	0.00317	0.00151	0.00351	0.00082
2	0.00351	0.00167	0.00389	0.02229
3	0.00367	0.00188	0.00413	0.00907
4	0.00514	0.00298	0.00594	0.00019
5	0.00547	0.00325	0.00636	0.00241
6	0.00839	0.00619	0.01043	0.00333
7	0.01097	0.01431	0.01803	0.00124
8	0.02969	0.06696	0.07325	0.01733
9	–	–	–	–

Table 8.25: Systematic uncertainties of the CLD method and systematic uncertainty of the flux for hadrons for the semi-inclusive deuteron asymmetry $A_1^{\bar{p}}$. The sources of the systematic uncertainties are the error ($[\delta\sigma_{\mathrm{CLD}}]_{\mathrm{Fit\ Err}}$) of the fit to the distributions for the mean value of the asymmetry and the standard deviation ($[\delta\sigma_{\mathrm{CLD}}]_{\mathrm{Stat}}$) in the distributions for the statistical uncertainty of the asymmetry. Additionally the total uncertainty ($\delta\sigma_{\mathrm{CLD}}^{\mathrm{Total}}$) of the sources is shown in the table. The uncertainty ($\delta A_1^{\mathrm{Flux}}$) of the flux for hadrons on the asymmetry is shown in the last column of the table.

Semi-inclusive asymmetry $A_1^{\bar{p}}$					
Bin	$[\delta A_1]_{P_{\mathrm{B}}}$	$[\delta A_1]_{P_{\mathrm{T}}}$	$[\delta A_1]_R$	$[\delta A_1]_{g_2}$	$\delta A_1^{\mathrm{Total}}$
1	0.0012	0.0028	0.0009	0.0008	0.0032
2	0.0053	0.0125	0.0048	0.0017	0.0145
3	0.0063	0.0148	0.0061	0.0028	0.0174
4	0.0003	0.0007	0.0003	0.0043	0.0043
5	0.0050	0.0117	0.0041	0.0063	0.0148
6	0.0023	0.0054	0.0019	0.0088	0.0107
7	0.0122	0.0285	0.0103	0.0123	0.0349
8	0.0038	0.0089	0.0034	0.0205	0.0229
9	0.0465	0.1088	0.0450	0.0318	0.1305

Table 8.26: Systematic uncertainties of the experiment for the semi-inclusive deuteron asymmetry $A_1^{\bar{p}}$. The sources of the systematic uncertainties are the measurements of the beam polarization ($[\delta A_1]_{P_{\mathrm{B}}}$), the target polarization ($[\delta A_1]_{P_{\mathrm{T}}}$), the cross section ratio R ($[\delta A_1]_R$) and the spin-dependent structure function g_2 ($[\delta A_1]_{g_2}$). Additionally the total uncertainty ($\delta A_1^{\mathrm{Total}}$) of the sources is shown in the table.

Appendix A

Spin Asymmetry for combined Statistics of K^+ and K^-

The $A_1^{K^+ + K^-}$ asymmetry for the combined statistics of K^+ and K^- on the deuteron allows to access the nonstrange and strange spin polarizations [105] of the sea quarks, $\Delta q(x)/q(x)$ and $\Delta s(x)/s(x)$, respectively by using the technique [2] of the flavor decomposition for the quark polarizations as:

$$\vec{A}(x) = \mathcal{P}(x) \cdot \vec{Q}(x), \tag{A.1}$$

where $\vec{A}(x) = (A_1(x), A_1^{K^+ + K^-}(x))$. $A_1(x)$ is the inclusive asymmetry on the deuteron. Also where $\vec{Q}(x) = (\Delta q(x)/q(x), \Delta s(x)/s(x))$. $q(x)$ is defined as $q(x) = u(x) + \bar{u}(x) + d(x) + \bar{d}(x)$ and $s(x)$ is the total polarization of the strange quark. $\mathcal{P}(x)$ is written as:

$$\mathcal{P}(x) = \begin{pmatrix} P_q(x) & P_s(x) \\ P_q^{K^+ + K^-}(x) & P_s^{K^+ + K^-} \end{pmatrix}, \tag{A.2}$$

where

$$P_q(x) = \frac{5q(x)}{5q(x) + 2s(x)}, \tag{A.3}$$

$$P_q^{K^+ + K^-}(x) = \frac{5q(x)\int_{0.2}^{1} dz D_q^{K^+ + K^-}(x)z}{5q(x)\int_{0.2}^{1} dz' D_q^{K^+ + K^-}(x)z' + 2s(x)\int_{0.2}^{1} dz' D_s^{K^+ + K^-}(x)z'}. \tag{A.4}$$

Here $D_q^{K^+ + K^-}(x)$ and $D_s^{K^+ + K^-}(x)$ are the fragmentation functions in leading order for the total flux of kaons at the average Q^2 of 2.5 GeV^2 in the HERMES experiment and can be derived in the analysis [106] from the experiments of the e^+e^- collisions. Figure A.1 shows the $K^+ + K^-$ asymmetry corrected by the CLD method in $rQp > 0.0$. The $K^+ + K^-$ asymmetry is used as an input to $\vec{A}(x)$. Table A.1 is the numerical values related to the asymmetry. The numerical values for the systematic uncertainties of the CLD method and the systematic uncertainty of the flux for

hadrons are shown in table A.2. The systematic uncertainties of the experiment is shown in table A.3.

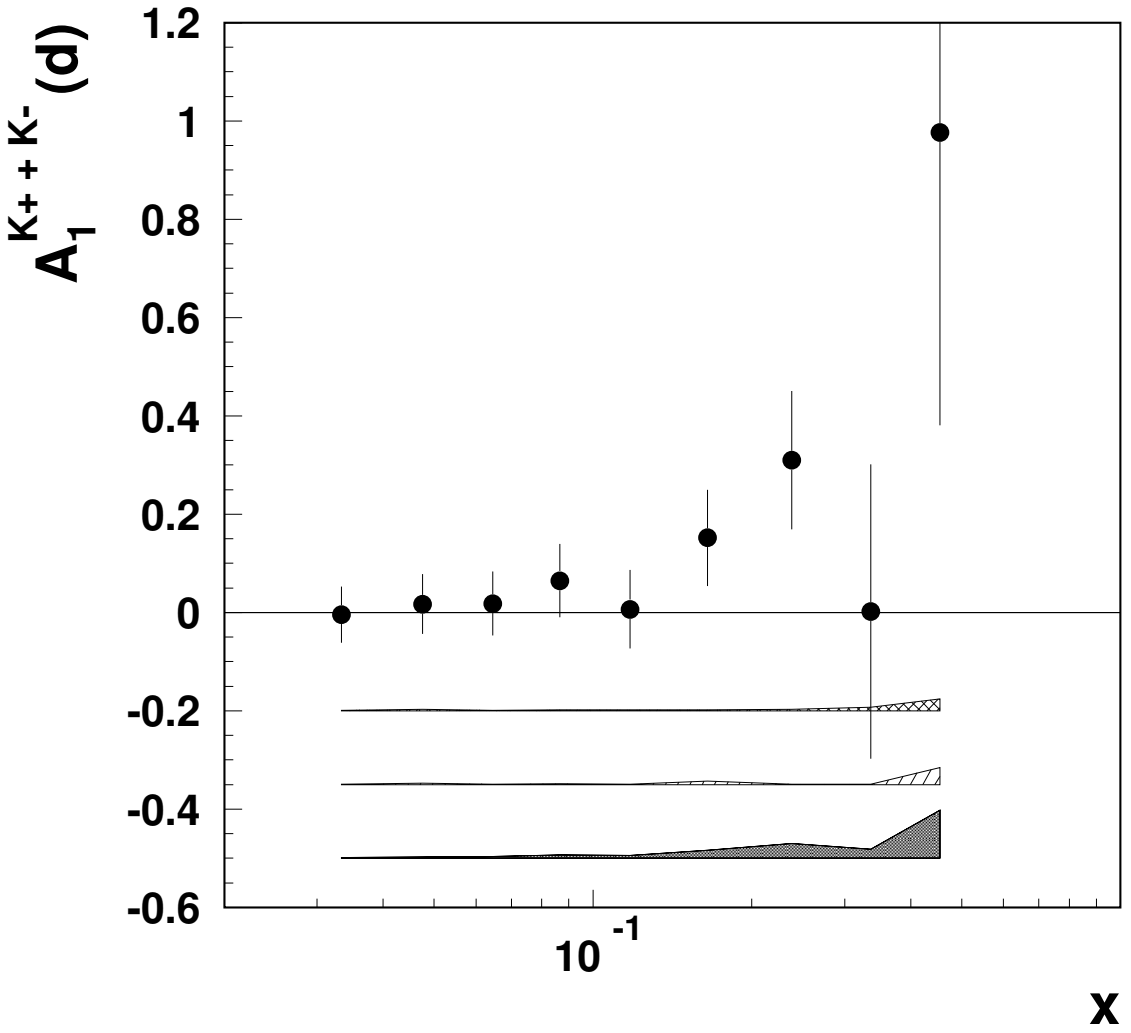

Figure A.1: Result of the $K^+ + K^-$ asymmetry on the deuterium target. The asymmetry was corrected by the assignment of the true type of hadron to the identified type of hadron by the RICH detector in the CLD method. The assignment was performed more than 600 times. The most upper band represents the total systematic uncertainty of the CLD method, the middle band the systematic uncertainty of the flux and the lowest band the total systematic uncertainty of the experiment.

Semi-inclusive asymmetry $A_1^{\mathrm{K}^+ + \mathrm{K}^-}$							
Bin	x	y	Q^2	$A_1^{\mathrm{K}^+ + \mathrm{K}^-}$ $\pm$ stat.	$N^{\vec{\Rightarrow}}$	$N^{\vec{\Leftarrow}}$	$N^{\vec{\Rightarrow}} + N^{\vec{\Leftarrow}}$
1	0.033	0.710	1.22	-0.0045 ± 0.0574	1726	1687	3412
2	0.047	0.614	1.50	0.0170 ± 0.0607	2110	2086	4196
3	0.064	0.561	1.87	0.0180 ± 0.0649	2193	2168	4360
4	0.087	0.530	2.37	0.0648 ± 0.0747	1771	1786	3557
5	0.118	0.508	3.09	0.0066 ± 0.0795	1634	1607	3244
6	0.165	0.490	4.18	0.1518 ± 0.0979	1041	1091	2131
7	0.238	0.472	5.81	0.3096 ± 0.1409	478	538	1016
8	0.336	0.452	7.87	0.0022 ± 0.2994	116	114	230
9	0.454	0.431	10.16	0.9768 ± 0.5962	22	33	55

Table A.1: Semi-inclusive deuteron asymmetry $A_1^{\mathrm{K}^+ + \mathrm{K}^-}$, x, y, Q^2, statistics in each spin state of beam and target, and their total. After the correction by the CLD method the sum of $N^{\vec{\Rightarrow}}$ and $N^{\vec{\Leftarrow}}$ does not become equal to $N^{\vec{\Rightarrow}} + N^{\vec{\Leftarrow}}$ as a matter of course because these numbers are determined from the average ones on the distributions. For the values of statistics the fractions are rounded off to integral place.

Semi-inclusive asymmetry $A_1^{\mathrm{K}^+ + \mathrm{K}^-}$				
Bin	$[\delta\sigma_{\mathrm{CLD}}]_{\mathrm{Fit\ Err}}$	$[\delta\sigma_{\mathrm{CLD}}]_{\mathrm{Stat}}$	$\delta\sigma_{\mathrm{CLD}}^{\mathrm{Total}}$	$\delta A_1^{\mathrm{Flux}}$
1	0.00118	0.00025	0.00121	0.00011
2	0.00113	0.00025	0.00270	0.00242
3	0.00122	0.00026	0.00125	0.00089
4	0.00138	0.00034	0.00143	0.00143
5	0.00141	0.00039	0.00146	0.00011
6	0.00180	0.00056	0.00188	0.00745
7	0.00255	0.00111	0.00278	0.00108
8	0.00514	0.00446	0.00681	0.00034
9	0.01015	0.02186	0.02410	0.03462

Table A.2: Systematic uncertainties of the CLD method and systematic uncertainty of the flux for hadrons for the semi-inclusive deuteron asymmetry $A_1^{\mathrm{K}^+ + \mathrm{K}^-}$. The sources of the systematic uncertainties are the error ($[\delta\sigma_{\mathrm{CLD}}]_{\mathrm{Fit\ Err}}$) of the fit to the distributions for the mean value of the asymmetry and the standard deviation ($[\delta\sigma_{\mathrm{CLD}}]_{\mathrm{Stat}}$) in the distributions for the statistical uncertainty of the asymmetry. Additionally the total uncertainty ($\delta\sigma_{\mathrm{CLD}}^{\mathrm{Total}}$) of the sources is shown in the table. The uncertainty ($\delta A_1^{\mathrm{Flux}}$) of the flux for hadrons on the asymmetry is shown in the last column of the table.

Semi-inclusive asymmetry $A_1^{\mathrm{K}^+ + \mathrm{K}^-}$					
Bin	$[\delta A_1]_{P_{\mathrm{B}}}$	$[\delta A_1]_{P_{\mathrm{T}}}$	$[\delta A_1]_R$	$[\delta A_1]_{g_2}$	$\delta A_1^{\mathrm{Total}}$
1	0.0002	0.0004	0.0001	0.0009	0.0010
2	0.0006	0.0014	0.0005	0.0017	0.0023
3	0.0006	0.0014	0.0006	0.0027	0.0032
4	0.0022	0.0052	0.0022	0.0039	0.0072
5	0.0002	0.0005	0.0002	0.0053	0.0053
6	0.0052	0.0121	0.0042	0.0074	0.0157
7	0.0106	0.0248	0.0089	0.0111	0.0304
8	0.0007	0.0002	0.0001	0.0185	0.0185
9	0.0334	0.0781	0.0325	0.0362	0.0979

Table A.3: Systematic uncertainties of the experiment for the semi-inclusive deuteron asymmetry $A_1^{\mathrm{K}^+ + \mathrm{K}^-}$. The sources of the systematic uncertainties are the measurements of the beam polarization ($[\delta A_1]_{P_{\mathrm{B}}}$), the target polarization ($[\delta A_1]_{P_{\mathrm{T}}}$), the cross section ratio R ($[\delta A_1]_R$) and the spin-dependent structure function g_2 ($[\delta A_1]_{g_2}$). Additionally the total uncertainty ($\delta A_1^{\mathrm{Total}}$) of the sources is shown in the table.

Appendix B

Tests for Stability of Asymmetry

The kinematical variables of both z and x_{F} use the mass of each type of hadrons for their calculations. The cuts of z and x_{F} are required to separate the hadrons of the current fragments from the ones of the target remnants. The stability of the asymmetry is tested for z and x_{F} in the two different conditions as follows:

- The mass of proton is applied instead of the mass of pion when the asymmetry of pion is extracted.
- Both kinematical cuts z and x_{F} are neglected in the extraction of the asymmetry.

For the first item, figures B.1 and B.2 show the comparison of the π^+ and π^- asymmetries between the mass of proton and the mass of pion. Tables B.1 and B.2 show the comparison of statistics between both. The results of the pion asymmetries which are extracted in the application of the mass of proton agree with the ones which are extracted in the application of the correct mass, namely, the mass of pion, within their statistical uncertainties. It is found from the tables that if the mass of proton is applied in the extraction of the pion asymmetries, statistics are significantly lost. This can happen if the misidentification between pions and protons is done as seen in the most upper parts of figures 5.12, 5.13 and 5.14.

For the second item, figures B.3 and B.4 show the comparison of the K^+ and K^- asymmetries between no cut and with cut on z and x_{F}. The asymmetries are extracted consistently imposing the momentum threshold of 3.25 GeV. In each figure the results between both are in agreement within their statistical uncertainties. It is assumed that the cuts of z and x_{F} play no significant roles in the extraction of the asymmetries when the momentum threshold of 3.25 GeV is imposed.

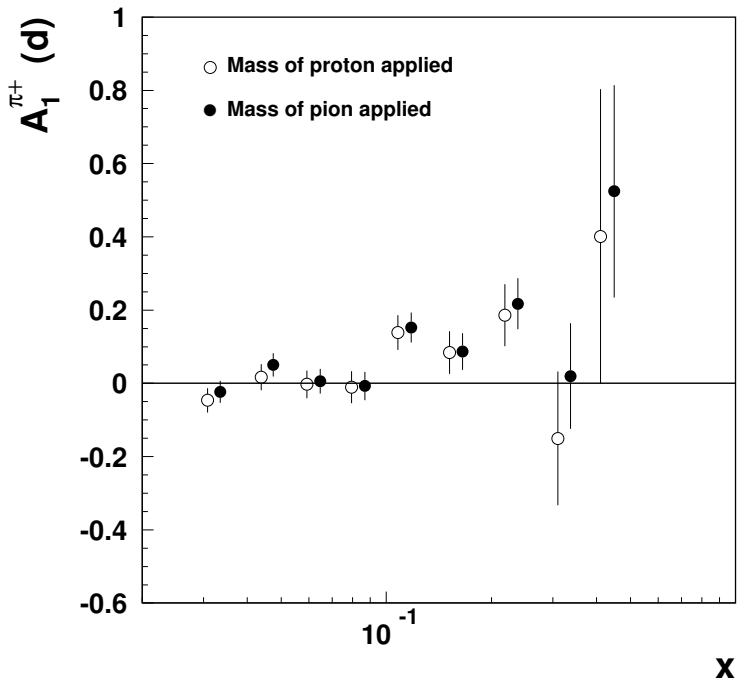

Figure B.1: Comparison of the π^+ asymmetry between the mass of proton (open circles) and the mass of pion (closed circles). The asymmetries are the results obtained by the CLD method in $rQp > 0.0$.

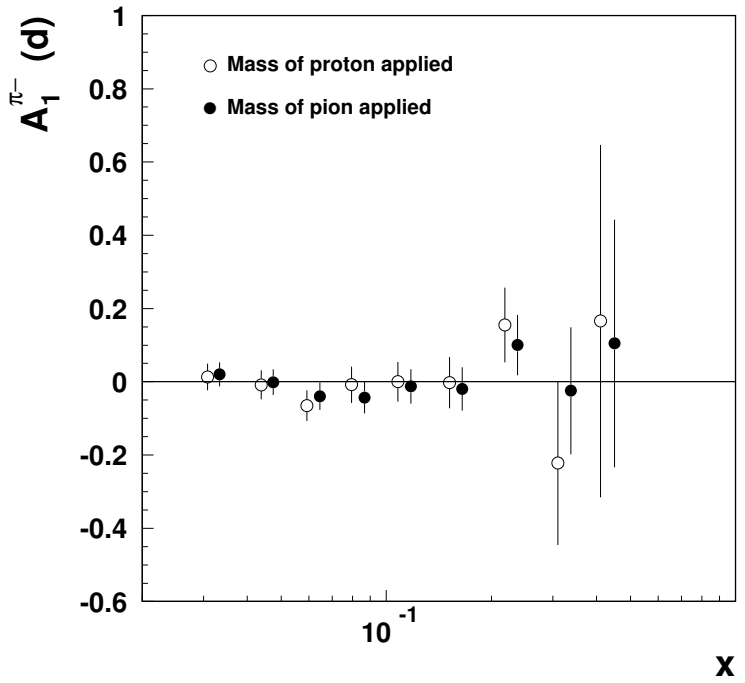

Figure B.2: Comparison of the π^- asymmetry between the mass of proton (open circles) and the mass of pion (closed circles). The asymmetries are the results obtained by the CLD method in $rQp > 0.0$.

Statistics for $A_1^{\pi^+}$				
Mass	Proton		Pion	
Bin	$N^{\vec{\Rightarrow}}$	$N^{\vec{\Leftarrow}}$	$N^{\vec{\Rightarrow}}$	$N^{\vec{\Leftarrow}}$
1	5211	4970	6394	6180
2	6481	6406	8128	8166
3	7189	7038	9369	9207
4	6236	6086	8416	8225
5	5602	5802	7834	8143
6	3589	3638	5298	5371
7	1637	1731	2585	2760
8	104	315	592	586
9	57	66	112	138

Table B.1: Comparison of statistics with application of the mass of proton and the mass of pion in the π^+ asymmetry. Statistics of the asymmetries were determined from the average value by the Gaussian fit to the distribution for statistics obtained by the assignment of the true type of hadron more than 600 times. The value of the quality parameter is $rQp > 0.0$. For the values of statistics the fractions are rounded off to integral place.

Statistics for $A_1^{\pi^-}$				
Mass	Proton		Pion	
Bin	$N^{\vec{\Rightarrow}}$	$N^{\vec{\Leftarrow}}$	$N^{\vec{\Rightarrow}}$	$N^{\vec{\Leftarrow}}$
1	4323	4270	5305	5263
2	5301	5176	6776	6639
3	5872	5589	7624	7346
4	4769	4659	6554	6314
5	4285	4200	6046	5898
6	2596	2543	3867	3761
7	1136	1186	1895	1932
8	238	213	423	411
9	43	45	92	96

Table B.2: Comparison of statistics with application of the mass of proton and the mass of pion in the π^- asymmetry. Statistics of the asymmetries were determined from the average value by the Gaussian fit to the distribution for statistics obtained by the assignment of the true type of hadron more than 600 times. The value of the quality parameter is $rQp > 0.0$. For the values of statistics the fractions are rounded off to integral place.

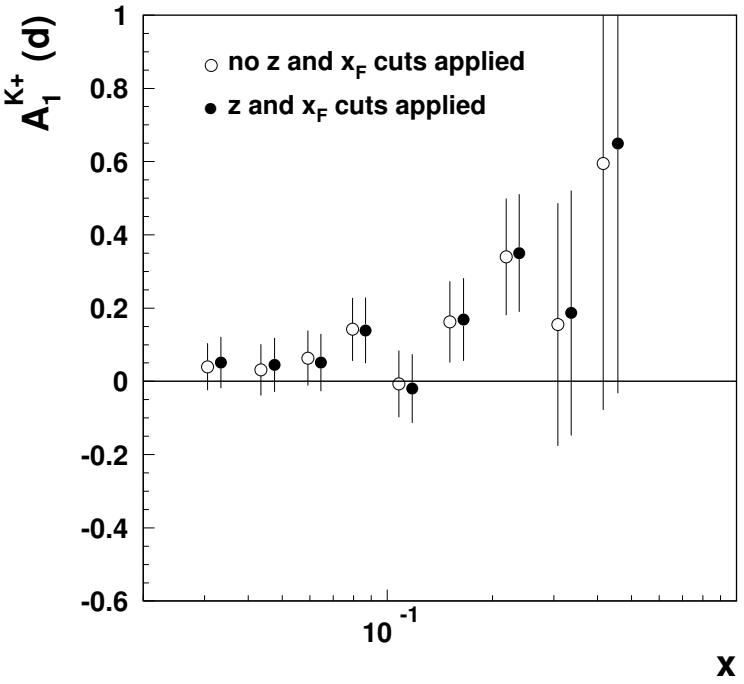

Figure B.3: Comparison of the K^+ asymmetry between no cut (open circles) and with cut (closed circles) on z and x_F. The asymmetries are the results obtained by the CLD method in $rQp > 0.0$.

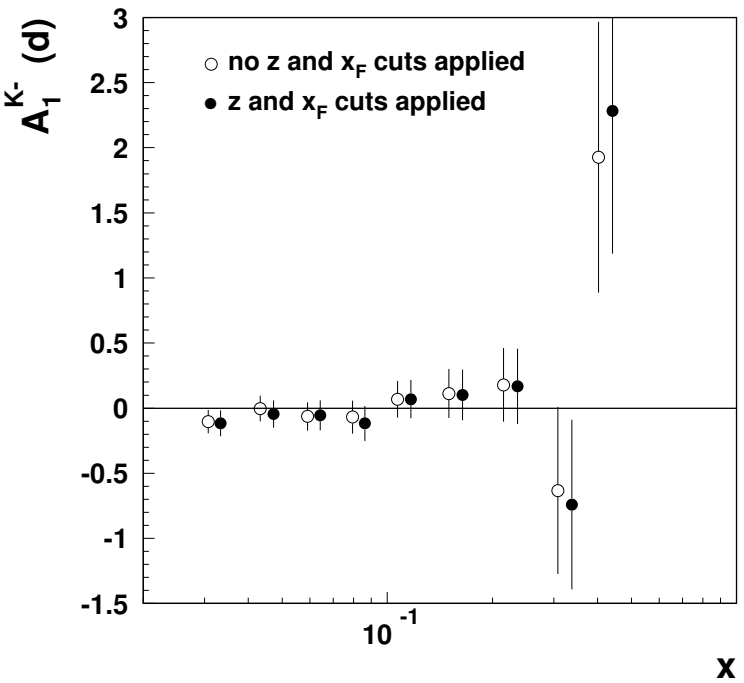

Figure B.4: Comparison of the K^- asymmetry between no cut (open circles) and with cut (closed circles) on z and x_F. The asymmetries are the results obtained by the CLD method in $rQp > 0.0$.

Appendix C

Particle Identification with direct Ray Tracing

Another method for the particle identification by the RICH detector besides the IRT method is direct ray tracing (DRT) [83, 84, 85]. The problem of the DRT method can be formulated as follows. Given point E the emission point and $\overrightarrow{\mathrm{P}}$ momentum vector of the photon, determine the point S where the photon is reflected from the surface of the mirror and the point D where the photon is detected. For the purpose of constructing the Čerenkov ring and/or its center on the plane of the photon detector, it is sufficient to determine only $\overrightarrow{\mathrm{D}}$. It, however, is also necessary to determine the incident angle in the plane of the photon detector. Finally $\overrightarrow{\mathrm{SD}}$ can be determined. Figure C.1 shows the problem of the DRT including the definitions which are used in the further derivation.

ρ is the perpendicular distance of C, the center of the spherical mirror, to the line ES. It follows that:

$$\begin{aligned} \rho &= a \sin\theta \\ &= R \sin\beta. \end{aligned} \tag{C.1}$$

When one defines $b = |\overrightarrow{\mathrm{ES}}|$, it follows that:

$$\begin{aligned} b &= |\overrightarrow{\mathrm{ES}}| \\ &= a\cos\theta + R\cos\beta. \end{aligned} \tag{C.2}$$

Since ρ can be eliminated in equation (C.1) β is derived. Then b is directly calculated. b defines the reflection point S and the angle at which the photon is reflected in S.

Switching to the Euclidean coordinate system with E as the origin, the u axis will be along $\overrightarrow{\mathrm{P}}$. The v axis is perpendicular to the u axis in the ECS plane and the v element of $\overrightarrow{\mathrm{C}}$ is positive. Then the unit vectors are expressed as follows:

$$\hat{\mathrm{u}} = \frac{\overrightarrow{\mathrm{P}}}{|\overrightarrow{\mathrm{P}}|}, \tag{C.3}$$

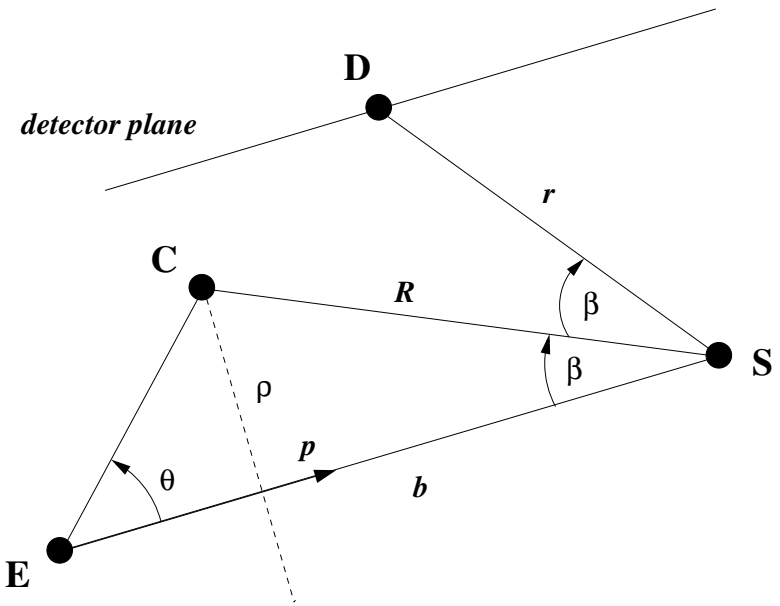

Figure C.1: Definition of the vectors and the angles in the direct ray tracing.

$$\hat{\mathrm{v}} = \frac{\overrightarrow{\mathrm{EC}} - (a\cos\theta)\cdot\hat{\mathrm{u}}}{a\sin\theta}. \tag{C.4}$$

Moreover one can write as follows:

$$\overrightarrow{\mathrm{ES}} = (b,0,0), \tag{C.5}$$

$$\overrightarrow{\mathrm{ED}} = \overrightarrow{\mathrm{ES}} + r\cdot(-\cos(2\beta),\sin(2\beta),0). \tag{C.6}$$

Using equation (C.3) and (C.4) then:

$$\overrightarrow{\mathrm{ED}} = \left[b - r\left(\cos(2\beta) - \frac{\sin(2\beta)\cos\theta}{\sin\theta}\right)\right]\cdot\frac{\overrightarrow{\mathrm{P}}}{|\overrightarrow{\mathrm{P}}|} \tag{C.7}$$

$$+ \; r\sin(2\beta)\cdot\frac{\overrightarrow{\mathrm{EC}}}{a\sin\theta}, \tag{C.8}$$

$$\overrightarrow{\mathrm{D}} = \overrightarrow{\mathrm{E}} + \left[b - r\left(\cos(2\beta) - \frac{\sin(2\beta)\cos\theta}{\sin\theta}\right)\right]\cdot\frac{\overrightarrow{\mathrm{P}}}{|\overrightarrow{\mathrm{P}}|} \tag{C.9}$$

$$+ \; r\sin(2\beta)\cdot\frac{\overrightarrow{\mathrm{EC}}}{a\sin\theta}. \tag{C.10}$$

The only variable which has not been determined in these equations is r. r can be solved from the requirement that lies on the plane of the photon detector. The plane of the photon detector is described by:

$$\overrightarrow{\mathrm{N}}\cdot\overrightarrow{\mathrm{D}} = c, \tag{C.11}$$

where $\overrightarrow{\mathrm{N}}$ is a vector perpendicular to the plane and c is a constant that can be determined by multiplying any vector which is known to be in the plane of the photon detector with $\overrightarrow{\mathrm{N}}$. This yields an equation for r. Defining the tilt angle r of the plane of the photon detector as the angle between the w axis and $\overrightarrow{\mathrm{N}}$, this can be written as:

$$\overrightarrow{\mathrm{N}} = (0, \cos\gamma, -\sin\gamma). \tag{C.12}$$

Equation (C.11) for r is written:

$$c = \overrightarrow{\mathrm{E}} \cdot \overrightarrow{\mathrm{N}} + \left[b - r\left(\cos(2\beta) - \frac{\sin(2\beta)\cos\theta}{\sin\theta}\right)\right] \cdot \frac{\overrightarrow{\mathrm{P}} \cdot \overrightarrow{\mathrm{N}}}{|\overrightarrow{\mathrm{P}}|} \tag{C.13}$$

$$+ \; r \cdot \sin(2\beta) \cdot \frac{\overrightarrow{\mathrm{EC}} \cdot \overrightarrow{\mathrm{N}}}{a\sin\theta}. \tag{C.14}$$

The solution for r is as follows:

$$r = \frac{c - \overrightarrow{\mathrm{E}} \cdot \overrightarrow{\mathrm{N}} - \left(b - \dfrac{\sin(2\beta)\cos\theta}{\sin\theta}\right) \cdot \dfrac{\overrightarrow{\mathrm{P}} \cdot \overrightarrow{\mathrm{N}}}{|\overrightarrow{\mathrm{P}}|}}{\dfrac{\sin(2\beta) \cdot \overrightarrow{\mathrm{EC}} \cdot \overrightarrow{\mathrm{N}}}{a\sin\theta} - \cos(2\beta) \cdot \dfrac{\overrightarrow{\mathrm{P}} \cdot \overrightarrow{\mathrm{N}}}{|\overrightarrow{\mathrm{P}}|}}. \tag{C.15}$$

If S has been calculated intermediately, the solution for r can be obtained from:

$$c = (\overrightarrow{\mathrm{S}} + r \cdot \hat{\mathrm{SD}}) \cdot \hat{\mathrm{N}}, \tag{C.16}$$

$$r = \frac{c - \overrightarrow{\mathrm{S}} \cdot \overrightarrow{\mathrm{N}}}{\hat{\mathrm{SD}} \cdot \overrightarrow{\mathrm{N}}}. \tag{C.17}$$

Therefore the procedure is to calculate a and θ, then deduce β and b. Then $\frac{\overrightarrow{\mathrm{P}} \cdot \overrightarrow{\mathrm{N}}}{|\overrightarrow{\mathrm{P}}|}$, $\overrightarrow{\mathrm{E}} \cdot \overrightarrow{\mathrm{N}}$ and $\overrightarrow{\mathrm{EC}} \cdot \overrightarrow{\mathrm{N}}$ are calculated, which allows the calculation of r. r is then used to determine D.

The tables for the numerical values of the P and Q matrices by using the DRT method, which are studied by the Monte Carlo simulation, are shown in appendix D.

Appendix D

Tables of Results for P and Q Matrices

Here the elements of the P matrices for the identification efficiencies and the Q matrices for the identification purities and contaminations are shown for each of $rQp > 0.0$, $rQp > 0.5$ and $rQp > 1.0$ in both the IRT and DRT methods taking into account the number of the tracks ($N_{\rm tracks} = 1$, $= 2$ and > 2) per detector half of the RICH detector, which are studied by the Monte Carlo simulation. The mean values for the elements of the Q matrices in the IRT method at $rQp > 0.0$ are used for the final results of the semi-inclusive asymmetries.

D.1 Elements of P and Q Matrices with the IRT Method

The tables of the results for the elements of the P and Q matrices obtained with the IRT method are shown in the following pages.

Momentum range	$\mathcal{P}_{\pi}^{\pi}$	$\mathcal{P}_{\pi}^{\mathrm{K}}$	$\mathcal{P}_{\pi}^{\mathrm{p}}$	$\mathcal{P}_{\mathrm{K}}^{\pi}$	$\mathcal{P}_{\mathrm{K}}^{\mathrm{K}}$	$\mathcal{P}_{\mathrm{K}}^{\mathrm{p}}$	$\mathcal{P}_{\mathrm{p}}^{\pi}$	$\mathcal{P}_{\mathrm{p}}^{\mathrm{K}}$	$\mathcal{P}_{\mathrm{p}}^{\mathrm{p}}$
0.00 - 0.50	–	–	–	–	–	–	–	–	–
0.50 - 1.00	1.00000±0.02200	–	–	1.00000±0.70711	–	–	–	–	–
1.00 - 1.50	1.00000±0.01020	–	–	1.00000±0.13245	–	–	1.00000±0.06901	–	–
1.50 - 2.00	0.99864±0.00855	0.00022±0.00009	0.00114±0.00020	0.86486±0.06959	0.00601±0.00426	0.12913±0.02092	0.85114±0.03407	0.00295±0.00148	0.14591±0.01110
2.00 - 2.25	0.92885±0.01072	0.03423±0.00151	0.03692±0.00157	0.10526±0.00963	0.49442±0.02427	0.40032±0.02114	0.12463±0.00544	0.07360±0.00408	0.80177±0.01745
2.25 - 2.50	0.91957±0.01061	0.04305±0.00169	0.03738±0.00157	0.06178±0.00712	0.80927±0.03363	0.12896±0.01060	0.12098±0.00536	0.08841±0.00451	0.79061±0.01730
2.50 - 2.75	0.91549±0.01077	0.05059±0.00187	0.03392±0.00152	0.07287±0.00726	0.84345±0.03239	0.08367±0.00782	0.13136±0.00562	0.08665±0.00448	0.78199±0.01722
2.75 - 3.00	0.91901±0.01092	0.04756±0.00184	0.03342±0.00153	0.05563±0.00613	0.86701±0.03217	0.07737±0.00730	0.11798±0.00556	0.10464±0.00520	0.77739±0.01798
3.00 - 3.25	0.92013±0.01121	0.04755±0.00188	0.03232±0.00154	0.06238±0.00656	0.88044±0.03280	0.05718±0.00627	0.11108±0.00575	0.10035±0.00544	0.78857±0.01945
3.25 - 3.50	0.98359±0.01214	0.00718±0.00074	0.00922±0.00084	0.02192±0.00380	0.91812±0.03370	0.05996±0.00640	0.02913±0.00303	0.12879±0.00668	0.84207±0.02181
3.50 - 3.75	0.99435±0.01256	0.00151±0.00035	0.00414±0.00057	0.01807±0.00351	0.93842±0.03489	0.04351±0.00551	0.01733±0.00247	0.14315±0.00753	0.83952±0.02314
3.75 - 4.00	0.99562±0.01319	0.00114±0.00032	0.00324±0.00053	0.01531±0.00322	0.96671±0.03558	0.01798±0.00349	0.06201±0.00719	0.22449±0.01469	0.71350±0.03098
4.00 - 4.25	0.99770±0.01355	0.00230±0.00046	–	0.02789±0.00436	0.93493±0.03466	0.03718±0.00506	0.02998±0.00403	0.11257±0.00812	0.85744±0.02894
4.25 - 4.50	0.99684±0.01403	0.00257±0.00050	0.00059±0.00024	0.02348±0.00407	0.93992±0.03549	0.03660±0.00512	0.02314±0.00341	0.07681±0.00638	0.90005±0.02902
4.50 - 4.75	0.99822±0.01444	0.00146±0.00039	0.00031±0.00018	0.02555±0.00437	0.94088±0.03651	0.03358±0.00503	0.02253±0.00356	0.06484±0.00616	0.91264±0.03097
4.75 - 5.00	0.99692±0.01507	0.00251±0.00054	0.00057±0.00026	0.02812±0.00457	0.93295±0.03606	0.03893±0.00540	0.02485±0.00375	0.05687±0.00576	0.91828±0.03119
5.00 - 5.25	0.99866±0.01560	0.00110±0.00037	0.00024±0.00017	0.02147±0.00410	0.93865±0.03736	0.03988±0.00564	0.02135±0.00360	0.04152±0.00506	0.93713±0.03281
5.25 - 5.50	0.99688±0.01608	0.00260±0.00058	0.00052±0.00026	0.02601±0.00439	0.92702±0.03593	0.04697±0.00596	0.01612±0.00325	0.04900±0.00576	0.93488±0.03415
5.50 - 5.75	0.99814±0.01690	0.00143±0.00045	0.00043±0.00025	0.01867±0.00393	0.94643±0.03867	0.03490±0.00541	0.02000±0.00389	0.04741±0.00606	0.93259±0.03654
5.75 - 6.00	0.99938±0.01764	0.00062±0.00031	–	0.02521±0.00466	0.94202±0.03921	0.03277±0.00533	0.02513±0.00443	0.05941±0.00692	0.91546±0.03654
6.00 - 6.50	0.99922±0.01319	0.00070±0.00025	0.00009±0.00009	0.02068±0.00311	0.94118±0.02898	0.03814±0.00427	0.02089±0.00298	0.04302±0.00433	0.93609±0.02751
6.50 - 7.00	0.99940±0.01415	0.00060±0.00025	–	0.02646±0.00372	0.93384±0.03032	0.03969±0.00458	0.03015±0.00398	0.05110±0.00524	0.91875±0.03001
7.00 - 7.50	0.99914±0.01569	0.00086±0.00033	–	0.02551±0.00389	0.93623±0.03242	0.03826±0.00480	0.01446±0.00304	0.05028±0.00576	0.93526±0.03373
7.50 - 8.00	0.99928±0.01692	0.00072±0.00032	–	0.01247±0.00288	0.93766±0.03453	0.04987±0.00586	0.01660±0.00335	0.03984±0.00524	0.94356±0.03490
8.00 - 8.50	0.99950±0.01827	0.00050±0.00029	–	0.02350±0.00427	0.93935±0.03716	0.03715±0.00540	0.01449±0.00354	0.04945±0.00665	0.93606±0.03931
8.50 - 9.00	0.99940±0.01994	0.00060±0.00034	–	0.02369±0.00453	0.92893±0.03894	0.04738±0.00648	0.02056±0.00464	0.04522±0.00697	0.93422±0.04309
9.00 - 9.50	0.99954±0.02151	0.00046±0.00033	–	0.03140±0.00555	0.89058±0.04003	0.07802±0.00895	0.02071±0.00493	0.04718±0.00754	0.93211±0.04552
9.50 - 10.0	0.99917±0.02346	0.00028±0.00028	0.00055±0.00039	0.02417±0.00534	0.87572±0.04348	0.10011±0.01126	0.01235±0.00414	0.04801±0.00831	0.93964±0.05000
10.0 - 11.0	0.99857±0.01892	0.00090±0.00040	0.00054±0.00031	0.02843±0.00450	0.85645±0.03321	0.11512±0.00944	0.01792±0.00415	0.00660±0.00250	0.97547±0.04264
11.0 - 12.0	0.99620±0.02245	0.00355±0.00095	0.00025±0.00025	0.05529±0.00752	0.92531±0.04157	0.01940±0.00438	0.00502±0.00252	0.00502±0.00252	0.98996±0.04972
12.0 - 13.0	0.99543±0.02750	0.00419±0.00127	0.00038±0.00038	0.10246±0.01242	0.89754±0.04824	–	0.00224±0.00224	0.00897±0.00450	0.98879±0.06640
13.0 - 14.0	0.99717±0.03359	0.00283±0.00127	–	0.17021±0.01963	0.82979±0.05419	–	–	0.00330±0.00331	0.99670±0.08104
14.0 - 15.0	0.99633±0.04270	0.00275±0.00159	0.00092±0.00092	0.21477±0.02959	0.78524±0.06859	–	0.00575±0.00576	0.01724±0.01004	0.97701±0.10536
15.0 - 30.0	0.99385±0.03490	0.00430±0.00163	0.00184±0.00107	0.44686±0.03745	0.54881±0.04294	0.00434±0.00307	0.00905±0.00643	0.00905±0.00643	0.98190±0.09384

Table D.1: Identification efficiencies for pions, kaons and protons in $N_{\mathrm{tracks}} = 1$ with the IRT method at $rQp > 0.0$.

Momentum range	$\mathcal{P}_{\pi}^{\pi}$	$\mathcal{P}_{\pi}^{\mathrm{K}}$	$\mathcal{P}_{\pi}^{\mathrm{p}}$	$\mathcal{P}_{\mathrm{K}}^{\pi}$	$\mathcal{P}_{\mathrm{K}}^{\mathrm{K}}$	$\mathcal{P}_{\mathrm{K}}^{\mathrm{p}}$	$\mathcal{P}_{\mathrm{p}}^{\pi}$	$\mathcal{P}_{\mathrm{p}}^{\mathrm{K}}$	$\mathcal{P}_{\mathrm{p}}^{\mathrm{p}}$
0.00 - 0.50	–	–	–	–	–	–	–	–	–
0.50 - 1.00	1.00000±0.02075	–	–	1.00000±0.57735	–	–	–	–	–
1.00 - 1.50	1.00000±0.00979	–	–	1.00000±0.07603	–	–	1.00000±0.04154	–	–
1.50 - 2.00	0.99801±0.00858	0.00089±0.00018	0.00111±0.00020	0.96787±0.05049	0.00535±0.00268	0.02677±0.00607	0.95429±0.02485	0.00497±0.00129	0.04074±0.00375
2.00 - 2.25	0.85553±0.01050	0.10305±0.00281	0.04143±0.00173	0.28295±0.01786	0.39192±0.02189	0.32513±0.01946	0.31417±0.00976	0.17151±0.00681	0.51431±0.01341
2.25 - 2.50	0.83862±0.01058	0.12457±0.00319	0.03681±0.00166	0.18129±0.01331	0.68295±0.03085	0.13576±0.01130	0.33548±0.01035	0.21856±0.00798	0.44596±0.01242
2.50 - 2.75	0.82976±0.01084	0.13358±0.00342	0.03666±0.00171	0.18074±0.01298	0.74428±0.03201	0.07498±0.00798	0.32518±0.01048	0.23726±0.00865	0.43756±0.01266
2.75 - 3.00	0.83275±0.01129	0.13878±0.00363	0.02847±0.00156	0.16056±0.01169	0.77933±0.03188	0.06012±0.00684	0.30238±0.01056	0.25170±0.00944	0.44592±0.01351
3.00 - 3.25	0.82622±0.01161	0.14081±0.00379	0.03297±0.00174	0.16171±0.01229	0.79566±0.03390	0.04264±0.00598	0.29287±0.01093	0.26513±0.01028	0.44199±0.01418
3.25 - 3.50	0.95946±0.01375	0.02756±0.00169	0.01298±0.00115	0.07757±0.00797	0.89658±0.03596	0.02586±0.00449	0.12368±0.00766	0.38793±0.01508	0.48839±0.01752
3.50 - 3.75	0.98681±0.01468	0.00572±0.00079	0.00747±0.00091	0.07238±0.00781	0.88120±0.03611	0.04642±0.00618	0.09189±0.00700	0.42327±0.01716	0.48485±0.01876
3.75 - 4.00	0.99026±0.01549	0.00329±0.00063	0.00646±0.00089	0.08326±0.00908	0.87100±0.03861	0.04575±0.00662	0.14125±0.01137	0.48395±0.02401	0.37480±0.02034
4.00 - 4.25	0.99655±0.01625	0.00226±0.00055	0.00119±0.00040	0.10038±0.01028	0.80210±0.03717	0.09751±0.01012	0.10850±0.00955	0.26480±0.01594	0.62671±0.02781
4.25 - 4.50	0.99458±0.01752	0.00464±0.00085	0.00077±0.00035	0.09859±0.01044	0.79276±0.03781	0.10865±0.01101	0.10125±0.00904	0.21203±0.01373	0.68672±0.02915
4.50 - 4.75	0.99572±0.01845	0.00360±0.00079	0.00069±0.00034	0.09911±0.01101	0.78508±0.03950	0.11581±0.01200	0.10016±0.00951	0.17241±0.01288	0.72742±0.03212
4.75 - 5.00	0.99640±0.01941	0.00303±0.00076	0.00057±0.00033	0.07448±0.00989	0.80220±0.04201	0.12332±0.01301	0.09786±0.01001	0.15843±0.01308	0.74371±0.03476
5.00 - 5.25	0.99768±0.02049	0.00211±0.00067	0.00021±0.00021	0.08367±0.01106	0.78812±0.04361	0.12821±0.01397	0.09602±0.01037	0.16956±0.01423	0.73442±0.03607
5.25 - 5.50	0.99859±0.02169	0.00094±0.00047	0.00047±0.00033	0.10986±0.01310	0.77324±0.04395	0.11690±0.01356	0.08896±0.01019	0.12433±0.01224	0.78671±0.03881
5.50 - 5.75	0.99806±0.02350	0.00166±0.00068	0.00028±0.00028	0.09211±0.01213	0.77485±0.04484	0.13304±0.01485	0.07956±0.01025	0.12362±0.01304	0.79682±0.04186
5.75 - 6.00	0.99883±0.02415	0.00117±0.00058	–	0.09760±0.01354	0.78253±0.04887	0.11986±0.01516	0.08889±0.01159	0.14306±0.01507	0.76806±0.04343
6.00 - 6.50	0.99824±0.01876	0.00159±0.00053	0.00018±0.00018	0.11963±0.01170	0.75971±0.03697	0.12065±0.01176	0.08961±0.00857	0.12048±0.01008	0.78991±0.03263
6.50 - 7.00	0.99911±0.02109	0.00067±0.00039	0.00022±0.00022	0.10240±0.01109	0.76797±0.03846	0.12963±0.01263	0.08780±0.00965	0.10732±0.01077	0.80488±0.03765
7.00 - 7.50	0.99919±0.02327	0.00027±0.00027	0.00054±0.00038	0.10458±0.01229	0.78301±0.04272	0.11242±0.01279	0.08385±0.01067	0.11639±0.01275	0.79975±0.04244
7.50 - 8.00	0.99965±0.02645	0.00035±0.00035	–	0.10287±0.01383	0.80607±0.04955	0.09106±0.01294	0.10590±0.01331	0.13616±0.01530	0.75794±0.04490
8.00 - 8.50	1.00000±0.03015	–	–	0.09055±0.01394	0.83465±0.05490	0.07480±0.01258	0.08644±0.01358	0.11002±0.01549	0.80354±0.05336
8.50 - 9.00	1.00000±0.03382	–	–	0.08506±0.01457	0.81609±0.05837	0.09885±0.01580	0.08763±0.01567	0.10825±0.01758	0.80412±0.06115
9.00 - 9.50	1.00000±0.03796	–	–	0.11411±0.01954	0.78378±0.06480	0.10210±0.01838	0.07962±0.01655	0.08599±0.01725	0.83439±0.06982
9.50 - 10.0	1.00000±0.04245	–	–	0.10791±0.02074	0.78417±0.07094	0.10791±0.02074	0.08936±0.02035	0.05957±0.01639	0.85106±0.08188
10.0 - 11.0	0.97294±0.03517	0.02706±0.00423	–	0.11924±0.01902	0.72629±0.05829	0.15447±0.02198	0.08743±0.01612	0.04918±0.01187	0.86339±0.06630
11.0 - 12.0	0.96410±0.04407	0.03590±0.00618	–	0.10800±0.02188	0.86400±0.08026	0.02800±0.01073	0.06438±0.01715	0.02575±0.01065	0.90987±0.08636
12.0 - 13.0	0.98077±0.05828	0.01923±0.00585	–	0.12422±0.02945	0.85714±0.09943	0.01863±0.01086	0.03252±0.01652	0.00813±0.00816	0.95935±0.12362
13.0 - 14.0	0.97476±0.07793	0.02524±0.00903	–	0.25581±0.06112	0.74419±0.12285	–	0.05000±0.02562	0.07500±0.03175	0.87500±0.14320
14.0 - 15.0	1.00000±0.10000	–	–	0.41667±0.09919	0.58333±0.12407	–	0.05556±0.04036	–	0.94444±0.22586
15.0 - 30.0	0.99490±0.10063	–	0.00510±0.00512	0.49152±0.11147	0.50848±0.11402	–	–	0.11429±0.06032	0.88571±0.21845

Table D.2: Identification efficiencies for pions, kaons and protons in $N_{\mathrm{tracks}} = 2$ with the IRT method at $rQp > 0.0$.

Table D.3: Identification efficiencies for pions, kaons and protons in $N_{\text{tracks}} > 2$ with the IRT method at $rQp > 0.0$.

Momentum range	$\mathcal{P}_{\pi}^{\pi}$	$\mathcal{P}_{\pi}^{\mathrm{K}}$	$\mathcal{P}_{\pi}^{\mathrm{p}}$	$\mathcal{P}_{\mathrm{K}}^{\pi}$	$\mathcal{P}_{\mathrm{K}}^{\mathrm{K}}$	$\mathcal{P}_{\mathrm{K}}^{\mathrm{p}}$	$\mathcal{P}_{\mathrm{p}}^{\pi}$	$\mathcal{P}_{\mathrm{p}}^{\mathrm{K}}$	$\mathcal{P}_{\mathrm{p}}^{\mathrm{p}}$
0.00 - 0.50	–	–	–	–	–	–	–	–	–
0.50 - 1.00	1.00000±0.04010	–	–	1.00000±1.00000	–	–	–	–	–
1.00 - 1.50	1.00000±0.01897	–	–	1.00000±0.12649	–	–	1.00000±0.07943	–	–
1.50 - 2.00	0.99810±0.01709	0.00073±0.00033	0.00117±0.00041	0.98016±0.08776	–	0.01984±0.00896	0.96714±0.04725	0.00469±0.00235	0.02817±0.00583
2.00 - 2.25	0.83938±0.02068	0.12656±0.00628	0.03406±0.00312	0.38095±0.04230	0.38095±0.04230	0.23810±0.03166	0.40919±0.02453	0.20981±0.01628	0.38100±0.02344
2.25 - 2.50	0.80150±0.02079	0.16467±0.00758	0.03383±0.00324	0.29107±0.03291	0.61383±0.05343	0.09510±0.01732	0.44262±0.02642	0.26011±0.01893	0.29727±0.02053
2.50 - 2.75	0.79195±0.02112	0.17599±0.00806	0.03206±0.00322	0.26629±0.03091	0.68272±0.05705	0.05099±0.01232	0.42056±0.02642	0.28505±0.02069	0.29439±0.02110
2.75 - 3.00	0.77847±0.02186	0.19462±0.00896	0.02692±0.00309	0.23030±0.02930	0.73939±0.06243	0.03030±0.00973	0.36341±0.02458	0.33049±0.02316	0.30610±0.02208
3.00 - 3.25	0.79663±0.02396	0.18692±0.00943	0.01645±0.00259	0.21875±0.03043	0.73264±0.06639	0.04861±0.01330	0.37265±0.02619	0.31635±0.02363	0.31099±0.02338
3.25 - 3.50	0.95630±0.02918	0.03823±0.00425	0.00546±0.00158	0.09667±0.01880	0.88000±0.07426	0.02333±0.00892	0.10495±0.01515	0.56040±0.04161	0.33465±0.02974
3.50 - 3.75	0.98264±0.03065	0.00964±0.00217	0.00771±0.00194	0.15101±0.02415	0.82215±0.07090	0.02685±0.00962	0.12208±0.01886	0.57403±0.04844	0.30390±0.03208
3.75 - 4.00	0.99238±0.03282	0.00272±0.00122	0.00490±0.00164	0.09339±0.01993	0.84436±0.07784	0.06226±0.01604	0.20270±0.02870	0.56757±0.05482	0.22973±0.03089
4.00 - 4.25	0.99169±0.03553	0.00511±0.00181	0.00319±0.00143	0.14286±0.02836	0.69951±0.07653	0.15763±0.02998	0.13910±0.02441	0.37218±0.04382	0.48872±0.05230
4.25 - 4.50	0.99779±0.03834	0.00147±0.00104	0.00074±0.00074	0.14655±0.02691	0.65948±0.06868	0.19397±0.03159	0.15947±0.02478	0.23920±0.03138	0.60133±0.05656
4.50 - 4.75	0.99092±0.04035	0.00578±0.00219	0.00330±0.00165	0.13043±0.03026	0.65838±0.08235	0.21118±0.03986	0.09091±0.01862	0.21678±0.03037	0.69231±0.06400
4.75 - 5.00	1.00000±0.04334	–	–	0.10323±0.02711	0.70968±0.08848	0.18710±0.03785	0.10843±0.02197	0.22088±0.03291	0.67068±0.06708
5.00 - 5.25	0.99566±0.04645	0.00434±0.00218	–	0.11258±0.02880	0.74172±0.09250	0.14569±0.03325	0.11274±0.02480	0.21078±0.03537	0.67647±0.07456
5.25 - 5.50	0.99878±0.04934	–	0.00122±0.00122	0.12500±0.03216	0.69853±0.09340	0.17647±0.03907	0.09906±0.02266	0.20283±0.03392	0.69811±0.07478
5.50 - 5.75	0.99849±0.05494	0.00151±0.00151	–	0.19084±0.04165	0.68702±0.09406	0.12214±0.03235	0.16564±0.03442	0.14110±0.03143	0.69325±0.08486
5.75 - 6.00	0.99837±0.05705	0.00163±0.00163	–	0.15652±0.03967	0.63478±0.09499	0.20870±0.04683	0.15672±0.03678	0.15672±0.03678	0.68657±0.09296
6.00 - 6.50	0.99896±0.04547	–	0.00104±0.00104	0.15385±0.03241	0.72189±0.08576	0.12426±0.02875	0.11111±0.02254	0.19342±0.03082	0.69547±0.06966
6.50 - 7.00	0.99862±0.05247	0.00138±0.00138	–	0.12667±0.03084	0.70000±0.08907	0.17333±0.03682	0.09290±0.02355	0.16393±0.03229	0.74317±0.08414
7.00 - 7.50	0.99832±0.05786	0.00168±0.00168	–	0.18699±0.04248	0.61789±0.09015	0.19512±0.04354	0.09756±0.02951	0.19512±0.04354	0.70732±0.09909
7.50 - 8.00	1.00000±0.07170	–	–	0.13187±0.04050	0.80220±0.12604	0.06593±0.02779	0.08257±0.02864	0.11009±0.03348	0.80734±0.11570
8.00 - 8.50	1.00000±0.07956	–	–	0.07692±0.03259	0.79487±0.13524	0.12821±0.04306	0.07812±0.03628	0.21875±0.06454	0.70312±0.13679
8.50 - 9.00	1.00000±0.09225	–	–	0.16949±0.05796	0.67797±0.13886	0.15254±0.05459	0.06667±0.03443	0.20000±0.06325	0.73333±0.14555
9.00 - 9.50	1.00000±0.09806	–	–	0.23684±0.08780	0.63158±0.16467	0.13158±0.06260	0.09302±0.04863	0.04651±0.03364	0.86047±0.19295
9.50 - 10.0	1.00000±0.12356	–	–	0.25000±0.10564	0.71429±0.20912	0.03571±0.03635	0.16129±0.07773	0.06452±0.04707	0.77419±0.21050
10.0 - 11.0	0.96154±0.10180	0.03846±0.01481	–	0.14583±0.05900	0.79167±0.17190	0.06250±0.03719	0.10345±0.06274	–	0.89655±0.24214
11.0 - 12.0	0.97531±0.15422	0.02469±0.01767	–	0.11765±0.08795	0.88235±0.31257	–	0.16667±0.12729	–	0.83333±0.35681
12.0 - 13.0	1.00000±0.26726	–	–	0.25000±0.19764	0.75000±0.40505	–	–	–	1.00000±0.44721
13.0 - 14.0	0.94118±0.32783	0.05882±0.06053	–	0.20000±0.21909	0.80000±0.53666	–	0.20000±0.15492	–	0.80000±0.37947
14.0 - 15.0	1.00000±0.44721	–	–	0.14286±0.15272	0.85714±0.47687	–	–	–	1.00000±0.53452
15.0 - 30.0	1.00000±0.36515	–	–	0.33333±0.38490	0.66667±0.60858	–	–	–	1.00000±1.00000

Momentum range	Q_π^π	Q_π^K	Q_π^p	Q_K^π	Q_K^K	Q_K^p	Q_p^π	Q_p^K	Q_p^p
0.00 - 0.50	–	–	–	–	–	–	–	–	–
0.50 - 1.00	0.99903±0.02197	0.00097±0.00048	–	–	–	–	–	–	–
1.00 - 1.50	0.97296±0.00986	0.00577±0.00054	0.02126±0.00105	–	–	–	–	–	–
1.50 - 2.00	0.94971±0.00803	0.01004±0.00059	0.04026±0.00121	0.50000±0.25000	0.16667±0.12729	0.33333±0.19245	0.11397±0.02160	0.15809±0.02594	0.72794±0.06800
2.00 - 2.25	0.95248±0.01106	0.00868±0.00076	0.03885±0.00163	0.35529±0.01790	0.41251±0.01969	0.23220±0.01380	0.11803±0.00520	0.10287±0.00482	0.77910±0.01685
2.25 - 2.50	0.95673±0.01115	0.00531±0.00060	0.03796±0.00162	0.31527±0.01392	0.48949±0.01845	0.19524±0.01044	0.13048±0.00573	0.03719±0.00293	0.83233±0.01843
2.50 - 2.75	0.95024±0.01128	0.00741±0.00072	0.04235±0.00174	0.31585±0.01310	0.51610±0.01797	0.16804±0.00900	0.11903±0.00556	0.02877±0.00262	0.85220±0.01914
2.75 - 3.00	0.95830±0.01151	0.00614±0.00066	0.03556±0.00161	0.28053±0.01197	0.54110±0.01824	0.17837±0.00916	0.12551±0.00599	0.03074±0.00284	0.84375±0.01988
3.00 - 3.25	0.96204±0.01185	0.00714±0.00073	0.03081±0.00154	0.27868±0.01219	0.56529±0.01921	0.15603±0.00867	0.13042±0.00651	0.02528±0.00273	0.84430±0.02115
3.25 - 3.50	0.99018±0.01225	0.00259±0.00044	0.00723±0.00074	0.04899±0.00515	0.73440±0.02563	0.21661±0.01166	0.04120±0.00381	0.03141±0.00331	0.92739±0.02457
3.50 - 3.75	0.99388±0.01255	0.00215±0.00041	0.00398±0.00056	0.01036±0.00239	0.76445±0.02712	0.22519±0.01227	0.02048±0.00287	0.02560±0.00322	0.95392±0.02709
3.75 - 4.00	0.99111±0.01312	0.00201±0.00042	0.00689±0.00078	0.00742±0.00207	0.82924±0.02943	0.16334±0.01042	0.03803±0.00637	0.02775±0.00541	0.93422±0.04309
4.00 - 4.25	0.99094±0.01344	0.00384±0.00059	0.00522±0.00069	0.01518±0.00306	0.85489±0.03103	0.12993±0.00944	–	0.03321±0.00451	0.96679±0.03358
4.25 - 4.50	0.99203±0.01395	0.00335±0.00057	0.00463±0.00068	0.01685±0.00333	0.88205±0.03280	0.10110±0.00849	0.00318±0.00130	0.02809±0.00391	0.96873±0.03179
4.50 - 4.75	0.99210±0.01433	0.00364±0.00062	0.00426±0.00067	0.00985±0.00265	0.90711±0.03489	0.08304±0.00796	0.00175±0.00101	0.02690±0.00402	0.97135±0.03346
4.75 - 5.00	0.99048±0.01495	0.00442±0.00071	0.00510±0.00076	0.01550±0.00333	0.91191±0.03505	0.07259±0.00741	0.00290±0.00130	0.03136±0.00433	0.96574±0.03320
5.00 - 5.25	0.99224±0.01548	0.00339±0.00064	0.00436±0.00073	0.00691±0.00231	0.93937±0.03739	0.05372±0.00659	0.00122±0.00087	0.03182±0.00448	0.96695±0.03412
5.25 - 5.50	0.99211±0.01599	0.00465±0.00078	0.00323±0.00065	0.01450±0.00327	0.93038±0.03609	0.05511±0.00649	0.00263±0.00132	0.04279±0.00542	0.95457±0.03505
5.50 - 5.75	0.99288±0.01679	0.00328±0.00068	0.00385±0.00074	0.00806±0.00256	0.94032±0.03836	0.05161±0.00662	0.00230±0.00133	0.03295±0.00511	0.96475±0.03811
5.75 - 6.00	0.99028±0.01744	0.00463±0.00085	0.00509±0.00089	0.00333±0.00167	0.93184±0.03868	0.06484±0.00758	–	0.03143±0.00511	0.96857±0.03920
6.00 - 6.50	0.99178±0.01307	0.00389±0.00058	0.00433±0.00061	0.00371±0.00131	0.94859±0.02926	0.04771±0.00481	0.00043±0.00043	0.03570±0.00399	0.96387±0.02853
6.50 - 7.00	0.98899±0.01397	0.00516±0.00072	0.00585±0.00076	0.00309±0.00126	0.94539±0.03078	0.05152±0.00528	–	0.04158±0.00480	0.95842±0.03163
7.00 - 7.50	0.99180±0.01555	0.00538±0.00081	0.00281±0.00059	0.00411±0.00156	0.94888±0.03296	0.04700±0.00538	–	0.04247±0.00534	0.95753±0.03473
7.50 - 8.00	0.99373±0.01680	0.00271±0.00062	0.00356±0.00071	0.00335±0.00150	0.95649±0.03539	0.04016±0.00529	–	0.05077±0.00597	0.94923±0.03516
8.00 - 8.50	0.99204±0.01810	0.00514±0.00093	0.00282±0.00068	0.00231±0.00133	0.95308±0.03784	0.04462±0.00599	–	0.04272±0.00623	0.95728±0.04042
8.50 - 9.00	0.99053±0.01972	0.00552±0.00105	0.00395±0.00088	0.00262±0.00151	0.95895±0.04050	0.03843±0.00590	–	0.05803±0.00798	0.94197±0.04354
9.00 - 9.50	0.98832±0.02121	0.00756±0.00132	0.00412±0.00097	0.00204±0.00145	0.95608±0.04371	0.04188±0.00668	–	0.09193±0.01061	0.90807±0.04407
9.50 - 10.0	0.99179±0.02325	0.00575±0.00126	0.00246±0.00082	0.00125±0.00126	0.95483±0.04839	0.04391±0.00758	0.00258±0.00183	0.11240±0.01271	0.88501±0.04643
10.0 - 11.0	0.98934±0.01870	0.00729±0.00114	0.00338±0.00078	0.00401±0.00180	0.99038±0.03976	0.00561±0.00213	0.00249±0.00144	0.13799±0.01142	0.85952±0.03645
11.0 - 12.0	0.98472±0.02213	0.01428±0.00190	0.00100±0.00050	0.01440±0.00388	0.98148±0.04473	0.00412±0.00206	0.00123±0.00124	0.02469±0.00559	0.97407±0.04872
12.0 - 13.0	0.97175±0.02669	0.02788±0.00326	0.00037±0.00037	0.01637±0.00498	0.97768±0.05364	0.00595±0.00299	0.00226±0.00227	–	0.99774±0.06715
13.0 - 14.0	0.95238±0.03172	0.04762±0.00520	–	0.01149±0.00517	0.98621±0.06710	0.00230±0.00230	–	–	1.00000±0.08138
14.0 - 15.0	0.94358±0.03990	0.05556±0.00713	0.00087±0.00087	0.01250±0.00726	0.97500±0.08957	0.01250±0.00726	0.00585±0.00587	–	0.99415±0.10767
15.0 - 30.0	0.88603±0.03026	0.11288±0.00830	0.00110±0.00078	0.02672±0.01023	0.96565±0.08512	0.00763±0.00542	0.01351±0.00785	0.00901±0.00640	0.97748±0.09331

Table D.4: Identification purities and contaminations for pions, kaons and protons in $N_\mathrm{tracks} = 1$ with the IRT method at $rQp > 0.0$.

Momentum range	Q_{π}^{π}	Q_{π}^{K}	Q_{π}^{p}	Q_{K}^{π}	$Q_{\mathrm{K}}^{\mathrm{K}}$	$Q_{\mathrm{K}}^{\mathrm{p}}$	Q_{p}^{π}	$Q_{\mathrm{p}}^{\mathrm{K}}$	$Q_{\mathrm{p}}^{\mathrm{p}}$
0.00 - 0.50	–	–	–	–	–	–	–	–	–
0.50 - 1.00	0.99871±0.02072	0.00129±0.00053	–	–	–	–	–	–	–
1.00 - 1.50	0.93275±0.00898	0.01546±0.00084	0.05179±0.00156	–	–	–	–	–	–
1.50 - 2.00	0.88236±0.00736	0.02360±0.00089	0.09404±0.00183	0.55814±0.14221	0.09302±0.04863	0.34884±0.10461	0.17341±0.03430	0.11561±0.02730	0.71098±0.08386
2.00 - 2.25	0.87989±0.01086	0.02298±0.00130	0.09713±0.00276	0.55535±0.01797	0.16679±0.00853	0.27786±0.01152	0.18685±0.00833	0.11581±0.00636	0.69734±0.01925
2.25 - 2.50	0.87688±0.01118	0.01662±0.00113	0.10650±0.00299	0.49667±0.01467	0.23878±0.00925	0.26454±0.00984	0.19992±0.00973	0.06467±0.00521	0.73541±0.02243
2.50 - 2.75	0.87697±0.01160	0.01872±0.00125	0.10431±0.00307	0.47959±0.01404	0.26187±0.00958	0.25854±0.00951	0.20735±0.01046	0.04156±0.00435	0.75109±0.02399
2.75 - 3.00	0.88570±0.01218	0.01945±0.00133	0.09485±0.00304	0.45988±0.01363	0.29413±0.01026	0.24599±0.00921	0.17067±0.01000	0.04104±0.00462	0.78829±0.02656
3.00 - 3.25	0.89111±0.01274	0.01937±0.00138	0.08952±0.00307	0.46271±0.01410	0.29037±0.01049	0.24692±0.00951	0.20230±0.01155	0.02906±0.00405	0.76864±0.02730
3.25 - 3.50	0.96023±0.01377	0.01027±0.00102	0.02950±0.00175	0.11551±0.00737	0.49705±0.01771	0.38744±0.01505	0.09773±0.00902	0.02576±0.00447	0.87652±0.03530
3.50 - 3.75	0.96975±0.01436	0.00994±0.00104	0.02031±0.00150	0.02552±0.00358	0.54956±0.02044	0.42493±0.01724	0.06077±0.00759	0.05273±0.00704	0.88651±0.03866
3.75 - 4.00	0.96820±0.01506	0.01084±0.00114	0.02096±0.00160	0.01707±0.00331	0.60177±0.02468	0.38116±0.01824	0.09298±0.01335	0.08772±0.01294	0.81930±0.05114
4.00 - 4.25	0.96804±0.01567	0.01353±0.00133	0.01843±0.00156	0.01411±0.00345	0.69627±0.03131	0.28963±0.01761	0.00961±0.00322	0.10886±0.01135	0.88154±0.04207
4.25 - 4.50	0.96457±0.01687	0.01471±0.00150	0.02071±0.00178	0.02710±0.00501	0.71183±0.03318	0.26107±0.01725	0.00477±0.00214	0.10296±0.01040	0.89228±0.04012
4.50 - 4.75	0.96498±0.01774	0.01477±0.00158	0.02025±0.00185	0.02244±0.00495	0.75321±0.03756	0.22436±0.01713	0.00402±0.00202	0.10463±0.01078	0.89135±0.04118
4.75 - 5.00	0.96942±0.01875	0.01124±0.00145	0.01934±0.00191	0.01898±0.00479	0.77936±0.04056	0.20166±0.01695	0.00333±0.00192	0.11197±0.01175	0.88470±0.04299
5.00 - 5.25	0.96811±0.01974	0.01267±0.00162	0.01921±0.00200	0.01316±0.00419	0.76842±0.04228	0.21842±0.01871	0.00123±0.00123	0.11656±0.01264	0.88221±0.04514
5.25 - 5.50	0.96340±0.02074	0.01773±0.00203	0.01887±0.00209	0.00598±0.00300	0.82063±0.04726	0.17339±0.01744	0.00244±0.00173	0.10134±0.01167	0.89621±0.04555
5.50 - 5.75	0.96570±0.02255	0.01688±0.00214	0.01742±0.00218	0.00942±0.00386	0.83203±0.04892	0.15856±0.01698	0.00135±0.00135	0.12248±0.01360	0.87618±0.04704
5.75 - 6.00	0.96581±0.02316	0.01611±0.00215	0.01808±0.00228	0.00709±0.00356	0.81028±0.05100	0.18262±0.01957	–	0.11236±0.01416	0.88764±0.05186
6.00 - 6.50	0.95996±0.01787	0.01985±0.00185	0.02019±0.00187	0.00987±0.00331	0.81469±0.04026	0.17544±0.01504	0.00086±0.00086	0.10103±0.00976	0.89812±0.03820
6.50 - 7.00	0.96062±0.02008	0.02012±0.00210	0.01926±0.00205	0.00367±0.00212	0.86186±0.04429	0.13447±0.01366	0.00106±0.00106	0.12593±0.01225	0.87302±0.04160
7.00 - 7.50	0.96166±0.02218	0.02087±0.00236	0.01748±0.00215	0.00144±0.00144	0.86436±0.04822	0.13420±0.01482	0.00275±0.00195	0.11829±0.01349	0.87896±0.04766
7.50 - 8.00	0.95616±0.02502	0.02041±0.00264	0.02343±0.00283	0.00176±0.00176	0.84007±0.05212	0.15817±0.01794	–	0.09730±0.01387	0.90270±0.05563
8.00 - 8.50	0.96070±0.02868	0.02009±0.00299	0.01921±0.00292	–	0.88333±0.05887	0.11667±0.01647	–	0.08501±0.01436	0.91499±0.06261
8.50 - 9.00	0.96099±0.03218	0.02033±0.00338	0.01868±0.00323	–	0.89421±0.06532	0.10579±0.01717	–	0.12113±0.01956	0.87887±0.06820
9.00 - 9.50	0.95658±0.03592	0.02619±0.00430	0.01723±0.00348	–	0.90625±0.07745	0.09375±0.01887	–	0.11486±0.02080	0.88514±0.07508
9.50 - 10.0	0.95607±0.04013	0.02584±0.00478	0.01809±0.00398	–	0.93966±0.08863	0.06034±0.01661	–	0.13043±0.02532	0.86957±0.08407
10.0 - 11.0	0.95208±0.03423	0.02774±0.00424	0.02018±0.00360	0.12805±0.02099	0.81707±0.06728	0.05488±0.01329	–	0.15282±0.02173	0.84718±0.06477
11.0 - 12.0	0.95723±0.04368	0.02749±0.00536	0.01527±0.00397	0.13619±0.02454	0.84047±0.07758	0.02335±0.00964	–	0.03196±0.01227	0.96804±0.09327
12.0 - 13.0	0.95897±0.05667	0.03419±0.00777	0.00684±0.00343	0.07333±0.02291	0.92000±0.10852	0.00667±0.00669	–	0.02479±0.01449	0.97521±0.12617
13.0 - 14.0	0.92239±0.07275	0.06567±0.01445	0.01194±0.00601	0.10256±0.03808	0.82051±0.13839	0.07692±0.03259	–	–	1.00000±0.16903
14.0 - 15.0	0.88106±0.08545	0.11013±0.02321	0.00881±0.00626	–	1.00000±0.23905	–	–	–	1.00000±0.24254
15.0 - 30.0	0.87054±0.08526	0.12946±0.02555	–	–	0.88235±0.22102	0.11765±0.06219	0.03125±0.03173	–	0.96875±0.24413

Table D.5: Identification purities and contaminations for pions, kaons and protons in $N_{\mathrm{tracks}} = 2$ with the IRT method at $rQp > 0.0$.

Momentum range	Q_π^π	Q_π^K	Q_π^p	Q_K^π	Q_K^K	Q_K^p	Q_p^π	Q_p^K	Q_p^p
0.00 - 0.50	–	–	–	–	–	–	–	–	–
0.50 - 1.00	0.99840±0.04002	0.00161±0.00114	–	–	–	–	–	–	–
1.00 - 1.50	0.92630±0.01725	0.02084±0.00188	0.05286±0.00305	–	–	–	–	–	–
1.50 - 2.00	0.86424±0.01429	0.03131±0.00202	0.10445±0.00382	0.55556±0.30987	–	0.44444±0.26708	0.21622±0.08430	0.13514±0.06439	0.64865±0.17001
2.00 - 2.25	0.85743±0.02123	0.03168±0.00304	0.11089±0.00590	0.59351±0.03505	0.14546±0.01471	0.26104±0.02068	0.22043±0.02196	0.12545±0.01591	0.65412±0.04403
2.25 - 2.50	0.84103±0.02206	0.03173±0.00321	0.12724±0.00671	0.54945±0.02916	0.21279±0.01606	0.23776±0.01715	0.27033±0.02866	0.07895±0.01428	0.65072±0.05069
2.50 - 2.75	0.84734±0.02294	0.03161±0.00331	0.12105±0.00675	0.53588±0.02806	0.23062±0.01648	0.23349±0.01660	0.27419±0.03065	0.04839±0.01168	0.67742±0.05527
2.75 - 3.00	0.85779±0.02462	0.02890±0.00336	0.11331±0.00693	0.52271±0.02716	0.22614±0.01603	0.25116±0.01707	0.23009±0.02889	0.02950±0.00946	0.74041±0.06165
3.00 - 3.25	0.85346±0.02607	0.02707±0.00346	0.11947±0.00758	0.51040±0.02906	0.23111±0.01765	0.25849±0.01888	0.14286±0.02385	0.04878±0.01335	0.80836±0.07137
3.25 - 3.50	0.96244±0.02941	0.01328±0.00248	0.02428±0.00338	0.13312±0.01546	0.41838±0.03067	0.44849±0.03209	0.06383±0.01901	0.03723±0.01433	0.89894±0.09529
3.50 - 3.75	0.95681±0.02965	0.02113±0.00318	0.02207±0.00325	0.04115±0.00939	0.50411±0.03950	0.45473±0.03689	0.11348±0.02994	0.05674±0.02062	0.82979±0.10377
3.75 - 4.00	0.95593±0.03132	0.01259±0.00259	0.03148±0.00413	0.01282±0.00577	0.55641±0.04712	0.43077±0.03975	0.09677±0.03378	0.17204±0.04656	0.73118±0.11667
4.00 - 4.25	0.95921±0.03408	0.01792±0.00336	0.02287±0.00380	0.03213±0.01154	0.57028±0.05997	0.39759±0.04724	0.02994±0.01359	0.19162±0.03698	0.77844±0.09105
4.25 - 4.50	0.94286±0.03573	0.02369±0.00411	0.03345±0.00491	0.00881±0.00626	0.67401±0.07050	0.31718±0.04290	0.00441±0.00441	0.19824±0.03235	0.79736±0.07946
4.50 - 4.75	0.96234±0.03890	0.01683±0.00370	0.02083±0.00413	0.04000±0.01542	0.60571±0.07455	0.35429±0.05236	0.01695±0.00855	0.14407±0.02643	0.83898±0.08086
4.75 - 5.00	0.96119±0.04125	0.01444±0.00364	0.02437±0.00475	–	0.66667±0.08206	0.33333±0.05190	–	0.14796±0.02944	0.85204±0.08973
5.00 - 5.25	0.95820±0.04428	0.01776±0.00435	0.02403±0.00507	0.02516±0.01274	0.70440±0.08690	0.27044±0.04649	–	0.13750±0.03127	0.86250±0.10020
5.25 - 5.50	0.95566±0.04670	0.01984±0.00486	0.02450±0.00541	–	0.68841±0.09177	0.31159±0.05442	0.00578±0.00580	0.13873±0.03022	0.85549±0.09579
5.50 - 5.75	0.92697±0.05009	0.03511±0.00714	0.03792±0.00744	0.00877±0.00881	0.78947±0.11132	0.20175±0.04612	–	0.12403±0.03287	0.87597±0.11287
5.75 - 6.00	0.94009±0.05293	0.02765±0.00661	0.03226±0.00715	0.01053±0.01058	0.76842±0.11960	0.22105±0.05330	–	0.20690±0.04640	0.79310±0.11072
6.00 - 6.50	0.94794±0.04259	0.02554±0.00507	0.02652±0.00517	–	0.72189±0.08576	0.27811±0.04586	0.00524±0.00525	0.10995±0.02528	0.88482±0.09344
6.50 - 7.00	0.95263±0.04947	0.02500±0.00581	0.02237±0.00549	0.00735±0.00738	0.77206±0.10030	0.22059±0.04449	–	0.16049±0.03391	0.83951±0.09763
7.00 - 7.50	0.94444±0.05399	0.03651±0.00775	0.01905±0.00555	0.00990±0.00995	0.75248±0.11427	0.23762±0.05396	–	0.21622±0.04867	0.78378±0.11223
7.50 - 8.00	0.94878±0.06715	0.02927±0.00857	0.02195±0.00740	–	0.85882±0.13704	0.14118±0.04354	–	0.06383±0.02688	0.93617±0.13886
8.00 - 8.50	0.96636±0.07623	0.01835±0.00756	0.01529±0.00689	–	0.81579±0.13961	0.18421±0.05358	–	0.18182±0.06250	0.81818±0.16446
8.50 - 9.00	0.94378±0.08583	0.04016±0.01295	0.01606±0.00810	–	0.76923±0.16178	0.23077±0.07391	–	0.16981±0.06122	0.83019±0.16932
9.00 - 9.50	0.94118±0.09092	0.04072±0.01385	0.01810±0.00913	–	0.92308±0.26129	0.07692±0.05645	–	0.11905±0.05632	0.88095±0.19863
9.50 - 10.0	0.91608±0.11079	0.04895±0.01895	0.03497±0.01591	–	0.90909±0.28087	0.09091±0.06714	–	0.04000±0.04079	0.96000±0.27434
10.0 - 11.0	0.94595±0.09975	0.03784±0.01457	0.01622±0.00944	0.15556±0.06320	0.84444±0.18604	–	–	0.10345±0.06274	0.89655±0.24214
11.0 - 12.0	0.95181±0.14961	0.02410±0.01724	0.02410±0.01724	0.11765±0.08795	0.88235±0.31257	–	–	–	1.00000±0.44721
12.0 - 13.0	0.93333±0.24525	0.06667±0.04869	–	–	1.00000±0.57735	–	–	–	1.00000±0.44721
13.0 - 14.0	0.84210±0.28574	0.05263±0.05400	0.10526±0.07825	0.20000±0.21909	0.80000±0.53666	–	–	–	1.00000±0.50000
14.0 - 15.0	0.90909±0.39721	0.09091±0.09495	–	–	1.00000±0.57735	–	–	–	1.00000±0.53452
15.0 - 30.0	0.93750±0.33693	0.06250±0.06442	–	–	1.00000±1.00000	–	–	–	1.00000±1.00000

Table D.6: Identification purities and contaminations for pions, kaons and protons in $N_{\text{tracks}} > 2$ with the IRT method at $rQp > 0.0$.

Momentum range	$\mathcal{P}_{\pi}^{\pi}$	$\mathcal{P}_{\pi}^{\mathrm{K}}$	$\mathcal{P}_{\pi}^{\mathrm{p}}$	$\mathcal{P}_{\mathrm{K}}^{\pi}$	$\mathcal{P}_{\mathrm{K}}^{\mathrm{K}}$	$\mathcal{P}_{\mathrm{K}}^{\mathrm{p}}$	$\mathcal{P}_{\mathrm{p}}^{\pi}$	$\mathcal{P}_{\mathrm{p}}^{\mathrm{K}}$	$\mathcal{P}_{\mathrm{p}}^{\mathrm{p}}$
0.00 - 0.50	–	–	–	–	–	–	–	–	–
0.50 - 1.00	1.00000±0.02202	–	–	1.00000±0.70711	–	–	–	–	–
1.00 - 1.50	1.00000±0.01021	–	–	1.00000±0.13304	–	–	1.00000±0.06942	–	–
1.50 - 2.00	0.99886±0.00856	–	0.00114±0.00020	0.86364±0.06984	0.00606±0.00430	0.13030±0.02113	0.84903±0.03425	0.00299±0.00150	0.14798±0.01127
2.00 - 2.25	0.95437±0.01128	0.00634±0.00066	0.03928±0.00167	0.08692±0.00893	0.48945±0.02480	0.42363±0.02256	0.11266±0.00523	0.05884±0.00368	0.82850±0.01817
2.25 - 2.50	0.94940±0.01127	0.01042±0.00085	0.04018±0.00169	0.03417±0.00543	0.82667±0.03547	0.13917±0.01149	0.11212±0.00520	0.07721±0.00425	0.81067±0.01784
2.50 - 2.75	0.95188±0.01154	0.01133±0.00091	0.03679±0.00165	0.02829±0.00465	0.87938±0.03508	0.09233±0.00867	0.11476±0.00531	0.07621±0.00425	0.80903±0.01795
2.75 - 3.00	0.95370±0.01172	0.00988±0.00086	0.03642±0.00167	0.02246±0.00401	0.89263±0.03443	0.08491±0.00804	0.10064±0.00520	0.08818±0.00484	0.81119±0.01894
3.00 - 3.25	0.95362±0.01205	0.01099±0.00093	0.03539±0.00169	0.01779±0.00359	0.91957±0.03545	0.06263±0.00688	0.09750±0.00545	0.08611±0.00510	0.81639±0.02030
3.25 - 3.50	0.98643±0.01222	0.00435±0.00058	0.00923±0.00084	0.01832±0.00349	0.92081±0.03402	0.06086±0.00650	0.02775±0.00297	0.12550±0.00660	0.84675±0.02196
3.50 - 3.75	0.99443±0.01256	0.00143±0.00034	0.00414±0.00057	0.01743±0.00345	0.93901±0.03493	0.04357±0.00552	0.01737±0.00248	0.14107±0.00748	0.84156±0.02321
3.75 - 4.00	0.99606±0.01320	0.00105±0.00030	0.00289±0.00050	0.01576±0.00331	0.97875±0.03643	0.00548±0.00194	0.06534±0.00759	0.21174±0.01457	0.72291±0.03210
4.00 - 4.25	0.99806±0.01356	0.00194±0.00042	–	0.02941±0.00460	0.96149±0.03634	0.00910±0.00254	0.03224±0.00434	0.07805±0.00690	0.88971±0.03084
4.25 - 4.50	0.99713±0.01404	0.00237±0.00049	0.00049±0.00022	0.02504±0.00435	0.96318±0.03732	0.01178±0.00296	0.02478±0.00366	0.05219±0.00538	0.92304±0.03059
4.50 - 4.75	0.99854±0.01445	0.00115±0.00035	0.00031±0.00018	0.02745±0.00470	0.96549±0.03858	0.00706±0.00236	0.02423±0.00383	0.03132±0.00437	0.94444±0.03294
4.75 - 5.00	0.99738±0.01508	0.00217±0.00050	0.00046±0.00023	0.03009±0.00489	0.96065±0.03812	0.00926±0.00269	0.02658±0.00401	0.02481±0.00388	0.94861±0.03304
5.00 - 5.25	0.99866±0.01560	0.00110±0.00037	0.00024±0.00017	0.02301±0.00440	0.96549±0.03949	0.01150±0.00309	0.02281±0.00385	0.01584±0.00319	0.96134±0.03457
5.25 - 5.50	0.99727±0.01609	0.00221±0.00054	0.00052±0.00026	0.02826±0.00478	0.96154±0.03848	0.01020±0.00284	0.01731±0.00349	0.02285±0.00402	0.95983±0.03609
5.50 - 5.75	0.99828±0.01690	0.00143±0.00045	0.00029±0.00020	0.01990±0.00419	0.97059±0.04068	0.00952±0.00288	0.02160±0.00420	0.01280±0.00322	0.96560±0.03897
5.75 - 6.00	0.99938±0.01764	0.00062±0.00031	–	0.02688±0.00497	0.96595±0.04125	0.00717±0.00254	0.02730±0.00482	0.02316±0.00443	0.94954±0.03913
6.00 - 6.50	0.99922±0.01319	0.00070±0.00025	0.00009±0.00009	0.02213±0.00334	0.96606±0.03057	0.01181±0.00242	0.02232±0.00319	0.01339±0.00246	0.96429±0.02908
6.50 - 7.00	0.99940±0.01415	0.00060±0.00025	–	0.02834±0.00399	0.96349±0.03211	0.00817±0.00212	0.03247±0.00430	0.01926±0.00329	0.94827±0.03189
7.00 - 7.50	0.99914±0.01569	0.00086±0.00033	–	0.02752±0.00421	0.95497±0.03417	0.01751±0.00334	0.01553±0.00326	0.01823±0.00354	0.96624±0.03582
7.50 - 8.00	0.99928±0.01692	0.00072±0.00032	–	0.01392±0.00322	0.97070±0.03744	0.01538±0.00338	0.01796±0.00362	0.01293±0.00307	0.96911±0.03703
8.00 - 8.50	0.99950±0.01827	0.00050±0.00029	–	0.02607±0.00474	0.96215±0.03985	0.01177±0.00317	0.01595±0.00390	0.01782±0.00413	0.96623±0.04222
8.50 - 9.00	0.99940±0.01994	0.00060±0.00034	–	0.02664±0.00510	0.94957±0.04197	0.02379±0.00481	0.02265±0.00512	0.01359±0.00395	0.96376±0.04630
9.00 - 9.50	0.99954±0.02151	0.00046±0.00033	–	0.03833±0.00680	0.92334±0.04542	0.03833±0.00680	0.02302±0.00549	0.01151±0.00386	0.96547±0.04926
9.50 - 10.0	0.99917±0.02346	0.00028±0.00028	0.00055±0.00039	0.03120±0.00691	0.91531±0.05104	0.05349±0.00915	0.01366±0.00458	0.02731±0.00653	0.95903±0.05339
10.0 - 11.0	0.99928±0.01894	0.00018±0.00018	0.00054±0.00031	0.02232±0.00405	0.86033±0.03395	0.11735±0.00972	0.01724±0.00410	0.00575±0.00235	0.97701±0.04301
11.0 - 12.0	0.99822±0.02253	0.00153±0.00062	0.00025±0.00025	0.03590±0.00618	0.94359±0.04337	0.02051±0.00463	0.00377±0.00218	0.00377±0.00218	0.99245±0.04987
12.0 - 13.0	0.99847±0.02763	0.00115±0.00066	0.00038±0.00038	0.05128±0.00930	0.94872±0.05443	–	0.00225±0.00225	0.00450±0.00319	0.99324±0.06678
13.0 - 14.0	0.99772±0.03374	0.00228±0.00114	–	0.09950±0.01650	0.90050±0.06525	–	–	0.00330±0.00331	0.99670±0.08104
14.0 - 15.0	0.99907±0.04304	–	0.00093±0.00093	0.13744±0.02722	0.86256±0.08726	–	–	0.00585±0.00587	0.99415±0.10767
15.0 - 30.0	0.99748±0.03540	0.00063±0.00063	0.00189±0.00109	0.44082±0.05092	0.55102±0.05906	0.00816±0.00580	0.00922±0.00655	0.00461±0.00462	0.98618±0.09501

Table D.7: Identification efficiencies for pions, kaons and protons in $N_{\mathrm{tracks}} = 1$ with the IRT method at $rQp > 0.5$.

Momentum range	$\mathcal{P}_{\pi}^{\pi}$	$\mathcal{P}_{\pi}^{\mathrm{K}}$	$\mathcal{P}_{\pi}^{\mathrm{p}}$	$\mathcal{P}_{\mathrm{K}}^{\pi}$	$\mathcal{P}_{\mathrm{K}}^{\mathrm{K}}$	$\mathcal{P}_{\mathrm{K}}^{\mathrm{p}}$	$\mathcal{P}_{\mathrm{p}}^{\pi}$	$\mathcal{P}_{\mathrm{p}}^{\mathrm{K}}$	$\mathcal{P}_{\mathrm{p}}^{\mathrm{p}}$
0.00 - 0.50	–	–	–	–	–	–	–	–	–
0.50 - 1.00	1.00000±0.02076	–	–	1.00000±0.57735	–	–	–	–	–
1.00 - 1.50	1.00000±0.00979	–	–	1.00000±0.07603	–	–	1.00000±0.04176	–	–
1.50 - 2.00	0.99867±0.00859	0.00022±0.00009	0.00111±0.00020	0.97135±0.05111	0.00136±0.00137	0.02729±0.00618	0.95620±0.02510	0.00236±0.00089	0.04144±0.00381
2.00 - 2.25	0.92657±0.01228	0.02298±0.00141	0.05044±0.00212	0.24897±0.01789	0.37037±0.02285	0.38066±0.02325	0.29590±0.00983	0.14304±0.00642	0.56107±0.01485
2.25 - 2.50	0.92257±0.01273	0.03108±0.00171	0.04635±0.00211	0.11611±0.01164	0.71234±0.03572	0.17155±0.01450	0.31979±0.01045	0.19767±0.00783	0.48254±0.01360
2.50 - 2.75	0.91917±0.01323	0.03376±0.00186	0.04707±0.00221	0.09216±0.01033	0.80720±0.03931	0.10064±0.01083	0.30268±0.01055	0.21298±0.00854	0.48434±0.01424
2.75 - 3.00	0.92738±0.01400	0.03521±0.00200	0.03741±0.00206	0.06853±0.00841	0.85232±0.03904	0.07915±0.00908	0.27577±0.01060	0.22151±0.00929	0.50271±0.01553
3.00 - 3.25	0.92113±0.01449	0.03510±0.00208	0.04376±0.00233	0.06438±0.00857	0.87875±0.04209	0.05687±0.00803	0.26057±0.01094	0.22850±0.01011	0.51093±0.01677
3.25 - 3.50	0.97349±0.01413	0.01310±0.00117	0.01341±0.00119	0.06902±0.00761	0.90431±0.03675	0.02667±0.00463	0.12010±0.00761	0.38183±0.01507	0.49806±0.01792
3.50 - 3.75	0.98681±0.01468	0.00572±0.00079	0.00747±0.00091	0.07244±0.00782	0.88110±0.03613	0.04646±0.00619	0.09220±0.00703	0.42129±0.01714	0.48651±0.01883
3.75 - 4.00	0.99098±0.01551	0.00317±0.00062	0.00585±0.00085	0.08966±0.00981	0.89557±0.04090	0.01478±0.00384	0.15766±0.01282	0.48739±0.02556	0.35496±0.02082
4.00 - 4.25	0.99695±0.01626	0.00226±0.00055	0.00080±0.00033	0.11851±0.01223	0.84989±0.04212	0.03160±0.00607	0.13645±0.01216	0.20706±0.01544	0.65649±0.03221
4.25 - 4.50	0.99489±0.01753	0.00449±0.00084	0.00062±0.00031	0.11751±0.01255	0.85731±0.04369	0.02518±0.00556	0.12958±0.01172	0.14460±0.01247	0.72582±0.03430
4.50 - 4.75	0.99589±0.01845	0.00360±0.00079	0.00051±0.00030	0.12732±0.01433	0.84692±0.04731	0.02575±0.00615	0.12656±0.01216	0.09751±0.01054	0.77593±0.03781
4.75 - 5.00	0.99678±0.01942	0.00265±0.00071	0.00057±0.00033	0.09356±0.01253	0.87577±0.05019	0.03067±0.00696	0.12515±0.01295	0.07390±0.00973	0.80095±0.04146
5.00 - 5.25	0.99768±0.02049	0.00211±0.00067	0.00021±0.00021	0.10745±0.01436	0.87175±0.05318	0.02080±0.00607	0.12651±0.01385	0.04845±0.00827	0.82503±0.04502
5.25 - 5.50	0.99882±0.02169	0.00071±0.00041	0.00047±0.00033	0.14004±0.01693	0.83124±0.05228	0.02873±0.00728	0.11528±0.01336	0.03472±0.00706	0.85000±0.04673
5.50 - 5.75	0.99806±0.02350	0.00166±0.00068	0.00028±0.00028	0.11909±0.01587	0.85066±0.05455	0.03025±0.00767	0.10204±0.01329	0.04396±0.00849	0.85400±0.04986
5.75 - 6.00	0.99883±0.02415	0.00117±0.00058	–	0.12180±0.01709	0.83974±0.05746	0.03846±0.00924	0.11874±0.01570	0.02597±0.00703	0.85529±0.05426
6.00 - 6.50	0.99841±0.01876	0.00159±0.00053	–	0.15476±0.01538	0.81614±0.04428	0.02910±0.00629	0.11464±0.01110	0.04239±0.00652	0.84297±0.03869
6.50 - 7.00	0.99933±0.02109	0.00067±0.00039	–	0.13409±0.01473	0.84308±0.04708	0.02282±0.00577	0.11250±0.01251	0.02875±0.00608	0.85875±0.04467
7.00 - 7.50	0.99973±0.02328	–	0.00027±0.00027	0.13180±0.01568	0.84514±0.05069	0.02306±0.00623	0.10485±0.01346	0.03756±0.00781	0.85759±0.04993
7.50 - 8.00	0.99965±0.02645	0.00035±0.00035	–	0.13090±0.01782	0.84979±0.05808	0.01931±0.00650	0.14199±0.01814	0.04057±0.00925	0.81744±0.05490
8.00 - 8.50	1.00000±0.03015	–	–	0.11247±0.01749	0.87042±0.06309	0.01711±0.00652	0.10864±0.01725	0.03951±0.01007	0.85185±0.06241
8.50 - 9.00	1.00000±0.03382	–	–	0.11246±0.01950	0.86626±0.07010	0.02128±0.00813	0.11724±0.02125	0.02759±0.00989	0.85517±0.07396
9.00 - 9.50	1.00000±0.03796	–	–	0.15261±0.02658	0.80321±0.07627	0.04418±0.01361	0.09470±0.01982	0.02273±0.00938	0.88258±0.07933
9.50 - 10.0	1.00000±0.04245	–	–	0.15306±0.03001	0.78061±0.08421	0.06633±0.01900	0.11053±0.02542	0.01053±0.00748	0.87895±0.09323
10.0 - 11.0	0.99137±0.03621	0.00863±0.00240	–	0.09172±0.01721	0.75740±0.06275	0.15089±0.02267	0.08757±0.01640	0.03107±0.00951	0.88136±0.06844
11.0 - 12.0	0.98506±0.04568	0.01494±0.00402	–	0.07658±0.01927	0.89189±0.08718	0.03153±0.01210	0.06140±0.01691	0.00877±0.00623	0.92983±0.08871
12.0 - 13.0	0.99283±0.05955	0.00717±0.00360	–	0.07246±0.02373	0.90580±0.11184	0.02174±0.01269	0.02459±0.01437	0.00820±0.00823	0.96721±0.12488
13.0 - 14.0	0.99355±0.07993	0.00645±0.00458	–	0.14754±0.05268	0.85246±0.16090	–	0.05128±0.02629	0.05128±0.02629	0.89744±0.14775
14.0 - 15.0	1.00000±0.10025	–	–	0.30303±0.10939	0.69697±0.18932	–	0.05556±0.04036	–	0.94444±0.22586
15.0 - 30.0	0.99465±0.10300	–	0.00535±0.00536	0.43243±0.12939	0.56757±0.15507	–	–	0.08824±0.05314	0.91177±0.22642

Table D.8: Identification efficiencies for pions, kaons and protons in $N_{\mathrm{tracks}} = 2$ with the IRT method at $rQp > 0.5$.

Table D.9: Identification efficiencies for pions, kaons and protons in $N_{\text{tracks}} > 2$ with the IRT method at $rQp > 0.5$.

Momentum range	$\mathcal{P}^{\pi}_{\pi}$	$\mathcal{P}^{\mathrm{K}}_{\pi}$	$\mathcal{P}^{\mathrm{p}}_{\pi}$	$\mathcal{P}^{\pi}_{\mathrm{K}}$	$\mathcal{P}^{\mathrm{K}}_{\mathrm{K}}$	$\mathcal{P}^{\mathrm{p}}_{\mathrm{K}}$	$\mathcal{P}^{\pi}_{\mathrm{p}}$	$\mathcal{P}^{\mathrm{K}}_{\mathrm{p}}$	$\mathcal{P}^{\mathrm{p}}_{\mathrm{p}}$
0.00 - 0.50	–	–	–	–	–	–	–	–	–
0.50 - 1.00	1.00000±0.04010	–	–	1.00000±1.00000	–	–	–	–	–
1.00 - 1.50	1.00000±0.01898	–	–	1.00000±0.12700	–	–	1.00000±0.07943	–	–
1.50 - 2.00	0.99868±0.01712	0.00015±0.00015	0.00117±0.00042	0.98016±0.08776	–	0.01984±0.00896	0.96923±0.04753	0.00237±0.00168	0.02840±0.00588
2.00 - 2.25	0.93086±0.02544	0.02485±0.00303	0.04429±0.00408	0.33621±0.04400	0.36207±0.04611	0.30172±0.04115	0.39706±0.02607	0.15564±0.01485	0.44730±0.02817
2.25 - 2.50	0.91025±0.02713	0.04191±0.00430	0.04784±0.00461	0.15487±0.02813	0.69912±0.07250	0.14602±0.02721	0.43020±0.02794	0.22462±0.01868	0.34518±0.02427
2.50 - 2.75	0.90735±0.02810	0.04610±0.00469	0.04655±0.00472	0.15584±0.02792	0.76623±0.07654	0.07792±0.01907	0.40246±0.02775	0.25375±0.02083	0.34379±0.02511
2.75 - 3.00	0.90526±0.02996	0.05414±0.00545	0.04060±0.00469	0.09677±0.02212	0.85714±0.08565	0.04608±0.01490	0.34932±0.02658	0.27436±0.02290	0.37631±0.02787
3.00 - 3.25	0.92550±0.03383	0.04817±0.00569	0.02633±0.00417	0.08108±0.02177	0.84324±0.09166	0.07568±0.02098	0.34184±0.02793	0.26360±0.02380	0.39456±0.03059
3.25 - 3.50	0.97431±0.03025	0.01998±0.00311	0.00571±0.00165	0.08276±0.01758	0.89310±0.07636	0.02414±0.00923	0.09259±0.01443	0.55967±0.04238	0.34774±0.03105
3.50 - 3.75	0.98264±0.03065	0.00964±0.00217	0.00771±0.00194	0.15101±0.02415	0.82215±0.07090	0.02685±0.00962	0.12208±0.01886	0.57403±0.04844	0.30390±0.03208
3.75 - 4.00	0.99346±0.03286	0.00164±0.00095	0.00491±0.00164	0.10959±0.02356	0.86301±0.08568	0.02740±0.01134	0.23346±0.03347	0.55253±0.05777	0.21401±0.03179
4.00 - 4.25	0.99233±0.03555	0.00448±0.00170	0.00320±0.00143	0.19079±0.03866	0.79605±0.09699	0.01316±0.00937	0.18974±0.03402	0.31795±0.04636	0.49231±0.06138
4.25 - 4.50	0.99779±0.03834	0.00147±0.00104	0.00074±0.00074	0.21250±0.04013	0.75000±0.09057	0.03750±0.01559	0.21145±0.03359	0.16300±0.02890	0.62555±0.06693
4.50 - 4.75	0.99174±0.04039	0.00578±0.00219	0.00248±0.00143	0.18584±0.04416	0.74336±0.10709	0.07080±0.02590	0.12808±0.02668	0.13301±0.02725	0.73892±0.07956
4.75 - 5.00	1.00000±0.04334	–	–	0.15094±0.04048	0.78302±0.11477	0.06604±0.02577	0.15517±0.03210	0.08621±0.02320	0.75862±0.08756
5.00 - 5.25	0.99674±0.04651	0.00326±0.00189	–	0.15888±0.04148	0.82243±0.11835	0.01869±0.01334	0.15862±0.03560	0.08966±0.02596	0.75172±0.09530
5.25 - 5.50	0.99878±0.04934	–	0.00122±0.00122	0.18085±0.04766	0.73404±0.11637	0.08511±0.03134	0.14000±0.03262	0.10000±0.02708	0.76000±0.09443
5.50 - 5.75	1.00000±0.05505	–	–	0.25773±0.05781	0.72165±0.11317	0.02062±0.01473	0.22131±0.04707	0.04098±0.01870	0.73771±0.10251
5.75 - 6.00	0.99837±0.05705	0.00163±0.00163	–	0.24000±0.06299	0.74667±0.13187	0.01333±0.01342	0.20202±0.04953	0.04040±0.02061	0.75758±0.11597
6.00 - 6.50	1.00000±0.04553	–	–	0.22609±0.04910	0.75652±0.10749	0.01739±0.01240	0.16364±0.03397	0.04242±0.01637	0.79394±0.09291
6.50 - 7.00	0.99862±0.05247	0.00138±0.00138	–	0.20430±0.05144	0.79570±0.12395	–	0.14167±0.03671	0.03333±0.01694	0.82500±0.11201
7.00 - 7.50	0.99832±0.05786	0.00168±0.00168	–	0.27059±0.06360	0.70588±0.11902	0.02353±0.01683	0.13636±0.04196	0.05682±0.02612	0.80682±0.12871
7.50 - 8.00	1.00000±0.07170	–	–	0.18182±0.05706	0.80303±0.14811	0.01515±0.01527	0.13433±0.04769	0.01493±0.01504	0.85075±0.15330
8.00 - 8.50	1.00000±0.07956	–	–	0.12766±0.05534	0.85106±0.18308	0.02128±0.02150	0.13889±0.06629	0.02778±0.02816	0.83333±0.20601
8.50 - 9.00	1.00000±0.09225	–	–	0.22727±0.07962	0.77273±0.17644	–	0.10000±0.05244	0.05000±0.03623	0.85000±0.19827
9.00 - 9.50	1.00000±0.09806	–	–	0.32143±0.12316	0.64286±0.19421	0.03571±0.03635	0.13333±0.07097	–	0.86667±0.23222
9.50 - 10.0	1.00000±0.12356	–	–	0.36842±0.16289	0.63158±0.23289	–	0.21739±0.10727	–	0.78261±0.24628
10.0 - 11.0	0.97753±0.10421	0.02247±0.01136	–	0.09756±0.05110	0.82927±0.19235	0.07317±0.04376	0.10345±0.06274	–	0.89655±0.24214
11.0 - 12.0	0.98684±0.16062	0.01316±0.01324	–	0.06250±0.06442	0.93750±0.33693	–	0.09091±0.09495	–	0.90909±0.39721
12.0 - 13.0	1.00000±0.26726	–	–	0.25000±0.27951	0.75000±0.57282	–	–	–	1.00000±0.44721
13.0 - 14.0	1.00000±0.37796	–	–	0.20000±0.21909	0.80000±0.53666	–	0.20000±0.15492	–	0.80000±0.37947
14.0 - 15.0	1.00000±0.47141	–	–	0.16667±0.18002	0.83333±0.50461	–	–	–	1.00000±0.53452
15.0 - 30.0	1.00000±0.40825	–	–	1.00000±1.41421	–	–	–	–	1.00000±1.00000

Momentum range	Q_π^π	Q_π^K	Q_π^p	Q_K^π	Q_K^K	Q_K^p	Q_p^π	Q_p^K	Q_p^p
0.00 - 0.50	–	–	–	–	–	–	–	–	–
0.50 - 1.00	0.99903±0.02200	0.00097±0.00048	–	–	–	–	–	–	–
1.00 - 1.50	0.97323±0.00987	0.00573±0.00054	0.02104±0.00104	–	–	–	–	–	–
1.50 - 2.00	0.95037±0.00805	0.00995±0.00059	0.03968±0.00120	–	0.33333±0.27217	0.66667±0.43033	0.11397±0.02160	0.15809±0.02594	0.72794±0.06800
2.00 - 2.25	0.95757±0.01133	0.00705±0.00070	0.03538±0.00158	0.09862±0.01072	0.61506±0.03246	0.28632±0.01976	0.11803±0.00520	0.10287±0.00482	0.77910±0.01685
2.25 - 2.50	0.96126±0.01144	0.00285±0.00045	0.03589±0.00161	0.10133±0.00863	0.66133±0.02706	0.23733±0.01399	0.13048±0.00573	0.03719±0.00293	0.83233±0.01843
2.50 - 2.75	0.95958±0.01166	0.00275±0.00045	0.03767±0.00168	0.09377±0.00780	0.70089±0.02660	0.20534±0.01212	0.11903±0.00556	0.02877±0.00262	0.85220±0.01914
2.75 - 3.00	0.96681±0.01192	0.00239±0.00042	0.03079±0.00154	0.07583±0.00679	0.71986±0.02647	0.20430±0.01180	0.12551±0.00599	0.03074±0.00284	0.84375±0.01988
3.00 - 3.25	0.97018±0.01231	0.00198±0.00040	0.02783±0.00151	0.08089±0.00708	0.74125±0.02721	0.17785±0.01096	0.13042±0.00651	0.02528±0.00273	0.84430±0.02115
3.25 - 3.50	0.99096±0.01229	0.00214±0.00041	0.00689±0.00073	0.03046±0.00410	0.75200±0.02654	0.21753±0.01190	0.04088±0.00379	0.03142±0.00331	0.92770±0.02458
3.50 - 3.75	0.99396±0.01255	0.00207±0.00041	0.00398±0.00056	0.00986±0.00234	0.76767±0.02727	0.22247±0.01221	0.02048±0.00287	0.02560±0.00322	0.95392±0.02709
3.75 - 4.00	0.99111±0.01312	0.00201±0.00042	0.00689±0.00078	0.00708±0.00205	0.84198±0.03024	0.15094±0.01012	0.03607±0.00639	0.00874±0.00310	0.95519±0.04518
4.00 - 4.25	0.99094±0.01344	0.00384±0.00059	0.00522±0.00069	0.01371±0.00301	0.89621±0.03331	0.09008±0.00801	–	0.00820±0.00228	0.99180±0.03529
4.25 - 4.50	0.99203±0.01395	0.00335±0.00057	0.00463±0.00068	0.01677±0.00345	0.91405±0.03497	0.06918±0.00719	0.00282±0.00126	0.00903±0.00227	0.98815±0.03330
4.50 - 4.75	0.99210±0.01433	0.00364±0.00062	0.00426±0.00067	0.00849±0.00257	0.95058±0.03784	0.04093±0.00574	0.00186±0.00108	0.00559±0.00187	0.99255±0.03505
4.75 - 5.00	0.99048±0.01495	0.00442±0.00071	0.00510±0.00076	0.01455±0.00336	0.95329±0.03776	0.03216±0.00504	0.00247±0.00123	0.00740±0.00214	0.99014±0.03485
5.00 - 5.25	0.99224±0.01548	0.00339±0.00064	0.00436±0.00073	0.00744±0.00249	0.97188±0.03981	0.02068±0.00418	0.00130±0.00092	0.00913±0.00245	0.98956±0.03584
5.25 - 5.50	0.99211±0.01599	0.00465±0.00078	0.00323±0.00065	0.01333±0.00326	0.96078±0.03844	0.02588±0.00456	0.00285±0.00143	0.00927±0.00258	0.98788±0.03741
5.50 - 5.75	0.99288±0.01679	0.00328±0.00068	0.00385±0.00074	0.00871±0.00277	0.97735±0.04103	0.01394±0.00351	0.00164±0.00116	0.00902±0.00273	0.98934±0.04017
5.75 - 6.00	0.99028±0.01744	0.00463±0.00085	0.00509±0.00089	0.00360±0.00181	0.97117±0.04153	0.02523±0.00483	–	0.00692±0.00246	0.99308±0.04138
6.00 - 6.50	0.99178±0.01307	0.00389±0.00058	0.00433±0.00061	0.00400±0.00142	0.98102±0.03116	0.01499±0.00276	0.00046±0.00046	0.01098±0.00225	0.98856±0.02999
6.50 - 7.00	0.98899±0.01397	0.00516±0.00072	0.00585±0.00076	0.00332±0.00136	0.97734±0.03268	0.01935±0.00330	–	0.00863±0.00224	0.99137±0.03370
7.00 - 7.50	0.99180±0.01555	0.00538±0.00081	0.00281±0.00059	0.00448±0.00170	0.97822±0.03521	0.01730±0.00336	–	0.01919±0.00366	0.98081±0.03649
7.50 - 8.00	0.99373±0.01680	0.00271±0.00062	0.00356±0.00071	0.00371±0.00166	0.98294±0.03803	0.01335±0.00317	–	0.01533±0.00337	0.98467±0.03777
8.00 - 8.50	0.99204±0.01810	0.00514±0.00093	0.00282±0.00068	0.00257±0.00149	0.98113±0.04083	0.01630±0.00377	–	0.01341±0.00361	0.98659±0.04333
8.50 - 9.00	0.99053±0.01972	0.00552±0.00105	0.00395±0.00088	0.00296±0.00171	0.98519±0.04394	0.01185±0.00344	–	0.02854±0.00579	0.97146±0.04676
9.00 - 9.50	0.98832±0.02121	0.00756±0.00132	0.00412±0.00097	0.00248±0.00176	0.98635±0.04930	0.01117±0.00374	–	0.04188±0.00744	0.95812±0.04879
9.50 - 10.0	0.99179±0.02325	0.00575±0.00126	0.00246±0.00082	0.00157±0.00158	0.97008±0.05486	0.02835±0.00678	0.00299±0.00211	0.05373±0.00919	0.94328±0.05231
10.0 - 11.0	0.99127±0.01875	0.00552±0.00099	0.00321±0.00076	0.00083±0.00083	0.99418±0.04061	0.00499±0.00204	0.00253±0.00146	0.13744±0.01148	0.86003±0.03673
11.0 - 12.0	0.99041±0.02231	0.00884±0.00150	0.00076±0.00044	0.00646±0.00265	0.99031±0.04606	0.00323±0.00187	0.00123±0.00124	0.02469±0.00559	0.97407±0.04872
12.0 - 13.0	0.98751±0.02726	0.01211±0.00215	0.00038±0.00038	0.00503±0.00291	0.99162±0.05752	0.00335±0.00237	0.00226±0.00227	–	0.99774±0.06715
13.0 - 14.0	0.97762±0.03289	0.02238±0.00358	–	0.01090±0.00548	0.98638±0.07307	0.00272±0.00273	–	–	1.00000±0.08138
14.0 - 15.0	0.97378±0.04169	0.02622±0.00493	–	–	0.99454±0.10411	0.00546±0.00548	0.00585±0.00587	–	0.99415±0.10767
15.0 - 30.0	0.93514±0.03266	0.06368±0.00632	0.00118±0.00083	0.00730±0.00733	0.98540±0.11950	0.00730±0.00733	0.01370±0.00796	0.00913±0.00649	0.97717±0.09393

Table D.10: Identification purities and contaminations for pions, kaons and protons in $N_\mathrm{tracks} = 1$ with the IRT method at $rQp > 0.5$.

Momentum range	Q_π^π	Q_π^{K}	Q_π^{p}	Q_{K}^π	$Q_{\mathrm{K}}^{\mathrm{K}}$	$Q_{\mathrm{K}}^{\mathrm{p}}$	Q_{p}^π	$Q_{\mathrm{p}}^{\mathrm{K}}$	$Q_{\mathrm{p}}^{\mathrm{p}}$
0.00 - 0.50	–	–	–	–	–	–	–	–	–
0.50 - 1.00	0.99871±0.02073	0.00129±0.00053	–	–	–	–	–	–	–
1.00 - 1.50	0.93322±0.00898	0.01548±0.00084	0.05130±0.00155	–	–	–	–	–	–
1.50 - 2.00	0.88381±0.00738	0.02330±0.00088	0.09289±0.00182	0.42857±0.20912	0.07143±0.07394	0.50000±0.23145	0.17341±0.03430	0.11561±0.02730	0.71098±0.08386
2.00 - 2.25	0.88557±0.01161	0.01954±0.00127	0.09489±0.00290	0.22667±0.01522	0.30000±0.01803	0.47333±0.02411	0.18685±0.00833	0.11581±0.00636	0.69734±0.01925
2.25 - 2.50	0.88224±0.01205	0.00970±0.00093	0.10805±0.00324	0.19048±0.01127	0.38151±0.01718	0.42801±0.01850	0.19992±0.00973	0.06467±0.00521	0.73541±0.02243
2.50 - 2.75	0.88864±0.01269	0.00835±0.00090	0.10300±0.00330	0.18309±0.01080	0.41034±0.01765	0.40657±0.01755	0.20735±0.01046	0.04156±0.00435	0.75109±0.02399
2.75 - 3.00	0.90041±0.01350	0.00756±0.00090	0.09202±0.00327	0.16912±0.01021	0.46523±0.01895	0.36565±0.01622	0.17067±0.01000	0.04104±0.00462	0.78829±0.02656
3.00 - 3.25	0.90927±0.01426	0.00702±0.00091	0.08370±0.00326	0.16992±0.01068	0.47015±0.01992	0.35993±0.01676	0.20230±0.01155	0.02906±0.00405	0.76864±0.02730
3.25 - 3.50	0.96229±0.01393	0.00904±0.00097	0.02867±0.00174	0.05817±0.00533	0.53232±0.01941	0.40951±0.01632	0.09773±0.00902	0.02576±0.00447	0.87652±0.03530
3.50 - 3.75	0.96975±0.01436	0.00994±0.00104	0.02031±0.00150	0.02562±0.00360	0.55123±0.02052	0.42315±0.01722	0.06077±0.00759	0.05273±0.00704	0.88651±0.03866
3.75 - 4.00	0.96832±0.01507	0.01084±0.00114	0.02084±0.00159	0.01762±0.00348	0.61585±0.02597	0.36653±0.01842	0.10503±0.01594	0.03282±0.00861	0.86214±0.05927
4.00 - 4.25	0.96804±0.01567	0.01353±0.00133	0.01843±0.00156	0.01722±0.00421	0.76292±0.03691	0.21986±0.01648	0.00831±0.00341	0.03878±0.00747	0.95291±0.05077
4.25 - 4.50	0.96457±0.01687	0.01471±0.00150	0.02071±0.00178	0.03229±0.00609	0.79621±0.03991	0.17149±0.01496	0.00501±0.00251	0.02632±0.00582	0.96867±0.04888
4.50 - 4.75	0.96498±0.01774	0.01477±0.00158	0.02025±0.00185	0.02970±0.00658	0.83734±0.04665	0.13296±0.01460	0.00390±0.00226	0.02341±0.00558	0.97269±0.04995
4.75 - 5.00	0.96942±0.01875	0.01124±0.00145	0.01934±0.00191	0.02164±0.00585	0.88253±0.05067	0.09583±0.01274	0.00432±0.00250	0.02878±0.00653	0.96691±0.05231
5.00 - 5.25	0.96811±0.01974	0.01267±0.00162	0.01921±0.00200	0.01821±0.00581	0.91621±0.05655	0.06557±0.01128	0.00160±0.00160	0.01917±0.00559	0.97923±0.05564
5.25 - 5.50	0.96340±0.02074	0.01773±0.00203	0.01887±0.00209	0.00611±0.00354	0.94297±0.06109	0.05092±0.01044	0.00317±0.00225	0.02540±0.00643	0.97143±0.05513
5.50 - 5.75	0.96570±0.02255	0.01688±0.00214	0.01742±0.00218	0.01240±0.00509	0.92975±0.06089	0.05785±0.01124	0.00178±0.00178	0.02852±0.00723	0.96970±0.05835
5.75 - 6.00	0.96581±0.02316	0.01611±0.00215	0.01808±0.00228	0.00973±0.00489	0.95620±0.06746	0.03406±0.00926	–	0.03758±0.00902	0.96242±0.06279
6.00 - 6.50	0.95996±0.01787	0.01985±0.00185	0.02019±0.00187	0.01343±0.00451	0.92090±0.05138	0.06567±0.01022	–	0.02453±0.00529	0.97547±0.04635
6.50 - 7.00	0.96062±0.02008	0.02012±0.00210	0.01926±0.00205	0.00486±0.00281	0.95786±0.05513	0.03728±0.00792	–	0.02276±0.00575	0.97724±0.05243
7.00 - 7.50	0.96166±0.02218	0.02087±0.00236	0.01748±0.00215	–	0.95531±0.05898	0.04469±0.00932	0.00178±0.00178	0.02487±0.00673	0.97336±0.05841
7.50 - 8.00	0.95616±0.02502	0.02041±0.00264	0.02343±0.00283	0.00240±0.00240	0.94964±0.06663	0.04796±0.01098	–	0.02184±0.00736	0.97815±0.06853
8.00 - 8.50	0.96070±0.02868	0.02009±0.00299	0.01921±0.00292	–	0.95699±0.07095	0.04301±0.01098	–	0.01989±0.00759	0.98011±0.07425
8.50 - 9.00	0.96099±0.03218	0.02033±0.00338	0.01868±0.00323	–	0.97270±0.08093	0.02730±0.00978	–	0.02745±0.01052	0.97255±0.08674
9.00 - 9.50	0.95658±0.03592	0.02619±0.00430	0.01723±0.00348	–	0.97087±0.09638	0.02913±0.01206	–	0.04508±0.01390	0.95492±0.08747
9.50 - 10.0	0.95607±0.04013	0.02584±0.00478	0.01809±0.00398	–	0.98710±0.11249	0.01290±0.00918	–	0.07222±0.02074	0.92778±0.09968
10.0 - 11.0	0.96013±0.03479	0.01994±0.00362	0.01994±0.00362	0.04643±0.01317	0.91429±0.07906	0.03929±0.01208	–	0.14050±0.02101	0.85950±0.06635
11.0 - 12.0	0.96750±0.04467	0.01782±0.00436	0.01468±0.00395	0.06542±0.01805	0.92523±0.09123	0.00935±0.00664	–	0.03196±0.01227	0.96804±0.09327
12.0 - 13.0	0.97707±0.05837	0.01764±0.00563	0.00529±0.00306	0.03077±0.01562	0.96154±0.12045	0.00769±0.00772	–	0.02479±0.01449	0.97521±0.12617
13.0 - 14.0	0.95950±0.07653	0.02804±0.00948	0.01246±0.00627	0.03448±0.02480	0.89655±0.17122	0.06897±0.03565	–	–	1.00000±0.16903
14.0 - 15.0	0.94313±0.09320	0.04739±0.01534	0.00948±0.00673	–	1.00000±0.29488	–	–	–	1.00000±0.24254
15.0 - 30.0	0.92079±0.09357	0.07921±0.02057	–	–	0.87500±0.26146	0.12500±0.07655	0.03125±0.03173	–	0.96875±0.24413

Table D.11: Identification purities and contaminations for pions, kaons and protons in $N_{\mathrm{tracks}} = 2$ with the IRT method at $rQp > 0.5$.

Momentum range	Q_{π}^{π}	Q_{π}^{K}	Q_{π}^{p}	Q_{K}^{π}	$Q_{\mathrm{K}}^{\mathrm{K}}$	$Q_{\mathrm{K}}^{\mathrm{p}}$	Q_{p}^{π}	$Q_{\mathrm{p}}^{\mathrm{K}}$	$Q_{\mathrm{p}}^{\mathrm{p}}$
0.00 - 0.50	–	–	–	–	–	–	–	–	–
0.50 - 1.00	0.99840±0.04002	0.00161±0.00114	–	–	–	–	–	–	–
1.00 - 1.50	0.92644±0.01725	0.02068±0.00188	0.05288±0.00305	–	–	–	–	–	–
1.50 - 2.00	0.86450±0.01431	0.03140±0.00203	0.10411±0.00382	0.33333±0.38490	–	0.66667±0.60858	0.21622±0.08430	0.13514±0.06439	0.64865±0.17001
2.00 - 2.25	0.86542±0.02325	0.02611±0.00300	0.10847±0.00634	0.24643±0.03312	0.30000±0.03732	0.45357±0.04852	0.22043±0.02196	0.12545±0.01591	0.65412±0.04403
2.25 - 2.50	0.85182±0.02500	0.01387±0.00236	0.13431±0.00777	0.22811±0.02541	0.36406±0.03383	0.40783±0.03637	0.27033±0.02866	0.07895±0.01428	0.65072±0.05069
2.50 - 2.75	0.85727±0.02620	0.01552±0.00261	0.12721±0.00786	0.21767±0.02390	0.38147±0.03370	0.40086±0.03479	0.27419±0.03065	0.04839±0.01168	0.67742±0.05527
2.75 - 3.00	0.87255±0.02863	0.01054±0.00231	0.11691±0.00809	0.21987±0.02381	0.39324±0.03403	0.38689±0.03368	0.23009±0.02889	0.02950±0.00946	0.74041±0.06165
3.00 - 3.25	0.86964±0.03132	0.00905±0.00235	0.12130±0.00906	0.19430±0.02452	0.40414±0.03834	0.40155±0.03818	0.14286±0.02385	0.04878±0.01335	0.80836±0.07137
3.25 - 3.50	0.96741±0.02998	0.01134±0.00233	0.02126±0.00320	0.07330±0.01172	0.45201±0.03384	0.47469±0.03495	0.06383±0.01901	0.03723±0.01433	0.89894±0.09529
3.50 - 3.75	0.95681±0.02965	0.02113±0.00318	0.02207±0.00325	0.04115±0.00939	0.50411±0.03950	0.45473±0.03689	0.11348±0.02994	0.05674±0.02062	0.82979±0.10377
3.75 - 4.00	0.95593±0.03132	0.01259±0.00259	0.03148±0.00413	0.00898±0.00521	0.56587±0.05151	0.42515±0.04259	0.12857±0.04553	0.08571±0.03646	0.78571±0.14158
4.00 - 4.25	0.95921±0.03408	0.01792±0.00336	0.02287±0.00380	0.03684±0.01418	0.63684±0.07407	0.32632±0.04773	0.04854±0.02223	0.01942±0.01386	0.93204±0.13222
4.25 - 4.50	0.94286±0.03573	0.02369±0.00411	0.03345±0.00491	0.01258±0.00895	0.75472±0.09126	0.23270±0.04247	0.00671±0.00673	0.04027±0.01677	0.95302±0.11177
4.50 - 4.75	0.96234±0.03890	0.01683±0.00370	0.02083±0.00413	0.05932±0.02308	0.71186±0.10162	0.22881±0.04881	0.01863±0.01086	0.04969±0.01800	0.93168±0.10573
4.75 - 5.00	0.96119±0.04125	0.01444±0.00364	0.02437±0.00475	–	0.84694±0.12634	0.15306±0.04244	–	0.05036±0.01951	0.94964±0.11541
5.00 - 5.25	0.95820±0.04428	0.01776±0.00435	0.02403±0.00507	0.02885±0.01689	0.84615±0.12256	0.12500±0.03677	–	0.01802±0.01285	0.98198±0.13242
5.25 - 5.50	0.95566±0.04670	0.01984±0.00486	0.02450±0.00541	–	0.82143±0.13346	0.17857±0.05005	0.00813±0.00816	0.06504±0.02373	0.92683±0.12050
5.50 - 5.75	0.92697±0.05009	0.03511±0.00714	0.03792±0.00744	–	0.93333±0.15511	0.06667±0.03079	–	0.02174±0.01554	0.97826±0.14504
5.75 - 6.00	0.94154±0.05303	0.02769±0.00662	0.03077±0.00699	0.01639±0.01653	0.91803±0.16990	0.06557±0.03384	–	0.01316±0.01324	0.98684±0.16062
6.00 - 6.50	0.94794±0.04259	0.02554±0.00507	0.02652±0.00517	–	0.92553±0.13769	0.07447±0.02918	–	0.01504±0.01071	0.98496±0.12124
6.50 - 7.00	0.95263±0.04947	0.02500±0.00581	0.02237±0.00549	0.01266±0.01274	0.93671±0.15154	0.05063±0.02595	–	–	1.00000±0.14213
7.00 - 7.50	0.94444±0.05399	0.03651±0.00775	0.01905±0.00555	0.01515±0.01527	0.90909±0.16216	0.07576±0.03514	–	0.02740±0.01964	0.97260±0.16212
7.50 - 8.00	0.94878±0.06715	0.02927±0.00857	0.02195±0.00740	–	0.98148±0.18977	0.01852±0.01869	–	0.01724±0.01739	0.98276±0.18329
8.00 - 8.50	0.96636±0.07623	0.01835±0.00756	0.01529±0.00689	–	0.97561±0.21682	0.02439±0.02469	–	0.03226±0.03277	0.96774±0.24785
8.50 - 9.00	0.94378±0.08583	0.04016±0.01295	0.01606±0.00810	–	0.94444±0.22586	0.05556±0.04036	–	–	1.00000±0.24254
9.00 - 9.50	0.94118±0.09092	0.04072±0.01385	0.01810±0.00913	–	1.00000±0.33333	–	–	0.03704±0.03772	0.96296±0.26459
9.50 - 10.0	0.91608±0.11079	0.04895±0.01895	0.03497±0.01591	–	1.00000±0.40825	–	–	–	1.00000±0.33333
10.0 - 11.0	0.96133±0.10206	0.02210±0.01117	0.01657±0.00965	0.10526±0.05533	0.89474±0.21122	–	–	0.10345±0.06274	0.89655±0.24214
11.0 - 12.0	0.97403±0.15802	0.01299±0.01307	0.01299±0.01307	0.06250±0.06442	0.93750±0.33693	–	–	–	1.00000±0.44721
12.0 - 13.0	0.96552±0.25581	0.03448±0.03507	–	–	1.00000±0.81650	–	–	–	1.00000±0.44721
13.0 - 14.0	0.82353±0.29722	0.05882±0.06053	0.11765±0.08795	–	1.00000±0.70711	–	–	–	1.00000±0.50000
14.0 - 15.0	0.90000±0.41352	0.10000±0.10488	–	–	1.00000±0.63246	–	–	–	1.00000±0.53452
15.0 - 30.0	0.92308±0.36953	0.07692±0.07983	–	–	–	–	–	–	1.00000±1.00000

Table D.12: Identification purities and contaminations for pions, kaons and protons in $N_{\mathrm{tracks}} > 2$ with the IRT method at $rQp > 0.5$.

Momentum range	$\mathcal{P}_{\pi}^{\pi}$	$\mathcal{P}_{\pi}^{\mathrm{K}}$	$\mathcal{P}_{\pi}^{\mathrm{p}}$	$\mathcal{P}_{\mathrm{K}}^{\pi}$	$\mathcal{P}_{\mathrm{K}}^{\mathrm{K}}$	$\mathcal{P}_{\mathrm{K}}^{\mathrm{p}}$	$\mathcal{P}_{\mathrm{p}}^{\pi}$	$\mathcal{P}_{\mathrm{p}}^{\mathrm{K}}$	$\mathcal{P}_{\mathrm{p}}^{\mathrm{p}}$
0.00 - 0.50	–	–	–	–	–	–	–	–	–
0.50 - 1.00	1.00000±0.00000	–	–	1.00000±0.00000	–	–	–	–	–
1.00 - 1.50	1.00000±0.00000	–	–	1.00000±0.00000	–	–	1.00000±0.00000	–	–
1.50 - 2.00	0.99881±0.00021	–	0.00119±0.00021	0.87013±0.01915	0.00325±0.00324	0.12662±0.01895	0.84240±0.01031	0.00320±0.00160	0.15440±0.01022
2.00 - 2.25	0.95698±0.00173	0.00290±0.00046	0.04012±0.00167	0.08084±0.00821	0.48138±0.01506	0.43778±0.01495	0.10635±0.00469	0.05375±0.00343	0.83990±0.00558
2.25 - 2.50	0.95397±0.00180	0.00478±0.00059	0.04125±0.00171	0.02873±0.00500	0.82855±0.01129	0.14273±0.01048	0.10713±0.00470	0.06779±0.00382	0.82508±0.00578
2.50 - 2.75	0.95747±0.00177	0.00522±0.00063	0.03731±0.00166	0.02024±0.00401	0.88259±0.00916	0.09717±0.00843	0.10731±0.00474	0.07076±0.00393	0.82193±0.00586
2.75 - 3.00	0.95783±0.00179	0.00499±0.00063	0.03718±0.00168	0.01293±0.00312	0.89734±0.00837	0.08973±0.00788	0.09250±0.00468	0.08153±0.00442	0.82597±0.00613
3.00 - 3.25	0.95814±0.00183	0.00528±0.00066	0.03657±0.00172	0.01216±0.00302	0.92401±0.00730	0.06383±0.00674	0.08953±0.00492	0.07975±0.00466	0.83071±0.00646
3.25 - 3.50	0.98758±0.00099	0.00353±0.00053	0.00889±0.00084	0.01842±0.00351	0.92087±0.00705	0.06071±0.00624	0.02806±0.00298	0.12333±0.00594	0.84861±0.00647
3.50 - 3.75	0.99451±0.00067	0.00141±0.00034	0.00408±0.00058	0.01677±0.00339	0.94060±0.00625	0.04263±0.00534	0.01672±0.00244	0.13953±0.00661	0.84375±0.00692
3.75 - 4.00	0.99614±0.00059	0.00092±0.00029	0.00294±0.00052	0.01661±0.00343	0.97906±0.00385	0.00433±0.00176	0.06624±0.00749	0.20145±0.01208	0.73230±0.01334
4.00 - 4.25	0.99836±0.00040	0.00164±0.00040	–	0.03046±0.00468	0.96880±0.00474	0.00074±0.00074	0.03313±0.00447	0.06688±0.00625	0.90000±0.00750
4.25 - 4.50	0.99772±0.00049	0.00187±0.00044	0.00042±0.00021	0.02584±0.00444	0.96789±0.00493	0.00626±0.00221	0.02516±0.00374	0.03602±0.00446	0.93882±0.00573
4.50 - 4.75	0.99857±0.00040	0.00110±0.00035	0.00033±0.00019	0.02886±0.00488	0.96774±0.00515	0.00340±0.00169	0.02543±0.00397	0.02225±0.00372	0.95232±0.00537
4.75 - 5.00	0.99760±0.00054	0.00204±0.00049	0.00036±0.00021	0.03120±0.00498	0.96470±0.00529	0.00411±0.00183	0.02774±0.00412	0.01576±0.00313	0.95649±0.00512
5.00 - 5.25	0.99872±0.00040	0.00115±0.00038	0.00013±0.00013	0.02469±0.00461	0.97443±0.00469	0.00088±0.00088	0.02396±0.00400	0.01027±0.00264	0.96578±0.00476
5.25 - 5.50	0.99713±0.00063	0.00232±0.00056	0.00055±0.00027	0.02685±0.00468	0.96812±0.00509	0.00503±0.00205	0.01722±0.00356	0.01272±0.00307	0.97006±0.00466
5.50 - 5.75	0.99879±0.00043	0.00106±0.00040	0.00015±0.00015	0.02045±0.00431	0.97769±0.00450	0.00186±0.00131	0.02316±0.00440	0.00772±0.00256	0.96913±0.00507
5.75 - 6.00	0.99935±0.00033	0.00065±0.00033	–	0.02778±0.00509	0.96647±0.00557	0.00575±0.00234	0.02509±0.00468	0.01165±0.00321	0.96326±0.00563
6.00 - 6.50	0.99927±0.00026	0.00073±0.00026	–	0.02309±0.00344	0.96957±0.00393	0.00735±0.00196	0.02305±0.00329	0.00768±0.00191	0.96926±0.00378
6.50 - 7.00	0.99937±0.00026	0.00063±0.00026	–	0.02929±0.00408	0.96602±0.00439	0.00469±0.00165	0.03397±0.00442	0.01192±0.00265	0.95411±0.00511
7.00 - 7.50	0.99923±0.00032	0.00077±0.00032	–	0.02804±0.00432	0.96101±0.00506	0.01094±0.00272	0.01463±0.00325	0.01244±0.00300	0.97293±0.00439
7.50 - 8.00	0.99925±0.00033	0.00075±0.00033	–	0.01420±0.00342	0.97410±0.00459	0.01170±0.00311	0.01788±0.00370	0.01011±0.00279	0.97201±0.00460
8.00 - 8.50	0.99948±0.00030	0.00053±0.00030	–	0.02880±0.00527	0.96127±0.00608	0.00993±0.00312	0.01474±0.00391	0.01368±0.00377	0.97158±0.00539
8.50 - 9.00	0.99938±0.00036	0.00062±0.00036	–	0.03117±0.00614	0.95012±0.00769	0.01870±0.00478	0.02405±0.00545	0.01266±0.00398	0.96329±0.00669
9.00 - 9.50	0.99952±0.00034	0.00048±0.00034	–	0.05482±0.00928	0.90698±0.01184	0.03821±0.00781	0.02526±0.00605	0.00743±0.00331	0.96731±0.00685
9.50 - 10.0	0.99913±0.00050	0.00029±0.00029	0.00058±0.00041	0.04861±0.01035	0.91898±0.01313	0.03241±0.00852	0.01599±0.00529	0.01776±0.00557	0.96625±0.00761
10.0 - 11.0	0.99943±0.00033	–	0.00057±0.00033	0.01484±0.00338	0.86562±0.00953	0.11953±0.00907	0.01820±0.00425	0.00506±0.00226	0.97674±0.00479
11.0 - 12.0	0.99920±0.00046	0.00053±0.00038	0.00027±0.00027	0.01734±0.00444	0.96069±0.00661	0.02197±0.00498	0.00407±0.00234	0.00136±0.00135	0.99458±0.00270
12.0 - 13.0	0.99919±0.00057	0.00041±0.00041	0.00041±0.00041	0.01793±0.00592	0.98207±0.00592	–	0.00235±0.00234	0.00469±0.00331	0.99296±0.00405
13.0 - 14.0	0.99815±0.00107	0.00185±0.00107	–	0.05986±0.01408	0.94014±0.01408	–	–	–	1.00000±0.00000
14.0 - 15.0	0.99901±0.00098	–	0.00099±0.00098	0.12143±0.02760	0.87857±0.02760	–	–	0.00606±0.00604	0.99394±0.00604
15.0 - 30.0	0.99780±0.00127	–	0.00220±0.00127	0.29032±0.04707	0.68817±0.04804	0.02151±0.01504	0.01010±0.00711	0.00505±0.00504	0.98485±0.00868

Table D.13: Identification efficiencies for pions, kaons and protons in $N_{\mathrm{tracks}} = 1$ with the IRT method at $rQp > 1.0$.

Momentum range	$\mathcal{P}_{\pi}^{\pi}$	$\mathcal{P}_{\pi}^{\mathrm{K}}$	$\mathcal{P}_{\pi}^{\mathrm{p}}$	$\mathcal{P}_{\mathrm{K}}^{\pi}$	$\mathcal{P}_{\mathrm{K}}^{\mathrm{K}}$	$\mathcal{P}_{\mathrm{K}}^{\mathrm{p}}$	$\mathcal{P}_{\mathrm{p}}^{\pi}$	$\mathcal{P}_{\mathrm{p}}^{\mathrm{K}}$	$\mathcal{P}_{\mathrm{p}}^{\mathrm{p}}$
0.00 - 0.50	–	–	–	–	–	–	–	–	–
0.50 - 1.00	1.00000±0.00000	–	–	1.00000±0.00000	–	–	–	–	–
1.00 - 1.50	1.00000±0.00000	–	–	1.00000±0.00000	–	–	1.00000±0.00000	–	–
1.50 - 2.00	0.99887±0.00021	0.00004±0.00004	0.00109±0.00021	0.97230±0.00627	0.00146±0.00146	0.02624±0.00610	0.95554±0.00390	0.00179±0.00080	0.04267±0.00383
2.00 - 2.25	0.93602±0.00235	0.01063±0.00099	0.05335±0.00216	0.22094±0.01407	0.37284±0.01640	0.40621±0.01666	0.28925±0.00748	0.13225±0.00559	0.57850±0.00815
2.25 - 2.50	0.93628±0.00246	0.01441±0.00120	0.04931±0.00218	0.09434±0.01004	0.72288±0.01537	0.18278±0.01327	0.31085±0.00776	0.18746±0.00654	0.50169±0.00838
2.50 - 2.75	0.93260±0.00265	0.01649±0.00134	0.05091±0.00232	0.06963±0.00882	0.82233±0.01324	0.10804±0.01076	0.28965±0.00798	0.20260±0.00707	0.50775±0.00880
2.75 - 3.00	0.94263±0.00260	0.01700±0.00145	0.04038±0.00220	0.04111±0.00662	0.87333±0.01109	0.08556±0.00932	0.26294±0.00826	0.21119±0.00766	0.52587±0.00937
3.00 - 3.25	0.93450±0.00288	0.01790±0.00154	0.04760±0.00248	0.03367±0.00637	0.90150±0.01052	0.06484±0.00870	0.24553±0.00868	0.21341±0.00826	0.54106±0.01005
3.25 - 3.50	0.97540±0.00163	0.01125±0.00111	0.01335±0.00121	0.06767±0.00726	0.90560±0.00845	0.02673±0.00466	0.11649±0.00686	0.38191±0.01038	0.50160±0.01069
3.50 - 3.75	0.98694±0.00122	0.00543±0.00079	0.00762±0.00093	0.07386±0.00753	0.88216±0.00929	0.04398±0.00591	0.09317±0.00661	0.41253±0.01120	0.49431±0.01137
3.75 - 4.00	0.99130±0.00105	0.00281±0.00060	0.00588±0.00086	0.09295±0.00949	0.89744±0.00992	0.00962±0.00319	0.16516±0.01178	0.48540±0.01586	0.34945±0.01513
4.00 - 4.25	0.99721±0.00062	0.00195±0.00052	0.00084±0.00034	0.12091±0.01157	0.86650±0.01207	0.01259±0.00396	0.14394±0.01155	0.19372±0.01300	0.66234±0.01556
4.25 - 4.50	0.99480±0.00092	0.00471±0.00087	0.00049±0.00028	0.12385±0.01196	0.86034±0.01258	0.01581±0.00453	0.14056±0.01138	0.11052±0.01027	0.74893±0.01420
4.50 - 4.75	0.99641±0.00080	0.00323±0.00076	0.00036±0.00025	0.13057±0.01345	0.85510±0.01405	0.01433±0.00474	0.13450±0.01167	0.07251±0.00887	0.79298±0.01386
4.75 - 5.00	0.99664±0.00081	0.00277±0.00074	0.00059±0.00034	0.10118±0.01238	0.88533±0.01308	0.01349±0.00474	0.13351±0.01243	0.06142±0.00877	0.80507±0.01447
5.00 - 5.25	0.99756±0.00073	0.00222±0.00070	0.00022±0.00022	0.11494±0.01396	0.87740±0.01436	0.00766±0.00382	0.13573±0.01353	0.02964±0.00670	0.83463±0.01467
5.25 - 5.50	0.99876±0.00055	0.00074±0.00043	0.00050±0.00035	0.14764±0.01574	0.84055±0.01624	0.01181±0.00479	0.11943±0.01294	0.01752±0.00523	0.86306±0.01372
5.50 - 5.75	0.99826±0.00071	0.00174±0.00071	–	0.12447±0.01516	0.85865±0.01600	0.01688±0.00592	0.11490±0.01351	0.02334±0.00640	0.86176±0.01462
5.75 - 6.00	0.99877±0.00061	0.00122±0.00061	–	0.12440±0.01614	0.85646±0.01715	0.01914±0.00670	0.13008±0.01517	0.01626±0.00570	0.85366±0.01593
6.00 - 6.50	0.99853±0.00052	0.00147±0.00052	–	0.16740±0.01431	0.82232±0.01465	0.01028±0.00387	0.11803±0.01067	0.02732±0.00539	0.85464±0.01165
6.50 - 7.00	0.99930±0.00041	0.00070±0.00041	–	0.14514±0.01407	0.84689±0.01438	0.00797±0.00355	0.12571±0.01246	0.02260±0.00559	0.85169±0.01336
7.00 - 7.50	0.99972±0.00028	–	0.00028±0.00028	0.13846±0.01515	0.85769±0.01532	0.00385±0.00271	0.11797±0.01374	0.01633±0.00540	0.86570±0.01453
7.50 - 8.00	0.99963±0.00037	0.00037±0.00037	–	0.14910±0.01806	0.83548±0.01880	0.01542±0.00625	0.15262±0.01716	0.02961±0.00809	0.81777±0.01842
8.00 - 8.50	1.00000±0.00000	–	–	0.13897±0.01901	0.84894±0.01968	0.01208±0.00601	0.11561±0.01719	0.02890±0.00901	0.85549±0.01890
8.50 - 9.00	1.00000±0.00000	–	–	0.13821±0.02200	0.85366±0.02253	0.00813±0.00573	0.13750±0.02223	0.01250±0.00717	0.85000±0.02305
9.00 - 9.50	1.00000±0.00000	–	–	0.20000±0.03068	0.77059±0.03225	0.02941±0.01296	0.11374±0.02186	0.01422±0.00815	0.87204±0.02300
9.50 - 10.0	1.00000±0.00000	–	–	0.21875±0.03654	0.75781±0.03787	0.02344±0.01337	0.13245±0.02759	–	0.86755±0.02759
10.0 - 11.0	0.99929±0.00071	0.00071±0.00071	–	0.07029±0.01445	0.76997±0.02379	0.15974±0.02071	0.07951±0.01496	0.02446±0.00854	0.89602±0.01688
11.0 - 12.0	0.99886±0.00114	0.00115±0.00114	–	0.04787±0.01557	0.91489±0.02035	0.03723±0.01381	0.04245±0.01385	0.00472±0.00471	0.95283±0.01456
12.0 - 13.0	0.99614±0.00272	0.00386±0.00272	–	0.03571±0.01754	0.93750±0.02287	0.02679±0.01526	0.02542±0.01449	0.00847±0.00844	0.96610±0.01666
13.0 - 14.0	1.00000±0.00000	–	–	0.08108±0.04487	0.91892±0.04487	–	0.04286±0.02421	0.01429±0.01418	0.94286±0.02774
14.0 - 15.0	1.00000±0.00000	–	–	0.25000±0.09682	0.75000±0.09682	–	0.05714±0.03923	–	0.94286±0.03923
15.0 - 30.0	1.00000±0.00000	–	–	0.47619±0.10898	0.52381±0.10898	–	–	–	1.00000±0.00000

Table D.14: Identification efficiencies for pions, kaons and protons in $N_{\mathrm{tracks}} = 2$ with the IRT method at $rQp > 1.0$.

Momentum range	$\mathcal{P}_{\pi}^{\pi}$	$\mathcal{P}_{\pi}^{\mathrm{K}}$	$\mathcal{P}_{\pi}^{\mathrm{p}}$	$\mathcal{P}_{\mathrm{K}}^{\pi}$	$\mathcal{P}_{\mathrm{K}}^{\mathrm{K}}$	$\mathcal{P}_{\mathrm{K}}^{\mathrm{p}}$	$\mathcal{P}_{\mathrm{p}}^{\pi}$	$\mathcal{P}_{\mathrm{p}}^{\mathrm{K}}$	$\mathcal{P}_{\mathrm{p}}^{\mathrm{p}}$
0.00 - 0.50	–	–	–	–	–	–	–	–	–
0.50 - 1.00	1.00000±0.00000	–	–	1.00000±0.00000	–	–	–	–	–
1.00 - 1.50	1.00000±0.00000	–	–	1.00000±0.00000	–	–	1.00000±0.00000	–	–
1.50 - 2.00	0.99861±0.00046	0.00015±0.00015	0.00123±0.00044	0.97934±0.00914	–	0.02066±0.00914	0.96894±0.00611	0.00248±0.00175	0.02857±0.00587
2.00 - 2.25	0.94433±0.00462	0.00853±0.00185	0.04714±0.00427	0.30846±0.03258	0.36816±0.03402	0.32338±0.03299	0.39290±0.01770	0.15112±0.01298	0.45598±0.01805
2.25 - 2.50	0.93205±0.00552	0.01639±0.00279	0.05157±0.00485	0.09677±0.02168	0.74731±0.03186	0.15591±0.02660	0.41758±0.01828	0.21978±0.01535	0.36264±0.01782
2.50 - 2.75	0.92968±0.00590	0.01811±0.00308	0.05221±0.00513	0.10440±0.02267	0.79670±0.02983	0.09890±0.02213	0.38249±0.01905	0.24270±0.01680	0.37481±0.01897
2.75 - 3.00	0.92830±0.00644	0.02556±0.00394	0.04613±0.00524	0.06145±0.01795	0.88268±0.02405	0.05587±0.01717	0.32995±0.01934	0.26396±0.01813	0.40609±0.02020
3.00 - 3.25	0.94749±0.00615	0.02131±0.00398	0.03120±0.00480	0.03125±0.01376	0.88125±0.02557	0.08750±0.02234	0.32341±0.02084	0.25992±0.01954	0.41667±0.02196
3.25 - 3.50	0.97680±0.00338	0.01715±0.00292	0.00605±0.00174	0.07554±0.01585	0.90288±0.01776	0.02158±0.00872	0.09492±0.01377	0.55629±0.02334	0.34879±0.02239
3.50 - 3.75	0.98279±0.00293	0.00911±0.00214	0.00810±0.00202	0.15957±0.02181	0.81206±0.02326	0.02837±0.00989	0.12707±0.01750	0.56354±0.02607	0.30939±0.02430
3.75 - 4.00	0.99317±0.00197	0.00171±0.00099	0.00513±0.00170	0.11274±0.02214	0.88235±0.02256	0.00490±0.00489	0.24779±0.02872	0.55310±0.03307	0.19911±0.02656
4.00 - 4.25	0.99205±0.00229	0.00464±0.00175	0.00331±0.00148	0.19858±0.03360	0.79433±0.03404	0.00709±0.00707	0.22981±0.03316	0.31677±0.03666	0.45342±0.03923
4.25 - 4.50	0.99770±0.00133	0.00154±0.00109	0.00077±0.00077	0.22069±0.03444	0.76552±0.03518	0.01379±0.00969	0.22843±0.02991	0.16244±0.02628	0.60914±0.03476
4.50 - 4.75	0.99216±0.00260	0.00610±0.00230	0.00174±0.00123	0.19388±0.03993	0.78571±0.04145	0.02041±0.01428	0.14444±0.02620	0.11667±0.02393	0.73889±0.03274
4.75 - 5.00	1.00000±0.00000	–	–	0.15730±0.03859	0.80899±0.04167	0.03371±0.01913	0.17763±0.03100	0.04605±0.01700	0.77632±0.03380
5.00 - 5.25	0.99772±0.00161	0.00228±0.00161	–	0.17895±0.03933	0.82105±0.03933	–	0.17797±0.03521	0.06780±0.02314	0.75424±0.03963
5.25 - 5.50	0.99872±0.00128	–	0.00128±0.00128	0.21795±0.04675	0.78205±0.04675	–	0.14062±0.03073	0.09375±0.02576	0.76562±0.03744
5.50 - 5.75	1.00000±0.00000	–	–	0.27160±0.04942	0.71605±0.05010	0.01235±0.01227	0.24038±0.04190	0.02885±0.01641	0.73077±0.04349
5.75 - 6.00	0.99830±0.00170	0.00170±0.00170	–	0.31034±0.06075	0.68966±0.06075	–	0.21111±0.04302	0.01111±0.01105	0.77778±0.04382
6.00 - 6.50	1.00000±0.00000	–	–	0.24742±0.04381	0.74227±0.04441	0.01031±0.01026	0.17105±0.03054	0.02632±0.01298	0.80263±0.03228
6.50 - 7.00	0.99855±0.00145	0.00145±0.00145	–	0.21951±0.04571	0.78049±0.04571	–	0.15686±0.03601	0.01961±0.01373	0.82353±0.03775
7.00 - 7.50	0.99826±0.00174	0.00174±0.00174	–	0.29167±0.05357	0.68056±0.05495	0.02778±0.01937	0.15584±0.04133	0.03896±0.02205	0.80519±0.04513
7.50 - 8.00	1.00000±0.00000	–	–	0.27273±0.06714	0.72727±0.06714	–	0.16000±0.05185	0.02000±0.01980	0.82000±0.05433
8.00 - 8.50	1.00000±0.00000	–	–	0.16667±0.06211	0.80556±0.06596	0.02778±0.02739	0.13333±0.06206	0.03333±0.03277	0.83333±0.06804
8.50 - 9.00	1.00000±0.00000	–	–	0.31250±0.08194	0.68750±0.08194	–	0.09677±0.05310	–	0.90323±0.05310
9.00 - 9.50	1.00000±0.00000	–	–	0.44444±0.11712	0.50000±0.11785	0.05556±0.05399	0.17391±0.07903	–	0.82609±0.07903
9.50 - 10.0	1.00000±0.00000	–	–	0.43750±0.12402	0.56250±0.12402	–	0.26316±0.10102	–	0.73684±0.10102
10.0 - 11.0	1.00000±0.00000	–	–	0.10256±0.04858	0.82051±0.06145	0.07692±0.04267	0.10714±0.05845	–	0.89286±0.05845
11.0 - 12.0	1.00000±0.00000	–	–	–	1.00000±0.00000	–	0.11111±0.10476	–	0.88889±0.10476
12.0 - 13.0	1.00000±0.00000	–	–	–	1.00000±0.00000	–	–	–	1.00000±0.00000
13.0 - 14.0	1.00000±0.00000	–	–	–	1.00000±0.00000	–	–	–	1.00000±0.00000
14.0 - 15.0	1.00000±0.00000	–	–	0.33333±0.27217	0.66667±0.27217	–	–	–	1.00000±0.00000
15.0 - 30.0	1.00000±0.00000	–	–	1.00000±0.00000	–	–	–	–	1.00000±0.00000

Table D.15: Identification efficiencies for pions, kaons and protons in $N_{\mathrm{tracks}} > 2$ with the IRT method at $rQp > 1.0$.

Momentum range	Q_{π}^{π}	Q_{π}^{K}	Q_{π}^{p}	Q_{K}^{π}	$Q_{\mathrm{K}}^{\mathrm{K}}$	$Q_{\mathrm{K}}^{\mathrm{p}}$	Q_{p}^{π}	$Q_{\mathrm{p}}^{\mathrm{K}}$	$Q_{\mathrm{p}}^{\mathrm{p}}$
0.00 - 0.50	–	–	–	–	–	–	–	–	–
0.50 - 1.00	0.99898±0.00051	0.00102±0.00051	–	–	–	–	–	–	–
1.00 - 1.50	0.97367±0.00117	0.00548±0.00054	0.02086±0.00104	–	–	–	–	–	–
1.50 - 2.00	0.95158±0.00130	0.00982±0.00060	0.03859±0.00117	–	0.20000±0.17888	0.80000±0.17888	0.11787±0.01988	0.14829±0.02191	0.73384±0.02725
2.00 - 2.25	0.96011±0.00167	0.00648±0.00068	0.03341±0.00153	0.04988±0.00769	0.66085±0.01672	0.28928±0.01601	0.11867±0.00474	0.10343±0.00446	0.77790±0.00609
2.25 - 2.50	0.96325±0.00162	0.00238±0.00042	0.03438±0.00157	0.05074±0.00613	0.72053±0.01254	0.22873±0.01174	0.13089±0.00515	0.03710±0.00289	0.83201±0.00571
2.50 - 2.75	0.96272±0.00166	0.00193±0.00039	0.03535±0.00162	0.04658±0.00551	0.74657±0.01138	0.20685±0.01060	0.11813±0.00503	0.02917±0.00262	0.85270±0.00553
2.75 - 3.00	0.97021±0.00152	0.00137±0.00033	0.02842±0.00149	0.04051±0.00500	0.75884±0.01085	0.20064±0.01016	0.12513±0.00540	0.03148±0.00285	0.84338±0.00594
3.00 - 3.25	0.97291±0.00150	0.00136±0.00034	0.02572±0.00146	0.04070±0.00502	0.78553±0.01043	0.17377±0.00963	0.13125±0.00586	0.02529±0.00272	0.84347±0.00630
3.25 - 3.50	0.99091±0.00085	0.00217±0.00042	0.00691±0.00074	0.02483±0.00370	0.76185±0.01012	0.21332±0.00973	0.03963±0.00369	0.03177±0.00331	0.92860±0.00487
3.50 - 3.75	0.99418±0.00069	0.00200±0.00041	0.00383±0.00056	0.00973±0.00235	0.77046±0.01006	0.21981±0.00991	0.02015±0.00285	0.02508±0.00317	0.95477±0.00421
3.75 - 4.00	0.99121±0.00089	0.00211±0.00044	0.00668±0.00078	0.00630±0.00199	0.85390±0.00886	0.13980±0.00870	0.03787±0.00657	0.00710±0.00289	0.95503±0.00713
4.00 - 4.25	0.99098±0.00093	0.00394±0.00061	0.00509±0.00070	0.01190±0.00287	0.91317±0.00745	0.07493±0.00697	–	0.00069±0.00069	0.99931±0.00069
4.25 - 4.50	0.99205±0.00090	0.00341±0.00059	0.00454±0.00068	0.01367±0.00320	0.93850±0.00662	0.04784±0.00588	0.00242±0.00121	0.00484±0.00171	0.99274±0.00209
4.50 - 4.75	0.99193±0.00093	0.00371±0.00063	0.00436±0.00069	0.00844±0.00266	0.96203±0.00555	0.02954±0.00492	0.00199±0.00115	0.00266±0.00133	0.99535±0.00175
4.75 - 5.00	0.99022±0.00107	0.00453±0.00073	0.00525±0.00079	0.01397±0.00336	0.96549±0.00523	0.02054±0.00407	0.00197±0.00113	0.00328±0.00146	0.99475±0.00185
5.00 - 5.25	0.99202±0.00100	0.00355±0.00067	0.00444±0.00075	0.00797±0.00265	0.97874±0.00429	0.01329±0.00341	0.00071±0.00071	0.00071±0.00071	0.99858±0.00100
5.25 - 5.50	0.99251±0.00101	0.00436±0.00077	0.00313±0.00065	0.01431±0.00345	0.97138±0.00484	0.01431±0.00345	0.00306±0.00153	0.00459±0.00187	0.99234±0.00241
5.50 - 5.75	0.99265±0.00105	0.00330±0.00070	0.00405±0.00078	0.00655±0.00247	0.98502±0.00372	0.00843±0.00280	0.00088±0.00088	0.00177±0.00125	0.99735±0.00153
5.75 - 6.00	0.99078±0.00122	0.00469±0.00087	0.00453±0.00085	0.00390±0.00195	0.98343±0.00399	0.01267±0.00349	–	0.00555±0.00226	0.99445±0.00226
6.00 - 6.50	0.99165±0.00087	0.00399±0.00060	0.00436±0.00063	0.00427±0.00151	0.98718±0.00260	0.00855±0.00213	–	0.00689±0.00184	0.99311±0.00184
6.50 - 7.00	0.98885±0.00107	0.00521±0.00074	0.00594±0.00078	0.00358±0.00146	0.98448±0.00302	0.01194±0.00265	–	0.00497±0.00175	0.99503±0.00175
7.00 - 7.50	0.99219±0.00100	0.00525±0.00082	0.00256±0.00057	0.00420±0.00171	0.98389±0.00333	0.01190±0.00287	–	0.01189±0.00295	0.98811±0.00295
7.50 - 8.00	0.99405±0.00094	0.00253±0.00061	0.00342±0.00071	0.00422±0.00188	0.98480±0.00356	0.01098±0.00303	–	0.01108±0.00294	0.98892±0.00294
8.00 - 8.50	0.99252±0.00114	0.00504±0.00093	0.00243±0.00065	0.00305±0.00176	0.98374±0.00403	0.01321±0.00364	–	0.01072±0.00337	0.98928±0.00337
8.50 - 9.00	0.99094±0.00136	0.00515±0.00103	0.00391±0.00090	0.00387±0.00223	0.98323±0.00461	0.01290±0.00405	–	0.01933±0.00494	0.98067±0.00494
9.00 - 9.50	0.98807±0.00168	0.00787±0.00136	0.00406±0.00098	0.00362±0.00255	0.98734±0.00475	0.00904±0.00403	–	0.03412±0.00699	0.96588±0.00699
9.50 - 10.0	0.99141±0.00156	0.00602±0.00131	0.00258±0.00086	0.00245±0.00245	0.97304±0.00802	0.02451±0.00766	0.00357±0.00252	0.02500±0.00660	0.97143±0.00704
10.0 - 11.0	0.99303±0.00114	0.00358±0.00082	0.00339±0.00080	–	0.99551±0.00200	0.00449±0.00200	0.00267±0.00154	0.13636±0.01025	0.86096±0.01033
11.0 - 12.0	0.99521±0.00113	0.00399±0.00103	0.00080±0.00046	0.00240±0.00169	0.99640±0.00207	0.00120±0.00120	0.00133±0.00133	0.02520±0.00571	0.97347±0.00585
12.0 - 13.0	0.99596±0.00127	0.00363±0.00121	0.00040±0.00040	0.00202±0.00201	0.99395±0.00348	0.00403±0.00285	0.00236±0.00236	–	0.99764±0.00236
13.0 - 14.0	0.98962±0.00251	0.01038±0.00251	–	0.01111±0.00638	0.98889±0.00638	–	–	–	1.00000±0.00000
14.0 - 15.0	0.98351±0.00397	0.01649±0.00397	–	–	0.99194±0.00803	0.00806±0.00803	0.00606±0.00604	–	0.99394±0.00604
15.0 - 30.0	0.97917±0.00383	0.01940±0.00370	0.00144±0.00102	–	0.98462±0.01527	0.01538±0.01527	0.01500±0.00860	0.01000±0.00704	0.97500±0.01104

Table D.16: Identification purities and contaminations for pions, kaons and protons in $N_{\mathrm{tracks}} = 1$ with the IRT method at $rQp > 1.0$.

Momentum range	Q_π^π	Q_π^{K}	Q_π^{p}	Q_{K}^π	$Q_{\mathrm{K}}^{\mathrm{K}}$	$Q_{\mathrm{K}}^{\mathrm{p}}$	Q_{p}^π	$Q_{\mathrm{p}}^{\mathrm{K}}$	$Q_{\mathrm{p}}^{\mathrm{p}}$
0.00 - 0.50	–	–	–	–	–	–	–	–	–
0.50 - 1.00	0.99887±0.00051	0.00113±0.00051	–	–	–	–	–	–	–
1.00 - 1.50	0.93410±0.00170	0.01520±0.00084	0.05069±0.00150	–	–	–	–	–	–
1.50 - 2.00	0.88530±0.00187	0.02296±0.00088	0.09174±0.00169	0.14286±0.13226	0.14286±0.13226	0.71429±0.17075	0.16970±0.02922	0.10909±0.02427	0.72121±0.03491
2.00 - 2.25	0.88971±0.00294	0.01687±0.00121	0.09342±0.00273	0.12432±0.01085	0.35027±0.01569	0.52541±0.01642	0.18881±0.00708	0.11551±0.00578	0.69568±0.00832
2.25 - 2.50	0.88611±0.00311	0.00768±0.00086	0.10620±0.00302	0.09986±0.00795	0.43108±0.01313	0.46906±0.01323	0.20033±0.00813	0.06389±0.00497	0.73578±0.00895
2.50 - 2.75	0.89396±0.00318	0.00619±0.00081	0.09985±0.00310	0.09953±0.00776	0.46066±0.01293	0.43981±0.01287	0.20906±0.00870	0.04117±0.00425	0.74977±0.00926
2.75 - 3.00	0.90583±0.00320	0.00444±0.00073	0.08973±0.00313	0.08936±0.00731	0.51643±0.01281	0.39422±0.01253	0.17054±0.00864	0.04065±0.00454	0.78881±0.00938
3.00 - 3.25	0.91611±0.00320	0.00359±0.00069	0.08030±0.00313	0.09565±0.00792	0.52391±0.01344	0.38044±0.01307	0.20242±0.00965	0.02999±0.00410	0.76759±0.01014
3.25 - 3.50	0.96340±0.00196	0.00882±0.00098	0.02778±0.00172	0.05045±0.00487	0.53610±0.01109	0.41345±0.01095	0.09672±0.00836	0.02558±0.00446	0.87770±0.00926
3.50 - 3.75	0.96947±0.00183	0.01010±0.00107	0.02043±0.00151	0.02465±0.00355	0.55742±0.01137	0.41793±0.01129	0.06145±0.00733	0.04935±0.00661	0.88920±0.00958
3.75 - 4.00	0.96864±0.00195	0.01087±0.00116	0.02049±0.00158	0.01637±0.00346	0.62500±0.01321	0.35863±0.01308	0.11443±0.01588	0.02239±0.00738	0.86318±0.01714
4.00 - 4.25	0.96898±0.00202	0.01300±0.00132	0.01801±0.00155	0.01589±0.00421	0.78093±0.01394	0.20318±0.01356	0.00955±0.00388	0.01592±0.00500	0.97452±0.00629
4.25 - 4.50	0.96457±0.00232	0.01480±0.00152	0.02063±0.00178	0.03694±0.00673	0.83185±0.01335	0.13121±0.01205	0.00421±0.00242	0.01683±0.00482	0.97896±0.00537
4.50 - 4.75	0.96571±0.00240	0.01427±0.00156	0.02001±0.00185	0.02917±0.00678	0.87034±0.01352	0.10049±0.01210	0.00290±0.00205	0.01306±0.00433	0.98403±0.00478
4.75 - 5.00	0.96924±0.00239	0.01153±0.00148	0.01922±0.00190	0.02393±0.00632	0.89744±0.01254	0.07863±0.01113	0.00489±0.00281	0.01303±0.00458	0.98208±0.00535
5.00 - 5.25	0.96835±0.00257	0.01292±0.00166	0.01873±0.00199	0.02053±0.00643	0.94045±0.01072	0.03901±0.00877	0.00185±0.00185	0.00741±0.00369	0.99074±0.00412
5.25 - 5.50	0.96405±0.00288	0.01797±0.00206	0.01797±0.00206	0.00680±0.00391	0.96825±0.00835	0.02494±0.00743	0.00364±0.00257	0.01091±0.00443	0.98545±0.00511
5.50 - 5.75	0.96557±0.00305	0.01652±0.00213	0.01792±0.00222	0.01408±0.00571	0.95540±0.01000	0.03052±0.00833	–	0.01639±0.00575	0.98361±0.00575
5.75 - 6.00	0.96566±0.00313	0.01539±0.00212	0.01895±0.00235	0.01081±0.00538	0.96757±0.00921	0.02162±0.00756	–	0.01869±0.00655	0.98131±0.00655
6.00 - 6.50	0.96064±0.00259	0.02021±0.00187	0.01915±0.00182	0.01349±0.00474	0.94435±0.00941	0.04216±0.00825	–	0.00887±0.00334	0.99113±0.00334
6.50 - 7.00	0.95955±0.00295	0.02045±0.00212	0.02000±0.00210	0.00545±0.00314	0.96545±0.00779	0.02909±0.00717	–	0.00822±0.00366	0.99178±0.00366
7.00 - 7.50	0.96248±0.00315	0.01972±0.00230	0.01780±0.00219	–	0.98022±0.00653	0.01978±0.00653	0.00208±0.00208	0.00417±0.00294	0.99375±0.00360
7.50 - 8.00	0.95600±0.00385	0.02042±0.00265	0.02358±0.00285	0.00295±0.00295	0.95870±0.01081	0.03835±0.01043	–	0.01644±0.00666	0.98356±0.00666
8.00 - 8.50	0.96064±0.00416	0.02105±0.00307	0.01831±0.00287	–	0.96564±0.01068	0.03436±0.01068	–	0.01333±0.00662	0.98667±0.00662
8.50 - 9.00	0.96138±0.00463	0.01960±0.00333	0.01902±0.00328	–	0.98591±0.00807	0.01408±0.00807	–	0.00971±0.00683	0.99029±0.00683
9.00 - 9.50	0.95833±0.00536	0.02443±0.00414	0.01724±0.00349	–	0.97761±0.01278	0.02239±0.01278	–	0.02645±0.01167	0.97354±0.01167
9.50 - 10.0	0.95644±0.00615	0.02541±0.00474	0.01815±0.00402	–	1.00000±0.00000	–	–	0.02239±0.01278	0.97761±0.01278
10.0 - 11.0	0.96699±0.00469	0.01513±0.00320	0.01788±0.00348	0.00400±0.00399	0.96400±0.01178	0.03200±0.01113	–	0.14577±0.01905	0.85423±0.01905
11.0 - 12.0	0.97977±0.00472	0.01011±0.00335	0.01011±0.00335	0.00575±0.00573	0.98851±0.00808	0.00575±0.00573	–	0.03349±0.01245	0.96651±0.01245
12.0 - 13.0	0.98662±0.00502	0.00765±0.00381	0.00574±0.00330	0.01852±0.01297	0.97222±0.01581	0.00926±0.00922	–	0.02564±0.01461	0.97436±0.01461
13.0 - 14.0	0.97931±0.00836	0.01034±0.00594	0.01034±0.00594	–	0.97143±0.02816	0.02857±0.02816	–	–	1.00000±0.00000
14.0 - 15.0	0.96429±0.01326	0.02551±0.01126	0.01020±0.00718	–	1.00000±0.00000	–	–	–	1.00000±0.00000
15.0 - 30.0	0.94152±0.01794	0.05848±0.01794	–	–	1.00000±0.00000	–	–	–	1.00000±0.00000

Table D.17: Identification purities and contaminations for pions, kaons and protons in $N_{\mathrm{tracks}} = 2$ with the IRT method at $rQp > 1.0$.

Momentum range	Q_{π}^{π}	Q_{π}^{K}	Q_{π}^{p}	Q_{K}^{π}	$Q_{\mathrm{K}}^{\mathrm{K}}$	$Q_{\mathrm{K}}^{\mathrm{p}}$	Q_{p}^{π}	$Q_{\mathrm{p}}^{\mathrm{K}}$	$Q_{\mathrm{p}}^{\mathrm{p}}$
0.00 - 0.50	–	–	–	–	–	–	–	–	–
0.50 - 1.00	0.99832±0.00119	0.00168±0.00119	–	–	–	–	–	–	–
1.00 - 1.50	0.92652±0.00344	0.02090±0.00189	0.05259±0.00295	–	–	–	–	–	–
1.50 - 2.00	0.86438±0.00395	0.03160±0.00202	0.10401±0.00353	0.33333±0.27217	–	0.66667±0.27217	0.22222±0.06929	0.13889±0.05764	0.63889±0.08005
2.00 - 2.25	0.86555±0.00658	0.02309±0.00290	0.11136±0.00607	0.10000±0.02070	0.35238±0.03297	0.54762±0.03435	0.21970±0.01802	0.12311±0.01430	0.65720±0.02066
2.25 - 2.50	0.85727±0.00736	0.00798±0.00187	0.13475±0.00719	0.10210±0.01659	0.41742±0.02702	0.48048±0.02738	0.26750±0.02213	0.07250±0.01297	0.66000±0.02369
2.50 - 2.75	0.86686±0.00757	0.00944±0.00216	0.12370±0.00734	0.10089±0.01641	0.43027±0.02697	0.46884±0.02718	0.27222±0.02346	0.05000±0.01149	0.67778±0.02463
2.75 - 3.00	0.87847±0.00794	0.00649±0.00195	0.11504±0.00775	0.11549±0.01696	0.44507±0.02638	0.43944±0.02634	0.22839±0.02332	0.03086±0.00961	0.74074±0.02435
3.00 - 3.25	0.88110±0.00861	0.00354±0.00158	0.11536±0.00850	0.09333±0.01680	0.47000±0.02882	0.43667±0.02864	0.15472±0.02221	0.05283±0.01374	0.79245±0.02491
3.25 - 3.50	0.96802±0.00393	0.01049±0.00228	0.02149±0.00324	0.06331±0.01051	0.46741±0.02153	0.46927±0.02154	0.06818±0.01900	0.03409±0.01368	0.89773±0.02284
3.50 - 3.75	0.95524±0.00459	0.02213±0.00326	0.02263±0.00330	0.03991±0.00922	0.50776±0.02354	0.45233±0.02344	0.11765±0.02763	0.05882±0.02018	0.82353±0.03269
3.75 - 4.00	0.95666±0.00477	0.01262±0.00261	0.03072±0.00404	0.00974±0.00560	0.58442±0.02808	0.40584±0.02798	0.16364±0.04988	0.01818±0.01802	0.81818±0.05201
4.00 - 4.25	0.95839±0.00505	0.01793±0.00336	0.02369±0.00385	0.04118±0.01524	0.65882±0.03636	0.30000±0.03515	0.06329±0.02739	0.01266±0.01258	0.92405±0.02981
4.25 - 4.50	0.94404±0.00620	0.02326±0.00406	0.03270±0.00479	0.01379±0.00969	0.76552±0.03518	0.22069±0.03444	0.00813±0.00810	0.01626±0.01140	0.97561±0.01391
4.50 - 4.75	0.96199±0.00556	0.01605±0.00365	0.02196±0.00426	0.06667±0.02434	0.73333±0.04316	0.20000±0.03904	0.01460±0.01025	0.01460±0.01025	0.97080±0.01438
4.75 - 5.00	0.96099±0.00597	0.01332±0.00354	0.02569±0.00488	–	0.91139±0.03197	0.08861±0.03197	–	0.02479±0.01414	0.97521±0.01414
5.00 - 5.25	0.95847±0.00660	0.01858±0.00446	0.02295±0.00495	0.02273±0.01589	0.88636±0.03383	0.09091±0.03065	–	–	1.00000±0.00000
5.25 - 5.50	0.95695±0.00712	0.02091±0.00502	0.02214±0.00516	–	0.83562±0.04338	0.16438±0.04338	0.01010±0.01005	–	0.98990±0.01005
5.50 - 5.75	0.93068±0.00975	0.03245±0.00680	0.03687±0.00724	–	0.95082±0.02769	0.04918±0.02769	–	0.01299±0.01290	0.98701±0.01290
5.75 - 6.00	0.94061±0.00947	0.02889±0.00671	0.03050±0.00689	0.02381±0.02352	0.95238±0.03286	0.02381±0.02352	–	–	1.00000±0.00000
6.00 - 6.50	0.94835±0.00711	0.02479±0.00500	0.02686±0.00520	–	0.94737±0.02561	0.05263±0.02561	–	0.00813±0.00810	0.99187±0.00810
6.50 - 7.00	0.95291±0.00788	0.02493±0.00580	0.02216±0.00548	0.01493±0.01481	0.95522±0.02527	0.02985±0.02079	–	–	1.00000±0.00000
7.00 - 7.50	0.94563±0.00920	0.03460±0.00742	0.01977±0.00565	0.01887±0.01869	0.92453±0.03628	0.05660±0.03174	–	0.03125±0.02175	0.96875±0.02175
7.50 - 8.00	0.94792±0.01134	0.03125±0.00888	0.02083±0.00729	–	0.96970±0.02984	0.03030±0.02984	–	–	1.00000±0.00000
8.00 - 8.50	0.96785±0.01000	0.01929±0.00780	0.01286±0.00639	–	0.96667±0.03277	0.03333±0.03277	–	0.03846±0.03771	0.96154±0.03771
8.50 - 9.00	0.94561±0.01467	0.04184±0.01295	0.01255±0.00720	–	1.00000±0.00000	–	–	–	1.00000±0.00000
9.00 - 9.50	0.94203±0.01624	0.03865±0.01340	0.01932±0.00957	–	1.00000±0.00000	–	–	0.05000±0.04873	0.95000±0.04873
9.50 - 10.0	0.91304±0.02399	0.05072±0.01868	0.03623±0.01591	–	1.00000±0.00000	–	–	–	1.00000±0.00000
10.0 - 11.0	0.95705±0.01588	0.02454±0.01212	0.01840±0.01053	–	1.00000±0.00000	–	–	0.10714±0.05845	0.89286±0.05845
11.0 - 12.0	0.98591±0.01398	–	0.01408±0.01398	–	1.00000±0.00000	–	–	–	1.00000±0.00000
12.0 - 13.0	1.00000±0.00000	–	–	–	1.00000±0.00000	–	–	–	1.00000±0.00000
13.0 - 14.0	1.00000±0.00000	–	–	–	1.00000±0.00000	–	–	–	1.00000±0.00000
14.0 - 15.0	0.88889±0.10476	0.11111±0.10476	–	–	1.00000±0.00000	–	–	–	1.00000±0.00000
15.0 - 30.0	0.92308±0.07391	0.07692±0.07391	–	–	–	–	–	–	1.00000±0.00000

Table D.18: Identification purities and contaminations for pions, kaons and protons in $N_{\mathrm{tracks}} > 2$ with the IRT method at $rQp > 1.0$.

D.2 Elements of P and Q Matrices with the DRT Method

The tables of the results for the elements of the P and Q matrices obtained with the DRT method are shown in the following pages.

Momentum range	$\mathcal{P}_{\pi}^{\pi}$	$\mathcal{P}_{\pi}^{\mathrm{K}}$	$\mathcal{P}_{\pi}^{\mathrm{p}}$	$\mathcal{P}_{\mathrm{K}}^{\pi}$	$\mathcal{P}_{\mathrm{K}}^{\mathrm{K}}$	$\mathcal{P}_{\mathrm{K}}^{\mathrm{p}}$	$\mathcal{P}_{\mathrm{p}}^{\pi}$	$\mathcal{P}_{\mathrm{p}}^{\mathrm{K}}$	$\mathcal{P}_{\mathrm{p}}^{\mathrm{p}}$
0.00 - 0.50	–	–	–	–	–	–	–	–	–
0.50 - 1.00	1.00000±0.02163	–	–	1.00000±0.53452	–	–	–	–	–
1.00 - 1.50	1.00000±0.01013	–	–	1.00000±0.11146	–	–	1.00000±0.05837	–	–
1.50 - 2.00	0.99916±0.00853	0.00004±0.00004	0.00080±0.00017	0.88915±0.06294	0.01415±0.00582	0.09670±0.01581	0.88189±0.03171	0.00606±0.00192	0.11205±0.00869
2.00 - 2.25	0.95878±0.01097	0.01064±0.00083	0.03058±0.00142	0.11483±0.01010	0.59410±0.02748	0.29107±0.01731	0.13391±0.00566	0.11409±0.00518	0.75200±0.01667
2.25 - 2.50	0.95356±0.01090	0.01620±0.00102	0.03023±0.00141	0.05019±0.00638	0.87104±0.03548	0.07876±0.00810	0.13261±0.00564	0.14234±0.00586	0.72504±0.01626
2.50 - 2.75	0.96343±0.01118	0.01389±0.00096	0.02268±0.00124	0.04318±0.00551	0.90823±0.03420	0.04858±0.00586	0.12944±0.00558	0.14328±0.00591	0.72727±0.01635
2.75 - 3.00	0.99195±0.01156	0.00271±0.00043	0.00535±0.00060	0.02941±0.00440	0.91368±0.03344	0.05691±0.00620	0.11774±0.00555	0.14607±0.00626	0.73619±0.01730
3.00 - 3.25	0.99267±0.01187	0.00135±0.00031	0.00598±0.00065	0.03054±0.00452	0.92203±0.03393	0.04743±0.00568	0.10545±0.00559	0.13630±0.00645	0.75825±0.01891
3.25 - 3.50	0.99415±0.01212	0.00059±0.00021	0.00526±0.00063	0.02053±0.00367	0.92816±0.03388	0.05131±0.00588	0.08916±0.00532	0.11713±0.00617	0.79371±0.02037
3.50 - 3.75	0.99545±0.01249	0.00118±0.00030	0.00338±0.00052	0.03515±0.00491	0.93037±0.03451	0.03448±0.00486	0.08591±0.00551	0.13147±0.00696	0.78262±0.02131
3.75 - 4.00	0.99419±0.01311	0.00139±0.00035	0.00442±0.00062	0.03539±0.00486	0.93694±0.03417	0.02767±0.00428	0.07864±0.00548	0.10415±0.00638	0.81722±0.02294
4.00 - 4.25	0.99680±0.01349	0.00146±0.00037	0.00174±0.00040	0.04092±0.00522	0.92711±0.03380	0.03197±0.00459	0.04829±0.00444	0.06153±0.00504	0.89019±0.02560
4.25 - 4.50	0.99773±0.01401	0.00049±0.00022	0.00177±0.00042	0.04639±0.00567	0.91518±0.03408	0.03844±0.00514	0.04364±0.00437	0.04238±0.00431	0.91397±0.02709
4.50 - 4.75	0.99771±0.01441	0.00073±0.00028	0.00156±0.00040	0.05289±0.00627	0.91114±0.03504	0.03597±0.00513	0.03761±0.00439	0.03216±0.00405	0.93023±0.02981
4.75 - 5.00	0.99750±0.01506	0.00148±0.00041	0.00102±0.00034	0.05278±0.00621	0.91042±0.03475	0.03681±0.00515	0.03338±0.00421	0.02363±0.00352	0.94299±0.03068
5.00 - 5.25	0.99805±0.01557	0.00109±0.00037	0.00085±0.00032	0.05543±0.00662	0.92060±0.03639	0.02397±0.00429	0.02798±0.00401	0.01679±0.00309	0.95523±0.03233
5.25 - 5.50	0.99702±0.01607	0.00233±0.00055	0.00065±0.00029	0.06395±0.00691	0.90794±0.03489	0.02811±0.00451	0.01784±0.00334	0.01661±0.00322	0.96556±0.03416
5.50 - 5.75	0.99928±0.01691	0.00029±0.00020	0.00043±0.00025	0.05868±0.00702	0.91673±0.03733	0.02458±0.00447	0.02339±0.00412	0.01347±0.00311	0.96315±0.03661
5.75 - 6.00	0.99953±0.01763	0.00031±0.00022	0.00016±0.00016	0.06021±0.00721	0.91131±0.03765	0.02848±0.00488	0.02575±0.00441	0.01840±0.00371	0.95585±0.03709
6.00 - 6.50	0.99913±0.01319	0.00052±0.00021	0.00035±0.00017	0.06556±0.00560	0.90211±0.02776	0.03233±0.00387	0.01735±0.00267	0.01614±0.00257	0.96652±0.02769
6.50 - 7.00	0.99930±0.01414	0.00020±0.00014	0.00050±0.00022	0.06850±0.00605	0.91150±0.02952	0.02000±0.00319	0.02779±0.00377	0.01687±0.00292	0.95534±0.03045
7.00 - 7.50	0.99938±0.01568	0.00012±0.00012	0.00049±0.00025	0.06214±0.00613	0.90935±0.03146	0.02851±0.00409	0.01398±0.00294	0.02492±0.00394	0.96109±0.03385
7.50 - 8.00	0.99986±0.01693	–	0.00014±0.00014	0.05595±0.00616	0.91511±0.03357	0.02894±0.00438	0.02531±0.00410	0.02596±0.00416	0.94873±0.03464
8.00 - 8.50	0.99933±0.01826	0.00033±0.00024	0.00033±0.00024	0.06440±0.00712	0.89563±0.03545	0.03997±0.00555	0.02647±0.00474	0.05790±0.00712	0.91563±0.03809
8.50 - 9.00	0.99980±0.01995	0.00020±0.00020	–	0.05111±0.00666	0.90437±0.03768	0.04452±0.00619	0.02792±0.00535	0.08175±0.00939	0.89033±0.04096
9.00 - 9.50	1.00000±0.02152	–	–	0.27793±0.01826	0.68545±0.03294	0.03662±0.00597	0.03160±0.00607	0.12867±0.01280	0.83973±0.04176
9.50 - 10.0	0.99917±0.02346	0.00055±0.00039	0.00028±0.00028	0.04730±0.00747	0.95045±0.04569	0.00225±0.00159	0.01740±0.00487	0.12316±0.01361	0.85944±0.04625
10.0 - 11.0	0.99928±0.01893	0.00018±0.00018	0.00054±0.00031	0.05336±0.00624	0.94456±0.03568	0.00208±0.00120	0.02642±0.00506	0.10472±0.01045	0.86887±0.03914
11.0 - 12.0	0.99975±0.02251	0.00025±0.00025	–	0.09020±0.00977	0.90883±0.04102	0.00097±0.00097	0.02008±0.00507	0.06650±0.00943	0.91343±0.04683
12.0 - 13.0	0.99962±0.02759	0.00038±0.00038	–	0.13525±0.01448	0.86475±0.04694	–	0.01345±0.00553	0.05381±0.01128	0.93273±0.06358
13.0 - 14.0	0.99830±0.03362	0.00170±0.00098	–	0.22824±0.02329	0.77176±0.05143	–	0.01980±0.00816	0.05611±0.01398	0.92409±0.07660
14.0 - 15.0	0.99908±0.04279	0.00092±0.00092	–	0.30537±0.03657	0.69463±0.06285	–	0.03448±0.01432	0.04598±0.01662	0.91954±0.10072
15.0 - 30.0	0.99631±0.03496	0.00123±0.00087	0.00246±0.00123	0.53796±0.04236	0.45770±0.03804	0.00434±0.00307	0.00905±0.00643	0.07240±0.01874	0.91855±0.08930

Table D.19: Identification efficiencies for pions, kaons and protons in $N_{\mathrm{tracks}} = 1$ with the DRT method at $rQp > 0.0$.

Momentum range	$\mathcal{P}_{\pi}^{\pi}$	$\mathcal{P}_{\pi}^{\mathrm{K}}$	$\mathcal{P}_{\pi}^{\mathrm{p}}$	$\mathcal{P}_{\mathrm{K}}^{\pi}$	$\mathcal{P}_{\mathrm{K}}^{\mathrm{K}}$	$\mathcal{P}_{\mathrm{K}}^{\mathrm{p}}$	$\mathcal{P}_{\mathrm{p}}^{\pi}$	$\mathcal{P}_{\mathrm{p}}^{\mathrm{K}}$	$\mathcal{P}_{\mathrm{p}}^{\mathrm{p}}$
0.00 - 0.50	–	–	–	–	–	–	–	–	–
0.50 - 1.00	1.00000±0.01993	–	–	1.00000±0.31623	–	–	–	–	–
1.00 - 1.50	1.00000±0.00963	–	–	1.00000±0.06202	–	–	1.00000±0.03471	–	–
1.50 - 2.00	0.99921±0.00848	0.00029±0.00010	0.00050±0.00013	0.98041±0.04361	0.00490±0.00220	0.01469±0.00382	0.96836±0.02179	0.00598±0.00122	0.02566±0.00256
2.00 - 2.25	0.95427±0.01138	0.03088±0.00149	0.01485±0.00102	0.30141±0.01857	0.54921±0.02734	0.14938±0.01228	0.36565±0.01074	0.27262±0.00895	0.36173±0.01066
2.25 - 2.50	0.94091±0.01151	0.04581±0.00186	0.01328±0.00099	0.18874±0.01363	0.76987±0.03358	0.04139±0.00597	0.36155±0.01085	0.33764±0.01039	0.30081±0.00967
2.50 - 2.75	0.94555±0.01193	0.04347±0.00187	0.01098±0.00093	0.16417±0.01228	0.81294±0.03411	0.02289±0.00430	0.37717±0.01151	0.35143±0.01100	0.27141±0.00938
2.75 - 3.00	0.98714±0.01280	0.00919±0.00088	0.00367±0.00055	0.11510±0.00970	0.86584±0.03442	0.01906±0.00377	0.34966±0.01156	0.34286±0.01142	0.30747±0.01067
3.00 - 3.25	0.99062±0.01327	0.00447±0.00063	0.00491±0.00066	0.10137±0.00948	0.88013±0.03649	0.01850±0.00389	0.33733±0.01193	0.32062±0.01155	0.34205±0.01203
3.25 - 3.50	0.99364±0.01392	0.00274±0.00052	0.00362±0.00060	0.11547±0.00986	0.87019±0.03505	0.01434±0.00331	0.32899±0.01276	0.32414±0.01265	0.34687±0.01319
3.50 - 3.75	0.99428±0.01463	0.00259±0.00053	0.00313±0.00058	0.10686±0.00961	0.86896±0.03559	0.02418±0.00440	0.31000±0.01320	0.35165±0.01429	0.33834±0.01394
3.75 - 4.00	0.99566±0.01548	0.00229±0.00053	0.00205±0.00050	0.12169±0.01097	0.85803±0.03749	0.02028±0.00427	0.27036±0.01298	0.27821±0.01321	0.45142±0.01793
4.00 - 4.25	0.99501±0.01614	0.00276±0.00060	0.00223±0.00054	0.16453±0.01323	0.78976±0.03594	0.04570±0.00661	0.17953±0.01100	0.16867±0.01062	0.65180±0.02481
4.25 - 4.50	0.99524±0.01747	0.00215±0.00058	0.00261±0.00063	0.17951±0.01437	0.78146±0.03685	0.03902±0.00629	0.17544±0.01158	0.11436±0.00910	0.71020±0.02809
4.50 - 4.75	0.99590±0.01842	0.00222±0.00062	0.00188±0.00057	0.19135±0.01570	0.75243±0.03776	0.05622±0.00801	0.17293±0.01235	0.07519±0.00780	0.75188±0.03147
4.75 - 5.00	0.99773±0.01941	0.00094±0.00042	0.00132±0.00050	0.17590±0.01579	0.78434±0.04106	0.03976±0.00706	0.16285±0.01291	0.05634±0.00724	0.78081±0.03499
5.00 - 5.25	0.99832±0.02047	0.00105±0.00047	0.00063±0.00036	0.20530±0.01810	0.75629±0.04194	0.03841±0.00727	0.13237±0.01203	0.04734±0.00692	0.82029±0.03798
5.25 - 5.50	0.99859±0.02167	0.00047±0.00033	0.00094±0.00047	0.25865±0.02122	0.70263±0.04068	0.03873±0.00746	0.12578±0.01213	0.04782±0.00722	0.82640±0.03961
5.50 - 5.75	1.00000±0.02352	–	–	0.23734±0.02062	0.72504±0.04254	0.03763±0.00752	0.08844±0.01065	0.04127±0.00712	0.87028±0.04381
5.75 - 6.00	0.99883±0.02414	0.00088±0.00051	0.00029±0.00029	0.21177±0.02077	0.75966±0.04740	0.02857±0.00703	0.10748±0.01273	0.02449±0.00584	0.86803±0.04697
6.00 - 6.50	0.99877±0.01876	0.00106±0.00043	0.00018±0.00018	0.25833±0.01811	0.71443±0.03516	0.02725±0.00531	0.09158±0.00859	0.03323±0.00504	0.87518±0.03481
6.50 - 7.00	0.99933±0.02108	0.00044±0.00031	0.00022±0.00022	0.24463±0.01807	0.72961±0.03680	0.02575±0.00532	0.07935±0.00905	0.03633±0.00600	0.88432±0.03991
7.00 - 7.50	0.99919±0.02326	0.00054±0.00038	0.00027±0.00027	0.25064±0.02007	0.71594±0.03974	0.03342±0.00666	0.10559±0.01204	0.04472±0.00762	0.84969±0.04419
7.50 - 8.00	1.00000±0.02645	–	–	0.25585±0.02318	0.71237±0.04517	0.03177±0.00740	0.12315±0.01433	0.09347±0.01231	0.78338±0.04553
8.00 - 8.50	1.00000±0.03015	–	–	0.24462±0.02441	0.71820±0.04914	0.03718±0.00869	0.10874±0.01530	0.11845±0.01604	0.77282±0.05158
8.50 - 9.00	0.99943±0.03379	–	0.00057±0.00057	0.22573±0.02499	0.71332±0.05252	0.06095±0.01208	0.13706±0.01989	0.14975±0.02090	0.71320±0.05569
9.00 - 9.50	0.99928±0.03793	–	0.00072±0.00072	0.42059±0.04192	0.53235±0.04898	0.04706±0.01204	0.12693±0.02104	0.13313±0.02161	0.73994±0.06313
9.50 - 10.0	1.00000±0.04245	–	–	0.24643±0.03312	0.75357±0.06870	–	0.14226±0.02608	0.15481±0.02735	0.70293±0.07077
10.0 - 11.0	1.00000±0.03590	–	–	0.21951±0.02693	0.77507±0.06106	0.00542±0.00384	0.15531±0.02211	0.16349±0.02277	0.68120±0.05586
11.0 - 12.0	1.00000±0.04529	–	–	0.17200±0.02840	0.82800±0.07781	–	0.11159±0.02307	0.15880±0.02810	0.72961±0.07359
12.0 - 13.0	1.00000±0.05913	–	–	0.24845±0.04389	0.75155±0.09042	–	0.02439±0.01425	0.18699±0.04248	0.78862±0.10709
13.0 - 14.0	1.00000±0.07943	–	–	0.36046±0.07551	0.63953±0.11042	–	0.12500±0.04193	0.12500±0.04193	0.75000±0.12809
14.0 - 15.0	1.00000±0.10000	–	–	0.51667±0.11428	0.48333±0.10931	–	0.08333±0.05008	0.08333±0.05008	0.83333±0.20601
15.0 - 30.0	1.00000±0.10101	–	–	0.64407±0.13397	0.35593±0.09044	–	0.13889±0.06629	0.22222±0.08686	0.63889±0.17054

Table D.20: Identification efficiencies for pions, kaons and protons in $N_{\mathrm{tracks}} = 2$ with the DRT method at $rQp > 0.0$.

Momentum range	$\mathcal{P}_{\pi}^{\pi}$	$\mathcal{P}_{\pi}^{\mathrm{K}}$	$\mathcal{P}_{\pi}^{\mathrm{p}}$	$\mathcal{P}_{\mathrm{K}}^{\pi}$	$\mathcal{P}_{\mathrm{K}}^{\mathrm{K}}$	$\mathcal{P}_{\mathrm{K}}^{\mathrm{p}}$	$\mathcal{P}_{\mathrm{p}}^{\pi}$	$\mathcal{P}_{\mathrm{p}}^{\mathrm{K}}$	$\mathcal{P}_{\mathrm{p}}^{\mathrm{p}}$
0.00 - 0.50	–	–	–	–	–	–	–	–	–
0.50 - 1.00	1.00000±0.03853	–	–	1.00000±0.57735	–	–	–	–	–
1.00 - 1.50	1.00000±0.01866	–	–	1.00000±0.11043	–	–	1.00000±0.06306	–	–
1.50 - 2.00	0.99957±0.01688	0.00043±0.00025	–	0.99171±0.07387	0.00829±0.00480	–	0.98576±0.04049	0.00419±0.00188	0.01005±0.00292
2.00 - 2.25	0.96649±0.02294	0.02686±0.00276	0.00665±0.00136	0.37075±0.04158	0.55782±0.05437	0.07143±0.01613	0.51044±0.02837	0.28601±0.01959	0.20355±0.01599
2.25 - 2.50	0.93234±0.02322	0.05808±0.00429	0.00958±0.00170	0.20461±0.02665	0.77522±0.06298	0.02017±0.00770	0.48415±0.02802	0.38142±0.02400	0.13443±0.01291
2.50 - 2.75	0.94249±0.02399	0.04745±0.00395	0.01006±0.00179	0.19830±0.02595	0.77620±0.06250	0.02550±0.00861	0.47780±0.02872	0.39252±0.02527	0.12967±0.01308
2.75 - 3.00	0.98309±0.02594	0.01449±0.00225	0.00242±0.00091	0.17273±0.02478	0.81515±0.06696	0.01212±0.00610	0.45366±0.02836	0.39024±0.02572	0.15610±0.01483
3.00 - 3.25	0.99318±0.02818	0.00481±0.00139	0.00201±0.00090	0.11806±0.02141	0.86806±0.07504	0.01389±0.00699	0.41421±0.02802	0.42225±0.02837	0.16354±0.01597
3.25 - 3.50	0.99422±0.02970	0.00445±0.00141	0.00133±0.00077	0.14950±0.02389	0.84385±0.07190	0.00664±0.00471	0.43500±0.03225	0.40000±0.03055	0.16500±0.01790
3.50 - 3.75	0.99332±0.03074	0.00573±0.00166	0.00095±0.00068	0.21854±0.02970	0.77815±0.06769	0.00331±0.00332	0.41280±0.03588	0.39956±0.03513	0.18764±0.02218
3.75 - 4.00	0.99838±0.03287	0.00054±0.00054	0.00108±0.00077	0.15299±0.02565	0.80970±0.07394	0.03731±0.01202	0.41509±0.03722	0.31604±0.03132	0.26887±0.02837
4.00 - 4.25	0.99558±0.03542	0.00253±0.00126	0.00189±0.00109	0.24644±0.03816	0.70616±0.07556	0.04739±0.01534	0.32198±0.03630	0.21053±0.02809	0.46749±0.04609
4.25 - 4.50	0.99853±0.03829	–	0.00147±0.00104	0.31897±0.04258	0.60776±0.06490	0.07328±0.01841	0.24534±0.03080	0.16770±0.02466	0.58696±0.05378
4.50 - 4.75	0.99918±0.04056	–	0.00082±0.00082	0.24074±0.04294	0.68519±0.08442	0.07407±0.02216	0.20066±0.02815	0.12829±0.02182	0.67105±0.06073
4.75 - 5.00	1.00000±0.04331	–	–	0.27564±0.04748	0.66026±0.08383	0.06410±0.02091	0.20077±0.03051	0.07722±0.01792	0.72201±0.06928
5.00 - 5.25	0.99568±0.04632	0.00324±0.00187	0.00108±0.00108	0.26797±0.04713	0.67320±0.08580	0.05882±0.02018	0.18868±0.03253	0.10377±0.02324	0.70755±0.07549
5.25 - 5.50	0.99878±0.04928	–	0.00122±0.00122	0.40146±0.06408	0.56204±0.08005	0.03650±0.01662	0.21101±0.03424	0.06422±0.01771	0.72477±0.07572
5.50 - 5.75	0.99547±0.05474	0.00452±0.00262	–	0.35556±0.05975	0.59259±0.08361	0.05185±0.02010	0.17442±0.03451	0.02907±0.01319	0.79651±0.09121
5.75 - 6.00	1.00000±0.05712	–	–	0.32759±0.06123	0.58621±0.08953	0.08621±0.02841	0.17647±0.03907	0.02206±0.01288	0.80147±0.10304
6.00 - 6.50	0.99896±0.04547	0.00104±0.00104	–	0.40116±0.05717	0.56395±0.07161	0.03488±0.01449	0.17959±0.02941	0.05714±0.01570	0.76326±0.07412
6.50 - 7.00	1.00000±0.05252	–	–	0.35762±0.05670	0.61589±0.08118	0.02649±0.01342	0.10753±0.02530	0.08602±0.02241	0.80645±0.08850
7.00 - 7.50	1.00000±0.05793	–	–	0.37903±0.06493	0.58871±0.08685	0.03226±0.01639	0.19048±0.04242	0.03968±0.01810	0.76984±0.10399
7.50 - 8.00	1.00000±0.07161	–	–	0.43956±0.08339	0.54945±0.09672	0.01099±0.01105	0.21101±0.04842	0.06422±0.02504	0.72477±0.10709
8.00 - 8.50	1.00000±0.07956	–	–	0.36709±0.07970	0.58228±0.10799	0.05063±0.02595	0.16667±0.05428	0.18182±0.05706	0.65151±0.12768
8.50 - 9.00	1.00000±0.09225	–	–	0.35593±0.09044	0.54237±0.11907	0.10169±0.04358	0.11667±0.04660	0.18333±0.06013	0.70000±0.14083
9.00 - 9.50	1.00000±0.09806	–	–	0.56410±0.15041	0.38461±0.11686	0.05128±0.03718	0.27273±0.08882	0.09091±0.04748	0.63636±0.15384
9.50 - 10.0	1.00000±0.12356	–	–	0.31034±0.11842	0.68966±0.20045	–	0.16129±0.07773	0.19355±0.08632	0.64516±0.18504
10.0 - 11.0	1.00000±0.10483	–	–	0.33333±0.09335	0.66667±0.14760	–	0.17241±0.08349	0.17241±0.08349	0.65517±0.19337
11.0 - 12.0	1.00000±0.15713	–	–	0.23529±0.13076	0.76471±0.28175	–	0.16667±0.12729	0.16667±0.12729	0.66667±0.30429
12.0 - 13.0	1.00000±0.26726	–	–	0.37500±0.25388	0.62500±0.35630	–	–	0.10000±0.10488	0.90000±0.41352
13.0 - 14.0	1.00000±0.34300	–	–	0.60000±0.43818	0.40000±0.33466	–	0.40000±0.23664	–	0.60000±0.30984
14.0 - 15.0	1.00000±0.44721	–	–	0.42857±0.29574	0.57143±0.35816	–	0.42857±0.29574	0.14286±0.15272	0.42857±0.29574
15.0 - 30.0	1.00000±0.36515	–	–	0.66667±0.60858	0.33333±0.38490	–	–	–	1.00000±1.00000

Table D.21: Identification efficiencies for pions, kaons and protons in $N_{\mathrm{tracks}} > 2$ with the DRT method at $rQp > 0.0$.

Momentum range	Q_{π}^{π}	Q_{π}^{K}	Q_{π}^{p}	Q_{K}^{π}	$Q_{\mathrm{K}}^{\mathrm{K}}$	$Q_{\mathrm{K}}^{\mathrm{p}}$	Q_{p}^{π}	$Q_{\mathrm{p}}^{\mathrm{K}}$	$Q_{\mathrm{p}}^{\mathrm{p}}$
0.00 - 0.50	–	–	–	–	–	–	–	–	–
0.50 - 1.00	0.99836±0.02159	0.00164±0.00062	–	–	–	–	–	–	–
1.00 - 1.50	0.96301±0.00967	0.00796±0.00063	0.02903±0.00122	–	–	–	–	–	–
1.50 - 2.00	0.93738±0.00788	0.01288±0.00067	0.04974±0.00134	0.05882±0.06053	0.35294±0.16760	0.58823±0.23443	0.08871±0.01973	0.16532±0.02787	0.74597±0.07247
2.00 - 2.25	0.95050±0.01085	0.00915±0.00077	0.04035±0.00163	0.11432±0.00937	0.51309±0.02312	0.37259±0.01877	0.10821±0.00522	0.08280±0.00451	0.80898±0.01822
2.25 - 2.50	0.95576±0.01093	0.00416±0.00052	0.04008±0.00163	0.12360±0.00822	0.54890±0.02034	0.32749±0.01454	0.11838±0.00575	0.02547±0.00255	0.85614±0.01992
2.50 - 2.75	0.95591±0.01108	0.00420±0.00053	0.03989±0.00165	0.09421±0.00680	0.60386±0.02084	0.30193±0.01328	0.08953±0.00505	0.01879±0.00224	0.89167±0.02098
2.75 - 3.00	0.96391±0.01116	0.00302±0.00045	0.03307±0.00150	0.01911±0.00305	0.68275±0.02343	0.29814±0.01360	0.02385±0.00271	0.02686±0.00289	0.94929±0.02363
3.00 - 3.25	0.96941±0.01152	0.00327±0.00048	0.02732±0.00140	0.00976±0.00225	0.72919±0.02545	0.26105±0.01301	0.02816±0.00312	0.02447±0.00290	0.94737±0.02487
3.25 - 3.50	0.97544±0.01183	0.00233±0.00041	0.02224±0.00129	0.00431±0.00153	0.77921±0.02732	0.21648±0.01191	0.02470±0.00297	0.02783±0.00315	0.94748±0.02533
3.50 - 3.75	0.97561±0.01218	0.00408±0.00056	0.02031±0.00126	0.00823±0.00213	0.77003±0.02735	0.22173±0.01219	0.01720±0.00265	0.02080±0.00291	0.96200±0.02748
3.75 - 4.00	0.97640±0.01282	0.00468±0.00063	0.01891±0.00128	0.00906±0.00228	0.82446±0.02918	0.16648±0.01049	0.02124±0.00301	0.01791±0.00276	0.96085±0.02801
4.00 - 4.25	0.98305±0.01326	0.00577±0.00072	0.01118±0.00101	0.00985±0.00248	0.89286±0.03226	0.09729±0.00811	0.00807±0.00186	0.02123±0.00303	0.97070±0.02850
4.25 - 4.50	0.98311±0.01376	0.00679±0.00081	0.01010±0.00099	0.00336±0.00151	0.92872±0.03471	0.06792±0.00698	0.00799±0.00189	0.02573±0.00342	0.96628±0.02903
4.50 - 4.75	0.98447±0.01417	0.00771±0.00089	0.00781±0.00090	0.00513±0.00194	0.94721±0.03677	0.04765±0.00605	0.00771±0.00200	0.02621±0.00372	0.96608±0.03124
4.75 - 5.00	0.98417±0.01481	0.00853±0.00098	0.00730±0.00091	0.00949±0.00264	0.95693±0.03697	0.03358±0.00503	0.00474±0.00158	0.02792±0.00389	0.96733±0.03166
5.00 - 5.25	0.98511±0.01532	0.00888±0.00104	0.00600±0.00085	0.00710±0.00237	0.96924±0.03880	0.02366±0.00437	0.00401±0.00152	0.01833±0.00327	0.97766±0.03328
5.25 - 5.50	0.98463±0.01582	0.01165±0.00123	0.00371±0.00069	0.01346±0.00319	0.96634±0.03770	0.02019±0.00393	0.00310±0.00139	0.02477±0.00396	0.97214±0.03445
5.50 - 5.75	0.98491±0.01660	0.01044±0.00122	0.00465±0.00081	0.00170±0.00120	0.98216±0.04067	0.01614±0.00373	0.00215±0.00124	0.02225±0.00404	0.97559±0.03720
5.75 - 6.00	0.98333±0.01727	0.01132±0.00132	0.00535±0.00091	0.00174±0.00123	0.97646±0.04102	0.02180±0.00441	0.00075±0.00075	0.02622±0.00449	0.97303±0.03792
6.00 - 6.50	0.98379±0.01294	0.01252±0.00104	0.00369±0.00056	0.00292±0.00119	0.97762±0.03067	0.01946±0.00311	0.00162±0.00081	0.02913±0.00348	0.96926±0.02779
6.50 - 7.00	0.98103±0.01382	0.01347±0.00116	0.00550±0.00074	0.00108±0.00076	0.98064±0.03232	0.01829±0.00317	0.00254±0.00114	0.02030±0.00324	0.97716±0.03132
7.00 - 7.50	0.98400±0.01538	0.01321±0.00127	0.00279±0.00058	0.00061±0.00061	0.97434±0.03428	0.02505±0.00396	0.00245±0.00122	0.03058±0.00439	0.96697±0.03411
7.50 - 8.00	0.98227±0.01655	0.01224±0.00132	0.00549±0.00088	–	0.97266±0.03621	0.02734±0.00438	0.00066±0.00066	0.02984±0.00451	0.96950±0.03558
8.00 - 8.50	0.98050±0.01784	0.01425±0.00154	0.00524±0.00093	0.00156±0.00110	0.94384±0.03783	0.05460±0.00670	0.00172±0.00122	0.04643±0.00646	0.95185±0.03997
8.50 - 9.00	0.98240±0.01952	0.01213±0.00155	0.00548±0.00104	0.00085±0.00085	0.92966±0.03899	0.06949±0.00794	–	0.05702±0.00798	0.94298±0.04399
9.00 - 9.50	0.93020±0.01967	0.06377±0.00382	0.00603±0.00114	–	0.86493±0.04372	0.13507±0.01348	–	0.04981±0.00817	0.95019±0.04865
9.50 - 10.0	0.98506±0.02305	0.01141±0.00177	0.00353±0.00098	0.00213±0.00151	0.89979±0.04269	0.09808±0.01072	0.00155±0.00155	0.00310±0.00220	0.99535±0.05549
10.0 - 11.0	0.98150±0.01851	0.01357±0.00156	0.00493±0.00093	0.00068±0.00068	0.92407±0.03472	0.07525±0.00741	0.00324±0.00187	0.00324±0.00187	0.99353±0.04622
11.0 - 12.0	0.97311±0.02176	0.02294±0.00241	0.00395±0.00099	0.00101±0.00101	0.94551±0.04308	0.05348±0.00754	–	0.00137±0.00137	0.99863±0.05232
12.0 - 13.0	0.96154±0.02628	0.03626±0.00371	0.00220±0.00090	0.00152±0.00152	0.96201±0.05356	0.03647±0.00758	–	–	1.00000±0.06934
13.0 - 14.0	0.93425±0.03095	0.06257±0.00594	0.00318±0.00130	0.00716±0.00415	0.95227±0.06661	0.04057±0.01004	–	–	1.00000±0.08452
14.0 - 15.0	0.91828±0.03852	0.07666±0.00834	0.00505±0.00207	0.00463±0.00464	0.95833±0.09321	0.03704±0.01333	–	–	1.00000±0.11180
15.0 - 30.0	0.86638±0.02940	0.13255±0.00896	0.00107±0.00076	0.00873±0.00620	0.92140±0.08793	0.06987±0.01807	0.01914±0.00966	0.00957±0.00680	0.97129±0.09571

Table D.22: Identification purities and contaminations for pions, kaons and protons in $N_{\mathrm{tracks}} = 1$ with the DRT method at $rQp > 0.0$.

Momentum range	Q_{π}^{π}	Q_{π}^{K}	Q_{π}^{p}	Q_{K}^{π}	$Q_{\mathrm{K}}^{\mathrm{K}}$	$Q_{\mathrm{K}}^{\mathrm{p}}$	Q_{p}^{π}	$Q_{\mathrm{p}}^{\mathrm{K}}$	$Q_{\mathrm{p}}^{\mathrm{p}}$
0.00 - 0.50	–	–	–	–	–	–	–	–	–
0.50 - 1.00	0.99604±0.01983	0.00396±0.00089	–	–	–	–	–	–	–
1.00 - 1.50	0.90826±0.00854	0.02188±0.00097	0.06986±0.00177	–	–	–	–	–	–
1.50 - 2.00	0.85038±0.00694	0.03064±0.00098	0.11898±0.00202	0.21622±0.08430	0.13514±0.06439	0.64865±0.17001	0.10606±0.02981	0.11364±0.03096	0.78030±0.10259
2.00 - 2.25	0.87710±0.01025	0.02188±0.00119	0.10103±0.00266	0.19769±0.01026	0.27765±0.01255	0.52466±0.01885	0.10969±0.00790	0.08713±0.00697	0.80318±0.02725
2.25 - 2.50	0.88164±0.01062	0.01551±0.00104	0.10285±0.00278	0.21224±0.00930	0.31282±0.01175	0.47494±0.01535	0.12274±0.00961	0.03353±0.00482	0.84373±0.03230
2.50 - 2.75	0.87867±0.01089	0.01495±0.00104	0.10637±0.00291	0.18916±0.00870	0.34669±0.01254	0.46415±0.01512	0.11489±0.01018	0.02346±0.00441	0.86165±0.03603
2.75 - 3.00	0.89466±0.01133	0.01188±0.00095	0.09346±0.00278	0.04396±0.00428	0.47202±0.01666	0.48401±0.01694	0.03806±0.00585	0.02249±0.00446	0.93945±0.03970
3.00 - 3.25	0.90263±0.01182	0.01026±0.00092	0.08711±0.00278	0.02314±0.00331	0.50625±0.01878	0.47062±0.01790	0.04729±0.00653	0.01978±0.00416	0.93293±0.03938
3.25 - 3.50	0.90747±0.01243	0.01367±0.00111	0.07887±0.00276	0.01365±0.00260	0.56217±0.02069	0.42418±0.01716	0.03749±0.00628	0.01925±0.00446	0.94326±0.04309
3.50 - 3.75	0.91470±0.01319	0.01360±0.00117	0.07170±0.00276	0.01226±0.00252	0.56924±0.02136	0.41850±0.01742	0.03420±0.00646	0.03656±0.00668	0.92924±0.04598
3.75 - 4.00	0.92297±0.01409	0.01543±0.00132	0.06161±0.00270	0.01219±0.00281	0.62412±0.02550	0.36369±0.01784	0.01771±0.00433	0.02396±0.00506	0.95833±0.04421
4.00 - 4.25	0.93880±0.01502	0.02230±0.00168	0.03890±0.00224	0.01780±0.00392	0.73220±0.03278	0.25000±0.01627	0.01408±0.00344	0.04142±0.00598	0.94449±0.03901
4.25 - 4.50	0.93450±0.01615	0.02655±0.00198	0.03896±0.00242	0.01413±0.00380	0.80827±0.03840	0.17760±0.01453	0.01478±0.00361	0.03478±0.00559	0.95044±0.04015
4.50 - 4.75	0.93476±0.01703	0.02837±0.00216	0.03686±0.00248	0.01607±0.00449	0.86032±0.04448	0.12361±0.01310	0.01035±0.00314	0.04892±0.00695	0.94073±0.04144
4.75 - 5.00	0.94102±0.01804	0.02602±0.00218	0.03297±0.00246	0.00694±0.00312	0.90417±0.04890	0.08889±0.01159	0.00755±0.00286	0.03560±0.00631	0.95685±0.04494
5.00 - 5.25	0.94213±0.01904	0.03072±0.00250	0.02715±0.00235	0.00800±0.00359	0.91360±0.05289	0.07840±0.01163	0.00341±0.00197	0.03292±0.00621	0.96368±0.04635
5.25 - 5.50	0.93237±0.01989	0.04106±0.00306	0.02657±0.00245	0.00360±0.00255	0.91367±0.05608	0.08273±0.01269	0.00484±0.00242	0.03386±0.00651	0.96131±0.04775
5.50 - 5.75	0.93797±0.02172	0.04256±0.00339	0.01947±0.00227	–	0.93470±0.05808	0.06530±0.01139	–	0.03403±0.00679	0.96597±0.04986
5.75 - 6.00	0.94346±0.02249	0.03475±0.00315	0.02179±0.00248	0.00634±0.00367	0.95560±0.06286	0.03805±0.00914	0.00152±0.00153	0.02591±0.00637	0.97256±0.05408
6.00 - 6.50	0.93714±0.01733	0.04235±0.00270	0.02051±0.00186	0.00791±0.00324	0.93281±0.04874	0.05929±0.00910	0.00082±0.00082	0.02226±0.00433	0.97692±0.03990
6.50 - 7.00	0.93526±0.01941	0.04746±0.00322	0.01728±0.00191	0.00278±0.00197	0.94444±0.05050	0.05278±0.00878	0.00105±0.00105	0.02526±0.00522	0.97368±0.04498
7.00 - 7.50	0.92944±0.02126	0.04914±0.00360	0.02142±0.00235	0.00336±0.00238	0.93613±0.05519	0.06050±0.01038	0.00141±0.00141	0.03657±0.00730	0.96203±0.05152
7.50 - 8.00	0.92372±0.02397	0.04945±0.00410	0.02683±0.00298	–	0.87117±0.05774	0.12883±0.01725	–	0.03473±0.00811	0.96527±0.05889
8.00 - 8.50	0.92398±0.02732	0.05250±0.00482	0.02352±0.00318	–	0.85748±0.06100	0.14252±0.01951	–	0.04556±0.01069	0.95444±0.06688
8.50 - 9.00	0.91907±0.03044	0.05255±0.00539	0.02838±0.00392	–	0.84267±0.06435	0.15733±0.02204	0.00324±0.00324	0.08738±0.01754	0.90938±0.07496
9.00 - 9.50	0.88295±0.03252	0.09097±0.00795	0.02608±0.00413	–	0.80804±0.08076	0.19196±0.03196	0.00391±0.00391	0.06250±0.01611	0.93359±0.08397
9.50 - 10.0	0.91509±0.03801	0.05688±0.00704	0.02803±0.00487	–	0.85081±0.07968	0.14919±0.02629	–	–	1.00000±0.10911
10.0 - 11.0	0.91834±0.03229	0.04793±0.00545	0.03373±0.00454	–	0.82659±0.06606	0.17341±0.02425	–	0.00794±0.00563	0.99206±0.08856
11.0 - 12.0	0.93391±0.04159	0.04119±0.00641	0.02490±0.00494	–	0.84836±0.08017	0.15164±0.02675	–	–	1.00000±0.10847
12.0 - 13.0	0.93008±0.05403	0.06504±0.01061	0.00488±0.00282	–	0.84028±0.10363	0.15972±0.03587	–	–	1.00000±0.14359
13.0 - 14.0	0.88548±0.06829	0.08659±0.01621	0.02793±0.00896	–	0.84615±0.15502	0.15385±0.05226	–	–	1.00000±0.18257
14.0 - 15.0	0.85470±0.08231	0.13248±0.02532	0.01282±0.00745	–	0.90625±0.23235	0.09375±0.05661	–	–	1.00000±0.25820
15.0 - 30.0	0.82008±0.07903	0.15900±0.02777	0.02092±0.00945	–	0.72414±0.20749	0.27586±0.11017	–	–	1.00000±0.29488

Table D.23: Identification purities and contaminations for pions, kaons and protons in $N_{\mathrm{tracks}} = 2$ with the DRT method at $rQp > 0.0$.

Momentum range	Q_{π}^{π}	Q_{π}^{K}	Q_{π}^{p}	Q_{K}^{π}	$Q_{\mathrm{K}}^{\mathrm{K}}$	$Q_{\mathrm{K}}^{\mathrm{p}}$	Q_{p}^{π}	$Q_{\mathrm{p}}^{\mathrm{K}}$	$Q_{\mathrm{p}}^{\mathrm{p}}$
0.00 - 0.50	–	–	–	–	–	–	–	–	–
0.50 - 1.00	0.99557±0.03832	0.00443±0.00181	–	–	–	–	–	–	–
1.00 - 1.50	0.89591±0.01628	0.02559±0.00202	0.07850±0.00363	–	–	–	–	–	–
1.50 - 2.00	0.82022±0.01322	0.04202±0.00226	0.13776±0.00428	0.27273±0.17764	0.27273±0.17764	0.45454±0.24516	–	–	1.00000±0.40825
2.00 - 2.25	0.85372±0.01968	0.02666±0.00259	0.11962±0.00572	0.18131±0.02001	0.30654±0.02736	0.51215±0.03805	0.10000±0.02141	0.08750±0.01991	0.81250±0.07833
2.25 - 2.50	0.85832±0.02097	0.01957±0.00235	0.12211±0.00615	0.23892±0.01909	0.33128±0.02331	0.42980±0.02751	0.19753±0.03821	0.04321±0.01668	0.75926±0.09080
2.50 - 2.75	0.86228±0.02149	0.02013±0.00243	0.11760±0.00615	0.19842±0.01768	0.36005±0.02537	0.44152±0.02892	0.21053±0.04095	0.05921±0.02031	0.73026±0.09117
2.75 - 3.00	0.86913±0.02226	0.01739±0.00232	0.11348±0.00621	0.06656±0.01061	0.42631±0.03104	0.50713±0.03480	0.05036±0.01951	0.02878±0.01459	0.92086±0.11281
3.00 - 3.25	0.87833±0.02419	0.01206±0.00208	0.10961±0.00657	0.02080±0.00607	0.43328±0.03281	0.54593±0.03824	0.03817±0.01739	0.03053±0.01550	0.93130±0.11718
3.25 - 3.50	0.87957±0.02551	0.01771±0.00266	0.10272±0.00668	0.01984±0.00634	0.50397±0.03878	0.47619±0.03735	0.02885±0.01689	0.01923±0.01373	0.95192±0.13366
3.50 - 3.75	0.89165±0.02688	0.02827±0.00353	0.08009±0.00609	0.02804±0.00821	0.54907±0.04458	0.42290±0.03750	0.02273±0.01625	0.01136±0.01143	0.96591±0.14690
3.75 - 4.00	0.89471±0.02868	0.01989±0.00314	0.08540±0.00671	0.00284±0.00284	0.61648±0.05321	0.38068±0.03864	0.01587±0.01131	0.07937±0.02607	0.90476±0.11695
4.00 - 4.25	0.90998±0.03167	0.03001±0.00422	0.06001±0.00606	0.01810±0.00913	0.67421±0.07147	0.30769±0.04267	0.01829±0.01066	0.06098±0.01986	0.92073±0.10384
4.25 - 4.50	0.89881±0.03360	0.04894±0.00583	0.05225±0.00603	–	0.72308±0.07993	0.27692±0.04258	0.00962±0.00683	0.08173±0.02062	0.90865±0.09131
4.50 - 4.75	0.92384±0.03679	0.02970±0.00483	0.04646±0.00609	–	0.74000±0.09265	0.26000±0.04673	0.00461±0.00462	0.05530±0.01640	0.94009±0.09168
4.75 - 5.00	0.91817±0.03895	0.03704±0.00575	0.04479±0.00635	–	0.83740±0.11184	0.16260±0.03920	–	0.05076±0.01645	0.94924±0.09691
5.00 - 5.25	0.91924±0.04194	0.04088±0.00651	0.03988±0.00643	0.02344±0.01369	0.80469±0.10651	0.17188±0.03967	0.00625±0.00627	0.05625±0.01927	0.93750±0.10655
5.25 - 5.50	0.89046±0.04273	0.05965±0.00828	0.04989±0.00754	–	0.84615±0.13102	0.15385±0.04417	0.00610±0.00612	0.03049±0.01384	0.96342±0.10740
5.50 - 5.75	0.89431±0.04791	0.06504±0.00969	0.04065±0.00757	0.03409±0.02002	0.90909±0.14044	0.05682±0.02612	–	0.04861±0.01881	0.95139±0.11354
5.75 - 6.00	0.90815±0.05067	0.05630±0.00939	0.03556±0.00739	–	0.95775±0.16251	0.04225±0.02491	–	0.08403±0.02767	0.91597±0.12144
6.00 - 6.50	0.89518±0.03967	0.06401±0.00795	0.04082±0.00628	0.00893±0.00897	0.86607±0.12012	0.12500±0.03543	–	0.03109±0.01289	0.96891±0.09942
6.50 - 7.00	0.90738±0.04654	0.06758±0.00950	0.02503±0.00567	–	0.85321±0.12044	0.14679±0.03930	–	0.02597±0.01315	0.97403±0.11174
7.00 - 7.50	0.89355±0.05037	0.07046±0.01063	0.03598±0.00748	–	0.93590±0.15241	0.06410±0.02957	–	0.03960±0.02019	0.96040±0.13653
7.50 - 8.00	0.86093±0.05947	0.08830±0.01456	0.05077±0.01085	–	0.87719±0.16997	0.12281±0.04918	–	0.01250±0.01258	0.98750±0.15663
8.00 - 8.50	0.88764±0.06860	0.08146±0.01573	0.03090±0.00946	–	0.79310±0.15659	0.20690±0.06561	–	0.08511±0.04433	0.91489±0.19307
8.50 - 9.00	0.89354±0.08021	0.07985±0.01811	0.02662±0.01019	–	0.74419±0.17374	0.25581±0.08644	–	0.12500±0.05413	0.87500±0.18488
9.00 - 9.50	0.85950±0.08127	0.09091±0.02024	0.04959±0.01467	–	0.78947±0.27268	0.21053±0.11582	–	0.06667±0.04869	0.93333±0.24525
9.50 - 10.0	0.90345±0.10890	0.06207±0.02132	0.03448±0.01568	–	0.76923±0.22879	0.23077±0.10452	–	–	1.00000±0.31623
10.0 - 11.0	0.89216±0.09097	0.08333±0.02104	0.02451±0.01109	–	0.87179±0.20455	0.12821±0.06090	–	–	1.00000±0.32444
11.0 - 12.0	0.93103±0.14375	0.04598±0.02351	0.02299±0.01644	–	0.86667±0.32841	0.13333±0.10037	–	–	1.00000±0.50000
12.0 - 13.0	0.90323±0.23548	0.09677±0.05851	–	–	0.83333±0.50461	0.16667±0.18002	–	–	1.00000±0.47141
13.0 - 14.0	0.70833±0.22454	0.12500±0.07655	0.16667±0.09001	–	1.00000±1.00000	–	–	–	1.00000±0.57735
14.0 - 15.0	0.62500±0.25195	0.18750±0.11797	0.18750±0.11797	–	0.80000±0.53666	0.20000±0.21909	–	–	1.00000±0.81650
15.0 - 30.0	0.88235±0.31257	0.11765±0.08795	–	–	1.00000±1.41421	–	–	–	1.00000±1.00000

Table D.24: Identification purities and contaminations for pions, kaons and protons in $N_{\mathrm{tracks}} > 2$ with the DRT method at $rQp > 0.0$.

Momentum range	$\mathcal{P}_{\pi}^{\pi}$	$\mathcal{P}_{\pi}^{\mathrm{K}}$	$\mathcal{P}_{\pi}^{\mathrm{p}}$	$\mathcal{P}_{\mathrm{K}}^{\pi}$	$\mathcal{P}_{\mathrm{K}}^{\mathrm{K}}$	$\mathcal{P}_{\mathrm{K}}^{\mathrm{p}}$	$\mathcal{P}_{\mathrm{p}}^{\pi}$	$\mathcal{P}_{\mathrm{p}}^{\mathrm{K}}$	$\mathcal{P}_{\mathrm{p}}^{\mathrm{p}}$
0.00 - 0.50	–	–	–	–	–	–	–	–	–
0.50 - 1.00	1.00000±0.02171	–	–	1.00000±0.53452	–	–	–	–	–
1.00 - 1.50	1.00000±0.01017	–	–	1.00000±0.11704	–	–	1.00000±0.06080	–	–
1.50 - 2.00	0.99996±0.00855	0.00004±0.00004	–	0.98315±0.07401	0.01685±0.00694	–	0.99334±0.03828	0.00666±0.00223	–
2.00 - 2.25	0.97102±0.01118	0.01025±0.00082	0.01873±0.00112	0.12463±0.01173	0.72228±0.03494	0.15309±0.01316	0.16851±0.00766	0.15628±0.00734	0.67522±0.01837
2.25 - 2.50	0.95907±0.01101	0.01453±0.00098	0.02640±0.00132	0.04609±0.00614	0.87656±0.03585	0.07734±0.00807	0.12258±0.00551	0.13801±0.00588	0.73942±0.01684
2.50 - 2.75	0.96833±0.01128	0.01223±0.00091	0.01944±0.00115	0.04164±0.00544	0.91058±0.03446	0.04778±0.00585	0.12312±0.00557	0.12873±0.00571	0.74815±0.01714
2.75 - 3.00	0.99335±0.01159	0.00251±0.00041	0.00414±0.00053	0.02918±0.00441	0.91634±0.03375	0.05447±0.00610	0.11298±0.00557	0.12851±0.00598	0.75851±0.01814
3.00 - 3.25	0.99387±0.01189	0.00121±0.00029	0.00492±0.00059	0.03084±0.00457	0.92454±0.03417	0.04462±0.00553	0.10299±0.00566	0.12190±0.00621	0.77511±0.01970
3.25 - 3.50	0.99444±0.01212	0.00059±0.00021	0.00496±0.00061	0.02031±0.00369	0.93512±0.03444	0.04456±0.00552	0.08727±0.00543	0.10311±0.00594	0.80963±0.02133
3.50 - 3.75	0.99584±0.01250	0.00079±0.00025	0.00338±0.00052	0.03406±0.00490	0.93869±0.03521	0.02725±0.00437	0.08383±0.00563	0.10793±0.00646	0.80824±0.02259
3.75 - 4.00	0.99513±0.01313	0.00104±0.00030	0.00382±0.00058	0.03578±0.00491	0.94014±0.03445	0.02407±0.00400	0.07593±0.00550	0.09074±0.00605	0.83333±0.02379
4.00 - 4.25	0.99735±0.01350	0.00119±0.00033	0.00146±0.00037	0.04013±0.00520	0.93074±0.03410	0.02913±0.00440	0.04627±0.00439	0.05345±0.00474	0.90028±0.02612
4.25 - 4.50	0.99852±0.01403	0.00039±0.00020	0.00108±0.00033	0.04615±0.00568	0.91639±0.03427	0.03746±0.00510	0.04126±0.00427	0.03743±0.00406	0.92131±0.02744
4.50 - 4.75	0.99844±0.01442	0.00063±0.00026	0.00094±0.00031	0.05196±0.00624	0.91388±0.03528	0.03416±0.00501	0.03652±0.00435	0.02601±0.00365	0.93747±0.03014
4.75 - 5.00	0.99806±0.01507	0.00137±0.00039	0.00057±0.00025	0.05123±0.00615	0.91509±0.03507	0.03368±0.00494	0.03226±0.00416	0.01769±0.00306	0.95005±0.03105
5.00 - 5.25	0.99927±0.01560	0.00073±0.00030	–	0.05383±0.00656	0.92419±0.03672	0.02199±0.00413	0.02809±0.00403	0.01629±0.00305	0.95562±0.03240
5.25 - 5.50	0.99779±0.01609	0.00195±0.00050	0.00026±0.00018	0.06188±0.00684	0.91252±0.03523	0.02560±0.00432	0.01737±0.00331	0.01675±0.00325	0.96588±0.03432
5.50 - 5.75	0.99957±0.01691	0.00014±0.00014	0.00029±0.00020	0.05382±0.00675	0.92209±0.03773	0.02410±0.00445	0.02359±0.00415	0.01001±0.00269	0.96640±0.03686
5.75 - 6.00	0.99984±0.01764	0.00016±0.00016	–	0.05519±0.00693	0.91927±0.03812	0.02554±0.00464	0.02457±0.00433	0.01564±0.00344	0.95979±0.03742
6.00 - 6.50	0.99956±0.01320	0.00035±0.00017	0.00009±0.00009	0.06152±0.00548	0.91506±0.02837	0.02342±0.00332	0.01710±0.00266	0.01303±0.00232	0.96987±0.02789
6.50 - 7.00	0.99980±0.01415	0.00020±0.00014	–	0.06609±0.00598	0.91968±0.02996	0.01423±0.00271	0.02714±0.00374	0.01357±0.00263	0.95930±0.03073
7.00 - 7.50	0.99988±0.01569	0.00012±0.00012	–	0.05869±0.00604	0.92312±0.03228	0.01819±0.00330	0.01314±0.00289	0.01815±0.00340	0.96871±0.03455
7.50 - 8.00	1.00000±0.01693	–	–	0.05152±0.00598	0.92668±0.03434	0.02180±0.00384	0.02482±0.00413	0.01543±0.00324	0.95976±0.03552
8.00 - 8.50	0.99983±0.01828	0.00017±0.00017	–	0.06072±0.00704	0.91161±0.03660	0.02767±0.00468	0.02537±0.00477	0.03762±0.00584	0.93701±0.03985
8.50 - 9.00	0.99980±0.01995	0.00020±0.00020	–	0.05056±0.00675	0.92459±0.03905	0.02485±0.00467	0.02781±0.00553	0.05989±0.00824	0.91230±0.04320
9.00 - 9.50	1.00000±0.02152	–	–	0.27897±0.01913	0.70051±0.03495	0.02051±0.00463	0.03562±0.00685	0.10178±0.01194	0.86260±0.04521
9.50 - 10.0	0.99945±0.02347	0.00055±0.00039	–	0.04535±0.00733	0.95352±0.04596	0.00113±0.00113	0.01903±0.00533	0.09956±0.01266	0.88141±0.04927
10.0 - 11.0	0.99946±0.01893	0.00018±0.00018	0.00036±0.00025	0.04513±0.00577	0.95275±0.03622	0.00212±0.00122	0.02451±0.00507	0.07865±0.00931	0.89683±0.04168
11.0 - 12.0	0.99975±0.02251	0.00025±0.00025	–	0.07325±0.00894	0.92574±0.04259	0.00102±0.00102	0.01704±0.00477	0.05505±0.00872	0.92792±0.04842
12.0 - 13.0	0.99962±0.02759	0.00038±0.00038	–	0.10977±0.01354	0.89023±0.05030	–	0.01174±0.00528	0.03521±0.00925	0.95305±0.06610
13.0 - 14.0	0.99830±0.03362	0.00170±0.00098	–	0.17471±0.02172	0.82529±0.05885	–	0.01742±0.00786	0.02787±0.00999	0.95470±0.08064
14.0 - 15.0	0.99908±0.04279	0.00092±0.00092	–	0.26778±0.03769	0.73222±0.07285	–	0.03550±0.01475	0.01775±0.01034	0.94675±0.10443
15.0 - 30.0	0.99631±0.03499	0.00123±0.00087	0.00246±0.00123	0.56374±0.04997	0.43060±0.04177	0.00567±0.00402	0.00922±0.00655	0.06452±0.01779	0.92627±0.09068

Table D.25: Identification efficiencies for pions, kaons and protons in $N_{\mathrm{tracks}} = 1$ with the DRT method at $rQp > 0.5$.

Momentum range	$\mathcal{P}_{\pi}^{\pi}$	$\mathcal{P}_{\pi}^{\mathrm{K}}$	$\mathcal{P}_{\pi}^{\mathrm{p}}$	$\mathcal{P}_{\mathrm{K}}^{\pi}$	$\mathcal{P}_{\mathrm{K}}^{\mathrm{K}}$	$\mathcal{P}_{\mathrm{K}}^{\mathrm{p}}$	$\mathcal{P}_{\mathrm{p}}^{\pi}$	$\mathcal{P}_{\mathrm{p}}^{\mathrm{K}}$	$\mathcal{P}_{\mathrm{p}}^{\mathrm{p}}$
0.00 - 0.50	–	–	–	–	–	–	–	–	–
0.50 - 1.00	1.00000±0.01997	–	–	1.00000±0.34300	–	–	–	–	–
1.00 - 1.50	1.00000±0.00965	–	–	1.00000±0.06408	–	–	1.00000±0.03586	–	–
1.50 - 2.00	0.99975±0.00849	0.00025±0.00010	–	0.99478±0.04551	0.00522±0.00234	–	0.99380±0.02312	0.00620±0.00130	–
2.00 - 2.25	0.96373±0.01155	0.02845±0.00144	0.00782±0.00074	0.32606±0.02070	0.61150±0.03125	0.06244±0.00811	0.42438±0.01318	0.32519±0.01113	0.25043±0.00949
2.25 - 2.50	0.94431±0.01160	0.04374±0.00183	0.01194±0.00094	0.18671±0.01365	0.77292±0.03395	0.04037±0.00594	0.36447±0.01125	0.33953±0.01076	0.29600±0.00988
2.50 - 2.75	0.95056±0.01204	0.03943±0.00179	0.01001±0.00089	0.15663±0.01206	0.82008±0.03462	0.02329±0.00438	0.38551±0.01213	0.34031±0.01121	0.27418±0.00981
2.75 - 3.00	0.98919±0.01284	0.00838±0.00084	0.00243±0.00045	0.11360±0.00972	0.86697±0.03478	0.01943±0.00385	0.35985±0.01233	0.32909±0.01166	0.31106±0.01126
3.00 - 3.25	0.99167±0.01330	0.00412±0.00061	0.00421±0.00062	0.09646±0.00934	0.88623±0.03712	0.01731±0.00381	0.34819±0.01278	0.32033±0.01214	0.33148±0.01240
3.25 - 3.50	0.99432±0.01393	0.00245±0.00049	0.00323±0.00056	0.11017±0.00971	0.87750±0.03563	0.01233±0.00310	0.35213±0.01410	0.31788±0.01323	0.32999±0.01354
3.50 - 3.75	0.99492±0.01465	0.00205±0.00047	0.00303±0.00057	0.10459±0.00964	0.87611±0.03636	0.01931±0.00398	0.32734±0.01434	0.33822±0.01463	0.33444±0.01453
3.75 - 4.00	0.99589±0.01549	0.00205±0.00050	0.00205±0.00050	0.11728±0.01083	0.86482±0.03800	0.01791±0.00404	0.28143±0.01389	0.26324±0.01334	0.45532±0.01883
4.00 - 4.25	0.99566±0.01616	0.00263±0.00059	0.00171±0.00047	0.16264±0.01326	0.79368±0.03637	0.04368±0.00651	0.18030±0.01127	0.15463±0.01032	0.66507±0.02571
4.25 - 4.50	0.99677±0.01751	0.00154±0.00049	0.00169±0.00051	0.17612±0.01436	0.78607±0.03738	0.03781±0.00625	0.17482±0.01173	0.10181±0.00867	0.72338±0.02890
4.50 - 4.75	0.99607±0.01843	0.00205±0.00059	0.00188±0.00057	0.18805±0.01572	0.75553±0.03830	0.05642±0.00812	0.17051±0.01238	0.06989±0.00758	0.75960±0.03204
4.75 - 5.00	0.99792±0.01941	0.00095±0.00042	0.00113±0.00046	0.17203±0.01580	0.79084±0.04187	0.03713±0.00690	0.16086±0.01292	0.05183±0.00698	0.78731±0.03546
5.00 - 5.25	0.99916±0.02049	0.00063±0.00036	0.00021±0.00021	0.20620±0.01831	0.75876±0.04241	0.03504±0.00699	0.12992±0.01202	0.03937±0.00635	0.83071±0.03869
5.25 - 5.50	0.99906±0.02168	0.00047±0.00033	0.00047±0.00033	0.25107±0.02117	0.71469±0.04181	0.03424±0.00711	0.12500±0.01215	0.04412±0.00696	0.83088±0.03997
5.50 - 5.75	1.00000±0.02352	–	–	0.23145±0.02056	0.72997±0.04329	0.03858±0.00771	0.08971±0.01081	0.03349±0.00643	0.87679±0.04437
5.75 - 6.00	0.99942±0.02416	0.00058±0.00041	–	0.20526±0.02083	0.76667±0.04875	0.02807±0.00712	0.10744±0.01280	0.02204±0.00557	0.87052±0.04736
6.00 - 6.50	0.99877±0.01876	0.00106±0.00043	0.00018±0.00018	0.25670±0.01824	0.71753±0.03564	0.02577±0.00522	0.08934±0.00855	0.03003±0.00482	0.88063±0.03526
6.50 - 7.00	0.99955±0.02109	0.00044±0.00031	–	0.24286±0.01821	0.73407±0.03740	0.02308±0.00509	0.07745±0.00905	0.03137±0.00563	0.89118±0.04065
7.00 - 7.50	0.99946±0.02327	0.00027±0.00027	0.00027±0.00027	0.24967±0.02030	0.72127±0.04050	0.02906±0.00629	0.10419±0.01209	0.03812±0.00709	0.85769±0.04499
7.50 - 8.00	1.00000±0.02645	–	–	0.25650±0.02363	0.72097±0.04637	0.02253±0.00632	0.12135±0.01446	0.08141±0.01163	0.79724±0.04691
8.00 - 8.50	1.00000±0.03015	–	–	0.24291±0.02472	0.72267±0.05020	0.03441±0.00849	0.11435±0.01628	0.09356±0.01458	0.79210±0.05432
8.50 - 9.00	1.00000±0.03382	–	–	0.22664±0.02549	0.71963±0.05377	0.05374±0.01150	0.14601±0.02147	0.11570±0.01886	0.73829±0.05946
9.00 - 9.50	0.99928±0.03793	–	0.00072±0.00072	0.41139±0.04287	0.54430±0.05158	0.04430±0.01210	0.13475±0.02329	0.09220±0.01890	0.77305±0.06972
9.50 - 10.0	1.00000±0.04245	–	–	0.23333±0.03265	0.76667±0.07083	–	0.15421±0.02884	0.14486±0.02784	0.70093±0.07464
10.0 - 11.0	1.00000±0.03590	–	–	0.20786±0.02656	0.78652±0.06283	0.00562±0.00398	0.15089±0.02267	0.15385±0.02292	0.69527±0.05905
11.0 - 12.0	1.00000±0.04529	–	–	0.15812±0.02797	0.84188±0.08140	–	0.10185±0.02279	0.13889±0.02706	0.75926±0.07864
12.0 - 13.0	1.00000±0.05913	–	–	0.20833±0.04181	0.79167±0.09925	–	0.02609±0.01526	0.14783±0.03841	0.82609±0.11453
13.0 - 14.0	1.00000±0.07943	–	–	0.35897±0.07908	0.64103±0.11613	–	0.13158±0.04426	0.10526±0.03913	0.76316±0.13306
14.0 - 15.0	1.00000±0.10000	–	–	0.51852±0.12075	0.48148±0.11493	–	0.08333±0.05008	0.08333±0.05008	0.83333±0.20601
15.0 - 30.0	1.00000±0.10101	–	–	0.63636±0.13760	0.36364±0.09495	–	0.15625±0.07514	0.12500±0.06629	0.71875±0.19648

Table D.26: Identification efficiencies for pions, kaons and protons in $N_{\mathrm{tracks}} = 2$ with the DRT method at $rQp > 0.5$.

Momentum range	$\mathcal{P}_{\pi}^{\pi}$	$\mathcal{P}_{\pi}^{\mathrm{K}}$	$\mathcal{P}_{\pi}^{\mathrm{p}}$	$\mathcal{P}_{\mathrm{K}}^{\pi}$	$\mathcal{P}_{\mathrm{K}}^{\mathrm{K}}$	$\mathcal{P}_{\mathrm{K}}^{\mathrm{p}}$	$\mathcal{P}_{\mathrm{p}}^{\pi}$	$\mathcal{P}_{\mathrm{p}}^{\mathrm{K}}$	$\mathcal{P}_{\mathrm{p}}^{\mathrm{p}}$
0.00 - 0.50	–	–	–	–	–	–	–	–	–
0.50 - 1.00	1.00000±0.03856	–	–	1.00000±0.57735	–	–	–	–	–
1.00 - 1.50	1.00000±0.01869	–	–	1.00000±0.11215	–	–	1.00000±0.06482	–	–
1.50 - 2.00	0.99957±0.01691	0.00043±0.00025	–	0.99125±0.07586	0.00875±0.00507	–	0.99559±0.04186	0.00441±0.00198	–
2.00 - 2.25	0.97116±0.02315	0.02520±0.00269	0.00364±0.00101	0.39114±0.04481	0.59410±0.05912	0.01476±0.00743	0.55718±0.03249	0.32117±0.02272	0.12165±0.01288
2.25 - 2.50	0.93620±0.02341	0.05534±0.00420	0.00847±0.00161	0.20772±0.02728	0.77448±0.06386	0.01780±0.00733	0.49190±0.02914	0.38194±0.02472	0.12616±0.01282
2.50 - 2.75	0.94700±0.02419	0.04348±0.00379	0.00952±0.00175	0.20058±0.02646	0.77326±0.06313	0.02616±0.00883	0.49431±0.03056	0.38053±0.02577	0.12516±0.01334
2.75 - 3.00	0.98510±0.02603	0.01317±0.00215	0.00173±0.00078	0.16718±0.02458	0.82353±0.06819	0.00929±0.00539	0.45989±0.02996	0.38235±0.02658	0.15775±0.01563
3.00 - 3.25	0.99477±0.02826	0.00443±0.00134	0.00080±0.00057	0.10954±0.02072	0.87633±0.07622	0.01413±0.00712	0.43852±0.03057	0.41926±0.02969	0.14222±0.01551
3.25 - 3.50	0.99422±0.02970	0.00445±0.00141	0.00133±0.00077	0.14286±0.02357	0.85374±0.07337	0.00340±0.00341	0.46125±0.03569	0.40265±0.03267	0.13611±0.01710
3.50 - 3.75	0.99426±0.03079	0.00478±0.00152	0.00096±0.00068	0.20339±0.02880	0.79322±0.06944	0.00339±0.00340	0.43373±0.03871	0.40482±0.03702	0.16145±0.02126
3.75 - 4.00	0.99838±0.03287	0.00054±0.00054	0.00108±0.00077	0.14176±0.02490	0.82376±0.07587	0.03448±0.01169	0.42857±0.03917	0.31830±0.03243	0.25313±0.02820
4.00 - 4.25	0.99558±0.03543	0.00253±0.00127	0.00190±0.00110	0.24638±0.03852	0.71015±0.07660	0.04348±0.01480	0.31803±0.03707	0.20656±0.02859	0.47541±0.04796
4.25 - 4.50	0.99853±0.03829	–	0.00147±0.00104	0.31579±0.04269	0.61403±0.06593	0.07018±0.01815	0.25159±0.03167	0.15287±0.02369	0.59554±0.05501
4.50 - 4.75	1.00000±0.04061	–	–	0.24359±0.04407	0.67949±0.08553	0.07692±0.02304	0.19595±0.02814	0.12838±0.02212	0.67568±0.06185
4.75 - 5.00	1.00000±0.04331	–	–	0.25343±0.04664	0.68493±0.08891	0.06164±0.02117	0.20000±0.03068	0.07451±0.01772	0.72549±0.07007
5.00 - 5.25	0.99568±0.04632	0.00324±0.00187	0.00108±0.00108	0.26846±0.04781	0.67114±0.08676	0.06040±0.02073	0.19512±0.03373	0.09268±0.02223	0.71220±0.07713
5.25 - 5.50	0.99878±0.04928	–	0.00122±0.00122	0.39850±0.06473	0.56391±0.08143	0.03759±0.01713	0.20283±0.03392	0.05660±0.01680	0.74057±0.07798
5.50 - 5.75	0.99547±0.05474	0.00452±0.00262	–	0.35821±0.06026	0.58955±0.08363	0.05224±0.02025	0.17262±0.03471	0.02976±0.01351	0.79762±0.09238
5.75 - 6.00	1.00000±0.05712	–	–	0.32759±0.06123	0.58621±0.08953	0.08621±0.02841	0.17424±0.03937	0.02273±0.01327	0.80303±0.10473
6.00 - 6.50	0.99896±0.04547	0.00104±0.00104	–	0.38889±0.05774	0.58025±0.07523	0.03086±0.01401	0.17373±0.02939	0.04661±0.01438	0.77966±0.07668
6.50 - 7.00	1.00000±0.05252	–	–	0.34931±0.05682	0.62329±0.08325	0.02740±0.01388	0.10870±0.02559	0.07609±0.02109	0.81522±0.08968
7.00 - 7.50	1.00000±0.05793	–	–	0.39831±0.06870	0.56780±0.08686	0.03390±0.01723	0.18400±0.04175	0.04000±0.01824	0.77600±0.10500
7.50 - 8.00	1.00000±0.07161	–	–	0.44828±0.08639	0.54023±0.09780	0.01149±0.01156	0.19608±0.04795	0.05882±0.02471	0.74510±0.11291
8.00 - 8.50	1.00000±0.07956	–	–	0.36000±0.08080	0.58667±0.11141	0.05333±0.02737	0.16923±0.05517	0.18462±0.05801	0.64615±0.12792
8.50 - 9.00	1.00000±0.09225	–	–	0.36842±0.09405	0.54386±0.12137	0.08772±0.04091	0.07692±0.03991	0.17308±0.06249	0.75000±0.15887
9.00 - 9.50	1.00000±0.09806	–	–	0.55263±0.15027	0.39474±0.12037	0.05263±0.03818	0.27273±0.08882	0.09091±0.04748	0.63636±0.15384
9.50 - 10.0	1.00000±0.12356	–	–	0.31034±0.11842	0.68966±0.20045	–	0.19231±0.09391	0.19231±0.09391	0.61538±0.19553
10.0 - 11.0	1.00000±0.10483	–	–	0.34694±0.09766	0.65306±0.14843	–	0.16667±0.09001	0.12500±0.07655	0.70833±0.22454
11.0 - 12.0	1.00000±0.15713	–	–	0.18750±0.11797	0.81250±0.30338	–	0.16667±0.12729	0.16667±0.12729	0.66667±0.30429
12.0 - 13.0	1.00000±0.26726	–	–	0.37500±0.25388	0.62500±0.35630	–	–	0.10000±0.10488	0.90000±0.41352
13.0 - 14.0	1.00000±0.34300	–	–	0.33333±0.38490	0.66667±0.60858	–	0.44444±0.26708	–	0.55556±0.30987
14.0 - 15.0	1.00000±0.44721	–	–	0.50000±0.35355	0.50000±0.35355	–	0.42857±0.29574	0.14286±0.15272	0.42857±0.29574
15.0 - 30.0	1.00000±0.36515	–	–	1.00000±1.00000	–	–	–	–	1.00000±1.00000

Table D.27: Identification efficiencies for pions, kaons and protons in $N_{\mathrm{tracks}} > 2$ with the DRT method at $rQp > 0.5$.

Momentum range	Q_{π}^{π}	Q_{π}^{K}	Q_{π}^{p}	Q_{K}^{π}	$Q_{\mathrm{K}}^{\mathrm{K}}$	$Q_{\mathrm{K}}^{\mathrm{p}}$	Q_{p}^{π}	$Q_{\mathrm{p}}^{\mathrm{K}}$	$Q_{\mathrm{p}}^{\mathrm{p}}$
0.00 - 0.50	–	–	–	–	–	–	–	–	–
0.50 - 1.00	0.99835±0.02166	0.00165±0.00062	–	–	–	–	–	–	–
1.00 - 1.50	0.96572±0.00973	0.00728±0.00061	0.02699±0.00118	–	–	–	–	–	–
1.50 - 2.00	0.94171±0.00794	0.01206±0.00065	0.04623±0.00129	0.06250±0.06442	0.37500±0.17952	0.56250±0.23438	–	–	–
2.00 - 2.25	0.95556±0.01096	0.00816±0.00073	0.03629±0.00155	0.11080±0.00932	0.51941±0.02360	0.36979±0.01891	0.10602±0.00658	0.05763±0.00475	0.83635±0.02382
2.25 - 2.50	0.96025±0.01103	0.00381±0.00050	0.03594±0.00155	0.11404±0.00802	0.56868±0.02126	0.31728±0.01455	0.10590±0.00551	0.02563±0.00261	0.86846±0.02050
2.50 - 2.75	0.95968±0.01116	0.00404±0.00052	0.03628±0.00158	0.08756±0.00675	0.63828±0.02237	0.27416±0.01293	0.07884±0.00480	0.01897±0.00229	0.90219±0.02156
2.75 - 3.00	0.96677±0.01121	0.00297±0.00044	0.03026±0.00144	0.01877±0.00311	0.71689±0.02499	0.26433±0.01302	0.01894±0.00245	0.02609±0.00288	0.95497±0.02408
3.00 - 3.25	0.97130±0.01155	0.00327±0.00048	0.02543±0.00135	0.00915±0.00223	0.75834±0.02679	0.23251±0.01242	0.02393±0.00291	0.02358±0.00289	0.95250±0.02539
3.25 - 3.50	0.97728±0.01186	0.00226±0.00041	0.02046±0.00123	0.00453±0.00160	0.80758±0.02874	0.18789±0.01124	0.02443±0.00302	0.02480±0.00304	0.95077±0.02601
3.50 - 3.75	0.97763±0.01221	0.00386±0.00055	0.01851±0.00121	0.00589±0.00187	0.81202±0.02945	0.18209±0.01126	0.01794±0.00276	0.01669±0.00266	0.96537±0.02813
3.75 - 4.00	0.97780±0.01285	0.00470±0.00063	0.01750±0.00123	0.00705±0.00204	0.84900±0.03037	0.14395±0.00984	0.01888±0.00287	0.01587±0.00263	0.96525±0.02853
4.00 - 4.25	0.98393±0.01327	0.00560±0.00071	0.01047±0.00098	0.00820±0.00228	0.90726±0.03304	0.08454±0.00761	0.00690±0.00173	0.01941±0.00292	0.97368±0.02879
4.25 - 4.50	0.98387±0.01377	0.00670±0.00081	0.00942±0.00096	0.00274±0.00137	0.93707±0.03524	0.06019±0.00661	0.00493±0.00149	0.02508±0.00339	0.97000±0.02925
4.50 - 4.75	0.98498±0.01418	0.00751±0.00088	0.00751±0.00088	0.00447±0.00183	0.95678±0.03735	0.03875±0.00548	0.00466±0.00156	0.02486±0.00363	0.97048±0.03147
4.75 - 5.00	0.98483±0.01482	0.00820±0.00096	0.00697±0.00089	0.00889±0.00258	0.96593±0.03750	0.02519±0.00437	0.00266±0.00119	0.02555±0.00373	0.97179±0.03193
5.00 - 5.25	0.98547±0.01533	0.00853±0.00102	0.00601±0.00085	0.00478±0.00196	0.97209±0.03910	0.02313±0.00434	–	0.01676±0.00314	0.98324±0.03357
5.25 - 5.50	0.98526±0.01583	0.01115±0.00120	0.00359±0.00068	0.01132±0.00294	0.96830±0.03793	0.02038±0.00396	0.00125±0.00089	0.02257±0.00380	0.97618±0.03478
5.50 - 5.75	0.98588±0.01663	0.00946±0.00116	0.00466±0.00081	0.00086±0.00086	0.98710±0.04107	0.01204±0.00324	0.00145±0.00102	0.02168±0.00400	0.97688±0.03735
5.75 - 6.00	0.98468±0.01730	0.01026±0.00126	0.00506±0.00088	0.00088±0.00088	0.98067±0.04131	0.01845±0.00406	–	0.02348±0.00427	0.97652±0.03824
6.00 - 6.50	0.98489±0.01296	0.01151±0.00100	0.00361±0.00056	0.00197±0.00099	0.98226±0.03098	0.01577±0.00281	0.00041±0.00041	0.02095±0.00296	0.97864±0.02821
6.50 - 7.00	0.98190±0.01384	0.01279±0.00113	0.00531±0.00072	0.00109±0.00077	0.98422±0.03260	0.01469±0.00285	–	0.01446±0.00275	0.98555±0.03178
7.00 - 7.50	0.98531±0.01541	0.01214±0.00122	0.00255±0.00056	0.00062±0.00062	0.98128±0.03483	0.01809±0.00339	–	0.01963±0.00356	0.98037±0.03507
7.50 - 8.00	0.98379±0.01659	0.01100±0.00125	0.00522±0.00086	–	0.98387±0.03700	0.01613±0.00339	–	0.02254±0.00397	0.97746±0.03634
8.00 - 8.50	0.98228±0.01788	0.01297±0.00147	0.00476±0.00089	0.00081±0.00081	0.96423±0.03924	0.03496±0.00542	–	0.03252±0.00551	0.96748±0.04147
8.50 - 9.00	0.98336±0.01954	0.01155±0.00151	0.00509±0.00100	0.00088±0.00088	0.94982±0.04038	0.04930±0.00675	–	0.03288±0.00621	0.96712±0.04644
9.00 - 9.50	0.93504±0.01979	0.05890±0.00368	0.00606±0.00115	–	0.89515±0.04715	0.10485±0.01232	–	0.02865±0.00650	0.97135±0.05238
9.50 - 10.0	0.98559±0.02306	0.01087±0.00173	0.00353±0.00098	0.00220±0.00155	0.92316±0.04415	0.07464±0.00938	–	0.00166±0.00166	0.99834±0.05752
10.0 - 11.0	0.98445±0.01858	0.01131±0.00142	0.00424±0.00087	0.00070±0.00070	0.94542±0.03588	0.05388±0.00630	0.00227±0.00160	0.00340±0.00196	0.99434±0.04739
11.0 - 12.0	0.97891±0.02192	0.01787±0.00212	0.00323±0.00090	0.00105±0.00105	0.95488±0.04426	0.04407±0.00695	–	0.00141±0.00141	0.99859±0.05306
12.0 - 13.0	0.97114±0.02661	0.02701±0.00320	0.00185±0.00083	0.00164±0.00165	0.97368±0.05622	0.02467±0.00645	–	–	1.00000±0.07019
13.0 - 14.0	0.95605±0.03185	0.04124±0.00483	0.00271±0.00121	0.00811±0.00470	0.97027±0.07188	0.02162±0.00773	–	–	1.00000±0.08544
14.0 - 15.0	0.93966±0.03964	0.05517±0.00708	0.00517±0.00212	0.00559±0.00560	0.97765±0.10393	0.01676±0.00976	–	–	1.00000±0.11180
15.0 - 30.0	0.88956±0.03039	0.10934±0.00816	0.00110±0.00078	0.01190±0.00847	0.90476±0.10128	0.08333±0.02318	0.01932±0.00975	0.00966±0.00686	0.97101±0.09616

Table D.28: Identification purities and contaminations for pions, kaons and protons in $N_{\mathrm{tracks}} = 1$ with the DRT method at $rQp > 0.5$.

Momentum range	Q_{π}^{π}	Q_{π}^{K}	Q_{π}^{p}	Q_{K}^{π}	$Q_{\mathrm{K}}^{\mathrm{K}}$	$Q_{\mathrm{K}}^{\mathrm{p}}$	Q_{p}^{π}	$Q_{\mathrm{p}}^{\mathrm{K}}$	$Q_{\mathrm{p}}^{\mathrm{p}}$
0.00 - 0.50	–	–	–	–	–	–	–	–	–
0.50 - 1.00	0.99662±0.01989	0.00338±0.00082	–	–	–	–	–	–	–
1.00 - 1.50	0.91324±0.00862	0.02069±0.00095	0.06607±0.00173	–	–	–	–	–	–
1.50 - 2.00	0.85661±0.00701	0.02946±0.00097	0.11393±0.00198	0.20000±0.08281	0.14286±0.06830	0.65714±0.17639	–	–	–
2.00 - 2.25	0.88346±0.01037	0.02124±0.00118	0.09530±0.00260	0.18773±0.01018	0.28671±0.01309	0.52556±0.01930	0.10622±0.01060	0.06029±0.00782	0.83349±0.03824
2.25 - 2.50	0.88626±0.01072	0.01527±0.00103	0.09847±0.00273	0.20947±0.00943	0.32246±0.01223	0.46807±0.01553	0.11863±0.00983	0.03493±0.00513	0.84643±0.03373
2.50 - 2.75	0.88403±0.01101	0.01419±0.00102	0.10178±0.00286	0.18261±0.00885	0.36993±0.01355	0.44746±0.01532	0.11111±0.01035	0.02517±0.00473	0.86372±0.03738
2.75 - 3.00	0.90013±0.01142	0.01159±0.00095	0.08828±0.00271	0.04312±0.00440	0.50022±0.01799	0.45666±0.01694	0.02746±0.00517	0.02462±0.00489	0.94792±0.04182
3.00 - 3.25	0.90838±0.01192	0.00960±0.00089	0.08203±0.00270	0.02254±0.00336	0.52670±0.01985	0.45076±0.01790	0.04608±0.00687	0.02059±0.00454	0.93333±0.04206
3.25 - 3.50	0.91151±0.01251	0.01283±0.00108	0.07566±0.00270	0.01299±0.00261	0.59169±0.02212	0.39532±0.01693	0.03933±0.00698	0.01907±0.00481	0.94160±0.04668
3.50 - 3.75	0.91803±0.01325	0.01296±0.00114	0.06901±0.00271	0.01042±0.00240	0.59737±0.02288	0.39221±0.01731	0.03689±0.00710	0.03162±0.00656	0.93149±0.04869
3.75 - 4.00	0.92623±0.01415	0.01471±0.00129	0.05906±0.00265	0.01153±0.00281	0.65492±0.02711	0.33356±0.01737	0.01914±0.00469	0.02252±0.00509	0.95833±0.04597
4.00 - 4.25	0.94075±0.01506	0.02174±0.00166	0.03751±0.00220	0.01765±0.00398	0.75375±0.03416	0.22860±0.01574	0.01107±0.00309	0.04003±0.00596	0.94889±0.03969
4.25 - 4.50	0.93663±0.01620	0.02561±0.00195	0.03776±0.00238	0.01050±0.00334	0.82983±0.03994	0.15966±0.01395	0.00974±0.00295	0.03366±0.00555	0.95660±0.04072
4.50 - 4.75	0.93701±0.01708	0.02732±0.00212	0.03567±0.00244	0.01527±0.00444	0.86896±0.04546	0.11578±0.01282	0.01047±0.00317	0.04853±0.00696	0.94101±0.04169
4.75 - 5.00	0.94303±0.01809	0.02483±0.00213	0.03215±0.00243	0.00712±0.00320	0.91026±0.04977	0.08262±0.01129	0.00654±0.00268	0.03272±0.00607	0.96074±0.04532
5.00 - 5.25	0.94343±0.01908	0.03037±0.00249	0.02620±0.00231	0.00495±0.00287	0.92904±0.05438	0.06601±0.01078	0.00115±0.00115	0.02985±0.00594	0.96900±0.04680
5.25 - 5.50	0.93504±0.01996	0.03876±0.00298	0.02621±0.00243	0.00367±0.00260	0.91927±0.05690	0.07706±0.01234	0.00245±0.00173	0.02938±0.00608	0.96818±0.04829
5.50 - 5.75	0.93992±0.02178	0.04057±0.00331	0.01951±0.00227	–	0.94615±0.05951	0.05385±0.01045	–	0.03426±0.00683	0.96574±0.05001
5.75 - 6.00	0.94607±0.02256	0.03236±0.00304	0.02157±0.00247	0.00440±0.00311	0.96044±0.06433	0.03516±0.00894	–	0.02469±0.00625	0.97531±0.05453
6.00 - 6.50	0.93900±0.01737	0.04127±0.00267	0.01972±0.00183	0.00809±0.00331	0.93800±0.04950	0.05391±0.00875	0.00083±0.00083	0.02085±0.00421	0.97832±0.04018
6.50 - 7.00	0.93741±0.01947	0.04611±0.00317	0.01648±0.00187	0.00285±0.00202	0.95157±0.05143	0.04558±0.00824	–	0.02258±0.00498	0.97742±0.04559
7.00 - 7.50	0.93155±0.02132	0.04774±0.00355	0.02071±0.00231	0.00173±0.00173	0.94627±0.05650	0.05199±0.00974	0.00143±0.00143	0.03152±0.00682	0.96705±0.05220
7.50 - 8.00	0.92642±0.02405	0.04797±0.00404	0.02561±0.00292	–	0.88699±0.05974	0.11301±0.01638	–	0.02444±0.00686	0.97556±0.06019
8.00 - 8.50	0.92632±0.02741	0.05053±0.00473	0.02316±0.00316	–	0.88806±0.06458	0.11194±0.01760	–	0.04271±0.01058	0.95729±0.06861
8.50 - 9.00	0.92101±0.03052	0.05108±0.00532	0.02791±0.00389	–	0.88000±0.06875	0.12000±0.01960	–	0.07904±0.01712	0.92096±0.07797
9.00 - 9.50	0.89203±0.03293	0.08355±0.00763	0.02442±0.00401	–	0.86869±0.09055	0.13131±0.02739	0.00429±0.00430	0.06009±0.01653	0.93562±0.08816
9.50 - 10.0	0.92040±0.03828	0.05224±0.00675	0.02736±0.00483	–	0.86975±0.08266	0.13025±0.02487	–	–	1.00000±0.11547
10.0 - 11.0	0.92546±0.03260	0.04413±0.00524	0.03041±0.00432	–	0.84337±0.06843	0.15663±0.02336	–	0.00844±0.00599	0.99156±0.09128
11.0 - 12.0	0.94294±0.04209	0.03578±0.00599	0.02128±0.00458	–	0.86784±0.08450	0.13216±0.02567	–	–	1.00000±0.11043
12.0 - 13.0	0.94546±0.05514	0.04959±0.00928	0.00496±0.00287	–	0.87023±0.11146	0.12977±0.03345	–	–	1.00000±0.14510
13.0 - 14.0	0.89296±0.06900	0.07887±0.01548	0.02817±0.00903	–	0.86207±0.16636	0.13793±0.05202	–	–	1.00000±0.18569
14.0 - 15.0	0.86580±0.08362	0.12121±0.02426	0.01299±0.00755	–	0.89655±0.24214	0.10345±0.06274	–	–	1.00000±0.25820
15.0 - 30.0	0.83051±0.08026	0.14830±0.02686	0.02119±0.00957	–	0.83333±0.25230	0.16667±0.09001	–	–	1.00000±0.29488

Table D.29: Identification purities and contaminations for pions, kaons and protons in $N_{\mathrm{tracks}} = 2$ with the DRT method at $rQp > 0.5$.

Momentum range	Q_π^π	Q_π^{K}	Q_π^{p}	Q_{K}^π	$Q_{\mathrm{K}}^{\mathrm{K}}$	$Q_{\mathrm{K}}^{\mathrm{p}}$	Q_{p}^π	$Q_{\mathrm{p}}^{\mathrm{K}}$	$Q_{\mathrm{p}}^{\mathrm{p}}$
0.00 - 0.50	–	–	–	–	–	–	–	–	–
0.50 - 1.00	0.99556±0.03835	0.00444±0.00182	–	–	–	–	–	–	–
1.00 - 1.50	0.90017±0.01640	0.02500±0.00201	0.07483±0.00356	–	–	–	–	–	–
1.50 - 2.00	0.82620±0.01336	0.04023±0.00223	0.13358±0.00423	0.27273±0.17764	0.27273±0.17764	0.45454±0.24516	–	–	–
2.00 - 2.25	0.86012±0.01992	0.02629±0.00259	0.11359±0.00560	0.17476±0.01997	0.31262±0.02823	0.51262±0.03880	0.11111±0.03248	0.03419±0.01738	0.85470±0.11640
2.25 - 2.50	0.86216±0.02114	0.01949±0.00235	0.11835±0.00607	0.23643±0.01943	0.33721±0.02414	0.42636±0.02803	0.19580±0.04046	0.04196±0.01749	0.76224±0.09692
2.50 - 2.75	0.86643±0.02167	0.02003±0.00244	0.11353±0.00606	0.19460±0.01817	0.37784±0.02719	0.42756±0.02944	0.21739±0.04379	0.06522±0.02244	0.71739±0.09449
2.75 - 3.00	0.87720±0.02254	0.01666±0.00229	0.10614±0.00602	0.06441±0.01078	0.45085±0.03330	0.48475±0.03493	0.03968±0.01810	0.02381±0.01391	0.93651±0.11997
3.00 - 3.25	0.88317±0.02438	0.01108±0.00200	0.10575±0.00646	0.02030±0.00618	0.45756±0.03508	0.52214±0.03829	0.01961±0.01400	0.03922±0.01999	0.94118±0.13383
3.25 - 3.50	0.88655±0.02576	0.01666±0.00259	0.09679±0.00649	0.02110±0.00674	0.52954±0.04134	0.44937±0.03707	0.03947±0.02324	0.01316±0.01324	0.94737±0.15580
3.50 - 3.75	0.89655±0.02707	0.02586±0.00338	0.07759±0.00600	0.02427±0.00777	0.56796±0.04649	0.40777±0.03733	0.02857±0.02049	0.01429±0.01439	0.95714±0.16359
3.75 - 4.00	0.89864±0.02884	0.01803±0.00299	0.08333±0.00663	0.00292±0.00292	0.62682±0.05452	0.37026±0.03846	0.01786±0.01274	0.08036±0.02784	0.90179±0.12374
4.00 - 4.25	0.91415±0.03186	0.02958±0.00420	0.05626±0.00587	0.01869±0.00943	0.68692±0.07359	0.29439±0.04220	0.01911±0.01114	0.05732±0.01965	0.92357±0.10637
4.25 - 4.50	0.90000±0.03365	0.04768±0.00575	0.05232±0.00604	–	0.74468±0.08313	0.25532±0.04129	0.00976±0.00693	0.07805±0.02026	0.91219±0.09224
4.50 - 4.75	0.92666±0.03693	0.02903±0.00478	0.04431±0.00595	–	0.73611±0.09421	0.26389±0.04813	–	0.05660±0.01680	0.94340±0.09299
4.75 - 5.00	0.92374±0.03924	0.03206±0.00535	0.04419±0.00632	–	0.84034±0.11400	0.15966±0.03945	–	0.04639±0.01582	0.95361±0.09799
5.00 - 5.25	0.92016±0.04199	0.03992±0.00644	0.03992±0.00644	0.02459±0.01437	0.81967±0.11057	0.15574±0.03841	0.00641±0.00643	0.05769±0.01978	0.93590±0.10777
5.25 - 5.50	0.89531±0.04302	0.05780±0.00817	0.04689±0.00732	–	0.86207±0.13583	0.13793±0.04247	0.00613±0.00615	0.03067±0.01393	0.96319±0.10771
5.50 - 5.75	0.89552±0.04799	0.06513±0.00970	0.03935±0.00745	0.03448±0.02025	0.90805±0.14112	0.05747±0.02643	–	0.04965±0.01922	0.95035±0.11465
5.75 - 6.00	0.90950±0.05076	0.05638±0.00940	0.03412±0.00724	–	0.95775±0.16251	0.04225±0.02491	–	0.08621±0.02841	0.91379±0.12278
6.00 - 6.50	0.90271±0.04008	0.05893±0.00764	0.03835±0.00610	0.00943±0.00948	0.88679±0.12564	0.10377±0.03287	–	0.02645±0.01199	0.97354±0.10083
6.50 - 7.00	0.91080±0.04676	0.06407±0.00925	0.02513±0.00569	–	0.86667±0.12413	0.13333±0.03794	–	0.02597±0.01315	0.97403±0.11174
7.00 - 7.50	0.89489±0.05046	0.07057±0.01065	0.03453±0.00732	–	0.93056±0.15796	0.06944±0.03212	–	0.03960±0.02019	0.96040±0.13653
7.50 - 8.00	0.86860±0.06012	0.08686±0.01450	0.04454±0.01018	–	0.88679±0.17768	0.11321±0.04876	–	0.01299±0.01307	0.98701±0.15959
8.00 - 8.50	0.89265±0.06908	0.07627±0.01523	0.03107±0.00951	–	0.78571±0.15829	0.21429±0.06817	–	0.08696±0.04533	0.91304±0.19486
8.50 - 9.00	0.90385±0.08135	0.08077±0.01832	0.01538±0.00775	–	0.77500±0.18545	0.22500±0.08301	–	0.11364±0.05363	0.88636±0.19494
9.00 - 9.50	0.86307±0.08168	0.08714±0.01983	0.04979±0.01473	–	0.78947±0.27268	0.21053±0.11582	–	0.06667±0.04869	0.93333±0.24525
9.50 - 10.0	0.90345±0.10890	0.06207±0.02132	0.03448±0.01568	–	0.80000±0.24000	0.20000±0.09798	–	–	1.00000±0.35355
10.0 - 11.0	0.89655±0.09152	0.08374±0.02114	0.01970±0.00995	–	0.91429±0.22362	0.08571±0.05156	–	–	1.00000±0.34300
11.0 - 12.0	0.94186±0.14583	0.03488±0.02049	0.02326±0.01663	–	0.86667±0.32841	0.13333±0.10037	–	–	1.00000±0.50000
12.0 - 13.0	0.90323±0.23548	0.09677±0.05851	–	–	0.83333±0.50461	0.16667±0.18002	–	–	1.00000±0.47141
13.0 - 14.0	0.77273±0.24953	0.04545±0.04648	0.18182±0.09883	–	1.00000±1.00000	–	–	–	1.00000±0.63246
14.0 - 15.0	0.62500±0.25195	0.18750±0.11797	0.18750±0.11797	–	0.75000±0.57282	0.25000±0.27951	–	–	1.00000±0.81650
15.0 - 30.0	0.88235±0.31257	0.11765±0.08795	–	–	–	–	–	–	1.00000±1.00000

Table D.30: Identification purities and contaminations for pions, kaons and protons in $N_{\mathrm{tracks}} > 2$ with the DRT method at $rQp > 0.5$.

Momentum range	$\mathcal{P}_{\pi}^{\pi}$	$\mathcal{P}_{\pi}^{\mathrm{K}}$	$\mathcal{P}_{\pi}^{\mathrm{p}}$	$\mathcal{P}_{\mathrm{K}}^{\pi}$	$\mathcal{P}_{\mathrm{K}}^{\mathrm{K}}$	$\mathcal{P}_{\mathrm{K}}^{\mathrm{p}}$	$\mathcal{P}_{\mathrm{p}}^{\pi}$	$\mathcal{P}_{\mathrm{p}}^{\mathrm{K}}$	$\mathcal{P}_{\mathrm{p}}^{\mathrm{p}}$
0.00 - 0.50	–	–	–	–	–	–	–	–	–
0.50 - 1.00	1.00000±0.00000	–	–	1.00000±0.00000	–	–	–	–	–
1.00 - 1.50	1.00000±0.00000	–	–	1.00000±0.00000	–	–	1.00000±0.00000	–	–
1.50 - 2.00	0.99996±0.00004	0.00004±0.00004	–	0.98095±0.00770	0.01905±0.00770	–	0.99312±0.00242	0.00688±0.00242	–
2.00 - 2.25	0.99031±0.00082	0.00969±0.00082	–	0.14092±0.01223	0.85908±0.01223	–	0.51521±0.01619	0.48479±0.01619	–
2.25 - 2.50	0.96974±0.00142	0.01327±0.00095	0.01700±0.00107	0.04431±0.00607	0.90356±0.00870	0.05213±0.00655	0.14043±0.00589	0.13755±0.00584	0.72201±0.00760
2.50 - 2.75	0.97266±0.00137	0.01102±0.00088	0.01632±0.00107	0.04348±0.00554	0.91157±0.00771	0.04495±0.00562	0.11895±0.00510	0.11919±0.00511	0.76186±0.00671
2.75 - 3.00	0.99400±0.00065	0.00250±0.00042	0.00350±0.00050	0.02718±0.00429	0.91847±0.00722	0.05436±0.00598	0.11057±0.00514	0.10950±0.00512	0.77993±0.00680
3.00 - 3.25	0.99573±0.00056	0.00097±0.00027	0.00330±0.00050	0.02943±0.00447	0.92922±0.00679	0.04135±0.00527	0.09631±0.00517	0.10646±0.00541	0.79723±0.00705
3.25 - 3.50	0.99533±0.00060	0.00047±0.00019	0.00420±0.00057	0.01870±0.00356	0.93975±0.00626	0.04155±0.00525	0.08846±0.00521	0.09351±0.00534	0.81803±0.00708
3.50 - 3.75	0.99655±0.00053	0.00058±0.00022	0.00288±0.00049	0.03233±0.00474	0.94181±0.00627	0.02586±0.00425	0.08072±0.00527	0.10501±0.00593	0.81427±0.00752
3.75 - 4.00	0.99635±0.00058	0.00055±0.00022	0.00311±0.00053	0.03586±0.00488	0.94138±0.00617	0.02276±0.00392	0.07368±0.00526	0.07571±0.00532	0.85061±0.00717
4.00 - 4.25	0.99875±0.00035	0.00106±0.00032	0.00019±0.00014	0.03994±0.00514	0.93113±0.00665	0.02893±0.00440	0.04567±0.00433	0.04438±0.00427	0.90995±0.00594
4.25 - 4.50	0.99907±0.00031	0.00041±0.00021	0.00052±0.00023	0.04603±0.00558	0.92210±0.00713	0.03187±0.00467	0.04077±0.00423	0.03115±0.00372	0.92808±0.00553
4.50 - 4.75	0.99891±0.00035	0.00055±0.00024	0.00055±0.00024	0.04973±0.00601	0.92119±0.00745	0.02907±0.00465	0.03482±0.00424	0.02035±0.00327	0.94483±0.00528
4.75 - 5.00	0.99820±0.00046	0.00144±0.00042	0.00036±0.00021	0.04597±0.00575	0.93142±0.00694	0.02261±0.00408	0.03123±0.00411	0.01339±0.00271	0.95538±0.00488
5.00 - 5.25	0.99924±0.00031	0.00076±0.00031	–	0.05238±0.00632	0.92748±0.00736	0.02014±0.00399	0.02657±0.00395	0.01208±0.00268	0.96135±0.00474
5.25 - 5.50	0.99768±0.00056	0.00205±0.00053	0.00027±0.00019	0.05753±0.00641	0.92279±0.00734	0.01968±0.00382	0.01587±0.00321	0.01389±0.00301	0.97024±0.00437
5.50 - 5.75	0.99955±0.00026	0.00015±0.00015	0.00030±0.00021	0.04836±0.00630	0.93351±0.00732	0.01813±0.00392	0.02301±0.00415	0.00997±0.00275	0.96703±0.00495
5.75 - 6.00	0.99984±0.00016	0.00016±0.00016	–	0.05044±0.00651	0.93628±0.00727	0.01327±0.00340	0.02238±0.00418	0.01439±0.00337	0.96323±0.00532
6.00 - 6.50	0.99963±0.00018	0.00037±0.00018	–	0.06084±0.00530	0.92836±0.00571	0.01079±0.00229	0.01751±0.00274	0.01138±0.00222	0.97112±0.00350
6.50 - 7.00	0.99979±0.00015	0.00021±0.00015	–	0.06291±0.00568	0.93381±0.00581	0.00328±0.00134	0.02694±0.00376	0.01293±0.00262	0.96013±0.00454
7.00 - 7.50	1.00000±0.00000	–	–	0.05734±0.00584	0.93321±0.00627	0.00945±0.00243	0.01293±0.00295	0.01293±0.00295	0.97413±0.00414
7.50 - 8.00	1.00000±0.00000	–	–	0.04892±0.00579	0.94460±0.00614	0.00647±0.00215	0.02446±0.00414	0.01079±0.00277	0.96475±0.00495
8.00 - 8.50	0.99982±0.00018	0.00018±0.00018	–	0.05907±0.00680	0.92429±0.00763	0.01664±0.00369	0.02339±0.00472	0.02827±0.00517	0.94834±0.00691
8.50 - 9.00	0.99979±0.00021	0.00021±0.00021	–	0.04731±0.00647	0.94341±0.00704	0.00928±0.00292	0.03149±0.00620	0.04534±0.00738	0.92317±0.00945
9.00 - 9.50	1.00000±0.00000	–	–	0.27357±0.01521	0.70780±0.01552	0.01863±0.00461	0.03858±0.00742	0.08160±0.01054	0.87982±0.01253
9.50 - 10.0	0.99942±0.00041	0.00058±0.00041	–	0.04217±0.00698	0.95783±0.00698	–	0.01937±0.00578	0.06866±0.01061	0.91197±0.01189
10.0 - 11.0	0.99981±0.00019	–	0.00019±0.00019	0.04236±0.00554	0.95613±0.00563	0.00151±0.00107	0.02604±0.00548	0.05799±0.00804	0.91598±0.00954
11.0 - 12.0	0.99974±0.00026	0.00026±0.00026	–	0.06757±0.00842	0.93131±0.00849	0.00113±0.00113	0.01679±0.00502	0.04275±0.00790	0.94046±0.00925
12.0 - 13.0	1.00000±0.00000	–	–	0.08362±0.01155	0.91638±0.01155	–	0.01031±0.00513	0.02062±0.00721	0.96907±0.00879
13.0 - 14.0	0.99820±0.00104	0.00180±0.00104	–	0.15057±0.01906	0.84943±0.01906	–	0.00769±0.00542	0.01923±0.00852	0.97308±0.01004
14.0 - 15.0	0.99904±0.00096	0.00096±0.00096	–	0.20670±0.03027	0.79330±0.03027	–	0.03205±0.01410	0.01282±0.00901	0.95513±0.01658
15.0 - 30.0	0.99675±0.00145	0.00065±0.00065	0.00260±0.00130	0.54546±0.03276	0.44589±0.03270	0.00866±0.00610	0.01010±0.00711	0.06566±0.01760	0.92424±0.01880

Table D.31: Identification efficiencies for pions, kaons and protons in $N_{\mathrm{tracks}} = 1$ with the DRT method at $rQp > 1.0$.

Momentum range	$\mathcal{P}_{\pi}^{\pi}$	$\mathcal{P}_{\pi}^{\mathrm{K}}$	$\mathcal{P}_{\pi}^{\mathrm{p}}$	$\mathcal{P}_{\mathrm{K}}^{\pi}$	$\mathcal{P}_{\mathrm{K}}^{\mathrm{K}}$	$\mathcal{P}_{\mathrm{K}}^{\mathrm{p}}$	$\mathcal{P}_{\mathrm{p}}^{\pi}$	$\mathcal{P}_{\mathrm{p}}^{\mathrm{K}}$	$\mathcal{P}_{\mathrm{p}}^{\mathrm{p}}$
0.00 - 0.50	–	–	–	–	–	–	–	–	–
0.50 - 1.00	1.00000±0.00000	–	–	1.00000±0.00000	–	–	–	–	–
1.00 - 1.50	1.00000±0.00000	–	–	1.00000±0.00000	–	–	1.00000±0.00000	–	–
1.50 - 2.00	0.99977±0.00009	0.00023±0.00009	–	0.99417±0.00260	0.00583±0.00260	–	0.99372±0.00137	0.00628±0.00137	–
2.00 - 2.25	0.97334±0.00139	0.02666±0.00139	–	0.33681±0.01608	0.66319±0.01608	–	0.56586±0.01032	0.43414±0.01032	–
2.25 - 2.50	0.95241±0.00188	0.04048±0.00174	0.00711±0.00074	0.18727±0.01185	0.78967±0.01238	0.02306±0.00456	0.39688±0.00864	0.35514±0.00845	0.24798±0.00762
2.50 - 2.75	0.95557±0.00188	0.03589±0.00169	0.00854±0.00084	0.15385±0.01061	0.82455±0.01118	0.02161±0.00427	0.38367±0.00865	0.33935±0.00842	0.27699±0.00796
2.75 - 3.00	0.98997±0.00093	0.00774±0.00082	0.00229±0.00045	0.10488±0.00874	0.87805±0.00933	0.01707±0.00369	0.36894±0.00901	0.31483±0.00868	0.31623±0.00869
3.00 - 3.25	0.99304±0.00081	0.00376±0.00059	0.00320±0.00055	0.09624±0.00872	0.88714±0.00936	0.01662±0.00378	0.36102±0.00953	0.29724±0.00907	0.34173±0.00941
3.25 - 3.50	0.99547±0.00068	0.00175±0.00042	0.00278±0.00053	0.10782±0.00890	0.88148±0.00927	0.01070±0.00295	0.35897±0.01036	0.30956±0.00998	0.33147±0.01016
3.50 - 3.75	0.99546±0.00072	0.00159±0.00042	0.00295±0.00058	0.10318±0.00892	0.87962±0.00954	0.01720±0.00381	0.33721±0.01088	0.32557±0.01078	0.33721±0.01088
3.75 - 4.00	0.99696±0.00062	0.00165±0.00046	0.00140±0.00042	0.11657±0.00996	0.86609±0.01057	0.01734±0.00405	0.28790±0.01119	0.24389±0.01062	0.46821±0.01234
4.00 - 4.25	0.99710±0.00063	0.00263±0.00060	0.00028±0.00020	0.15547±0.01148	0.80642±0.01251	0.03811±0.00606	0.17697±0.00973	0.14639±0.00902	0.67664±0.01193
4.25 - 4.50	0.99790±0.00058	0.00146±0.00049	0.00065±0.00032	0.16955±0.01233	0.79698±0.01322	0.03348±0.00591	0.17524±0.01023	0.09920±0.00804	0.72556±0.01201
4.50 - 4.75	0.99696±0.00074	0.00161±0.00054	0.00143±0.00051	0.18117±0.01330	0.76758±0.01458	0.05125±0.00761	0.16944±0.01081	0.06063±0.00688	0.76993±0.01213
4.75 - 5.00	0.99842±0.00056	0.00079±0.00039	0.00079±0.00039	0.16929±0.01359	0.80053±0.01448	0.03018±0.00620	0.15692±0.01136	0.04581±0.00653	0.79727±0.01255
5.00 - 5.25	0.99934±0.00038	0.00066±0.00038	–	0.20086±0.01512	0.76638±0.01597	0.03276±0.00672	0.12580±0.01083	0.03838±0.00627	0.83582±0.01210
5.25 - 5.50	0.99901±0.00050	0.00050±0.00035	0.00050±0.00035	0.24848±0.01687	0.72256±0.01748	0.02896±0.00655	0.12018±0.01095	0.03741±0.00639	0.84240±0.01227
5.50 - 5.75	1.00000±0.00000	–	–	0.23595±0.01701	0.72873±0.01781	0.03531±0.00739	0.08779±0.01009	0.03053±0.00614	0.88168±0.01152
5.75 - 6.00	0.99939±0.00043	0.00061±0.00043	–	0.20075±0.01735	0.76923±0.01825	0.03002±0.00739	0.10915±0.01198	0.01770±0.00506	0.87316±0.01278
6.00 - 6.50	0.99908±0.00041	0.00092±0.00041	–	0.25799±0.01453	0.72216±0.01487	0.01985±0.00463	0.08542±0.00793	0.02740±0.00463	0.88719±0.00898
6.50 - 7.00	0.99953±0.00033	0.00047±0.00033	–	0.23669±0.01462	0.74438±0.01501	0.01893±0.00469	0.07975±0.00878	0.02728±0.00528	0.89297±0.01001
7.00 - 7.50	0.99943±0.00040	0.00028±0.00028	0.00028±0.00028	0.24744±0.01651	0.73206±0.01695	0.02050±0.00542	0.10881±0.01156	0.03444±0.00677	0.85675±0.01300
7.50 - 8.00	1.00000±0.00000	–	–	0.25283±0.01888	0.72453±0.01941	0.02264±0.00646	0.12436±0.01362	0.07155±0.01064	0.80409±0.01638
8.00 - 8.50	1.00000±0.00000	–	–	0.23831±0.02011	0.73274±0.02088	0.02895±0.00791	0.11290±0.01519	0.07604±0.01272	0.81106±0.01879
8.50 - 9.00	1.00000±0.00000	–	–	0.22835±0.02151	0.72966±0.02275	0.04199±0.01028	0.14744±0.02007	0.09936±0.01694	0.75321±0.02441
9.00 - 9.50	1.00000±0.00000	–	–	0.40824±0.03008	0.55431±0.03042	0.03745±0.01162	0.13992±0.02225	0.07819±0.01722	0.78189±0.02649
9.50 - 10.0	1.00000±0.00000	–	–	0.22177±0.02638	0.77823±0.02638	–	0.16043±0.02684	0.11765±0.02356	0.72193±0.03276
10.0 - 11.0	1.00000±0.00000	–	–	0.20060±0.02191	0.79341±0.02215	0.00599±0.00422	0.16319±0.02178	0.14236±0.02059	0.69444±0.02714
11.0 - 12.0	1.00000±0.00000	–	–	0.14423±0.02436	0.85577±0.02436	–	0.09474±0.02125	0.12105±0.02366	0.78421±0.02984
12.0 - 13.0	1.00000±0.00000	–	–	0.20168±0.03678	0.79832±0.03678	–	0.03000±0.01706	0.11000±0.03129	0.86000±0.03470
13.0 - 14.0	1.00000±0.00000	–	–	0.33846±0.05869	0.66154±0.05869	–	0.13433±0.04166	0.08955±0.03488	0.77612±0.05093
14.0 - 15.0	1.00000±0.00000	–	–	0.58537±0.07694	0.41463±0.07694	–	0.05882±0.04035	0.08824±0.04864	0.85294±0.06074
15.0 - 30.0	1.00000±0.00000	–	–	0.60000±0.07746	0.40000±0.07746	–	0.16667±0.06804	0.10000±0.05477	0.73333±0.08074

Table D.32: Identification efficiencies for pions, kaons and protons in $N_{\mathrm{tracks}} = 2$ with the DRT method at $rQp > 1.0$.

Momentum range	$\mathcal{P}_{\pi}^{\pi}$	$\mathcal{P}_{\pi}^{\mathrm{K}}$	$\mathcal{P}_{\pi}^{\mathrm{p}}$	$\mathcal{P}_{\mathrm{K}}^{\pi}$	$\mathcal{P}_{\mathrm{K}}^{\mathrm{K}}$	$\mathcal{P}_{\mathrm{K}}^{\mathrm{p}}$	$\mathcal{P}_{\mathrm{p}}^{\pi}$	$\mathcal{P}_{\mathrm{p}}^{\mathrm{K}}$	$\mathcal{P}_{\mathrm{p}}^{\mathrm{p}}$
0.00 - 0.50	–	–	–	–	–	–	–	–	–
0.50 - 1.00	1.00000±0.00000	–	–	1.00000±0.00000	–	–	–	–	–
1.00 - 1.50	1.00000±0.00000	–	–	1.00000±0.00000	–	–	1.00000±0.00000	–	–
1.50 - 2.00	0.99955±0.00026	0.00045±0.00026	–	0.99013±0.00567	0.00987±0.00567	–	0.99517±0.00215	0.00483±0.00215	–
2.00 - 2.25	0.97683±0.00259	0.02317±0.00259	–	0.37917±0.03132	0.62083±0.03132	–	0.62423±0.01897	0.37577±0.01897	–
2.25 - 2.50	0.94279±0.00418	0.05268±0.00402	0.00452±0.00121	0.21122±0.02345	0.78218±0.02371	0.00660±0.00465	0.52080±0.01830	0.39195±0.01789	0.08725±0.01034
2.50 - 2.75	0.95295±0.00390	0.03859±0.00354	0.00846±0.00169	0.20128±0.02266	0.78275±0.02331	0.01597±0.00709	0.48787±0.01888	0.39230±0.01844	0.11983±0.01227
2.75 - 3.00	0.98722±0.00215	0.01205±0.00209	0.00073±0.00052	0.16333±0.02134	0.82667±0.02185	0.01000±0.00574	0.45675±0.01940	0.38543±0.01896	0.15782±0.01420
3.00 - 3.25	0.99581±0.00132	0.00336±0.00118	0.00084±0.00059	0.10448±0.01868	0.88060±0.01981	0.01493±0.00741	0.44974±0.02053	0.41738±0.02035	0.13288±0.01401
3.25 - 3.50	0.99441±0.00161	0.00419±0.00139	0.00140±0.00081	0.13879±0.02062	0.86121±0.02062	–	0.47881±0.02299	0.39195±0.02247	0.12924±0.01544
3.50 - 3.75	0.99448±0.00166	0.00452±0.00150	0.00100±0.00071	0.20290±0.02421	0.79348±0.02437	0.00362±0.00362	0.44444±0.02587	0.40379±0.02554	0.15176±0.01868
3.75 - 4.00	0.99887±0.00080	0.00057±0.00057	0.00057±0.00057	0.14056±0.02203	0.83534±0.02350	0.02410±0.00972	0.43228±0.02659	0.29971±0.02459	0.26801±0.02378
4.00 - 4.25	0.99803±0.00114	0.00131±0.00093	0.00066±0.00066	0.24742±0.03098	0.71134±0.03253	0.04124±0.01428	0.34340±0.02917	0.20000±0.02457	0.45660±0.03060
4.25 - 4.50	0.99923±0.00077	–	0.00077±0.00077	0.32211±0.03240	0.62500±0.03357	0.05288±0.01552	0.26071±0.02624	0.14286±0.02091	0.59643±0.02932
4.50 - 4.75	1.00000±0.00000	–	–	0.25170±0.03579	0.68707±0.03824	0.06122±0.01977	0.20788±0.02429	0.11470±0.01908	0.67742±0.02799
4.75 - 5.00	1.00000±0.00000	–	–	0.23308±0.03666	0.69925±0.03976	0.06767±0.02178	0.20165±0.02574	0.06996±0.01636	0.72840±0.02853
5.00 - 5.25	0.99548±0.00225	0.00339±0.00195	0.00113±0.00113	0.26241±0.03705	0.68085±0.03926	0.05674±0.01948	0.18325±0.02799	0.09424±0.02114	0.72251±0.03240
5.25 - 5.50	0.99872±0.00128	–	0.00128±0.00128	0.40323±0.04405	0.56452±0.04453	0.03226±0.01587	0.19192±0.02799	0.05051±0.01556	0.75758±0.03046
5.50 - 5.75	0.99684±0.00223	0.00316±0.00223	–	0.35246±0.04325	0.61475±0.04406	0.03279±0.01612	0.16250±0.02916	0.03125±0.01376	0.80625±0.03125
5.75 - 6.00	1.00000±0.00000	–	–	0.33981±0.04667	0.58252±0.04859	0.07767±0.02637	0.16260±0.03327	0.02439±0.01391	0.81301±0.03516
6.00 - 6.50	0.99891±0.00109	0.00109±0.00109	–	0.40541±0.04036	0.56757±0.04072	0.02703±0.01333	0.16964±0.02508	0.03571±0.01240	0.79464±0.02699
6.50 - 7.00	1.00000±0.00000	–	–	0.35252±0.04052	0.62590±0.04104	0.02158±0.01233	0.10843±0.02413	0.07229±0.02010	0.81928±0.02987
7.00 - 7.50	1.00000±0.00000	–	–	0.39286±0.04615	0.57143±0.04676	0.03571±0.01754	0.18803±0.03612	0.02564±0.01461	0.78633±0.03790
7.50 - 8.00	1.00000±0.00000	–	–	0.43210±0.05504	0.55556±0.05521	0.01235±0.01227	0.17977±0.04070	0.05618±0.02441	0.76404±0.04501
8.00 - 8.50	1.00000±0.00000	–	–	0.36765±0.05847	0.58823±0.05968	0.04412±0.02490	0.15790±0.04830	0.10526±0.04065	0.73684±0.05833
8.50 - 9.00	1.00000±0.00000	–	–	0.38776±0.06961	0.53061±0.07129	0.08163±0.03911	0.06250±0.03494	0.18750±0.05634	0.75000±0.06250
9.00 - 9.50	1.00000±0.00000	–	–	0.57143±0.08365	0.37143±0.08167	0.05714±0.03923	0.28947±0.07357	0.07895±0.04374	0.63158±0.07825
9.50 - 10.0	1.00000±0.00000	–	–	0.36000±0.09600	0.64000±0.09600	–	0.21739±0.08601	0.17391±0.07903	0.60870±0.10176
10.0 - 11.0	1.00000±0.00000	–	–	0.31111±0.06901	0.68889±0.06901	–	0.18182±0.08223	0.09091±0.06129	0.72727±0.09495
11.0 - 12.0	1.00000±0.00000	–	–	0.21429±0.10966	0.78571±0.10966	–	0.22222±0.13858	–	0.77778±0.13858
12.0 - 13.0	1.00000±0.00000	–	–	0.42857±0.18704	0.57143±0.18704	–	–	–	1.00000±0.00000
13.0 - 14.0	1.00000±0.00000	–	–	0.33333±0.27217	0.66667±0.27217	–	0.44444±0.16564	–	0.55556±0.16564
14.0 - 15.0	1.00000±0.00000	–	–	0.50000±0.25000	0.50000±0.25000	–	0.50000±0.20412	0.16667±0.15215	0.33333±0.19245
15.0 - 30.0	1.00000±0.00000	–	–	1.00000±0.00000	–	–	–	–	1.00000±0.00000

Table D.33: Identification efficiencies for pions, kaons and protons in $N_{\mathrm{tracks}} > 2$ with the DRT method at $rQp > 1.0$.

Momentum range	Q_{π}^{π}	Q_{π}^{K}	Q_{π}^{p}	Q_{K}^{π}	$Q_{\mathrm{K}}^{\mathrm{K}}$	$Q_{\mathrm{K}}^{\mathrm{p}}$	Q_{p}^{π}	$Q_{\mathrm{p}}^{\mathrm{K}}$	$Q_{\mathrm{p}}^{\mathrm{p}}$
0.00 - 0.50	–	–	–	–	–	–	–	–	–
0.50 - 1.00	0.99875±0.00056	0.00125±0.00056	–	–	–	–	–	–	–
1.00 - 1.50	0.96911±0.00126	0.00669±0.00059	0.02419±0.00112	–	–	–	–	–	–
1.50 - 2.00	0.94658±0.00136	0.01127±0.00064	0.04214±0.00121	0.06667±0.06441	0.40000±0.12649	0.53333±0.12881	–	–	–
2.00 - 2.25	0.95887±0.00164	0.00775±0.00072	0.03338±0.00148	0.10656±0.00857	0.53668±0.01386	0.35676±0.01331	–	–	–
2.25 - 2.50	0.96302±0.00156	0.00350±0.00049	0.03348±0.00149	0.11228±0.00763	0.60819±0.01180	0.27953±0.01085	0.08739±0.00532	0.02131±0.00272	0.89130±0.00587
2.50 - 2.75	0.96239±0.00159	0.00412±0.00054	0.03348±0.00150	0.08329±0.00638	0.66044±0.01094	0.25627±0.01009	0.06875±0.00437	0.01815±0.00230	0.91309±0.00486
2.75 - 3.00	0.96868±0.00145	0.00271±0.00043	0.02861±0.00139	0.01989±0.00333	0.74886±0.01034	0.23125±0.01005	0.01619±0.00229	0.02578±0.00288	0.95803±0.00365
3.00 - 3.25	0.97399±0.00136	0.00308±0.00047	0.02293±0.00128	0.00772±0.00213	0.78694±0.00998	0.20534±0.00984	0.01633±0.00244	0.02190±0.00282	0.96177±0.00369
3.25 - 3.50	0.97785±0.00129	0.00206±0.00040	0.02009±0.00123	0.00366±0.00149	0.82693±0.00934	0.16941±0.00926	0.02121±0.00286	0.02357±0.00301	0.95522±0.00410
3.50 - 3.75	0.97893±0.00129	0.00363±0.00054	0.01744±0.00118	0.00438±0.00165	0.81989±0.00961	0.17574±0.00952	0.01556±0.00261	0.01600±0.00265	0.96844±0.00369
3.75 - 4.00	0.97899±0.00136	0.00467±0.00065	0.01634±0.00120	0.00385±0.00157	0.87612±0.00835	0.12003±0.00823	0.01568±0.00267	0.01522±0.00263	0.96910±0.00372
4.00 - 4.25	0.98446±0.00120	0.00550±0.00072	0.01005±0.00097	0.00750±0.00225	0.92224±0.00699	0.07026±0.00668	0.00093±0.00066	0.01948±0.00298	0.97959±0.00305
4.25 - 4.50	0.98430±0.00126	0.00663±0.00082	0.00907±0.00096	0.00291±0.00145	0.94760±0.00601	0.04949±0.00585	0.00241±0.00108	0.02168±0.00320	0.97591±0.00336
4.50 - 4.75	0.98595±0.00122	0.00702±0.00087	0.00702±0.00087	0.00401±0.00179	0.96552±0.00517	0.03047±0.00487	0.00277±0.00124	0.02103±0.00338	0.97620±0.00359
4.75 - 5.00	0.98614±0.00127	0.00723±0.00092	0.00663±0.00088	0.00943±0.00271	0.97170±0.00465	0.01887±0.00381	0.00172±0.00099	0.01718±0.00311	0.98110±0.00326
5.00 - 5.25	0.98630±0.00130	0.00817±0.00101	0.00553±0.00083	0.00510±0.00208	0.97791±0.00428	0.01699±0.00377	–	0.01546±0.00307	0.98454±0.00307
5.25 - 5.50	0.98649±0.00134	0.01027±0.00117	0.00324±0.00066	0.01195±0.00307	0.97132±0.00471	0.01673±0.00362	0.00134±0.00095	0.01739±0.00338	0.98127±0.00351
5.50 - 5.75	0.98719±0.00137	0.00834±0.00111	0.00447±0.00081	0.00091±0.00091	0.98721±0.00340	0.01187±0.00327	0.00156±0.00110	0.01636±0.00354	0.98209±0.00370
5.75 - 6.00	0.98634±0.00147	0.00916±0.00121	0.00450±0.00085	0.00093±0.00093	0.98236±0.00401	0.01671±0.00391	–	0.01230±0.00315	0.98771±0.00315
6.00 - 6.50	0.98522±0.00115	0.01118±0.00100	0.00360±0.00057	0.00208±0.00104	0.98439±0.00283	0.01353±0.00263	–	0.00982±0.00208	0.99018±0.00208
6.50 - 7.00	0.98292±0.00132	0.01190±0.00110	0.00518±0.00073	0.00115±0.00082	0.98500±0.00292	0.01385±0.00281	–	0.00336±0.00137	0.99664±0.00137
7.00 - 7.50	0.98602±0.00132	0.01157±0.00121	0.00242±0.00055	–	0.98733±0.00289	0.01267±0.00289	–	0.01037±0.00266	0.98963±0.00266
7.50 - 8.00	0.98497±0.00148	0.01002±0.00121	0.00501±0.00086	–	0.98870±0.00290	0.01130±0.00290	–	0.00667±0.00221	0.99333±0.00221
8.00 - 8.50	0.98364±0.00166	0.01223±0.00144	0.00413±0.00084	0.00088±0.00088	0.97371±0.00474	0.02542±0.00466	–	0.02014±0.00446	0.97986±0.00446
8.50 - 9.00	0.98445±0.00177	0.01043±0.00145	0.00511±0.00102	0.00095±0.00095	0.96490±0.00567	0.03416±0.00559	–	0.01346±0.00423	0.98654±0.00423
9.00 - 9.50	0.94075±0.00356	0.05335±0.00339	0.00590±0.00115	–	0.91704±0.01071	0.08296±0.01071	–	0.02627±0.00648	0.97373±0.00648
9.50 - 10.0	0.98689±0.00192	0.00998±0.00168	0.00314±0.00094	0.00239±0.00169	0.95096±0.00747	0.04665±0.00729	–	–	1.00000±0.00000
10.0 - 11.0	0.98546±0.00163	0.01044±0.00139	0.00410±0.00087	–	0.96268±0.00523	0.03732±0.00523	0.00129±0.00129	0.00257±0.00182	0.99614±0.00222
11.0 - 12.0	0.98154±0.00217	0.01560±0.00200	0.00286±0.00086	0.00117±0.00117	0.96612±0.00618	0.03271±0.00608	–	0.00162±0.00162	0.99838±0.00162
12.0 - 13.0	0.97959±0.00280	0.01884±0.00269	0.00157±0.00078	–	0.98502±0.00526	0.01498±0.00526	–	–	1.00000±0.00000
13.0 - 14.0	0.96795±0.00425	0.03089±0.00418	0.00117±0.00082	0.00977±0.00561	0.97394±0.00909	0.01629±0.00722	–	–	1.00000±0.00000
14.0 - 15.0	0.96136±0.00585	0.03404±0.00550	0.00460±0.00205	0.00690±0.00687	0.97931±0.01182	0.01379±0.00969	–	–	1.00000±0.00000
15.0 - 30.0	0.92289±0.00655	0.07590±0.00650	0.00120±0.00085	0.00855±0.00851	0.88034±0.03001	0.11111±0.02905	0.02116±0.01047	0.01058±0.00744	0.96825±0.01275

Table D.34: Identification purities and contaminations for pions, kaons and protons in $N_{\mathrm{tracks}} = 1$ with the DRT method at $rQp > 1.0$.

Momentum range	Q_{π}^{π}	Q_{π}^{K}	Q_{π}^{p}	Q_{K}^{π}	$Q_{\mathrm{K}}^{\mathrm{K}}$	$Q_{\mathrm{K}}^{\mathrm{p}}$	Q_{p}^{π}	$Q_{\mathrm{p}}^{\mathrm{K}}$	$Q_{\mathrm{p}}^{\mathrm{p}}$
0.00 - 0.50	–	–	–	–	–	–	–	–	–
0.50 - 1.00	0.99685±0.00081	0.00315±0.00081	–	–	–	–	–	–	–
1.00 - 1.50	0.91854±0.00184	0.01954±0.00093	0.06192±0.00162	–	–	–	–	–	–
1.50 - 2.00	0.86286±0.00197	0.02801±0.00095	0.10913±0.00179	0.18750±0.06900	0.15625±0.06419	0.65625±0.08396	–	–	–
2.00 - 2.25	0.89056±0.00258	0.01994±0.00116	0.08950±0.00236	0.18436±0.00882	0.29674±0.01040	0.51890±0.01137	–	–	–
2.25 - 2.50	0.89191±0.00266	0.01486±0.00103	0.09323±0.00249	0.20605±0.00807	0.34049±0.00945	0.45346±0.00993	0.09978±0.00992	0.02741±0.00541	0.87281±0.01103
2.50 - 2.75	0.89241±0.00273	0.01378±0.00103	0.09382±0.00257	0.17609±0.00768	0.38796±0.00983	0.43595±0.01000	0.10269±0.00958	0.02493±0.00492	0.87238±0.01054
2.75 - 3.00	0.90468±0.00263	0.01037±0.00091	0.08495±0.00250	0.04251±0.00443	0.52174±0.01098	0.43575±0.01090	0.02728±0.00528	0.02204±0.00476	0.95068±0.00701
3.00 - 3.25	0.91137±0.00264	0.00949±0.00090	0.07914±0.00251	0.02211±0.00346	0.56053±0.01167	0.41736±0.01159	0.03692±0.00621	0.02063±0.00468	0.94245±0.00767
3.25 - 3.50	0.91467±0.00272	0.01241±0.00108	0.07292±0.00253	0.00970±0.00234	0.61130±0.01165	0.37900±0.01159	0.03595±0.00679	0.01731±0.00476	0.94674±0.00819
3.50 - 3.75	0.92048±0.00277	0.01260±0.00114	0.06691±0.00256	0.00847±0.00226	0.61925±0.01195	0.37228±0.01189	0.03807±0.00732	0.02928±0.00645	0.93265±0.00959
3.75 - 4.00	0.92997±0.00278	0.01431±0.00129	0.05572±0.00249	0.00992±0.00274	0.68574±0.01282	0.30435±0.01271	0.01384±0.00414	0.02264±0.00528	0.96352±0.00665
4.00 - 4.25	0.94410±0.00263	0.02029±0.00161	0.03561±0.00212	0.01813±0.00412	0.76718±0.01306	0.21469±0.01268	0.00185±0.00131	0.03519±0.00561	0.96296±0.00575
4.25 - 4.50	0.93923±0.00295	0.02391±0.00189	0.03686±0.00233	0.01018±0.00338	0.83484±0.01249	0.15498±0.01217	0.00386±0.00192	0.02989±0.00529	0.96625±0.00561
4.50 - 4.75	0.93988±0.00309	0.02567±0.00206	0.03445±0.00237	0.01240±0.00411	0.88705±0.01175	0.10055±0.01116	0.00818±0.00288	0.04397±0.00656	0.94785±0.00711
4.75 - 5.00	0.94578±0.00310	0.02412±0.00210	0.03010±0.00234	0.00605±0.00302	0.92284±0.01038	0.07110±0.01000	0.00473±0.00236	0.02722±0.00560	0.96805±0.00605
5.00 - 5.25	0.94575±0.00328	0.02953±0.00245	0.02472±0.00225	0.00520±0.00299	0.93241±0.01045	0.06239±0.01007	–	0.02850±0.00586	0.97150±0.00586
5.25 - 5.50	0.93744±0.00369	0.03791±0.00291	0.02465±0.00236	0.00393±0.00277	0.93124±0.01122	0.06483±0.01091	0.00262±0.00185	0.02487±0.00563	0.97251±0.00592
5.50 - 5.75	0.94121±0.00388	0.04001±0.00323	0.01878±0.00224	–	0.94979±0.00999	0.05021±0.00999	–	0.03077±0.00646	0.96923±0.00646
5.75 - 6.00	0.94747±0.00380	0.03105±0.00295	0.02147±0.00247	0.00472±0.00333	0.96698±0.00868	0.02830±0.00805	–	0.02632±0.00649	0.97368±0.00649
6.00 - 6.50	0.94104±0.00310	0.04058±0.00260	0.01838±0.00177	0.00720±0.00321	0.94380±0.00874	0.04899±0.00819	–	0.01609±0.00376	0.98391±0.00376
6.50 - 7.00	0.93935±0.00354	0.04395±0.00304	0.01670±0.00190	0.00304±0.00215	0.95738±0.00788	0.03957±0.00761	–	0.01845±0.00457	0.98155±0.00457
7.00 - 7.50	0.93410±0.00404	0.04491±0.00338	0.02099±0.00234	0.00190±0.00190	0.95057±0.00945	0.04753±0.00928	0.00157±0.00157	0.02198±0.00581	0.97645±0.00601
7.50 - 8.00	0.92921±0.00474	0.04583±0.00387	0.02497±0.00289	–	0.90141±0.01444	0.09859±0.01444	–	0.02479±0.00707	0.97521±0.00707
8.00 - 8.50	0.93082±0.00534	0.04745±0.00448	0.02173±0.00307	–	0.90884±0.01513	0.09116±0.01513	–	0.03562±0.00970	0.96438±0.00970
8.50 - 9.00	0.92615±0.00616	0.04831±0.00505	0.02554±0.00372	–	0.89968±0.01709	0.10032±0.01709	–	0.06374±0.01542	0.93625±0.01542
9.00 - 9.50	0.90318±0.00769	0.07380±0.00680	0.02302±0.00390	–	0.88623±0.02457	0.11377±0.02457	–	0.05000±0.01541	0.95000±0.01541
9.50 - 10.0	0.92537±0.00779	0.04829±0.00635	0.02634±0.00475	–	0.89767±0.02067	0.10233±0.02067	–	–	1.00000±0.00000
10.0 - 11.0	0.92826±0.00647	0.04216±0.00504	0.02958±0.00425	–	0.86601±0.01947	0.13399±0.01947	–	0.00990±0.00697	0.99010±0.00697
11.0 - 12.0	0.95132±0.00685	0.03043±0.00547	0.01826±0.00426	–	0.88557±0.02245	0.11443±0.02245	–	–	1.00000±0.00000
12.0 - 13.0	0.95337±0.00876	0.04145±0.00828	0.00518±0.00298	–	0.89623±0.02962	0.10377±0.02962	–	–	1.00000±0.00000
13.0 - 14.0	0.90577±0.01611	0.06687±0.01377	0.02736±0.00899	–	0.87755±0.04683	0.12245±0.04683	–	–	1.00000±0.00000
14.0 - 15.0	0.88288±0.02158	0.10811±0.02084	0.00901±0.00634	–	0.85000±0.07984	0.15000±0.07984	–	–	1.00000±0.00000
15.0 - 30.0	0.86574±0.02320	0.11111±0.02138	0.02315±0.01023	–	0.84210±0.08365	0.15790±0.08365	–	–	1.00000±0.00000

Table D.35: Identification purities and contaminations for pions, kaons and protons in $N_{\mathrm{tracks}} = 2$ with the DRT method at $rQp > 1.0$.

Momentum range	Q_{π}^{π}	Q_{π}^{K}	Q_{π}^{p}	Q_{K}^{π}	$Q_{\mathrm{K}}^{\mathrm{K}}$	$Q_{\mathrm{K}}^{\mathrm{p}}$	Q_{p}^{π}	$Q_{\mathrm{p}}^{\mathrm{K}}$	$Q_{\mathrm{p}}^{\mathrm{p}}$
0.00 - 0.50	–	–	–	–	–	–	–	–	–
0.50 - 1.00	0.99531±0.00191	0.00469±0.00191	–	–	–	–	–	–	–
1.00 - 1.50	0.90442±0.00378	0.02418±0.00198	0.07139±0.00331	–	–	–	–	–	–
1.50 - 2.00	0.83275±0.00418	0.03780±0.00214	0.12946±0.00376	0.27273±0.13428	0.27273±0.13428	0.45454±0.15013	–	–	–
2.00 - 2.25	0.86846±0.00549	0.02404±0.00249	0.10750±0.00503	0.16525±0.01710	0.31568±0.02139	0.51907±0.02300	–	–	–
2.25 - 2.50	0.86584±0.00587	0.01900±0.00235	0.11517±0.00550	0.23555±0.01613	0.34249±0.01804	0.42196±0.01877	0.17284±0.04201	0.02469±0.01724	0.80247±0.04424
2.50 - 2.75	0.87422±0.00584	0.01957±0.00244	0.10621±0.00543	0.17981±0.01525	0.38643±0.01934	0.43375±0.01968	0.21930±0.03875	0.04386±0.01918	0.73684±0.04124
2.75 - 3.00	0.88536±0.00577	0.01605±0.00227	0.09859±0.00540	0.06168±0.01040	0.46355±0.02156	0.47477±0.02159	0.01835±0.01285	0.02752±0.01567	0.95413±0.02004
3.00 - 3.25	0.89047±0.00605	0.01050±0.00197	0.09902±0.00578	0.01636±0.00574	0.48262±0.02260	0.50102±0.02261	0.02381±0.01663	0.04762±0.02324	0.92857±0.02810
3.25 - 3.50	0.88958±0.00640	0.01625±0.00258	0.09417±0.00596	0.02064±0.00681	0.55505±0.02380	0.42431±0.02367	0.04688±0.02642	–	0.95312±0.02642
3.50 - 3.75	0.90004±0.00639	0.02544±0.00336	0.07451±0.00560	0.02387±0.00786	0.58090±0.02541	0.39522±0.02518	0.03390±0.02356	0.01695±0.01680	0.94915±0.02860
3.75 - 4.00	0.90513±0.00664	0.01795±0.00301	0.07692±0.00603	0.00319±0.00319	0.66454±0.02669	0.33227±0.02662	0.01000±0.00995	0.06000±0.02375	0.93000±0.02551
4.00 - 4.25	0.91611±0.00681	0.02897±0.00412	0.05492±0.00560	0.01036±0.00729	0.71503±0.03249	0.27461±0.03213	0.00769±0.00766	0.06154±0.02108	0.93077±0.02226
4.25 - 4.50	0.90305±0.00779	0.04640±0.00554	0.05055±0.00577	–	0.76471±0.03253	0.23529±0.03253	0.00559±0.00557	0.06145±0.01795	0.93296±0.01869
4.50 - 4.75	0.92363±0.00753	0.02974±0.00482	0.04662±0.00598	–	0.75940±0.03706	0.24060±0.03706	–	0.04545±0.01480	0.95454±0.01480
4.75 - 5.00	0.92661±0.00790	0.02844±0.00503	0.04495±0.00628	–	0.84545±0.03446	0.15454±0.03446	–	0.04839±0.01573	0.95161±0.01573
5.00 - 5.25	0.92453±0.00855	0.03878±0.00625	0.03669±0.00609	0.02564±0.01461	0.82051±0.03548	0.15385±0.03336	0.00680±0.00678	0.05442±0.01871	0.93878±0.01977
5.25 - 5.50	0.89862±0.01024	0.05760±0.00791	0.04378±0.00694	–	0.87500±0.03698	0.12500±0.03698	0.00645±0.00643	0.02581±0.01274	0.96774±0.01419
5.50 - 5.75	0.90143±0.01127	0.06143±0.00908	0.03714±0.00715	0.02439±0.01703	0.91463±0.03086	0.06098±0.02642	–	0.03008±0.01481	0.96993±0.01481
5.75 - 6.00	0.91433±0.01105	0.05452±0.00896	0.03115±0.00686	–	0.95238±0.02683	0.04762±0.02683	–	0.07407±0.02520	0.92593±0.02520
6.00 - 6.50	0.90354±0.00926	0.05906±0.00740	0.03740±0.00595	0.01075±0.01069	0.90323±0.03066	0.08602±0.02908	–	0.02198±0.01087	0.97802±0.01087
6.50 - 7.00	0.91138±0.01034	0.06481±0.00895	0.02381±0.00554	–	0.87879±0.03280	0.12121±0.03280	–	0.02158±0.01233	0.97842±0.01233
7.00 - 7.50	0.89704±0.01200	0.06864±0.00999	0.03432±0.00719	–	0.95522±0.02527	0.04478±0.02527	–	0.04167±0.02039	0.95833±0.02039
7.50 - 8.00	0.87740±0.01608	0.08413±0.01361	0.03846±0.00943	–	0.90000±0.04243	0.10000±0.04243	–	0.01449±0.01439	0.98551±0.01439
8.00 - 8.50	0.89851±0.01650	0.07463±0.01436	0.02687±0.00883	–	0.86957±0.04966	0.13043±0.04966	–	0.06667±0.03718	0.93333±0.03718
8.50 - 9.00	0.91129±0.01805	0.07661±0.01689	0.01210±0.00694	–	0.74286±0.07388	0.25714±0.07388	–	0.10000±0.04743	0.90000±0.04743
9.00 - 9.50	0.86283±0.02288	0.08850±0.01889	0.04867±0.01431	–	0.81250±0.09758	0.18750±0.09758	–	0.07692±0.05226	0.92308±0.05226
9.50 - 10.0	0.90000±0.02535	0.06429±0.02073	0.03571±0.01568	–	0.80000±0.08944	0.20000±0.08944	–	–	1.00000±0.00000
10.0 - 11.0	0.90270±0.02179	0.07568±0.01944	0.02162±0.01069	–	0.93939±0.04154	0.06061±0.04154	–	–	1.00000±0.00000
11.0 - 12.0	0.93976±0.02612	0.03614±0.02049	0.02410±0.01683	–	1.00000±0.00000	–	–	–	1.00000±0.00000
12.0 - 13.0	0.90323±0.05310	0.09677±0.05310	–	–	1.00000±0.00000	–	–	–	1.00000±0.00000
13.0 - 14.0	0.76191±0.09294	0.04762±0.04647	0.19048±0.08569	–	1.00000±0.00000	–	–	–	1.00000±0.00000
14.0 - 15.0	0.66667±0.12172	0.13333±0.08777	0.20000±0.10328	–	0.66667±0.27217	0.33333±0.27217	–	–	1.00000±0.00000
15.0 - 30.0	0.93750±0.06052	0.06250±0.06052	–	–	–	–	–	–	1.00000±0.00000

Table D.36: Identification purities and contaminations for pions, kaons and protons in $N_{\mathrm{tracks}} > 2$ with the DRT method at $rQp > 1.0$.

Bibliography

[1] J. Ashman *et al.* (European Muon Collaboration), Phys. Rev. **D206** (1988) 364.

[2] K. Ackerstaff *et al.* (HERMES Collaboration), Phys. Lett. **B464** (1999) 123.

[3] R.L. Jaffe and A. Manohar, Nucl. Phys. **B337** (1990) 509.

[4] M. Anselmino *et al.*, Phys. Rep. **261** (1995) 1;
Erratum-ibid. **281** (1997) 399.

[5] C. Caso *et al.* (Particle Data Group), Eur. Phys. J. **C3** (1998) 1;
The Review of Particle Physics, `http://pdg.lbl.gov/pdg.html`.

[6] L.W. Whitlow *et al.*, Phys. Lett. **B282** (1992) 475.

[7] A.C. Benvenuti *et al.* (BCDMS Collaboration), Phys. Lett. **B237** (1990) 592.

[8] M.R. Adams *et al.* (Fermilab E665 Collaboration), Phys. Rev. **D54** (1996) 3006.

[9] M. Arneodo *et al.* (European Muon Collaboration), Phys. Lett. **B364** (1995) 107.

[10] K. Abe *et al.* (E143 Collaboration), Phys. Lett. **B452** (1999) 194.

[11] L.W. Whitlow *et al.*, Phys. Lett. **B250** (1990) 193.

[12] M. Arneodo *et al.* (European Muon Collaboration), Nucl. Phys. **B483** (1997) 3.

[13] D.H. Perkins, *Introduction to High Energy Physics: 2nd Edition, Revised, Enlarged, and Reset* (Benjamin/Cummings, California, 1982).

[14] F. Halzen and A.D. Martin, *Quarks and Leptons: An Introductory Course in Modern Particle Physics* (John Wiley & Sons, New York, 1984).

[15] B. Povh, K. Rith, C. Scholz and F. Zetsche, *Teilchen und Kerne – Eine Einführung in die physikalischen Konzepte* (Springer-Verlag, Berlin, 1994).

[16] C.G. Callan and D.G. Gross, Phys. Rev. Lett. **21** (1968) 311;
C.G. Callan and D.G. Gross, Phys. Rev. Lett. **22** (1969) 156.

[17] M.J. Alguard *et al.* (SLAC-Yale E80 Collaboration), Phys. Rev. Lett. **37** (1976) 1258;
M.J. Alguard *et al.* (SLAC-Yale E80 Collaboration), Phys. Rev. Lett. **41** (1978) 70.

[18] G. Baum *et al.* (SLAC-Yale E130 Collaboration), Phys. Rev. Lett. **51** (1983) 1135.

[19] K. Abe *et al.* (E143 Collaboration), Phys. Rev. Lett. **74** (1995) 346.

[20] J. Ashman *et al.* (European Muon Collaboration), Nucl. Phys. **B328** (1989) 1.

[21] B. Adeva *et al.* (Spin Muon Collaboration), Phys. Lett. **B412** (1997) 414.

[22] P.L. Anthony *et al.* (E142 Collaboration), Phys. Rev. Lett. **71** (1993) 959.

[23] K. Abe *et al.* (E143 Collaboration), Phys. Rev. Lett. **75** (1995) 25.

[24] K. Abe *et al.* (E154 Collaboration), Phys. Lett. **B405** (1997) 180.

[25] K. Ackerstaff *et al.* (HERMES Collaboration), Phys. Lett. **B404** (1997) 383; DESY-97-085 (1997).

[26] D. Adams *et al.* (Spin Muon Collaboration), Phys. Lett. **B396** (1997) 338.

[27] R.P. Feynman, *Photon-Hadron Interactions* (W.A. Benjamin, New York, 1972, Addison-Wesley, New York, 1989).

[28] J.D. Bjorken, Phys. Rev. **179** (1969) 1547;
J.D. Bjorken and E.A. Paschos, Phys. Rev. **185** (1969) 1975.

[29] M. Arneodo *et al.* (New Muon Collaboration), Phys. Lett. **B364** (1995) 107.

[30] M.G. Vincter, HERMES Internal Note 97-028 (1997).

[31] P. Amaudruz *et al.* (New Muon Collaboration), Nucl. Phys. **B371** (1992) 3.

[32] P. Amaudruz *et al.* (New Muon Collaboration), Phys. Rev. Lett. **66** (1991) 2712.

[33] M. Arneodo *et al.* (New Muon Collaboration), Phys. Rev. **D50** (1994) 1.

[34] K. Ackerstaff *et al.* (HERMES Collaboration), Phys. Rev. Lett. **81** (1998) 5519; DESY 98-078 (1998).

[35] K. Gottfried, Phys. Rev. Lett. **18** (1967) 1174.

[36] J. Ellis and R.L. Jaffe, Phys. Rev. **D9** (1974) 1444;
J. Ellis and R.L. Jaffe, Phys. Rev. **D10** (1974) 1669.

[37] F.E. Close and R.G. Roberts, Phys. Lett. **B316** (1993) 165.

[38] S.A. Larin *et al.*, Phys. Rev. Lett. **66** (1991) 862;
S.A. Larin and J.A.M Vermaseren, Phys. Lett. **B259** (1991) 345.

[39] S.A. Larin, Phys. Lett. **B334** (1994) 192.

[40] A.L. Kataev and V.V. Starshenko, Mod. Phys. Lett. **A10** (1995) 235.

[41] K. Abe *et al.* (E143 Collaboration), Phys. Rev. **D58** (1998) 112003.

[42] B. Adeva *et al.* (Spin Muon Collaboration), Phys. Lett. **B302** (1993) 533.

[43] D. Adams *et al.* (Spin Muon Collaboration), Phys. Lett. **B329** (1994) 399.

[44] D. Adams *et al.* (Spin Muon Collaboration), Phys. Rev. **D56** (1997) 5330.

[45] J.D. Bjorken, Phys. Rev. **148** (1966) 1467;
J.D. Bjorken, Phys. Rev. **D1** (1970) 1376.

[46] J. Ellis and M. Karliner, Phys. Lett. **B341** (1995) 397.

[47] A. Airapetian *et al.* (HERMES Collaboration), Phys. Rev. Lett. **84** (2000) 2584; DESY 99-071 (1999).

[48] X. Ji, Phys. Rev. Lett. **78** (1997) 610.

[49] R.D. Field and R.P. Feynman, Phys. Rev. **D15** (1977) 2590.

[50] R.D. Field and R.P. Feynman, Phys. Rev. **B136** (1978) 1.

[51] M. Althoff *et al.* (TASSO Collaboration), Zeit. Phys. **C22** (1984) 307.

[52] M. Arneodo *et al.* (European Muon Collaboration), Zeit. Phys. **C36** (1987) 527.

[53] M. Arneodo *et al.* (European Muon Collaboration), Nucl. Phys. **B321** (1989) 541.

[54] P. Geiger, PhD thesis, Ruprecht-Karls-Universität Heidelberg, Germany (1998).

[55] The HERMES Collaboration, *Technical Design Report*, DESY-PRC 93/06 (1993); MPIH-V20-1993 (1993).

[56] M. Düren, Habilitation thesis, DESY HERMES-95-02, Friedrich-Alexander-Universität Erlangen-Nürnberg, Germany (1995).

[57] L.H. Kramer *et al.*, Nucl. Instr. Meth. **A365** (1995) 49.

[58] A.A. Sokolov and I.M. Ternov, Sov. Phys. Comm. **82** (1964) 1203.

[59] A.W. Chao, Nucl. Instr. Meth. **180** (1981) 29;
Physics of High Energy Particle Accelerators, American Institute of Physics Proceedings **87** (1982) 395.

[60] D.P. Barber *et al.*, Phys. Lett. **B343** (1995) 436.

[61] D.P. Barber *et al.*, Nucl. Instr. Meth. **A329** (1993) 79.

[62] F. Stock *et al.*, Nucl. Instr. Meth. **A343** (1994) 334.

[63] B. Braun, Proceedings of the Workshop Polarized Gas Targets and Polarized Beams. Edited by R.J. Holt and M.A. Miller, Urbana-Champaign, USA, API Conf. Proc. **421** (1997) 156.

[64] K. Ackerstaff *et al.* (HERMES Collaboration), Nucl. Instr. Meth. **A417** (1998) 230; DESY-98-057 (1998).

[65] H. Avakian *et al.*, Nucl. Instr. Meth. **A417** (1998) 69.

[66] H. Avakian *et al.*, Nucl. Instr. Meth. **A378** (1996) 155.

[67] T.-A. Shibata, Y. Sakemi, H. Kobayashi, S. Yoneyama, T. Harano, K. Shibatani, M. Kurisuno, H. Ogami and C.A. Miller, Nucl. Instr. Meth. **A411** (1998) 75.

[68] E. Cisbani *et al.*, HERMES Internal Note 97-003 (1997).

[69] E. Cisbani, PhD thesis, Università degli Studi di Roma "La Sapienza", Italy (1998).

[70] J. Seguinot and T. Ypsilantis, Nucl. Instr. Meth. **A343** (1994) 1.

[71] H. Yokogawa and M. Yokoyama, J. Non-Cryst. Solids **186** (1995) 23.

[72] I. Adachi *et al.*, Nucl. Instr. Meth. **A355** (1995) 390.

[73] L.F. Zhang, Diploma thesis, Tokyo Institute of Technology, Japan (1999).

[74] E. Aschenauer *et al.*, Nucl. Instr. Meth. **A440** (2000) 338.

[75] R. De Leo *et al.*, Nucl. Instr. Meth. **A401** (1997) 187.

[76] P. Carter, PhD thesis, California Institute of Technology, USA (1999).

[77] P.C. Chen, T.T. Saha, A.M. Smith and R.C. Romeo, Optical Eng. **37**, No.2 (1998).

[78] M. Pommot Maia *et al.*, Nucl. Instr. Meth. **A326** (1993) 496.

[79] R.B. Kaiser *et al.*, *Online Monitoring at HERMES*, Proc. of CHEP97, Berlin, Germany, 1997.

[80] W. Wander, *DAD-Distributed ADAMO Database System at HERMES*, Proc. of CHEP95, Rio de Janeiro, Brazil, 1995.

[81] K. Ackerstaff and M.-A. Funk, *Pink: A Tcl/Tk based Database Interface to ADAMO and DAD*, Proc. of CHEP95, Rio de Janeiro, Brazil, 1995.

[82] R. Forty and O. Schneider, LHCb Internal Note LHCb-98-040 (1998).

[83] D. De Schepper, R.B. Kaiser and E. Cisbani, HERMES Internal Note 98-008 (1998).

[84] P. Jung, Diploma thesis, Humboldt-Universität, Germany (2000).

[85] A.T. Maas, Diploma thesis, Universität Darmstadt, Germany (2000).

[86] R.B. Kaiser, HERMES Internal Note 00-026 (2000).

[87] K. Negodaeva, HERMES Internal Note 99-022 (1999).

[88] H. Ihssen *et al.* (HERMES Monte Carlo Simulations Group), `http://www.desy.de/~ihssen/pepsi.html`.

[89] T. Sjöstrand, Comp. Phys. Comm. **82** (1994) 74; `http://www.thep.lu.se/tf2/staff/torbjrn/Pythia.html`.

[90] Application Software & Databases Group, Information Technology Division, CERN, Switzerland, `http://wwwinfo.cern.ch/asd/`; `http://wwwinfo.cern.ch/asd/geant/`.

[91] G. Ingelman *et al.*, Comp. Phys. Comm. **101** (1997) 108; DESY 96-057 (1996); `http://www3.tsl.uu.se/thep/lepto/`.

[92] B. Andersson *et al.*, Phys. Rep. **97** (1983) 31.

[93] F. Sato, HERMES Internal Note 00-011 (2000).

[94] CERN Program Library Long Writeup I101, CERN, Switzerland; `http://wwwinfo.cern.ch/asdoc/WWW/epio/epiomain/epiomain.html`.

[95] W. Wander, PhD thesis, Friedrich-Alexander-Universität Erlangen-Nürnberg, Germany (1996).

[96] Information, Process & Technology Group, Information Technology Division, CERN, Switzerland, `http://adamo.web.cern.ch/Adamo/ADAMO_ENTRY.html`.

[97] T. Lindemann and J. Wendland, Private communication (2000).

[98] R.B. Kaiser, D. Phil. thesis (partial fulfillment), Simon Fraser University, Canada (1999).

[99] H. Böttcher, Y. Gärber and U. Stösslein, HERMES Internal Note 99-053 (1999).

[100] J.L. Friar *et al.*, Phys. Rev. **C42** (1990) 2310.

[101] P.L. Anthony *et al.* (E155 Collaboration), Phys. Lett. **B458** (1999) 529.

[102] S. Wandzura and F. Wilczek, Phys. Lett. **B72** (1977) 195.

[103] R.L. Jaffe and X. Ji, Phys. Rev. **D43** (1991) 733.

[104] B. Adeva *et al.* (Spin Muon Collaboration), Phys. Lett. **B420** (1998) 180.

[105] H.E. Jackson, HERMES Internal Note 00-039 (2000).

[106] J. Binnewies, B.A. Kniehl and G. Kramer, Phys. Rev. **D52** (1995) 4947.

Acknowledgements

I would like to thank Prof. Dr. Toshiaki Shibata who gave me an opportunity to join the HERMES Collaboration and gave me advice throughout my analysis of this work.

I thank very much Yasuhiro Sakemi. His advice helped me to overcome the difficulties against my work and he discussed with me patiently.

I want to thank Hideyuki Kobayashi, who is the first collaborator of the HERMES experiment as a student from our university. I learned the procedures of the analyses from him.

I want to thank very much Stefan Bernreuther who gave helpful advice to me.

I want to thank very much Jiro Kanesaka. He stayed and worked at DESY with me.

I thank very much Kentaro Suetsugu. He is a one of my collaborators for the analysis and worked for the HERMES experiment together.

I thank very much Fumiko Sato. Her code included into the Monte Carlo simulations was very helpful.

I like to thank very much my colleagues, Hiroshi Ohsuga and Hidekazu Tanaka in our laboratory. They helped me to arrange my thesis.

I like to thank all members of our laboratory.

I would like to thank all members of the sub-groups of the HERMES Collaboration: As for the RICH group, I thank very much Ralf Bernd Kaiser, Peter Jung, Katerina Negodaeva, Elke-Caroline Aschenauer, Axel Torsten Maas, Wolf-Dieter Nowak, Vassili Djordjadze, Markus Ehrenfried, Harold E. Jr. Jackson, Dirk De Schepper, Brecht Hommez, Michael Tytgat, Katty Van de Kerckhove, Dirk Ryckbosch and Hamlet Zohrabyan. As for the Δq analysis group, I thank very much Thore Lindemann, Jürgen Wendland, Chiara Simani, Marc Beckmann, Manuella G. Vincter, Makins Naomi and Michael Düren.

I would like to thank Yorck Holler, Adolf Schwind, Felix Menden, Michael Ruh, Greg Rakness, James Ely, Jeffery Martin, Michael Gabriel M^{c}Andrew, Erika Garutti, Paolo Lenisa, Severino Tessarin and Alexandr Nagaitsev for the friendship they showed.

I thank very much all the collaborators of the HERMES experiment.

I want to thank Masaharu Oka and Haruko Kumamoto. They gave me delightful time and memories.

I thank very much Mr. and Mrs. Kohlmann, and Mr. and Mrs. Nishino for their kind considerations.

I thank my parents and brother. They always support me when I faced the difficulties.